# *Epi*-cyclophellitol cyclosulfate, a mechanism-based ER α-glucosidase II inhibitor, blocks replication of SARS-CoV-2 and other coronaviruses

Melissa Thaler[a], Tim P. Ofman[b], Ken Kok[b], Jurriaan J.A. Heming[b], Elisha Moran[c], Isabelle Pickles[c], Anouk A. Leijs[a], Adrianus M. C. H. van den Nieuwendijk[b], Richard J. B. H. N. van den Berg[b], Gijs Ruijgrok[b], Zach Armstrong[b], Clarisse Salgado-Benvindo[a], Dennis K. Ninaber[d], Eric J. Snijder[a], Constant A. A. van Boeckel[b], Marta Artola[b], Gideon J. Davies[c], Herman S. Overkleeft[b#], Martijn J. van Hemert[a#]

[a]Leiden University Center for Infectious Diseases (LUCID), Leiden University Medical Center, Leiden, The Netherlands.

[b]Leiden Institute of Chemistry, Leiden University, Leiden, The Netherlands.

[c]Department of Chemistry, University of York, YO10 5DD, York, United Kingdom.

[d]Department of Pulmonology, Leiden University Medical Center, Leiden, The Netherlands.

Running Head: Mechanism-based ER α-Glu-II inhibitor blocks coronavirus infection

#Address correspondence to:

Martijn J. van Hemert, m.j.van_hemert@lumc.nl or

Herman S. Overkleeft, h.s.overkleeft@chem.leidenuniv.nl

## Abstract

The combined inhibition of ER α-glucosidases I and II has been shown to inhibit replication of a broad range of viruses that rely on ER protein quality control. We found, by screening a panel of deoxynojirimycin and cyclitol glycomimetics, that the mechanism-based ER α-glucosidase II inhibitor, 1,6-*epi*-cyclophellitol cyclosulfate, potently blocks SARS-CoV-2 replication in lung epithelial cells, halting intracellular generation of mature Spike protein, reducing production of infectious progeny, and leading to reduced syncytium formation. Through activity-based protein profiling, we confirmed ER α-glucosidase II inhibition in primary airway epithelial cells, grown at the air-liquid interface. 1,6-*Epi*-cyclophellitol cyclosulfate inhibits early pandemic and more recent SARS-CoV-2 variants, as well as SARS-CoV and MERS-CoV. The reported antiviral activity is comparable to the best-in-class described glucosidase inhibitors, all competitive inhibitors also targeting ER α-glucosidase I and other glycoprocessing enzymes not involved in ER protein quality control. We propose selective blocking ER-resident α-glucosidase II in a covalent and irreversible manner as a new strategy in the search for effective antiviral agents targeting SARS-CoV-2 and other viruses that rely on ER protein quality control.


**Synopsis**

Screening of deoxynojirimycin and cyclitol glycomimetics identified mechanism-based ER α-glucosidase II inhibitor 1,6-*epi*-cyclophellitol cyclosulfate as a potent inhibitor of SARS-CoV-2 replication.

**Keywords**: glycomimetics, ER-resident α-glucosidase-II, SARS-CoV-2, Spike glycosylation, antiviral, carbohydrate-active enzymes

## Introduction

Coronaviruses, like many other virus groups, use the host machinery for co- and post-translational formation and processing of N-linked glycans. N-linked oligosaccharides are crucial for proper protein folding, stability and functioning of many proteins that are part of viral envelopes (1). In the endoplasmic reticulum (ER), α-glucosidases I and II (α-Glu I and α-Glu II) are responsible for trimming the terminal glucose moieties of nascent N-glycans (**Figure 1A**), and the resultant mono-glucosylated N-glycans are subsequently recognized by the ER chaperones calnexin and calreticulin (CNX-CRT cycle) (2, 3), which prevent protein aggregation and assist in polypeptide folding. When a protein fails to fold correctly, glycoprotein glycosyltransferase (UGGT) reconstructs the mono-glucosylated G1M9 N-glycan, enabling another round of refolding attempts facilitated by the CNX-CRT chaperones. Upon proper folding of the protein, the final glucose residue in high mannose-type N-glycans is removed by α-Glu II, leading to further trimming by ER α-mannosidase I (ERMI), after which the N-glycoproteins are routed to the Golgi apparatus for N-glycan maturation and further post-translational modification events en route to their final destination. Glycoproteins that fail to attain their proper conformation undergo mannose

trimming orchestrated by the ER degradation-enhancing mannosidase-like proteins (EDEMs) and ultimately are routed toward the ER-associated degradation (ERAD) machinery. Inhibition of ER α-Glu I and II has been shown to interfere with proper processing of nascent proteins through the CNX-CRT cycle, leading to their inappropriate folding, eventual dislocation from the ER and proteasomal degradation (4). This holds true for host and viral N-glycoproteins alike and ER α-Glu I/II inhibition has therefore been considered as a viable strategy for antiviral therapeutics development for several decades (5, 6). Many studies have reported the ability of iminosugars to inhibit replication of various viruses, through the blocking of ER protein quality control via ER α-Glu I/II inhibition (7). Iminosugars are polyhydroxylated glycomimetic alkaloids featuring a basic amine, replacing the sugar ring oxygen, that is thought to interact with glycosidase active site residues that partake in enzymatic glycosidic bond hydrolysis (8, 9). The potential of iminosugars as antivirals was first reported in 1987 (5, 10, 11) in the context of Human Immunodeficiency Virus (HIV), which relies on the host ER machinery for glycoprotein processing (12). These studies revealed that the two iminosugar compounds, deoxynojirimycin and castanospermine, as well as some structural analogues thereof, inhibit ER α-Glu I and II and block the production of HIV infectious progeny *in vitro*. Later studies using a host of structurally diverse iminosugars described blocking replication of a broad range of viruses *in vitro* and *in vivo*, including influenza viruses (13-15), severe acute respiratory syndrome coronavirus (SARS-CoV) (16), dengue virus and the hemorrhagic fever viruses Marburg and Ebola (17, 18). One of the studied iminosugars, UV-4B, showed promising results in mice, as a single high dose, which caused hallmarks of ER α-Glu I inhibition in vivo, protected the animals from a lethal dose of DENV or influenza virus(15).

Interestingly, patients that have N-glycosylation defects (defects in ER α-Glu I) due to a congenital disorder, have also reduced susceptibility to infection with enveloped viruses that depend on host glycan processing for their replication (19). Despite promising *in vitro* studies, phase II clinical trials with the iminosugar Celgosivir (a prodrug form of castanospermine) showed no beneficial outcomes when it was used as mono therapy for dengue and hepatitis C virus infections (20, 21). Most recently, a range of competitive α-glucosidase inhibitors have been studied during the search for antivirals against SARS-CoV-2 (22-24). The spike (S) protein of SARS-CoV-2, one of the envelope proteins on the virus surface, is heavily glycosylated with 23 reported N-glycan sites (25). Besides shielding of antibody epitopes (26), and modulating protein structure, N-glycosylation of S protein and its receptor binding domain (RBD) is crucial for virus infectivity, as the S protein drives virus entry by binding to the host receptor ACE2 and mediates fusion between the virus and host cell membrane (27). N-glycans and their modulation through deletion of specific sites on the RBD were reported to be important for conformational stability and accessibility of the RBD for ACE2 binding (28-31). Therefore, the incorporation of non-functional immaturely glycosylated S proteins can reduce the specific infectivity of progeny virions (16, 32). Disruption of the CNX-CRT-mediated glycoprotein processing, by iminosugars specifically, was reported to reduce the incorporation of S protein into SARS-CoV pseudovirus particles (16). In this study, it was suggested that ER α-Glu I/II inhibition could lead to both the degradation of improperly processed S proteins in the ER as well as the incorporation of incompletely glycosylated S proteins into virus particles, thus having a two-pronged mode of action.

Despite the decades of research on iminosugars, no small molecules inhibiting ER α-Glu have proceeded beyond phase II clinical trials (33, 34) as antivirals. With the aim of uncovering alternative inhibitor designs for antiviral drug discovery, and building upon our recent studies on mechanism-based, covalent and irreversible glycosidase inhibition (35-40), we decided to assess a panel of mechanism-based inhibitors, side by side with a set of classical *N*-alkyl iminosugars, for their ability to inhibit SARS-CoV-2 replication through inhibition of ER α-Glu I and II. While performing the same net transformation (hydrolysis of α-glucosidic linkages), ER α-Glu I and II do so with distinct mechanisms. Both enzymes feature a carboxylic acid and a carboxylate containing amino acid in their active site and process their substrate by acid catalysis (8, 9). Both enzymes are therefore amenable to inhibition by a basic, glucose-mimetic iminosugar. In contrast to ER α-Glu I, ER α-Glu II forms a covalent intermediate with its substrate during processing by utilizing one of the carboxylates as nucleophile. This nucleophile can be trapped by glucomimetic cyclitols endowed with an electrophile (epoxide, aziridine or cyclic sulfate). We have shown in the past that 1,6-*epi*-cyclophellitol (**9**, **Figure 1**) as well as its aziridine (**10**) and cyclic sulfate (**11**) analogues potently and selectively block ER α-Glu II (35). In this study, we screened members of both compound classes, cyclitols and iminosugars, for their inhibition of ER α-Glu II and antiviral activity against SARS-CoV-2. We demonstrate that 1,6-*epi*-cyclophellitol cyclosulfate (**11**) most potently reduces the enzyme activity of α-Glu II, and exerts the best antiviral efficacy against SARS-CoV-2. We also show that this compound blocks replication of all SARS-CoV-2 variants tested, as well as the pathogenic SARS-CoV and MERS-CoV, making it an interesting lead for further exploration towards a new class of antiviral drugs.

## Results

### Efficacy of glucosidase inhibitors against SARS-CoV-2 correlates with their activity against ER α-glucosidase II

The panel of iminosugars and cyclitols, subject of the here-presented studies, is depicted in **Figure 1B**. With respect to the iminosugars, and to keep in line with literature precedents, we selected *N*-alkyl deoxynojirimycins **1-8**. Deoxynojirimycin (DNJ) features the glucopyranose configuration and *N*-alkyl derivatives have been shown to be more effective glucosidase inhibitors compared to non-substituted DNJ (41-43). This includes the benchmark analogue, *N*-butyl-DNJ **1** (Miglustat, Zavesca) which is part of almost all antiviral studies on iminosugars targeting α-Glu I/II. In fact, Miglustat is a clinical drug for the treatment of Gaucher disease and acts as a glucosylceramidase (GCS) inhibitor (44). It also inhibits the human retaining β-glucosidases, GBA1, GBA2 and GBA3, displaying a rather broad activity profile across various glycoprocessing enzymes not involved in ER protein quality control. Besides Miglustat **1**, we included DNJ derivatives **2-8** to assess the influence of the hydrophobic *N*-alkyl substituent on antiviral activity. Compound **8** has the L-*ido*-configuration and comprises the C6-epimer (glucopyranose numbering) of DNJ derivative **5**. Compared to **5**, L-*ido*-DNJ **8** is a much weaker ER α-Glu inhibitor, which should be reflected in its antiviral potency. With respect to the cyclitols, we previously published 1,6-*epi*-cyclophellitol **9**, 1,6-*epi*-cyclophellitol aziridine **10** and 1,6-*epi*-cyclophellitol cyclosulfate **11** as potent and selective, mechanism-based, covalent and irreversible retaining α-glucosidase inhibitors (35, 45). Besides inhibiting ER α-Glu II, the single detected off-target (in the context of pharmacological ER protein quality control

interference) is the lysosomal α-glucosidase, human acid α-glucosidase GAA. These 1,6-*epi*-cyclophellitol analogues were designed to inhibit retaining α-glucosidases exclusively (so, not inverting ones like α-Glu I), and while epoxide **9** and aziridine **10** partially inhibit the retaining β-glucosidases, GBA1 and GBA2, cyclosulfate **11** is completely inactive towards these enzymes. We also found that tempering the electrophilicity, as in cyclosulfamidates **17**, **18** and cyclosulfamide **19** yields competitive retaining α-glucosidase inhibitors and to investigate the effect of going from covalent to competitive inhihition within the same compound class we included these compounds in our assays. In addition, we tested a number of structural cyclitol variations. These include 1,2-*epi*-cyclophellitols (**20**-**22**), which may block α-Glu II in a covalent, irreversible manner similar to the 1,6-*epi*-cyclophellitols (46). A number of partially *O*-methylated cyclosulfates (**12**-**16**) were included to assess the effect of polarity, while compounds **23**-**28** were designed to contain alkyl substituents also present in the iminosugar series tested. The synthesis of the iminosugar and cyclitol inhibitors **1**-**11**, **17**-**22**, **25** and **26** have been published previously (35, 41-43, 45, 47). The synthesis of methylated sulfates **12**-**16** and alkyl aziridines **23**, **24**, **27** and **28** can be found in the supporting information (**Scheme S1**-**S5**).

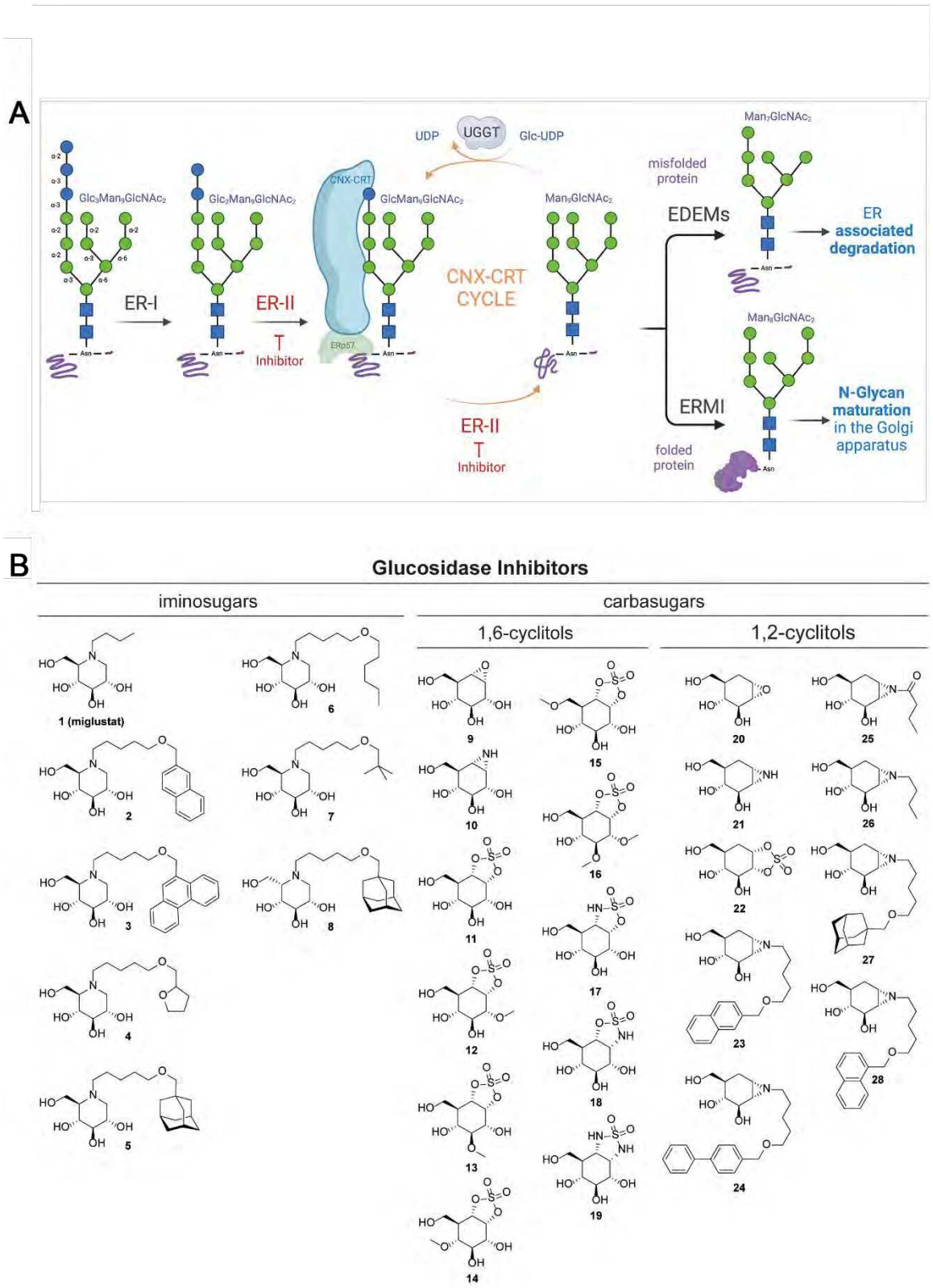


**Figure 1**: (A) Schematic of N-glycan processing of newly synthesized proteins in the ER lumen. Folding of nascent proteins in the ER is promoted by the calnexin-calreticulin cycle (CNX-CRT cycle), which relies on

glycan trimming by ER α-Glu II (ER-II). (B) Focused library of 28 iminosugars and cyclitols subject of the here-presented studies.

The inhibitory effect of all synthesized molecules on the activity of GAA and endoplasmic reticulum α-glucosidase II (ER α-Glu II, GANAB) was determined following *in vitro* enzyme activity methods reported previously (35), using 4-methylumbelliferyl-α-D-glucopyranoside (4-MU-α-Glc) as fluorogenic substrate and measuring the amount of 4-MU-mediated fluorescence (**Figure 2A**, left panel). *N*-alkyldeoxynojirimycins **1**-**8** all inhibited both ER α-Glu II as well as GAA, but with potencies varying from the nanomolar to the micromolar range. *N*-alkyl-iminosugars **2**-**7**, featuring an extended lipophilic *N*-alkyl moiety relative to *N*-butyl-DNJ **1**, inhibited both enzymes rather more potently than this benchmark iminosugar, with **2** showing high potencies for both ER α-Glu II ($IC_{50}$ = 0.3 ± 0.07 μM) and GAA ($IC_{50}$ = 1.1 ± 0.09 μM). L-*Ido*-deoxynojirimycin **8** is a much weaker ER α-Glu II inhibitor than its D-*gluco*-isoster **5** (both compounds containing the same adamantane-modified *N*-alkyl chain), and showed no activity against GAA at the measured concentrations. These results match the literature trend indicating that large, hydrophobic *N*-alkyl appendages positively influence glucosidase inhibitory potency in this class of compound (41-43, 47).

With respect to the cyclitol class of compounds, 1,6-*epi*-cyclophellitol cyclosulfate **11** proved to be the most potent ER α-Glu II inhibitor of all compounds tested, with an $IC_{50}$ value of 0.03 ± 0.007 μM. Cyclosulfate **11** was also, and together with naphthyl-iminosugar **2**, the most potent of the GAA inhibitors. Methylation of either of the four hydroxyls (or combinations thereof) in **11**, as in 1,6-*epi*-cyclophellitol cyclosulfates **12**-**16** proved detrimental to inhibitory potency, though 4-*O*-methyl derivative **14** with an $IC_{50}$ value of

8.2 ± 0.1 μM for ER α-Glu II and 2.2 ± 0.09 μM for GAA still outperformed Miglustat (**1**) as inhibitor of both of these enzymes. Moving from covalent (cyclosulfate, **11**) to competitive (**17-19**) cyclitol designs proved detrimental for ER α-Glu II inhibition, although compound **18** retains remarkable ($IC_{50}$ = 6.1 ± 1.3 μM) inhibitory activity against GAA. 1,2-*Epi*-cyclitols **20-22** turned out to be only moderately active ER α-Glu II inhibitors. In contrast to the 1,6-analogues (**9-11**), where the cyclosulfate was more potent compared to the aziridine and epoxide, epoxide **20** was the most potent of this series (46). Interestingly, 1,2-cyclosulfate **22** proved to be a rather potent GAA inhibitor, much more so than epoxide **20** and aziridine **21**, suggesting that conformational aspects (the epoxide and aziridine likely enforcing a half chair conformation with respect to the cyclitol ring where the cyclosulfate will allow a chair-like conformation) are in play for this enzyme. Finally, and in contrast to what was observed for the competitive inhibitor series **1-8**, 1,2-cyclophellitol aziridines **23-28** bearing an *N*-alkyl chain (and in case of **25** an *N*-acyl one) are much worse inhibitors for both enzymes tested (no significant inhibition up to 100 μM) when compared to the non-substituted aziridine **21**. In all, 1,6-*epi*-cyclophellitol cyclosulfate **11** is the most potent ER α-Glu II inhibitor, with naphthylated deoxynojirimycin **2** as the most effective of the competitive inhibitors almost on a par with **11**.

To confirm the stabilizing effect of these two compounds on the enzyme, we performed a thermal stability assay with these, as well as with the less potent inhibitors **20-22**, on recombinant *M. musculus* α-Glu II, a mouse enzyme with high sequence homology to the human enzyme (**Figure 2B**). ER α-Glu II denaturation as a consequence of heat exposure, as well as the effect of active site-binding inhibitors on the denaturation temperature, can

be monitored by a naturally quenched SYPRO orange dye. Upon denaturation of a protein, hydrophobic regions are exposed to which the dye binds, demonstrating a distinct difference in melting temperature ($T_m$) for each inhibitor compared to the unliganded ER α-Glu II control. *Mm*α-Glu II preincubated with compound **11** or **2** displayed melting temperatures ($T_m$) of 63.3 °C and 63.5 °C, respectively, whereas the unliganded enzyme denatured at approximately 15 °C lower ($T_m$ = 49.9 °C). In comparison, compounds **21** and **22** gave no (49.5 °C) to marginal (51.7 °C) $T_m$ increases, while epoxide **20**, which had the best efficacy of all 1,2-*epi*-cyclophellitols in the enzyme activity assay, gave a remarkably high $T_m$ of 64.7 °C.

To elucidate the structure-activity relationship and predict the binding mode of the compounds before and after the covalent reaction with the nucleophilic aspartate, docking into ER-α-Glu II was performed for compound **11**, **10** and **9**. The top scoring pose of **11**, **10** and **9** after non-covalent docking using Glide (in the Schrödinger Maestro GUI) was overlaid with the bound D-glucose molecule from the original PDB file (PDB:5H9O) as a measure of the accuracy of the pose. The compound adopted a near-identical conformation in the binding site (**Figure S1A**). The ligand was also subjected to covalent docking to mimic a post-reaction conformation. The outputted poses made the same hydrogen bonding interactions as the non-covalently docked pose. The top poses were overlaid with a PDB file containing a 5-fluoro-α-d-glucopyranosyl (PDB:5HJR); the poses overlaid well in a skewed boat confirmation (**Figure S1B-D**), suggesting confidence in the docking results. These binding pose predictions suggest compounds **11, 10** and **9** are orientated correctly in the binding site of ER α-Glu II to facilitate a covalent reaction with Asp564.

All compounds were then analyzed for their antiviral activity against SARS-CoV-2, in cytopathic effect (CPE) reduction assays, in which Vero E6 cells were pre-treated and infected with SARS-CoV-2 in the presence of various concentrations of compound. Three days post-infection cell viability was measured and $EC_{50}$ values (compound concentration at which 50% of cell viability is reached as compared to the non-treated, infected cells) were determined (**Figure 2A**, right panel). Simultaneously, uninfected cells were treated with the same concentrations of compound to determine the $CC_{50}$ (compound concentration at which cell viability is 50% of that of untreated cells due to cytotoxicity). All iminosugars **1-8** protected cells from SARS-CoV-2 infection in this assay, and naphthyl deoxynojirimycin **2**, being the most potent competitive ER α-Glu II inhibitor from the enzyme activity assay, also displayed the highest efficacy of the eight iminosugars assessed in blocking SARS-CoV-2 replication, with an $EC_{50}$ value of 6 ± 0.4 μM (**Figure 2D**). Similar deoxynojirimycin derivatives were previously reported to have activity against SARS-CoV-2 (24, 48). UV-4, an iminosugar that was previously described to be efficacious in a mouse model (13), was tested in parallel and its activity was compared to those of compounds **11** and **2**. The antiviral efficacy of UV-4 was similar to that of our iminosugar compound **2** (**Figure S2A**). In contrast, the $EC_{50}$ value in the CPE assay for Miglustat **1** was above 100 μM (**Figure 2C**), which correlates to other studies which found limited antiviral activity for this compound against SARS-CoV-2 (24, 49). 1,6-*Epi*-cyclophellitol cyclosulfate **11**, our most potent ER α-Glu II inhibitor, also proved to be the most potent SARS-CoV-2 replication inhibitor of all compounds tested with an $EC_{50}$ value of 0.48 ± 0.1 μM (**Figure 2E**). This matches our general finding that ER α-Glu II inhibitory potency correlates with anti-SARS-CoV-2 replication efficacy (**Figure 2A**). Selective ER

α-Glu II inhibition thus appears a promising strategy in the discovery of new antiviral agents. To validate the results obtained in the Vero E6 cell-based assays, CPE reduction assays on H1299/ACE2 lung epithelial cells were performed with compounds 11, 2 and UV-4. With these human lung cells, comparable EC50 values were obtained(**Figure S2B**). Given that 1,6-*epi*-cyclophellitol cyclosulfate **11** came out as the most potent compound in both the enzyme inhibition and SARS-CoV-2 CPE assays, and that this compound class, in contrast to that of iminosugars, comprises a new design class, we decided to further profile this inhibitor in more advanced virological assays to study its efficacy and mechanism of action.

A

| | Compound | Inhibitory activity against glucosidases (biochemical assay) | | Antiviral activity (CPE assay) | |
|---|---|---|---|---|---|
| | | IC50 GANAB (μM) (ER-Glu-II) | IC50 GAA (μM) | EC50 (μM) | CC50 (μM) |
| Iminosugars | 1 (Miglustat) | 200 | 6.58 ± 2.4 | 113.5 ± 10.3 | >200 |
| | 2 | 0.12 ± 0.07 | 0.19 ± 0.01 | 6 ± 0.4 | >200 |
| | 3 | 0.15 ± 0.09 | 0.034 ± 0.004 | 3.25 ± 0.42 | 50 |
| | 4 | 0.2 ± 0.05 | 0.82 ± 0.18 | 51.7 ± 3.37 | >200 |
| | 5 | 0.21 ± 0.07 | 0.64 ± 0.06 | 13.9 ± 8 | 200 |
| | 6 | 0.26 ± 0.1 | 0.47 ± 0.05 | 11.8 ± 0.8 | >200 |
| | 7 | 2.12 ± 0.38 | 2.19 ± 5.9 | 22.7 ± 4.3 | >200 |
| | 8 | 41.1 | >100 | 104 ± 12.4 | >200 |
| 1,6-cyclitols | 9 | 561 ± 22 | 6.7 ± 0.34 | >200 | >200 |
| | 10 | 1.47 ± 1.45 | 0.2 | 14 ± 3.2 | >200 |
| | 11 | 0.034 ± 0.004 | 0.038 ± 0.002 | 0.48 ± 0.1 | >200 |
| | 12 | >100 | >100 | >200 | >200 |
| | 13 | 39.8 | 37.3 | >200 | >200 |
| | 14 | 8.15 | 2.3 | 16.9 ± 2.1 | >200 |
| | 15 | >100 | >100 | >100 | >200 |
| | 16 | >100 | >100 | >200 | >200 |
| | 17 | 47 | 112 | 45.3 ± 1.52 | >200 |
| | 18 | >100 | 2.63 | >100 | >200 |
| | 19 | >100 | >100 | >200 | >200 |
| 1,2-cyclitols | 20 | 11.4 ± 2.3 | 13 | 17.7 ± 1.28 | >200 |
| | 21 | 43.8 | >100 | 67.6 ± 14.8 | >200 |
| | 22 | 20.3 ± 3.8 | 1.08 | >200 | >200 |
| | 23 | >100 | >100 | 64.9 ± 0.77 | >200 |
| | 24 | >100 | >100 | 28.6 ± 0.21 | 200 |
| | 25 | >100 | >100 | 22.25 ± 4.12 | >200 |
| | 26 | >100 | >100 | 91.38 ± 20.6 | >200 |
| | 27 | >100 | >100 | 26.9 ± 1.3 | 100 |
| | 28 | >100 | >100 | 56.7 ± 1.38 | >200 |

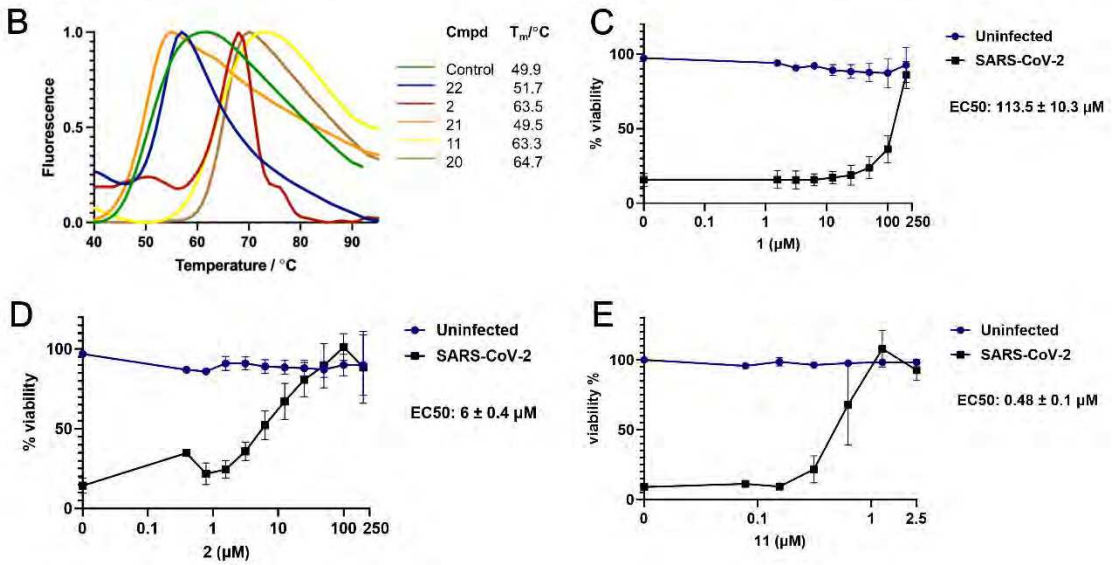


**Figure 2**: ER α-Glu II inhibitory potency correlates with reduction of SARS-CoV-2 mediated cytopathic effect in cell culture. (A) $IC_{50}$ values of compounds in *in vitro* enzyme activity assays with ER α-Glu-II and GAA, and $EC_{50}$ and $CC_{50}$ values of compounds determined by CPE reduction assays with SARS-CoV-2. (B) Thermal shift profile of preincubated ER-α-Glu II with inhibitors. (C-E) SARS-CoV-2 CPE reduction assay dose-response curves of (C) Miglustat **1**, (D) naphthyl-deoxynojirimycin **2**, and (E) cyclosulfate **11**. n=3 independent experiments. The viability of uninfected compound-treated cells was established by MTS assay

in parallel. Means ± SEM are shown. The 50% inhibitory concentration ($EC_{50}$) values were determined by non-linear regression with GraphPad Prism 6.

**1,6-*Epi*-cyclophellitol cyclosulfate reduces SARS-CoV-2 infectious progeny in cell culture**

To investigate further the results from the CPE reduction assays, the effect of the most potent glucosidase inhibitor, 1,6-*epi*-cyclophellitol cyclosulfate **11** was assessed in viral load reduction assays on infected H1299/ACE2 lung epithelial cells. Cells were pre-treated with **11** and infected with SARS-CoV-2 at an MOI of 1. At 16 hours post infection (hpi) supernatant was harvested to quantify the infectious virus titer by plaque assay and extracellular viral RNA copies by RT-qPCR. Treatment of infected H1299/ACE2 lung epithelial cells with **11** resulted in a 100-fold reduction of the infectious progeny virus titer (**Figure 3A**). The inhibitory effect reached a plateau at 1.6 μM, and higher concentrations of **11** did not lead to more inhibition of virus replication. In contrast, Miglustat **1** reduced infectious progeny production only minimally, even at a concentration as high as 100 μM. Cyclosulfate **11** only slightly reduced extracellular viral RNA copy numbers (**Figure 3B**), indicating no effect on viral RNA production. This is in line with the expected mechanism of action of the compound that involves viral (structural) protein maturation, likely resulting in reduced infectivity of progeny virus. We then calculated the specific infectivity (defined as the number of infectious particles per viral RNA copy) of treated and untreated samples for the data in **Figure 3A** and **3B** (**Figure 3C**). Treatment with compound **11** caused a decrease in specific infectivity, suggesting that the infectivity of released particles is affected. None of the treatments caused noticeable cytotoxicity in uninfected treated cells (**Figure 3B**). Similarly, treatment of infected Calu-3 lung epithelial cells with **11** reduced

infectious progeny virus titers by ~10-fold, while no reduction in extracellular viral RNA copies was observed (**Figure S3**).

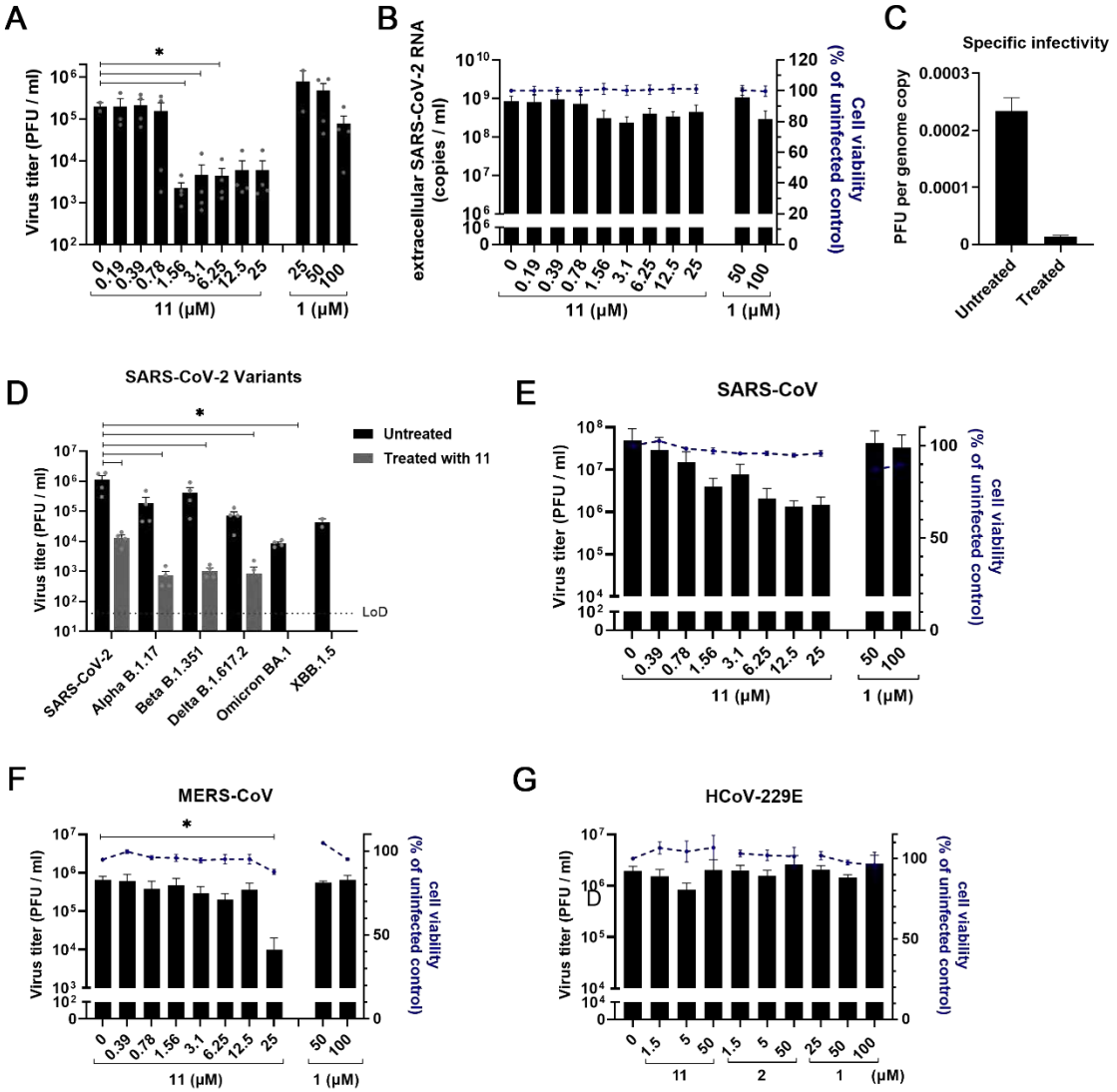


**Figure 3**: Spectrum of activity of 1,6-*Epi*-cyclophellitol cyclosulfate **11** and iminosugars **1** and **2** against various coronaviruses. (A-B) Viral load reduction assay on H1299/ACE2 cells with SARS-CoV-2 (MOI 1) in the presence of compounds **1** or **11**. (A) Infectious virus titer and (B) extracellular viral RNA copy numbers were quantified by plaque assay and RT-qPCR, respectively. Uninfected compound-treated cells were assessed by MTS assay in parallel to measure cytotoxicity of the compounds. n = 3 independent experiments. Mean ± SEM are shown. (C) The specific infectivity of treated (using 1.5 µM of compound **11**) and untreated

samples was calculated by dividing the infectious virus titer (PFU/mL) by the viral RNA copy number (copies/mL). Viral load reduction assays with (D) SARS-CoV-2 variants in H1299/ACE2 cells, (E) SARS-CoV in Vero E6 cells, (F) MERS-CoV in HuH-7 cells, and (G) HCoV-229E in H1299/ACE2 cells (all with MOI 1), and treatment with **1**, **2** or **11**. Supernatant was harvested at 16 hpi to quantify infectious progeny by plaque assay. n = 3 independent experiments. Uninfected compound-treated cells were measured by MTS assay in parallel to assess the cytotoxicity of the compounds. Mean ± SEM are shown. Statistical analysis was conducted using one-way ANOVA and significant differences are indicated by *$p$<0.05.

**1,6-*Epi*-cyclophellitol cyclosulfate inhibits infectious progeny of SARS-CoV-2 variants, SARS-CoV, and MERS-CoV, but not HCoV-229E**

To investigate the spectrum of activity against coronaviruses of 1,6-*epi*-cyclophellitol cyclosulfate **11**, its effect on the replication of SARS-CoV-2 variants alpha, beta, delta, omicron BA.1, and XBB.1.5 was tested (**Figure 3D**). As in the above experiments (**Figure 3A**), viral load reduction assays were performed, during which different cell lines were infected with the respective virus in the presence of compound, and at 16 hpi supernatant was harvested to quantify the infectious virus titer by plaque assay. Similar to the antiviral effect on the early pandemic SARS-CoV-2 isolate, treatment of H1299/ACE2 cells that were infected with other variants showed a ~100-fold reduction in infectious virus titer (**Figure 3D**). Viral load reduction assays with SARS-CoV on Vero E6 cells and MERS-CoV on HuH-7 cells showed a significant reduction of infectious progeny upon treatment with increasing concentrations of compound **11** (**Figure 3E** and **3F**), although the efficacy of the compound was slightly lower against SARS-CoV and clearly lower against MERS-CoV. Interestingly, the viral load reduction assay with HCoV-229E on H1299/ACE2 cells did not show any reduction in virus infectivity, upon treatment with either compound **11** or **2** (**Figure 3G**).

**1,6-*Epi*-cyclophellitol cyclosulfate strongly reduces α-glucosidase activity and inhibits SARS-CoV-2 in primary human bronchial epithelial cells cultured at the air-liquid interface**

We next evaluated the efficacy of 1,6-*epi*-cyclophellitol cyclosulfate **11**, in comparison to our most potent iminosugar, naphthyl-deoxynojirimycin **2**, as well as Miglustat **1** in a more advanced model of primary human bronchial epithelial cells that were cultured at the air-liquid interface (ALI-PBEC), as we described previously (50, 51). Thus, ALI-PBEC cells were infected with SARS-CoV-2 (10^5 PFU per insert; estimated MOI of ~0.1) and treated with compounds on the apical side of the cells for 2 hours. For uninfected controls, PBS was used instead of virus. The compounds were also present in the basal medium during the whole experiment until 48 hpi when samples were harvested. Treatment with 0.5 μM of compound **11** reduced the viral load significantly by up to 100-fold compared to the untreated control (**Figure 4A**). Deoxynojiriomycin derivative **2** reduced SARS-CoV-2 to similar titers, but at higher compound concentrations (10 and 100 μM), while Miglustat **1** had only a slight effect at the highest concentration measured (100 μM) (**Figure 4A**). Measurement of cell death (by LDH release in the supernatant) revealed that none of the compounds tested caused significant cytotoxicity at the highest concentrations (**Figure 4B**). We also evaluated the reduction of retaining α-glucosidases in the treated ALI-PBEC cell cultures by treatment of the cell lysate at 48 hpi with retaining α-glucosidase activity-based probe **29**, which labels GAA (isoforms at 70 and 76 kDa) and both isoforms of GANAB (~100 kDa) at pH 7 (52) (**Figure 4D**). In line with the *in vitro* enzyme activity assay results (**Figure 2A**), compound **11** was most efficient in inhibiting ER α-Glu II and

GAA at low concentrations (**Figure 4C** and **Figure S4**), suggesting that *in cellulo* ER α-Glu II inhibition potency correlated well with the efficacy to block SARS-CoV-2 replication.

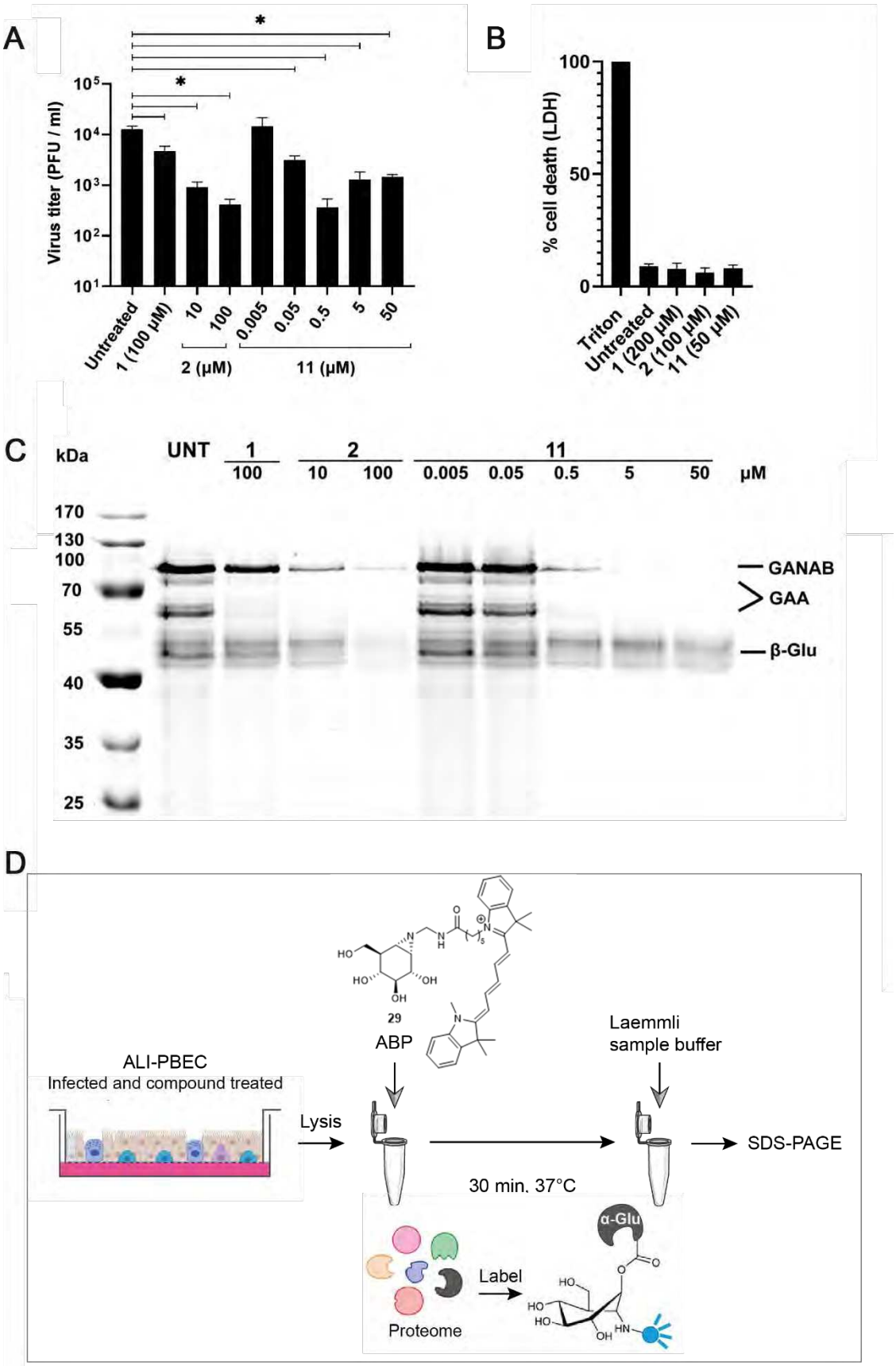
A
Virus titer (PFU / ml)
Untreated
1 (100 μM)
10
100
0.005
0.05
0.5
5
50
2 (μM)
11 (μM)
B
% cell death (LDH)
Triton
Untreated
1 (200 μM)
2 (100 μM)
11 (50 μM)
C
kDa
UNT
1
2
11
μM
170
130
100
70
55
40
35
25
GANAB
GAA
β-Glu
D
29
ABP
ALI-PBEC
Infected and compound treated
Lysis
Laemmli
sample buffer
SDS-PAGE
30 min. 37°C
α-Glu
Label
Proteome

**Figure 4**: Reduction of SARS-CoV-2 infection in primary bronchial epithelial cells is consistent with inhibition of active ER α-glucosidase II. (A) Viral load reduction assay in ALI-PBEC. Supernatant was harvested at 48 hpi to quantify infectious progeny by plaque assay. n = 3 independent experiments. Mean ± SEM are shown. Statistical analysis was conducted using one-way ANOVA and significant differences are indicated by *$p$<0.05. (B) The viability of uninfected compound-treated cells was measured by LDH release assay in parallel, to assess cytotoxicity of the compounds. Mean ± SEM are shown. (C) Following compound treatment, cells were lysed and the lysate at pH 7.0 was treated with activity-based probe (ABP) **29** to assess cellular retaining α-glucosidase activities in a competitive activity-based protein profiling experiment. A representative gel of three independent experiments (with two biological replicates/ALI-PBEC inserts each) is shown. (D) Schematic representation of ABP labelling. Part of the figure in (D) was adapted from (52), and partly generated using Servier Medical Art, provided by Servier, licensed under a Creative Commons Attribution 3.0 unported license. **Figure S4** shows the Gelcode Blue stained gel of C), which demonstrated that equal amounts of protein were loaded.

## 1,6-*Epi*-cyclophellitol cyclosulfate inhibits SARS-CoV-2 replication at a post-entry step of the viral replication cycle

We then investigated the mode of action of 1,6-*epi*-cyclophellitol cyclosulfate **11** by assessing which step in the viral replication cycle is inhibited. First, we assessed whether the compound affects the infectivity of virus particles, that is, has virucidal or neutralizing activity. Therefore, SARS-CoV-2 was incubated with a high concentration of compound **11** (50 μM) for 1 h at 37 $^{o}$C, and subsequently the infectious virus titer was quantified by plaque assay. Control treatment with 70% ethanol led to full inactivation of the virus, while compound **11** had no effect on the infectious titer (**Figure 5A**). Next, we assessed if treatment early during infection had an effect on virus replication. We infected H1299/ACE2 cells with SARS-CoV-2 at an MOI of 3 and started treatment with compound **11** at 1 hpi. At 2, 3 and 5 hpi, cells were harvested and RT-qPCR was performed to quantify

the intracellular viral genome copies. The kinetics of intracellular viral RNA accumulation were similar in untreated and compound **11** treated cells, suggesting the compound had no effect on (early) RNA replication (**Figure 5B**).

To evaluate whether compound **11** has an effect on host proteins (for instance, ACE2) involved in viral entry, we treated monolayers of H1299/ACE2 cells with compound **11** either 48 or 2 h before infection, during infection (0-1 h), or starting from 1 h post-infection (hpi). The cell monolayers were infeed with ~20 PFU of SARS-CoV-2 and after 1 h the inoculum was replaced with an overlay. In one well (Post Infection) the overlay contained compound **11**. Remdesivir, a viral RNA synthesis inhibitor, was added to the overlay of another well, as a positive control for blocking virus replication in the cell. At 3 dpi cells were fixed and stained with crystal violet. Pre-treatment of the cells with compound **11**, or treatment only during infection had no effect on the number of plaques that developed or their morphology. Only the presence of compound **11** after infection prevented the formation of plaques, similar to treatment with remdesivir (**Figure 5C and 5D**). This result suggests that the antiviral effect of **11** is not through modulating expression or functioning of host proteins (such as the ACE2 receptor) that are essential for viral attachment to, or entry into, the host cell.

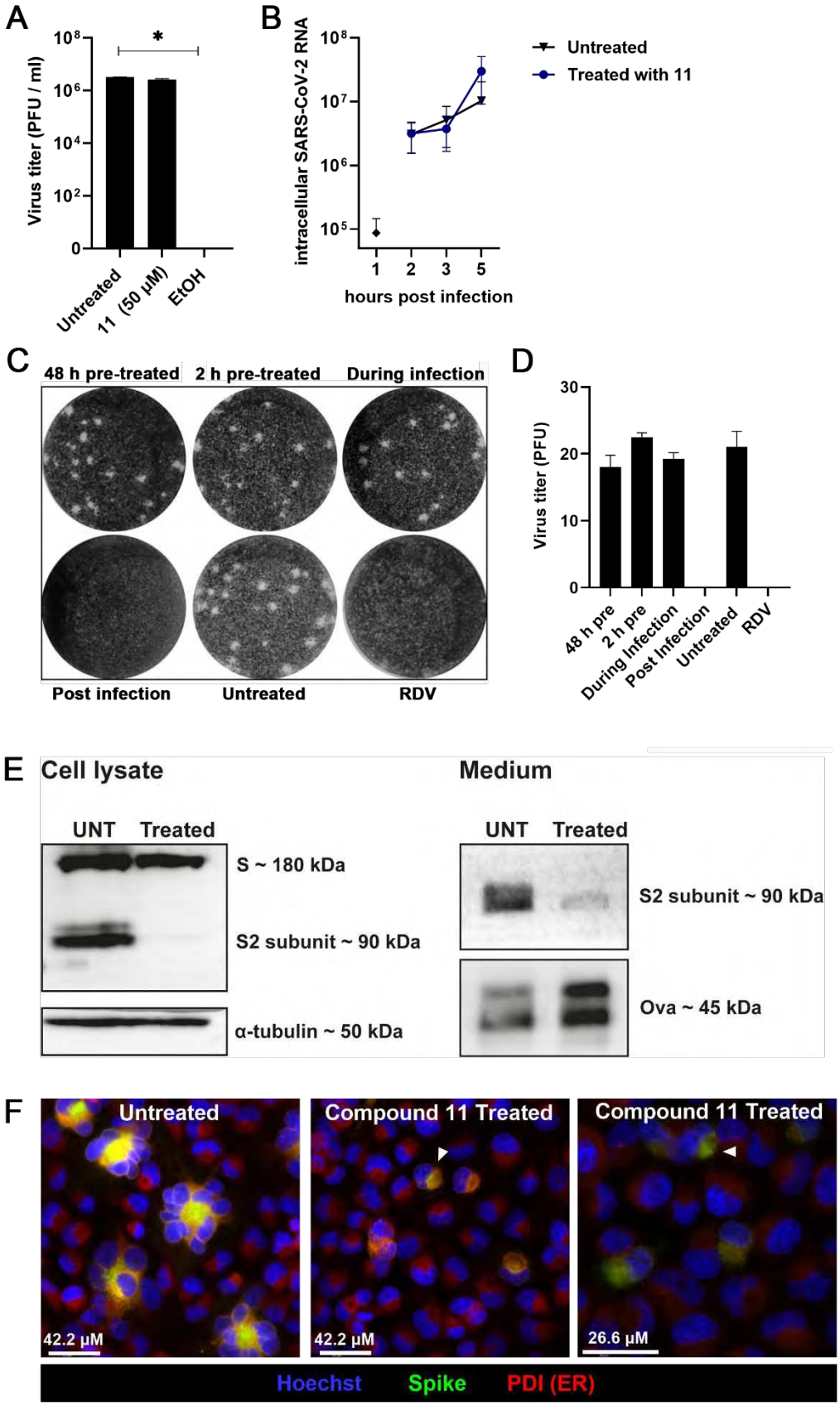
A
Virus titer (PFU / ml)
Untreated
11 (50 μM)
EtOH
B
intracellular SARS-CoV-2 RNA
hours post infection
Untreated
Treated with 11
C
48 h pre-treated
2 h pre-treated
During infection
Post infection
Untreated
RDV
D
Virus titer (PFU)
48 h pre
2 h pre
During Infection
Post Infection
Untreated
RDV
E
Cell lysate
Medium
UNT
Treated
S ~ 180 kDa
S2 subunit ~ 90 kDa
α-tubulin ~ 50 kDa
S2 subunit ~ 90 kDa
Ova ~ 45 kDa
F
Untreated
Compound 11 Treated
Compound 11 Treated
42.2 μM
42.2 μM
26.6 μM
Hoechst
Spike
PDI (ER)

**Figure 5**: 1,6-*Epi*-cyclophellitol cyclosulfate **11** inhibits SARS-CoV-2 replication and syncytium formation by reducing intracellular spike protein levels and processing. (A) Virucidal activity assay in which SARS-CoV-2 was incubated with compound **11** or 70% ethanol (as control) for 1 h at RT, and (remaining) infectious progeny was quantified by plaque assay. n = 2 independent experiments. Mean ± SEM are shown. Statistical analysis was conducted using one-way ANOVA and significant differences are indicated by *$p$<0.05. (B) H1299/ACE2 cells were infected with SARS-CoV-2 (MOI 3) and treated with **11** from 1 hpi until harvesting at the indicated time points. Intracellular viral RNA copies were quantified by RT-qPCR. n = 3 independent experiments. (C, D) Plaque reduction assay was performed with 1 h infection and incubation for 3 days until cells were fixed and stained with crystal violet. Cells were treated with 5 μM of compound **11**, either before infection (pre-treatment), during infection, or after infection (post infection) in the overlay. Treatment with RDV in the overlay was used as a control. n = 2 independent experiments. Means ± SEM are shown. (E) Western Blot analysis of viral S protein in the medium and cell lysates of untreated (UNT) or compound **11** treated (2 μM) H1299/ACE2 cells that were infected with SARS-CoV-2 (MOI 2) and analyzed at 10 hpi using an S2-specific antibody. The medium was spiked with ovalbumin (Ova) as a recovery control and was concentrated, before a sample corresponding to ~250 μL of the original medium volume was analyzed. α-tubulin was used as a loading control for cell lysates. (F) H1299/ACE2 cells were infected with SARS-CoV-2 (MOI 0.1), fixed at 10 hpi, and the viral S protein and ER marker PDI were visualized by immunofluorescence microscopy. Cells were stained with human anti-SARS-CoV-2 S protein antibody (green), mouse anti-PDI antibody for ER staining (red), and Hoechst for visualizing nuclei(blue). White arrows indicate co-localization of S with PDI. Images are representative of n = 2 independent experiments.

## 1,6-*Epi*-cyclophellitol cyclosulfate inhibits SARS-CoV-2 replication through effects on intracellular S protein maturation and infectivity of viral progeny

From the above-described experiments it became evident that treatment with 1,6-*epi*-cyclophellitol cyclosulfate **11** led to a reduction in virus infectivity, but not to a reduction in the number of viral genome copies (**Figure 3**), and that inhibition was not through an effect on the receptor or virus binding and entry, but at a post-entry step other than RNA

replication (**Figure 5A-D**). Therefore, we suspected an effect on the S protein. As shown in **Figure 4**, compound **11** effciently inhibited ER α-Glu II, which is crucial for the processing of N-glycosylated viral proteins such as S. To assess the effect of α-Glu II inhibition on S protein production/maturation, we performed viral load reduction assays on H1299/ACE2 cells. Cells were infected with SARS-CoV-2 (MOI of 2) and treated with 2 μM of compound **11** or cell culture medium. At 10 hpi medium and cell lysate were harvested to analyze S protein levels by Western blotting with an S2-specific antibody. Treatment with compound **11** led to a minor reduction in the amount of full-length S protein in the cell lysate and to the almost complete disappearance of the ~90 kDa S2 fragment, a product of proteolytic (furin) cleavage of mature S protein in the Golgi apparatus. This indicated that treatment with **11** impaired maturation of the S protein in the ER, leading to reduced trafficking to the Golgi (**Figure 5E**). The amount of (processed) S2 was also strongly reduced in the medium of compound-treated cells, suggesting the compound impaired biogenesis of particles or their S protein content (**Figure 5E**).

Next, we set out to analyze the effect of compound **11** treatment on the level and localization of the S protein in infected cells, and formation of syncytia, which are large multinucleated cells resulting from the interaction of S protein on the surface of infected cells with ACE2 receptors on neighbouring cells, which triggers cell fusion. To this end, SARS-CoV-2-infected H1299/ACE2 cells (MOI 0.1) were treated with 5 μM of compound **11** or cell culture medium as control, and at 10 hpi cells were fixed and analyzed by immunofluorescence staining for the viral S protein and the ER marker protein disulfide isomerase (**Figure 5F**). We observed a reduction in the amount of S protein in infected cells that were treated with compound **11** and the co-localization of S protein with the ER

marker, which suggests (partial) retention of S proteins in the ER. Treatment also led to reduced syncytium formation compared to untreated infected cells, likely due to impaired maturation, and subsequent impaired trafficking of S protein to the plasma membrane.

## Discussion

In this study we have assessed the ER α-Glu II inhibitory potency and anti-SARS-CoV-2 activity of selected members (28 compounds in total) of two classes of glycomimetics: iminosugars and cyclitol analogues, and to what extent these two effects correlate. Deoxynojirimycin-type iminosugars as competitive inhibitors have been studied for almost four decades as candidate-antivirals for pathogenic viruses that rely on ER-protein quality control, and in recent years have also been explored as anti-SARS-CoV-2 agents (14, 15, 18, 24, 53, 54). In contrast, cyclophellitol-type mechanism-based inhibitors have not been considered for this purpose. The results described here support the hypothesis that mechanism-based inactivation of ER α-Glu II may lead to effective new antiviral agents to treat infections with the numerous viruses that rely on host protein glycosylation for replication. In particular, 1,6-*epi*-cyclocyclosulfate **11**, the most potent ER α-Glu II inhibitor of the tested compounds, also blocked viral replication most effectively. Although 0.5 – 1.6 μM doses of compound 11 reduced infectious virus titers up to 2 logs in Calu3 cells and ALI-PBEC, higher concentrations did not lead to a further reduction and complete inhibition of virus replication was not observed at high doses. In ALI-PBEC the maximum antiviral effect was already reached at 0.5 μM, a concentration at which an almost full inhibition of ER α-Glu II was observed, suggesting that the remaining virus replication was not due to incomplete inhibition of this enzyme. Further investigations

revealed that the antiviral effect is not due to effects on (glycosylation or quantity of) host cell factors that play a role in virus binding and entry into the host cell, or replication of the viral genome, suggesting it does not (noticeably) target the SARS-CoV-2 non-structural proteins. The antiviral effect is on blocking N-glycosylation of the S protein, the most heavily N-glycosylated SARS-CoV-2 protein, which plays crucial roles in virus binding and entry. The absence of cleaved S2 fragment in compound treated cells, indicates that impairing processing of S protein at the ER led to reduced trafficking of S to the Golgi and prevention of (furin) cleavage of the S1/S2 site, ultimately leading to less mature S protein for incorporation into infectious virus particles. Thus, cyclosulfate **11** acts on protein N-glycosylation/ER protein quality control, just as the N-alkyl deoxynojirimycin derivatives tested by us and others, but, in addition compound **11** is much more selective compared to the iminosugars (35). Considering the mechanistic mode of action of inverting and retaining glucosidases, compound **11** inhibits retaining α-glucosidases exclusively over inverting α-glucosidases; with in the context of this work the lysosomal retaining α-glucosidase, GAA, as the single off-target. Deoxynojirimycin-type iminosugars in contrast also block inverting α-glucosidases including ER α-Glu I. The finding that blocking ER α-Glu II alone is sufficient (at least in the assays reported here) for halting SARS-CoV-2 replication may therefore be beneficial for situations in which ER inhibiting α-Glu I has adverse effects. Iminosugars have often also other human glycoprocessing enzymes as off-target. *N*-butyldeoxynojirimycin **1** (Miglustat) is applied in the clinic for the treatment of Gaucher disease where it acts as glucosylceramide synthase inhibitor (44, 55). It also inhibits the three human retaining β-glucosidases, GBA1, GBA2, GBA3 (56). None of these enzymes play a role in SARS-CoV-2 infections, and their inhibition may lead to

adverse effects as well. Such adverse effects in contrast are not to be expected from 1,6-*epi*-cyclophellitol cyclosulfate **11**, which does not inhibit any of these enzymes (GCS, GBA1, GBA2, GBA3) as we have shown before (35). Arguably, adverse effects as elicited by **11** may be the result of inhibition of the lysosomal α-glucosidase, GAA, however this enzyme is also inhibited by the iminosugars (57). We therefore conclude that compound **11**, which in contrast to the iminosugars is non-basic, thus not charged at physiological conditions, may be a good starting point for the development of new antiviral agents for the treatment of infections by SARS-CoV-2 and other (emerging) viruses that require ER-protein quality control for replication.

# Methods

## Compounds and cell lines

Inhibitors were synthesized at the department of bio-organic synthesis at the Leiden Institute of Chemistry. The synthesis of the cyclitol and iminosugar inhibitors **9–11, 17, 18–22, 25, 26, and 1–8** have been published previously (35, 41-43, 45, 47). The synthesis of methylated sulfates **12–16** and alkyl aziridines **23**, **24**, **27** and **28** can be found in the supporting information (**Scheme S1 – S5**). Lyophilized compounds were diluted in DMSO prior to use. Remdesivir, which was used as compound control in different assays, was purchased from Sigma-Aldrich and dissolved in DMSO. UV-4 (SP187) was purchased from MedChemExpress and dissolved in DMSO.

Vero E6 cells and HuH-7 cells were cultured as previously described (58). Human lung cell line H1299/ACE2 is described elsewhere (59). These cells were cultured in Dulbecco's modified Eagle's medium with 4.5 g/L glucose with L-glutamine (DMEM; Lonza, Basel,

Switzerland) supplemented with 10% fetal calf serum (FCS) (CapriCorn Scientific, Ebsdorfergrund, Germany), 100 U/mL of Penicillin/Streptomycin (P/S) (Sigma-Aldrich, St. Louis, MO, USA), and 1200 µg/mL G418 for selection (InvivoGen, San Diego, CA, USA). Infections of Vero E6 cells, HuH-7 cells, and H1299/ACE2 cells were performed in Eagle's minimal essential medium with 25 mM HEPES (EMEM; Lonza) supplemented with 2% FCS, 2 mM L-glutamine (Sigma-Aldrich), and 100 U/mL of P/S. Primary human bronchial epithelial cells (PBEC) were isolated and cultured as previously described (60). All cell cultures were maintained at 37 °C in an atmosphere of 5% CO2.

**Virus stocks**

All experiments with infectious SARS-CoV, SARS-CoV-2, or MERS-CoV were performed at the LUMC biosafety level 3 facilities. The clinical isolate SARS-CoV-2/Leiden-0008 (isolated at LUMC during the first wave of the Corona pandemic in March 2020 (GenBank: MT705206.1) was used for H1299/ACE2 and ALI-PBEC infections. This virus stock was not adapted to Vero E6 cells with regard to the spike S1/S2 cleavage site (confirmed by NGS). For CPE assays in Vero E6 cells SARS-CoV-2/Leiden0002 was used (GenBank: MT510999.1). SARS-CoV-2 variant B.1.1.7 (Alpha), variant B.1.351 (Beta), and variant B.1.617 (Delta) were obtained from the University of Leuven. SARS-CoV-2 variant BA.1 (Omicron) was obtained from RIVM (strain hCoV-19/Netherlands/NH-RIVM-72291/2021, lineage B.1.1.529, GenBank: OR427989.1) and variant XBB.1.5 was isolated from a patient sample at LUMC. SARS-CoV-2/Leiden-0008 (Passage 2), SARS-CoV-2/Leiden0002 and SARS-CoV isolate Frankfurt 1 (61) (Passage 4) were grown on Vero E6 cells. Alpha (Passage 4), Beta (Passage 4), Delta (Passage 4), Omicron BA.1 and XBB.1.5 (P3) variants were grown on Calu-3 cells. MERS-CoV (N3/Jordan) (GenBank:

KJ614529.1) (Passage 3) and HCoV-229E were grown on HuH-7 cells. Virus titers were determined by plaque assay on Vero E6 cells, and for MERS-CoV and HCoV-229E on HuH-7 cells, as described before (62).

***In vitro* GAA and GANAB enzyme activity assay**

Inhibition of the enzymes GAA and GANAB by the compounds was tested *in vitro* as described previously (35). Briefly, enzymes were preincubated with a range of inhibitor concentrations for 30 min at 37°C. The residual activity of the enzymes was then measured by adding the 4-MU–Glc substrate mixture at their corresponding optimal pH. Reactions were quenched with 1 M NaOH–glycine (pH 10.3) upon completion, and 4-MU fluorescence was measured with an LS55 fluorescence spectrophotometer (PerkinElmer) (λEX 366 nm; λEM 445 nm). IC50 values reported are the mean values from three technical replicates.

**Cytopathic Effect (CPE) reduction assay**

CPE reduction assays were performed as previously described (58). Briefly, Vero E6 cells were seeded in 96-well plates at a density of $5*10^3$ cells per well. The next day, cells were infected with SARS-CoV-2/Leiden0002 in the presence of 2-fold serial dilutions of compound. 4 days post infection the CellTiter 96 aqueous nonradioactive cell proliferation kit (Promega) was used to measure the cell viability of infected (protection) and non-infected cells (assessment of cytotoxicity). $EC_{50}$ values reported are the mean values from three independent experiments and were calculated using GraphPad Prism 6.

**Expression of Mmα-Glu-II**

The two subunits of *M. musculus* α-glucosidase II ganab and prkcsh were subcloned into separate vectors (pOPING and pOPINGS for ganab and prkcsh respectively) and codon

optimized for mammalian expression by Genscript. Each vector was transformed into DH5α (Thermofisher) cells by heat shock. Cultures of each subunit were grown at 37 °C in LB, and the amplified DNA was purified using the PureLink™ HiPure plasmid filter Maxiprep kit (Invitrogen) obtaining 750 μg of DNA for both constructs. The isolated DNA was co-transfected into a 600 mL suspension of 293-F cells following the Freestyle 293 Expression system protocol (ThermoFisher) and harvested after 4 days at 37°C, 8% $CO_2$, at 135 rpm.

**Purification of ER α-Glu-II**

Cells were pelleted at 200 *g*, for 20 minutes at 4 °C and the clarified media was then further centrifuged for 20 minutes, at 5000 *g* at 4 °C. The clarified media was loaded onto a pre-equilibrated 5 mL HisTrap excel column (Cytiva) with binding buffer (1x PBS, 20 mM imidazole, 5% glycerol w/v) and eluted using a buffer gradient 0-100% of elution buffer (1x PBS, 500 mM imidazole, 5% glycerol w/v) over 20 CVs. Fractions containing *Mm*α-Glu-II were concentrated and loaded onto size exclusion S200 column (Cytiva), which was pre-equilibrated with HEPES buffer (20 mM HEPES pH 7.5 and 150 mM NaCl). The *Mm*α-Glu-II containing fractions were pooled and a trypsinolysis was performed using sequencing grade modified trypsin (Promega), supplemented with 2 mM $CaCl_2$ for 4 hours at a ratio of 1:100 (trypsin: *Mm*α-Glu-II). The size exclusion was repeated and the resulting *Mm*α-Glu-II was pooled and concentrated to 8 mg/mL.

**Thermal shift assays**

Triplicate reactions of 10 μM *Mm*α-Glu-II unliganded control and 10 μM *Mm*α-Glu-II with 50 μM inhibitor were prepared to a final volume of 30 μL with buffer (20 mM HEPES pH 7.5 and 150 mM NaCl). Before the assay, 20x SYPRO orange dye was added to each

reaction mixture. The assay was performed using the Stratagene Mx3005P qPCR machine where the SYPRO orange dye was excited at $\lambda_{ex}$ 517 nm and monitored at 585 nm with 2 °C $min^{-1}$ increases from 25 °C – 95 °C. Readings were averaged to produce a thermal stability curve with fluorescence plotted against temperature and the $T_m$ estimated from the midpoint.

**Viral load reduction assays**

For SARS-CoV-2 (variants) and HCoV-229E infections, H1299/ACE2 cells were seeded in 96-well plates at a density of $10^4$ cells per well and the next day infected at MOI 1. Infections with SARS-CoV-2 were incubated at 37 °C, and infections with HCoV-229E at 33 °C. For SARS-CoV or MERS-CoV infections (MOI 1), Vero E6 or HuH-7 cells were seeded in 96-well plates at a density of $2*10^4$ cells per well. Cells were incubated at 37 °C. After removal of the inoculum at 1 hpi, cells were washed three times with warm PBS or medium after which they were incubated in infection medium (EMEM). Supernatant samples were harvested at 16 hpi and infectious virus titers were determined by plaque assay, and viral RNA copy numbers by RT-qPCR. In parallel, the cytotoxicity of compound treatment was measured on uninfected cells by the CellTiter 96 aqueous nonradioactive cell proliferation kit.

**Immunofluorescence staining**

For immunofluorescence imaging of viral spike protein H1299/ACE2 cells were seeded onto glass cover slips in 24-well plates at a density of $1.6*10^5$ cells per well. Thenext day they were infected with SARS-CoV-2/Leiden0008 (MOI 0.1) in Opti-MEM reduced serum medium (Thermo Fisher Scientific). At 16 hpi, cells were fixed with 3% warm paraformaldehyde. Immunofluorescent staining of viral spike protein was done using

human anti-spike antibody P52 (gift from King's college) and goat-α-human IgG Alexa 488 antibody (Thermo Fisher Scientific). Staining of endoplasmic reticulum was done using mouse anti-PDI antibody (Fuller)(63), and donkey-α-mouse Cy3 antibody (Jackson).

**Western Blot**

For western blot analysis, H1299/ACE2 cells were seeded in 6-well plates at a density of $6.5*10^5$ cells per well and the next day infected with SARS-CoV-2/Leiden0008 at an MOI of 2. At 10 hpi supernatant was harvested and 4000 µL medium was spiked with ovalbumin (internal recovery control), and concentrated to 150 µL using Amicon Ultra-0.5 centrifugal filter units (Merck), according to the manufacturer's instruction. An equal amount of Laemmli buffer was added and samples were heated at 95 °C for 5 min. Samples were analyzed by SDS-PAGE (10% gel, 30 min at 90 V, then 50 min at 120 V) and subsequently blotted for 30 min in a semi-dry blotting system (Bio-Rad). The membrane was blocked with 1% casein in PBST for 1 h at RT, before incubation with primary antibodies overnight at 4 °C. Spike proteins were detected using SARS/SARS-CoV-2 spike protein S2-specific mAb 1A9 (Invitrogen) as primary antibody . The loading control tubulin was detected with mouse-anti-α-tubulin antibody B-5-1-2 (abcam) and spiked ovalbumin was detected with mouse ovalbumin mAb 1D3D5 (ThermoFischer). The next day the membrane was washed three times for 5 min with PBST, and then incubated in 0.5% casein in PBST with a secondary goat-α-mouse-HRP antibody (P0447, Dako) for 1 h at RT. After washing again three times, the membrane was incubated in Clarity Western ECL Substrate (Bio-Rad) for 2 minutes and imaged with the Uvitec Alliance Q9 advanced imager.

**RNA isolation and RT-qPCR**

RNA was isolated by magnetic bead isolation, as described in (51). Equine arteritis virus (EAV) in AVL lysis buffer (Qiagen) was spiked into the isolation reagent as an internal control for extracellular RNA samples. RT-qPCR was performed using TaqMan Fast Virus 1-step master mix (Thermo Fisher Scientific) and as previously described (64). The cellular reference gene PGK1 served as a control for intracellular RNA. Primers and probes for EAV and PGK1 and the normalization procedure were described before (62). Primers and probes for SARS-CoV-2, as well as a standard curve, were used as described previously (64, 65).

**Plaque Assay**

To quantify infectious virus titers, plaque assays were done on Vero E6 cells (SARS-CoV-2 and variants, SARS-CoV), H1299/ACE2 (HCoV-229E) or HuH-7 (MERS-CoV). For SARS-CoV-2 and variants, $2x10^4$ cells/well were seeded in a 96-well plate, and serial dilutions of samples were inoculated for 1 h at 37 °C on a rocking platform. Inoculums were removed and 100 μL of methylcellulose overlay was added. Cells were incubated for 4 days until fixation and crystal violet staining. Alternatively, plaque assays for SARS-CoV-2 (variants) were done in 6-well plates, with avicel overlay and 3 days incubation. HCoV-229E samples were quantified in 12-well plates, using avicel overlay and incubating for 4 days. MERS-CoV samples were quantified in 12-well plates with avicel overlay or 96-well plates with methylcellulose overlay for 3 days.

**Infection of ALI-PBEC and activity-based probe labelling**

ALI-PBEC were pre-treated with compound in the basal medium for 3 hours. Cells were infected with 100 000 PFU of SARS-CoV-2/Leiden0008 per insert (estimated MOI of 0.1) with compounds present in the inoculum. After 2 hours at 37 °C on a rocking platform, the

inoculum was removed and cells were washed three times with warm PBS. Compounds stayed present in the basal medium until 48 h post infection. At 48 hpi the viral load was determined by plaque assay on a 200 µL apical wash (PBS incubated on the apical side of the inserts for 10 min at 37 °C). For assessing cytotoxicity with the CyQuant LDH cytotoxicity assay (Thermo Fisher Scientific), 10 µL of apical wash was diluted 5x with 40 µL PBS. 25 µL of this dilution was added to 25 µL assay reagent and incubated for 30 min at RT in the dark. The plate was fixed and measured at a wavelength of 490 nM (Envision reader, Perkin Elmer). For the activity-based probe labelling, the inserts were washed one more time with PBS and processed as described previously (52). Briefly, cells were lysed with 60 µL of potassium phosphate buffer per insert. A fluorescently-labelled Probe (JJB383) was diluted in McIlvaine buffer (pH 7) to a 10 µM stock and incubated for 5 min on ice. For labelling of the cell lysate, 10 µL of lysate was added to 10 µL of McIlvaine buffer and 5 µL of probe. The lysate was incubated for 30 mins at 37 °C, before addition of 10 µL of Laemmli sample buffer (4x). Samples were heated at 95 $^{o}$C for 5 min and separated in a 10% SDS-PAGE gel. Fluorescence was measured at a wavelength of 625 nm (Cy5) with a Uvitec Alliance Q9 imager (BioSPX). After imaging, the gels were stained with GelCode Blue stain reagent (Thermo Fisher Scientific) and visualized using a Uvitec Essential V6 system to check for equal loading.

**Plaque reduction assay**

H1299/ACE2 cells were seeded in a 6-well plate at a density of 1.3*10^5 cells/well (20 % confluency), 96 h prior to infection. Cells were treated with 5 µM of compound **11** either 48 or 2 h before infection, or during the 1 h infection in the inoculum. The monolayers were infected with ~20 PFU of SARS-CoV-2/Leiden0008. In the post infection treatment,

the compound (or RDV) was added to the avicel overlay. Cells were incubated for 4 days at 37 °C before fixation and crystal violet staining.

**Supporting Information:**

Additional experimental details: Synthesis of the methylated sulfamidates **12–16** and the alkyl aziridines **23**, **24**, **27** and **28**; and additional results: SARS-CoV-2 Viral load reduction assay on Calu-3 lung epithelial cells, SARS-CoV Viral load reduction assay on Vero E6 cells, GelCode Blue staining of SDS-PAGE gel of activity-based protein profiling experiment, SDS-PAGE gel of activity-based protein profiling at pH 4.

**Acknowledgements**

The authors are grateful for funding from the European Research Council (ERC-2020-SyG-951231 Carbocentre, to GJD and HSO). GJD is funded by the Royal Society Ken Murray research Professorship. ZA thanks the NWO for support through the Veni grant: VI.Veni.212.173. CSB was supported by the Coordination for the Improvement of Higher Education Personnel (CAPES) (Process nr. 88881.171440/2018-01), Ministry of Education, Brazil. Figure 1 was created with BioRender.com.

## References


1. Feng T, Zhang J, Chen Z, Pan W, Chen Z, Yan Y, Dai J. 2022. Glycosylation of viral proteins: Implication in virus–host interaction and virulence. Virulence 13:670-683.
2. O'Keefe S, Roebuck QP, Nakagome I, Hirono S, Kato A, Nash R, High S. 2019. Characterizing the selectivity of ER α-glucosidase inhibitors. Glycobiology 29:530-542.
3. Hebert DN, Foellmer B, Helenius A. 1995. Glucose trimming and reglucosylation determine glycoprotein association with calnexin in the endoplasmic reticulum. Cell 81:425-33.
4. Kostova Z, Wolf DH. 2003. For whom the bell tolls: protein quality control of the endoplasmic reticulum and the ubiquitin–proteasome connection. 22:2309-2317.
5. Gruters RA, Neefjes JJ, Tersmette M, de Goede RE, Tulp A, Huisman HG, Miedema F, Ploegh HL. 1987. Interference with HIV-induced syncytium formation and viral infectivity by inhibitors of trimming glucosidase. Nature 330:74-7.
6. Fuhrmann U, Bause E, Ploegh H. 1985. Inhibitors of oligosaccharide processing. Biochimica et Biophysica Acta (BBA) - Gene Structure and Expression 825:95-110.
7. Chang J, Block TM, Guo J-T. 2013. Antiviral therapies targeting host ER alpha-glucosidases: Current status and future directions. Antiviral Research 99:251-260.
8. Koshland Jr. DE. 1953. Stereochemistry and the mechanism of enzymatic reactions 28:416-436.
9. Koshland DE. 1958. Application of a Theory of Enzyme Specificity to Protein Synthesis. Proc Natl Acad Sci U S A 44:98-104.
10. Walker BD, Kowalski M, Goh WC, Kozarsky K, Krieger M, Rosen C, Rohrschneider L, Haseltine WA, Sodroski J. 1987. Inhibition of human immunodeficiency virus syncytium formation and virus replication by castanospermine. Proc Natl Acad Sci U S A 84:8120-4.
11. Fleet GW, Karpas A, Dwek RA, Fellows LE, Tyms AS, Petursson S, Namgoong SK, Ramsden NG, Smith PW, Son JC, et al. 1988. Inhibition of HIV replication by amino-sugar derivatives. FEBS Lett 237:128-32.
12. Montagnier L, Clavel F, Krust B, Chamaret S, Rey F, Barré-Sinoussi F, Chermann JC. 1985. Identification and antigenicity of the major envelope glycoprotein of lymphadenopathy-associated virus. Virology 144:283-9.
13. Warfield KL, Barnard DL, Enterlein SG, Smee DF, Khaliq M, Sampath A, Callahan MV, Ramstedt U, Day CW. 2016. The Iminosugar UV-4 is a Broad Inhibitor of Influenza A and B Viruses ex Vivo and in Mice. Viruses 8:71.
14. Stavale EJ, Vu H, Sampath A, Ramstedt U, Warfield KL. 2015. In vivo therapeutic protection against influenza A (H1N1) oseltamivir-sensitive and resistant viruses by the iminosugar UV-4. PLoS One 10:e0121662.
15. Warfield KL, Alonzi DS, Hill JC, Caputo AT, Roversi P, Kiappes JL, Sheets N, Duchars M, Dwek RA, Biggins J, Barnard D, Shresta S, Treston AM, Zitzmann N. 2020. Targeting Endoplasmic Reticulum α-Glucosidase I with a Single-Dose

Iminosugar Treatment Protects against Lethal Influenza and Dengue Virus Infections. J Med Chem 63:4205-4214.

16. Fukushi M, Yoshinaka Y, Matsuoka Y, Hatakeyama S, Ishizaka Y, Kirikae T, Sasazuki T, Miyoshi-Akiyama T. 2012. Monitoring of S Protein Maturation in the Endoplasmic Reticulum by Calnexin Is Important for the Infectivity of Severe Acute Respiratory Syndrome Coronavirus. 86:11745-11753.

17. Chang J, Warren TK, Zhao X, Gill T, Guo F, Wang L, Comunale MA, Du Y, Alonzi DS, Yu W, Ye H, Liu F, Guo J-T, Mehta A, Cuconati A, Butters TD, Bavari S, Xu X, Block TM. 2013. Small molecule inhibitors of ER α-glucosidases are active against multiple hemorrhagic fever viruses. Antiviral Research 98:432-440.

18. Perry ST, Buck MD, Plummer EM, Penmasta RA, Batra H, Stavale EJ, Warfield KL, Dwek RA, Butters TD, Alonzi DS, Lada SM, King K, Klose B, Ramstedt U, Shresta S. 2013. An iminosugar with potent inhibition of dengue virus infection in vivo. Antiviral Res 98:35-43.

19. Sadat MA, Moir S, Chun T-W, Lusso P, Kaplan G, Wolfe L, Memoli MJ, He M, Vega H, Kim LJY, Huang Y, Hussein N, Nievas E, Mitchell R, Garofalo M, Louie A, Ireland DC, Grunes C, Cimbro R, Patel V, Holzapfel G, Salahuddin D, Bristol T, Adams D, Marciano BE, Hegde M, Li Y, Calvo KR, Stoddard J, Justement JS, Jacques J, Long Priel DA, Murray D, Sun P, Kuhns DB, Boerkoel CF, Chiorini JA, Di Pasquale G, Verthelyi D, Rosenzweig SD. 2014. Glycosylation, Hypogammaglobulinemia, and Resistance to Viral Infections. 370:1615-1625.

20. Sung C, Wei Y, Watanabe S, Lee HS, Khoo YM, Fan L, Rathore AP, Chan KW, Choy MM, Kamaraj US, Sessions OM, Aw P, de Sessions PF, Lee B, Connolly JE, Hibberd ML, Vijaykrishna D, Wijaya L, Ooi EE, Low JG, Vasudevan SG. 2016. Extended Evaluation of Virological, Immunological and Pharmacokinetic Endpoints of CELADEN: A Randomized, Placebo-Controlled Trial of Celgosivir in Dengue Fever Patients. PLoS Negl Trop Dis 10:e0004851.

21. Durantel D. 2009. Celgosivir, an alpha-glucosidase I inhibitor for the potential treatment of HCV infection. Curr Opin Investig Drugs 10:860-70.

22. Clarke EC, Nofchissey RA, Ye C, Bradfute SB. 2021. The iminosugars celgosivir, castanospermine and UV-4 inhibit SARS-CoV-2 replication. Glycobiology 31:378-384.

23. Karade SS, Hill ML, Kiappes JL, Manne R, Aakula B, Zitzmann N, Warfield KL, Treston AM, Mariuzza RA. 2021. N-Substituted Valiolamine Derivatives as Potent Inhibitors of Endoplasmic Reticulum α-Glucosidases I and II with Antiviral Activity. Journal of Medicinal Chemistry doi:
.

24. Ferjancic Z, Bihelovic F, Vulovic B, Matovic R, Trmcic M, Jankovic A, Pavlovic M, Djurkovic F, Prodanovic R, Djurdjevic Djelmas A, Kalicanin N, Zlatovic M, Sladic D, Vallet T, Vignuzzi M, Saicic RN. 2024. Development of iminosugar-based glycosidase inhibitors as drug candidates for SARS-CoV-2 virus via molecular modelling and in vitro studies. J Enzyme Inhib Med Chem 39:2289007.

25. Gong Y, Qin S, Dai L, Tian Z. 2021. The glycosylation in SARS-CoV-2 and its receptor ACE2. Signal Transduction and Targeted Therapy 6:396.

26. Grant OC, Montgomery D, Ito K, Woods RJ. 2020. Analysis of the SARS-CoV-2 spike protein glycan shield reveals implications for immune recognition. Sci Rep 10:14991.
27. Jackson CB, Farzan M, Chen B, Choe H. 2022. Mechanisms of SARS-CoV-2 entry into cells. Nature Reviews Molecular Cell Biology 23:3-20.
28. Bouwman KM, Tomris I, Turner HL, van der Woude R, Shamorkina TM, Bosman GP, Rockx B, Herfst S, Snijder J, Haagmans BL, Ward AB, Boons G-J, de Vries RP. 2021. Multimerization- and glycosylation-dependent receptor binding of SARS-CoV-2 spike proteins. PLOS Pathogens 17:e1009282.
29. Henderson R, Edwards RJ, Mansouri K, Janowska K, Stalls V, Kopp M, Haynes BF, Acharya P. 2020. Glycans on the SARS-CoV-2 Spike Control the Receptor Binding Domain Conformation. bioRxiv.
30. Huang H-C, Lai Y-J, Liao C-C, Wang F-Y, Huang K-B, Lee IJ, Chou W-C, Wang S-H, Wang L-H, Hsu J-M, Sun C-P, Kuo C-T, Wang J, Hsiao T-C, Yang P-J, Lee T-A, Huang W, Li F-A, Shen C-Y, Lin Y-L, Tao M-H, Li C-W. 2021. Targeting conserved N-glycosylation blocks SARS-CoV-2 variant infection in vitro. eBioMedicine 74:103712.
31. Casalino L, Gaieb Z, Goldsmith JA, Hjorth CK, Dommer AC, Harbison AM, Fogarty CA, Barros EP, Taylor BC, McLellan JS, Fadda E, Amaro RE. 2020. Beyond Shielding: The Roles of Glycans in the SARS-CoV-2 Spike Protein. ACS Cent Sci 6:1722-1734.
32. Casas-Sanchez A, Romero-Ramirez A, Hargreaves E, Ellis CC, Grajeda BI, Estevao IL, Patterson EI, Hughes GL, Almeida IC, Zech T, Acosta-Serrano Á. 2022. Inhibition of Protein N-Glycosylation Blocks SARS-CoV-2 Infection. mBio 13:e03718-21.
33. Watanabe S, Chan KW-K, Dow G, Ooi EE, Low JG, Vasudevan SG. 2016. Optimizing celgosivir therapy in mouse models of dengue virus infection of serotypes 1 and 2: The search for a window for potential therapeutic efficacy. Antiviral Research 127:10-19.
34. Roussel HM. 1996. A randomized, double-blind active-controlled, dose-ranging study of safety and efficacy of chronically administered MDL 28,574A in the treatment of HIV-infected patients. NLM identifier: NCT00002151.
35. Artola M, Wu L, Ferraz MJ, Kuo C-L, Raich L, Breen IZ, Offen WA, Codée JDC, van der Marel GA, Rovira C, Aerts JMFG, Davies GJ, Overkleeft HS. 2017. 1,6-Cyclophellitol Cyclosulfates: A New Class of Irreversible Glycosidase Inhibitor. ACS Central Science 3:784-793.
36. Schröder SP, Petracca R, Minnee H, Artola M, Aerts JMFG, Codée JDC, van der Marel GA, Overkleeft HS. 2016. A Divergent Synthesis of l-arabino- and d-xylo-Configured Cyclophellitol Epoxides and Aziridines. 2016:4787-4794.
37. Jiang J, Artola M, Beenakker TJM, Schröder SP, Petracca R, de Boer C, Aerts JMFG, van der Marel GA, Codée JDC, Overkleeft HS. 2016. The Synthesis of Cyclophellitol-Aziridine and Its Configurational and Functional Isomers. 2016:3671-3678.
38. Willems LI, Jiang J, Li K-Y, Witte MD, Kallemeijn WW, Beenakker TJN, Schröder SP, Aerts JMFG, van der Marel GA, Codée JDC, Overkleeft HS. 2014.

From Covalent Glycosidase Inhibitors to Activity-Based Glycosidase Probes. 20:10864-10872.

39. de Boer C, McGregor NGS, Peterse E, Schröder SP, Florea BI, Jiang J, Reijngoud J, Ram AFJ, van Wezel GP, van der Marel GA, Codée JDC, Overkleeft HS, Davies GJ. 2020. Glycosylated cyclophellitol-derived activity-based probes and inhibitors for cellulases. RSC Chemical Biology 1:148-155.

40. Schröder SP, van de Sande JW, Kallemeijn WW, Kuo C-L, Artola M, van Rooden EJ, Jiang J, Beenakker TJM, Florea BI, Offen WA, Davies GJ, Minnaard AJ, Aerts JMFG, Codée JDC, van der Marel GA, Overkleeft HS. 2017. Towards broad spectrum activity-based glycosidase probes: synthesis and evaluation of deoxygenated cyclophellitol aziridines. Chemical Communications 53:12528-12531.

41. Wennekes T, Meijer AJ, Groen AK, Boot RG, Groener JE, van Eijk M, Ottenhoff R, Bijl N, Ghauharali K, Song H, O'Shea TJ, Liu H, Yew N, Copeland D, van den Berg RJ, van der Marel GA, Overkleeft HS, Aerts JM. 2010. Dual-Action Lipophilic Iminosugar Improves Glycemic Control in Obese Rodents by Reduction of Visceral Glycosphingolipids and Buffering of Carbohydrate Assimilation. Journal of Medicinal Chemistry 53:689-698.

42. Ghisaidoobe A, Bikker P, de Bruijn ACJ, Godschalk FD, Rogaar E, Guijt MC, Hagens P, Halma JM, van't Hart SM, Luitjens SB, van Rixel VHS, Wijzenbroek M, Zweegers T, Donker-Koopman WE, Strijland A, Boot R, van der Marel G, Overkleeft HS, Aerts JMFG, van den Berg RJBHN. 2011. Identification of Potent and Selective Glucosylceramide Synthase Inhibitors from a Library of N-Alkylated Iminosugars. ACS Medicinal Chemistry Letters 2:119-123.

43. Ghisaidoobe AT, van den Berg RJBHN, Butt SS, Strijland A, Donker-Koopman WE, Scheij S, van den Nieuwendijk AMCH, Koomen G-J, van Loevezijn A, Leemhuis M, Wennekes T, van der Stelt M, van der Marel GA, van Boeckel CAA, Aerts JMFG, Overkleeft HS. 2014. Identification and Development of Biphenyl Substituted Iminosugars as Improved Dual Glucosylceramide Synthase/Neutral Glucosylceramidase Inhibitors. Journal of Medicinal Chemistry 57:9096-9104.

44. Ficicioglu C. 2008. Review of miglustat for clinical management in Gaucher disease type 1. Ther Clin Risk Manag 4:425-31.

45. Kok K, Kuo C-L, Katzy RE, Lelieveld LT, Wu L, Roig-Zamboni V, van der Marel GA, Codée JDC, Sulzenbacher G, Davies GJ, Overkleeft HS, Aerts JMFG, Artola M. 2022. 1,6-epi-Cyclophellitol Cyclosulfamidate Is a Bona Fide Lysosomal α-Glucosidase Stabilizer for the Treatment of Pompe Disease. Journal of the American Chemical Society 144:14819-14827.

46. Ofman TP, Heming JJA, Nin-Hill A, Küllmer F, Steneker R, Klein A, Moran E, Bennett M, Ruijgrok G, Kok K, Armstrong ZWB, Aerts JMFG, van der Marel GA, Rovira C, Davies GJ, Artola M, Codée JDC, Overkleeft HS. 2024. Conformational and Electronic Variations in 1,2- and 1,6-Cyclophellitols and Their Impact on Retaining α-Glucosidase Inhibition. submitted to Chem Eur J.

47. Lahav D, Liu B, van den Berg RJBHN, van den Nieuwendijk AMCH, Wennekes T, Ghisaidoobe AT, Breen I, Ferraz MJ, Kuo C-L, Wu L, Geurink PP, Ovaa H, van der Marel GA, van der Stelt M, Boot RG, Davies GJ, Aerts JMFG, Overkleeft

HS. 2017. A Fluorescence Polarization Activity-Based Protein Profiling Assay in the Discovery of Potent, Selective Inhibitors for Human Nonlysosomal Glucosylceramidase. Journal of the American Chemical Society 139:14192-14197.

48. Karade SS, Franco EJ, Rojas AC, Hanrahan KC, Kolesnikov A, Yu W, MacKerell AD, Jr., Hill DC, Weber DJ, Brown AN, Treston AM, Mariuzza RA. 2023. Structure-Based Design of Potent Iminosugar Inhibitors of Endoplasmic Reticulum α-Glucosidase I with Anti-SARS-CoV-2 Activity. Journal of Medicinal Chemistry 66:2744-2760.

49. Rajasekharan S, Milan Bonotto R, Nascimento Alves L, Kazungu Y, Poggianella M, Martinez-Orellana P, Skoko N, Polez S, Marcello A. 2021. Inhibitors of Protein Glycosylation Are Active against the Coronavirus Severe Acute Respiratory Syndrome Coronavirus SARS-CoV-2. Viruses 13.

50. Thaler M, Wang Y, van der Does AM, Faiz A, Ninaber DK, Ogando NS, Beckert H, Taube C, Salgado-Benvindo C, Snijder EJ, Bredenbeek PJ, Hiemstra PS, van Hemert MJ. 2023. Impact of Changes in Human Airway Epithelial Cellular Composition and Differentiation on SARS-CoV-2 Infection Biology. Journal of Innate Immunity 15:562-580.

51. Thaler M, Salgado-Benvindo C, Leijs A, Tas A, Ninaber DK, Arbiser JL, Snijder EJ, van Hemert MJ. 2023. R-Propranolol Has Broad-Spectrum Anti-Coronavirus Activity and Suppresses Factors Involved in Pathogenic Angiogenesis. Int J Mol Sci 24.

52. Jiang J, Kuo C-L, Wu L, Franke C, Kallemeijn WW, Florea BI, van Meel E, van der Marel GA, Codée JDC, Boot RG, Davies GJ, Overkleeft HS, Aerts JMFG. 2016. Detection of Active Mammalian GH31 α-Glucosidases in Health and Disease Using In-Class, Broad-Spectrum Activity-Based Probes. ACS Central Science 2:351-358.

53. Warfield KL, Plummer EM, Sayce AC, Alonzi DS, Tang W, Tyrrell BE, Hill ML, Caputo AT, Killingbeck SS, Beatty PR, Harris E, Iwaki R, Kinami K, Ide D, Kiappes JL, Kato A, Buck MD, King K, Eddy W, Khaliq M, Sampath A, Treston AM, Dwek RA, Enterlein SG, Miller JL, Zitzmann N, Ramstedt U, Shresta S. 2016. Inhibition of endoplasmic reticulum glucosidases is required for in vitro and in vivo dengue antiviral activity by the iminosugar UV-4. Antiviral Res 129:93-98.

54. Fukushi M, Yoshinaka Y, Matsuoka Y, Hatakeyama S, Ishizaka Y, Kirikae T, Sasazuki T, Miyoshi-Akiyama T. 2012. Monitoring of S protein maturation in the endoplasmic reticulum by calnexin is important for the infectivity of severe acute respiratory syndrome coronavirus. J Virol 86:11745-53.

55. Elstein D, Hollak C, Aerts JMFG, van Weely S, Maas M, Cox TM, Lachmann RH, Hrebicek M, Platt FM, Butters TD, Dwek RA, Zimran A. 2004. Sustained therapeutic effects of oral miglustat (Zavesca, N-butyldeoxynojirimycin, OGT 918) in type I Gaucher disease. 27:757-766.

56. Kiappes JL, Hill ML, Alonzi DS, Miller JL, Iwaki R, Sayce AC, Caputo AT, Kato A, Zitzmann N. 2018. ToP-DNJ, a Selective Inhibitor of Endoplasmic Reticulum α-Glucosidase II Exhibiting Antiflaviviral Activity. ACS Chem Biol 13:60-65.

57. Fiege L, Duran I, Marquardt T. 2023. Improved Enzyme Replacement Therapy with Cipaglucosidase Alfa/Miglustat in Infantile Pompe Disease. Pharmaceuticals (Basel) 16.
58. Salgado-Benvindo C, Leijs AA, Thaler M, Tas A, Arbiser JL, Snijder EJ, van Hemert MJ. 2023. Honokiol Inhibits SARS-CoV-2 Replication in Cell Culture at a Post-Entry Step. Microbiol Spectr 11:e0327322.
59. Salgado-Benvindo C, Tas A, Zevenhoven-Dobbe JC, van der Meer Y, Sidorov IA, Leijs AA, Gelderloos AT, van Kasteren PB, Snijder EJ, van Hemert MJ. 2024. Characterization of SARS-CoV-2 replication in human H1299/ACE2 cells: a versatile and practical infection model for antiviral research and beyond. submitted to Antiviral Research
60. Ninaber DK, van der Does AM, Hiemstra PS. 2023. Isolating Bronchial Epithelial Cells from Resected Lung Tissue for Biobanking and Establishing Well-Differentiated Air-Liquid Interface Cultures. J Vis Exp.
61. Drosten C, Günther S, Preiser W, Van Der Werf S, Brodt H-R, Becker S, Rabenau H, Panning M, Kolesnikova L, Fouchier RA. 2003. Identification of a novel coronavirus in patients with severe acute respiratory syndrome. New England journal of medicine 348:1967-1976.
62. Kovacikova K, Morren BM, Tas A, Albulescu IC, van Rijswijk R, Jarhad DB, Shin YS, Jang MH, Kim G, Lee HW, Jeong LS, Snijder EJ, van Hemert MJ. 2020. 6'-β-Fluoro-Homoaristeromycin and 6'-Fluoro-Homoneplanocin A Are Potent Inhibitors of Chikungunya Virus Replication through Their Direct Effect on Viral Nonstructural Protein 1. Antimicrob Agents Chemother 64.
63. Vaux D, Tooze J, Fuller S. 1990. Identification by anti-idiotype antibodies of an intracellular membrane protein that recognizes a mammalian endoplasmic reticulum retention signal. Nature 345:495-502.
64. Salgado-Benvindo C, Thaler M, Tas A, Ogando NS, Bredenbeek PJ, Ninaber DK, Wang Y, Hiemstra PS, Snijder EJ, van Hemert MJ. 2020. Suramin Inhibits SARS-CoV-2 Infection in Cell Culture by Interfering with Early Steps of the Replication Cycle. Antimicrob Agents Chemother 64.
65. Corman VM, Landt O, Kaiser M, Molenkamp R, Meijer A, Chu DK, Bleicker T, Brunink S, Schneider J, Schmidt ML, Mulders DG, Haagmans BL, van der Veer B, van den Brink S, Wijsman L, Goderski G, Romette JL, Ellis J, Zambon M, Peiris M, Goossens H, Reusken C, Koopmans MP, Drosten C. 2020. Detection of 2019 novel coronavirus (2019-nCoV) by real-time RT-PCR. Euro Surveill 25.

## Graphical Abstract

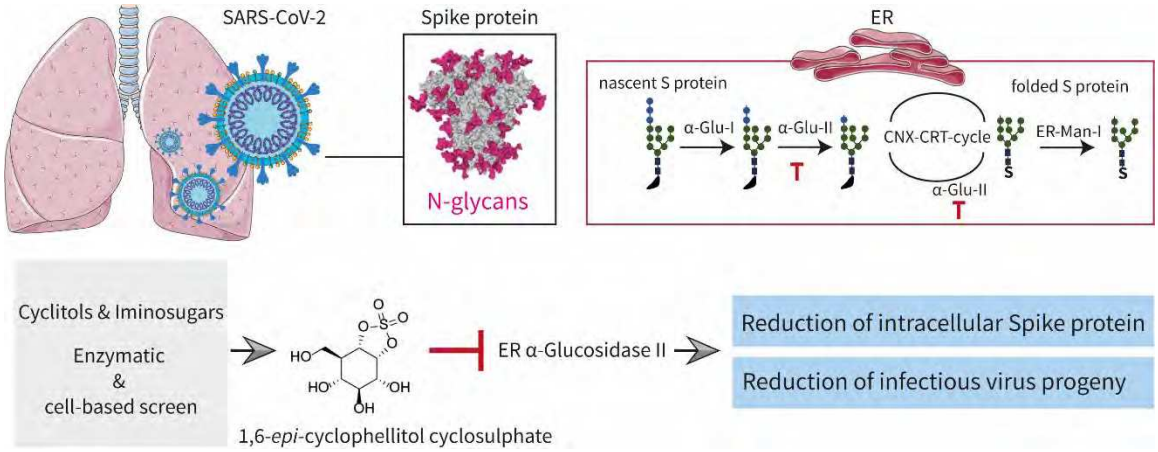


The Figure was partly generated using Servier Medical Art, provided by Servier, licensed under a Creative Commons Attribution 3.0 unported license.

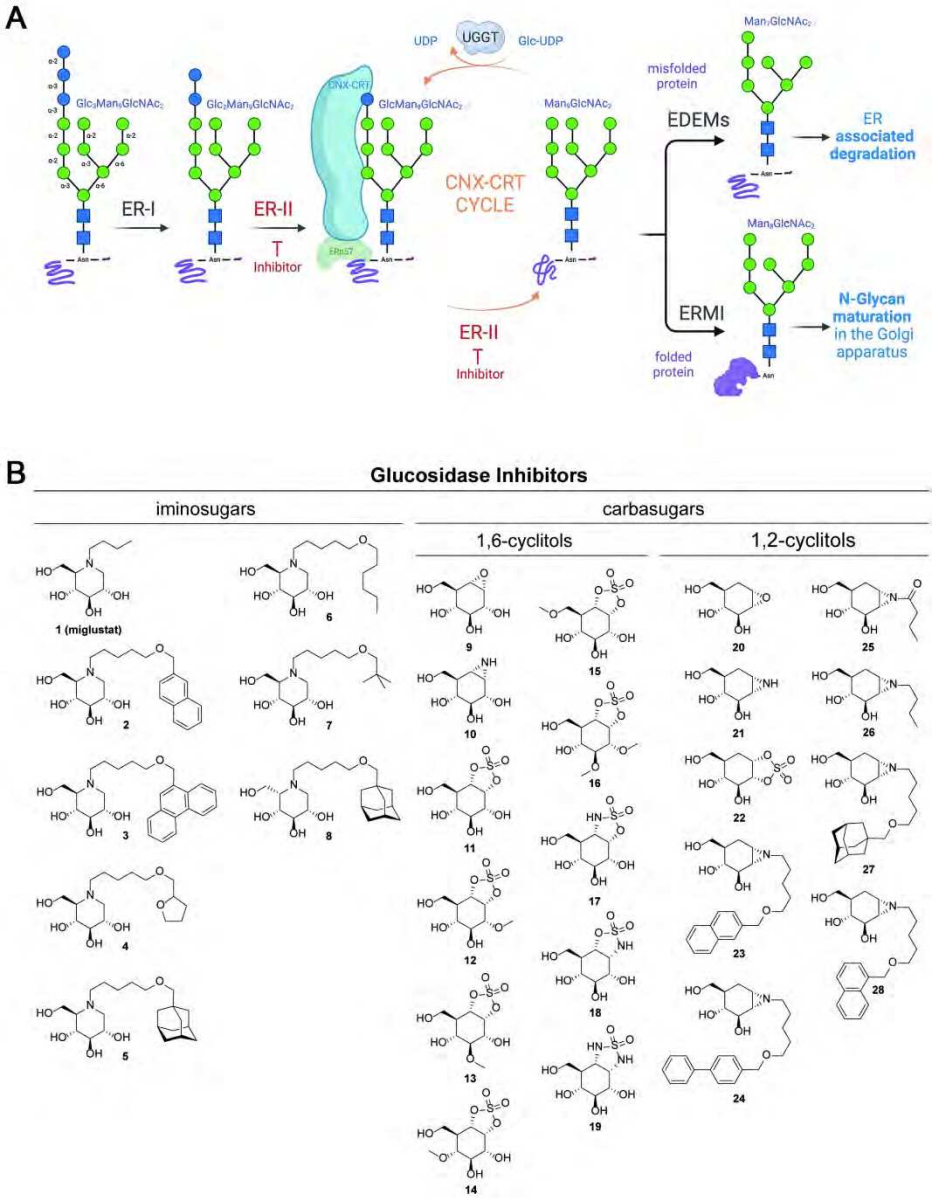


Figure 1

188x241mm (300 x 300 DPI)

A

| | Compound | Inhibitory activity against glucosidases (biochemical assay) | | Antiviral activity (CPE assay) | |
|---|---|---|---|---|---|
| | | IC50 GANAB (μM) (ER-Glu-II) | IC50 GAA (μM) | EC50 (μM) | CC50 (μM) |
| Iminosugars | 1 (Miglustat) | 200 | 6.58 ± 2.4 | 113.5 ± 10.3 | >200 |
| | 2 | 0.12 ± 0.07 | 0.19 ± 0.01 | 6 ± 0.4 | >200 |
| | 3 | 0.15 ± 0.09 | 0.034 ± 0.004 | 3.25 ± 0.42 | 50 |
| | 4 | 0.2 ± 0.05 | 0.82 ± 0.18 | 51.7 ± 3.37 | >200 |
| | 5 | 0.21 ± 0.07 | 0.64 ± 0.06 | 13.9 ± 8 | 200 |
| | 6 | 0.26 ± 0.1 | 0.47 ± 0.05 | 11.8 ± 0.8 | >200 |
| | 7 | 2.12 ± 0.38 | 2.19 ± 5.9 | 22.7 ± 4.3 | >200 |
| | 8 | 41.1 | >100 | 104 ± 12.4 | >200 |
| 1,6-cyclitols | 9 | 561 ± 22 | 6.7 ± 0.34 | >200 | >200 |
| | 10 | 1.47 ± 1.45 | 0.2 | 14 ± 3.2 | >200 |
| | 11 | 0.034 ± 0.004 | 0.038 ± 0.002 | 0.48 ± 0.1 | >200 |
| | 12 | >100 | >100 | >200 | >200 |
| | 13 | 39.8 | 37.3 | >200 | >200 |
| | 14 | 8.15 | 2.3 | 16.9 ± 2.1 | >200 |
| | 15 | >100 | >100 | >100 | >200 |
| | 16 | >100 | >100 | >200 | >200 |
| | 17 | 47 | 112 | 45.3 ± 1.52 | >200 |
| | 18 | >100 | 2.63 | >100 | >200 |
| | 19 | >100 | >100 | >200 | >200 |
| 1,2-cyclitols | 20 | 11.4 ± 2.3 | 13 | 17.7 ± 1.28 | >200 |
| | 21 | 43.8 | >100 | 67.6 ± 14.8 | >200 |
| | 22 | 20.3 ± 3.8 | 1.08 | >200 | >200 |
| | 23 | >100 | >100 | 64.9 ± 0.77 | >200 |
| | 24 | >100 | >100 | 28.6 ± 0.21 | 200 |
| | 25 | >100 | >100 | 22.25 ± 4.12 | >200 |
| | 26 | >100 | >100 | 91.38 ± 20.6 | >200 |
| | 27 | >100 | >100 | 26.9 ± 1.3 | 100 |
| | 28 | >100 | >100 | 56.7 ± 1.38 | >200 |

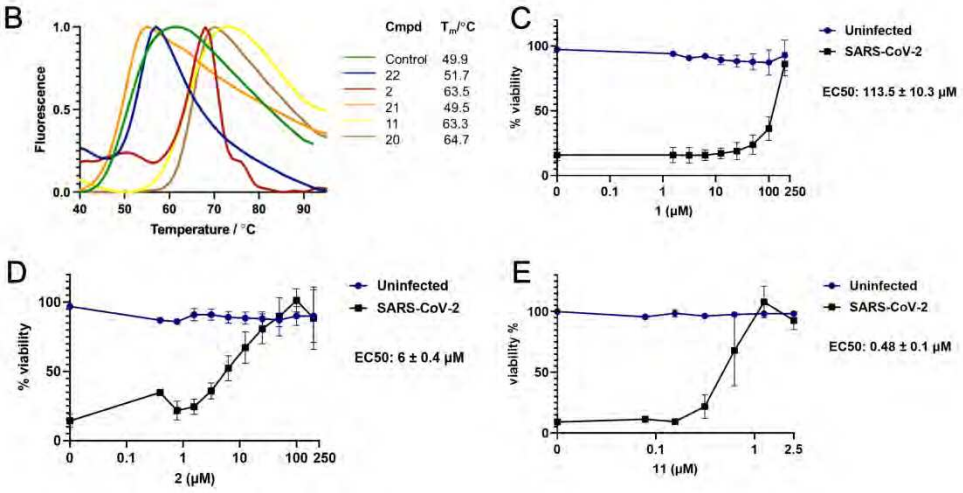


Figure 2

206x225mm (300 x 300 DPI)

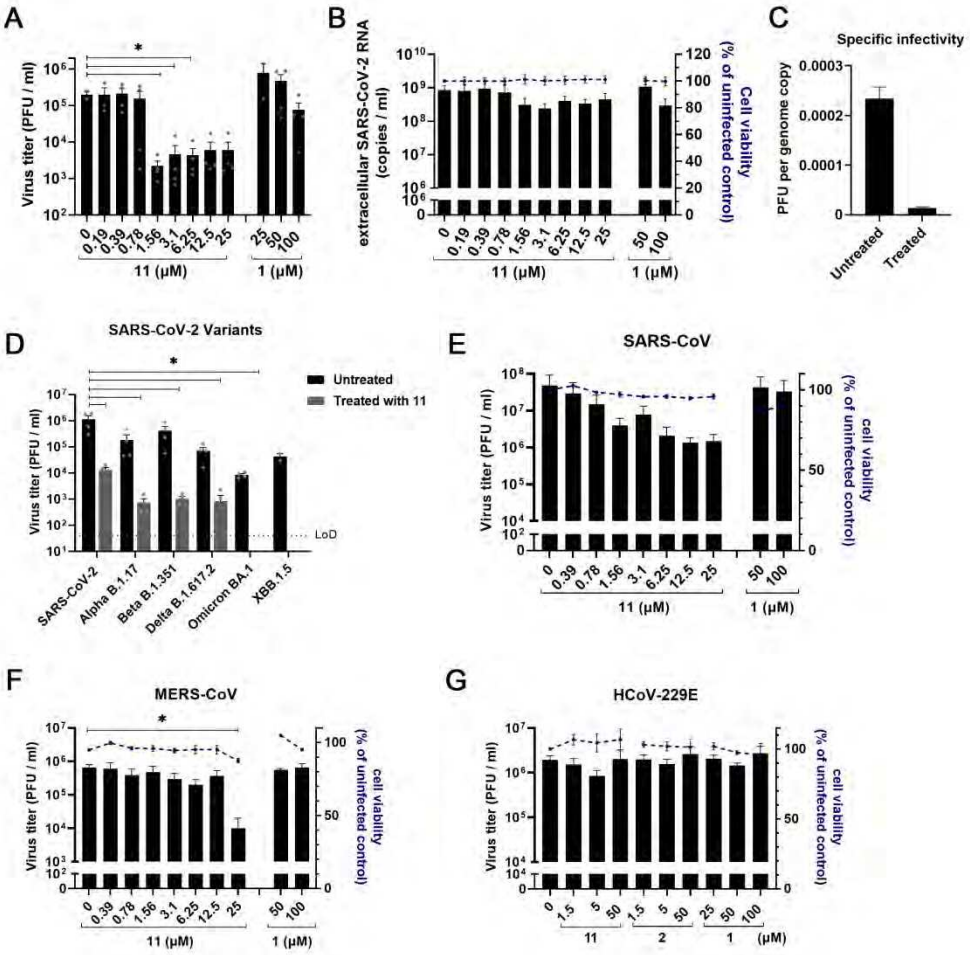


Figure 3

220x221mm (300 x 300 DPI)

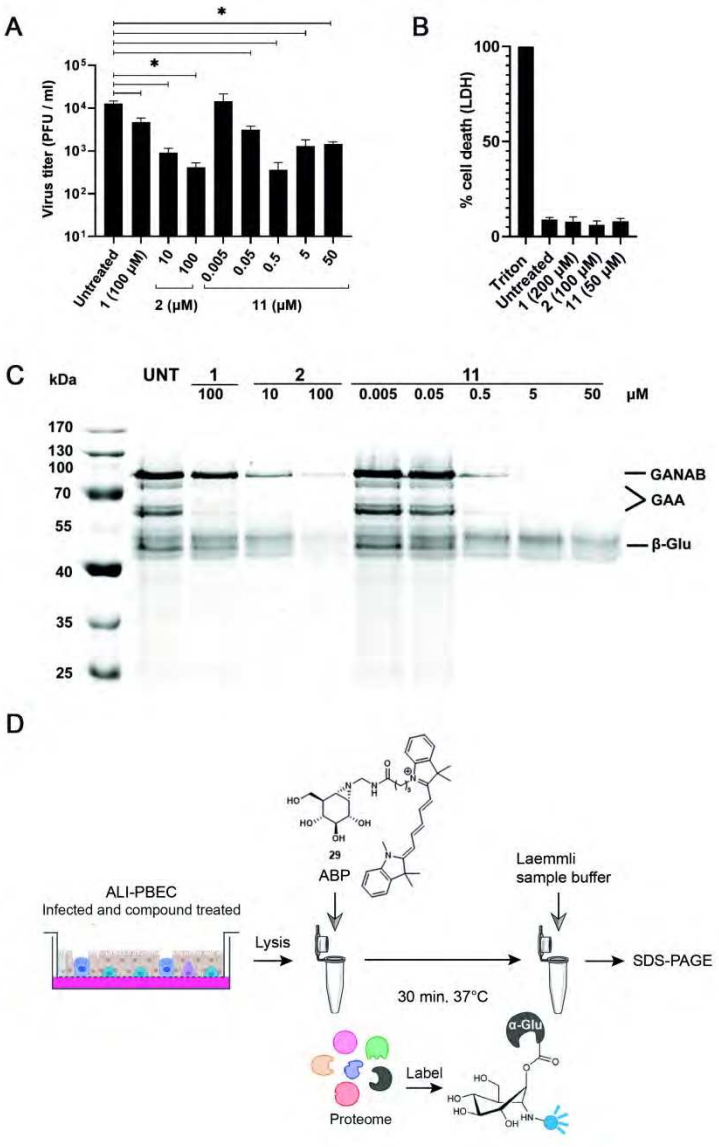


Figure 4

182x287mm (300 x 300 DPI)

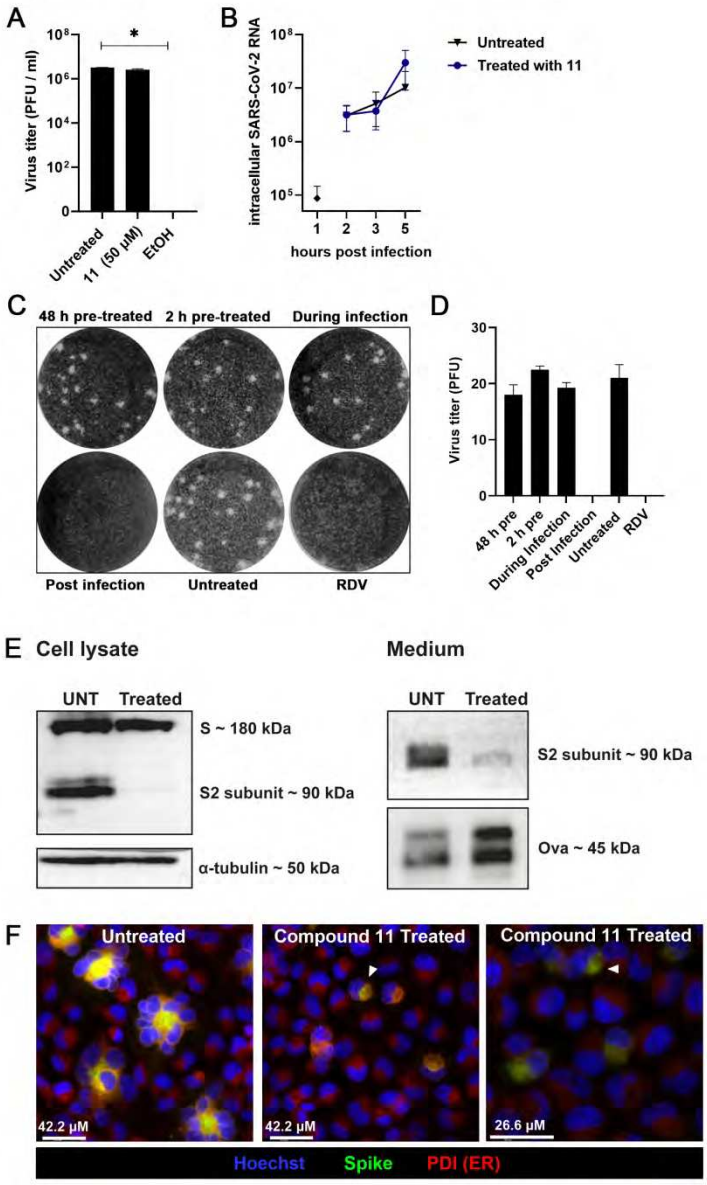


Figure 5

169x275mm (300 x 300 DPI)

# Supplementary information

## *Epi*-cyclophellitol cyclosulfate, a mechanism-based ER α-glucosidase II inhibitor, blocks replication of SARS-CoV-2 and other coronaviruses

Melissa Thaler[a], Tim P. Ofman[b], Ken Kok[b], Jurriaan J.A. Heming[b], Elisha Moran[c], Isabelle Pickles[c], Anouk A. Leijs[a], Adrianus M. C. H. van den Nieuwendijk[b], Richard J. B. H. N. van den Berg[b], Gijs Ruijgrok[b], Zach Armstrong[b], Clarisse Salgado-Benvindo[a], Dennis K. Ninaber[d], Eric J. Snijder[a], Constant A. A. van Boeckel[b], Marta Artola[b], Gideon J. Davies[c], Herman S. Overkleeft[b#], Martijn J. van Hemert[a#]

[a]Leiden University Center for Infectious Diseases (LUCID), Leiden University Medical Center, Leiden, The Netherlands.

[b]Leiden Institute of Chemistry, Leiden University, Leiden, The Netherlands.

[c]Department of Chemistry, University of York, YO10 5DD, York, United Kingdom.

[d]Department of Pulmonology, Leiden University Medical Center, Leiden, The Netherlands.

Running Head: Mechanism-based ER α-Glu-II inhibitor blocks coronavirus infection

#Address correspondence to:

Martijn J. van Hemert, m.j.van_hemert@lumc.nl or

Herman S. Overkleeft, h.s.overkleeft@chem.leidenuniv.nl

# Table of Contents



## Supplementary Figures

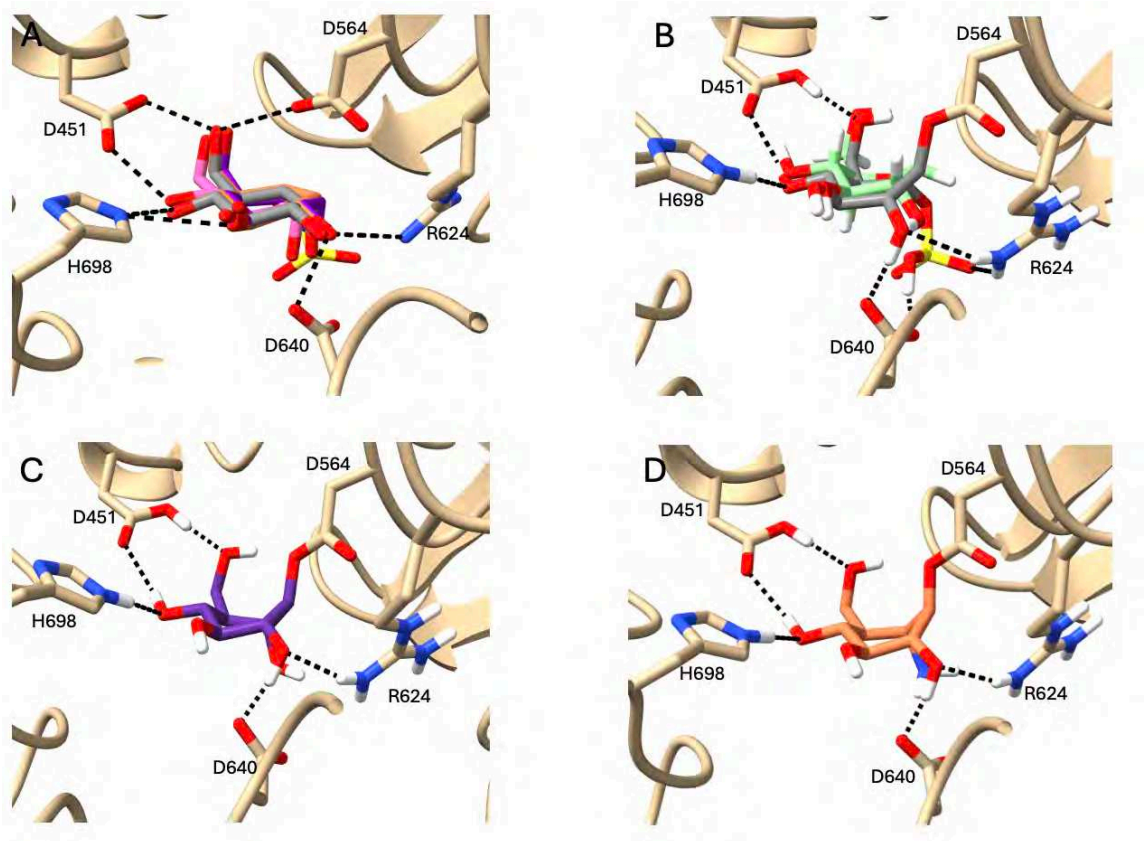


**Figure S1**: Docking of 1,6-cyclitols compounds into the α-glucosidase II active site (PDB 5H9O).
(A) Overlay of the top non-covalent dockings of compounds 10 (orange), 9 (purple) and 11 (grey) with glucose (pink PDB: 5H9O). Black lines indicating H-bond interactions with active site residues, including catalytic nucleophile D564.
(B) Top covalent docking for compound 11 (grey), the covalent bond formed between nucleophile D564 along with H-bond interactions and overlaid with covalent 5F-Glc (PDB: 5HJR, green).
(C) Top covalent docking of compound 9 covalently bound to catalytic nucleophile D564 along with H-bonds interactions (black dashes).
(D) Top covalent docking of compound 10 covalently bound to catalytic nucleophile D564 along with H-bonds interactions (black dashes).

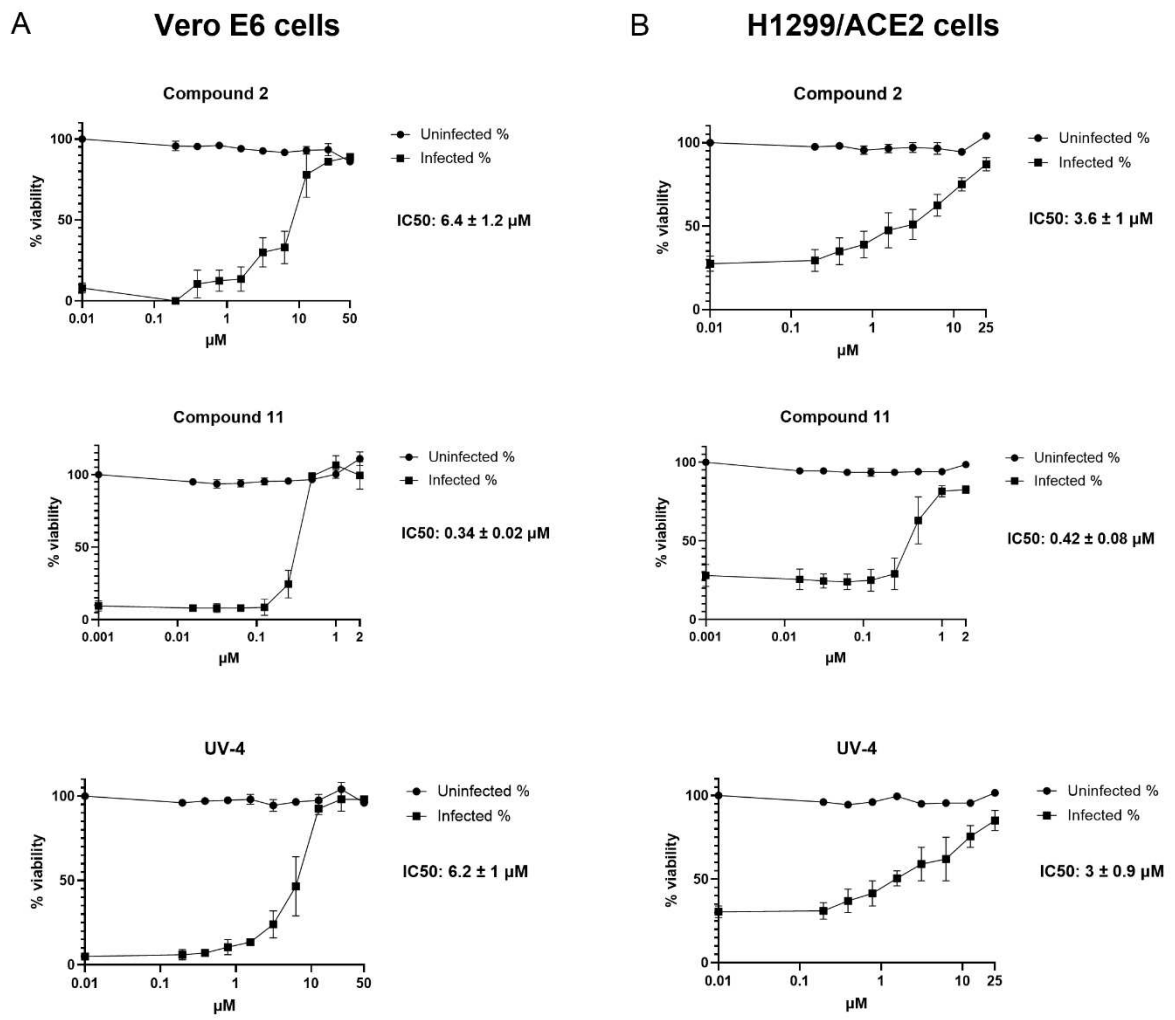


**Figure S2**: Cytopathic effect reduction assays on Vero E6 monkey kidney cells and H1299/ACE2 human lung epithelial cells. (A) SARS-CoV-2 CPE assay dose-response curves of naphthyl-deoxynojirimycin **2**, cyclosulfate **11**, and iminosugar **UV4** on (A) Vero E6 cells, and (B) H1299/ACE2 cells. n=2 independent experiments. The viability of uninfected compound-treated cells was established by MTS assay in parallel. Means ± SEM are shown. The 50% inhibitory concentration ($EC_{50}$) values were determined by non-linear regression with GraphPad Prism 6. Methods for the CPE assay on H1299/ACE2 cells can be found in this supplementary material.

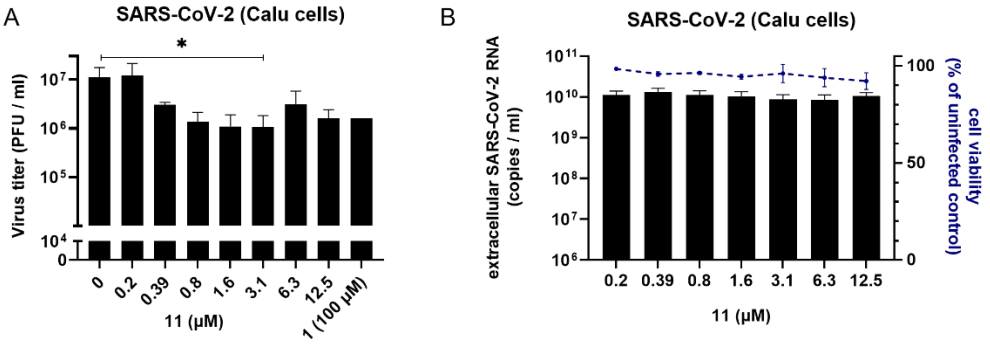


**Figure S3**: 1,6-*epi*-cyclophellitol cyclosulfate inhibits SARS-CoV-2 infectious progeny production in Calu-3 lung epithelial cells. (A-B) Viral load reduction assay in Calu-3 cells with SARS-CoV-2 (MOI 1) and samples harvested at 16 hpi. (A) Infectious virus titer and (B) extracellular viral RNA copy numbers were quantified by

plaque assay and RT-qPCR, respectively. Uninfected compound-treated cells were assessed by MTS assay in parallel to measure cytotoxicity of the compounds. n=3 independent experiments. Mean ± SEM are shown.

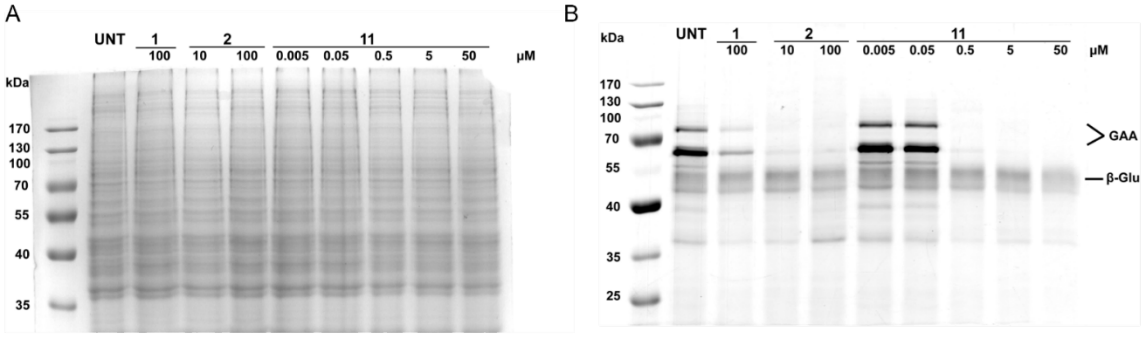


**Figure S4**: Activity-based probe labelling of cell lysate from SARS-CoV-2 infected ALI-PBEC that were treated with compound **11**, **1** and **2**. (A) performed at pH7. GelCode Blue staining of SDS-PAGE to visualize the total protein amount that was loaded. Gel was washed three times for 5 minutes with deionized water, stained over night with GelCode Blue staining reagent, and washed again three times, before imaging using a Uvitec Essential V6 system. (B) performed at pH4.

## Supporting synthesis schemes

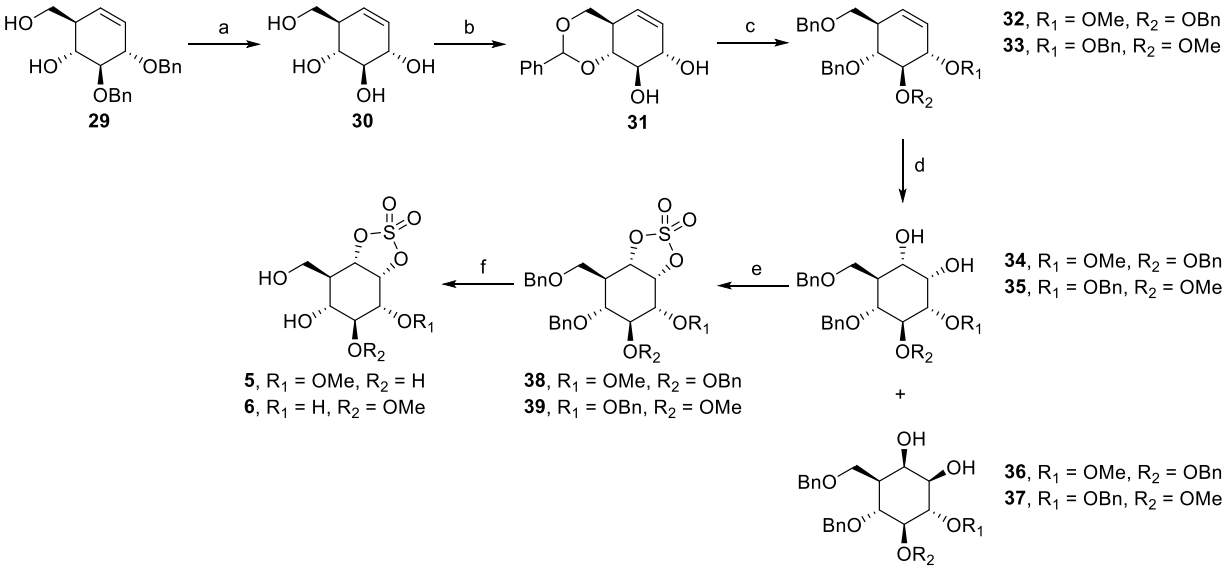


**Scheme S1**. Preparation of target compounds **5** and **6**. Reagents and conditions: (a) $BCl_3$, DCM, -78 °C, 4 h, 89% (b) Benzaldehyde dimethyl acetal, *p*-TsOH, DMF/MeCN, 4 h, 73% (c) i: KI, $K_2CO_3$, 2-aminoethyl diphenylborinate, alkyl halide, MeCN, 18 h ii: TFA, $H_2O$, DCM, 1.5 h, iii: alkyl halide, TBAI, 60% NaH, DMF, 2 h, 36% (**32**), 31% (**33**) (d) $RuCl_3{\cdot}H_2O$, $NaIO_4$, EtOAc/$H_2O$/MeCN, (e) i: $SOCl_2$, $Et_3N$, DCM, ii: $RuCl_3{\cdot}H_2O$, $NaIO_4$, EtOAc/$H_2O$/MeCN, 46% (**38**), 40% (**39**) over 3 steps (f) Pd/C, $H_2$, MeOH/THF, 4 h, 91% (**5**), 93% (**6**).

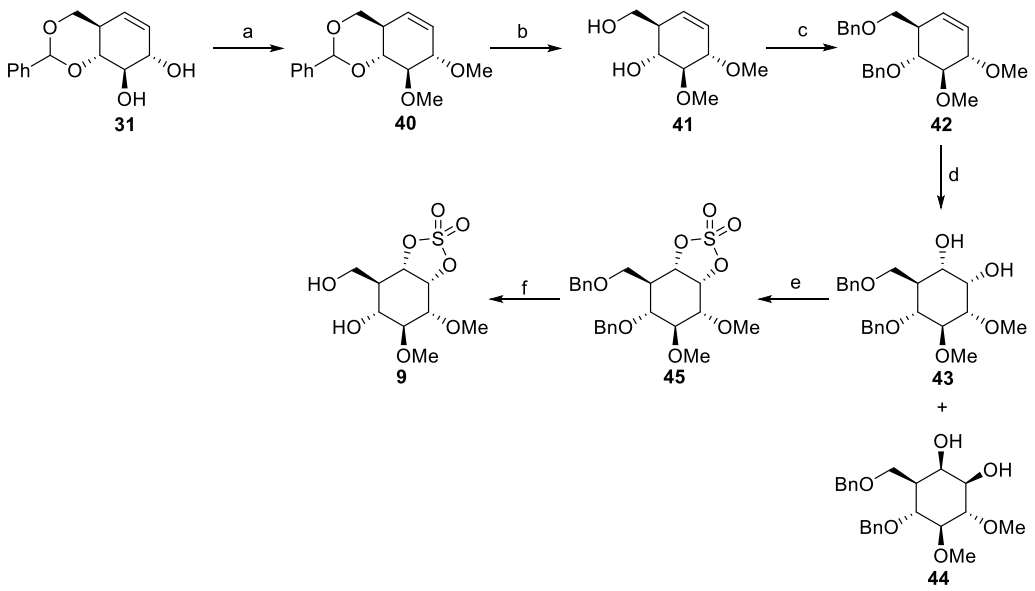

**Scheme S2**. Preparation of target compound **9**. Reagents and conditions: (a) MeI, 60% NaH, DMF, 4 h, 91%, (b) TFA, $H_2O$, DCM, 1.5 h, 83%, (c) BnBr, TBAI, 60% NaH, DMF, 5 h, 94%, (d) $RuCl_3 \cdot H_2O$, $NaIO_4$, EtOAc/$H_2O$/MeCN, 2 h, 39% (**43**), 29% (**44**), (e) i: $SOCl_2$, $Et_3N$, DCM, 1.5 h, ii: $RuCl_3 \cdot H_2O$, $NaIO_4$, EtOAc/$H_2O$/MeCN, 2.5 h, 73%, (f) Pd/C, $H_2$, MeOH/THF, 4 h, 93%.

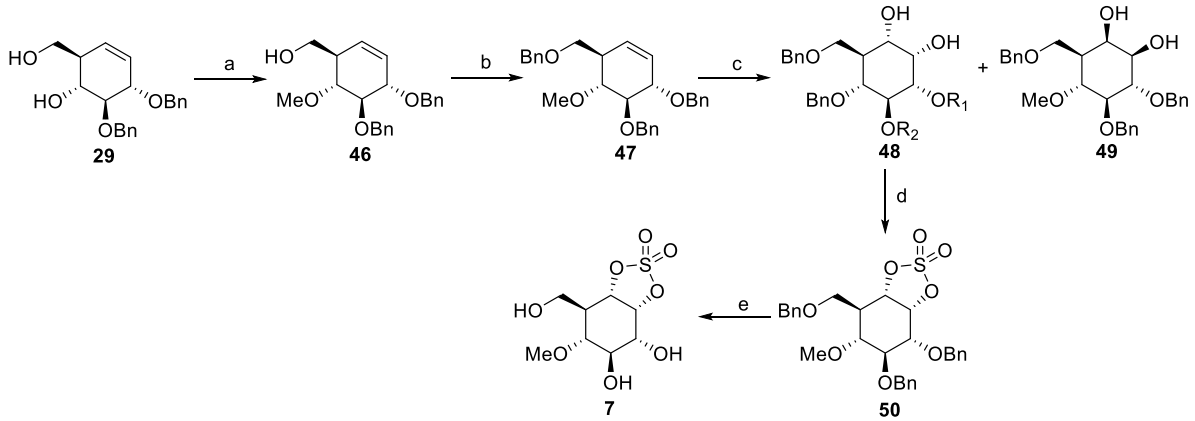

**Scheme S3**. Preparation of target compound **7**. Reagents and conditions: (a) i: TrtCl, DMAP, $Et_3N$, DMF, 18 h, ii: MeI, 60% NaH, DMF, 3 h, iii: *p*-TsOH, DCM/MeOH, 4 h, 62% over 3 steps (b) BnBr, TBAI, 60% NaH, DMF, 2 h, 95% (c) $RuCl_3 \cdot H_2O$, $NaIO_4$, EtOAc/$H_2O$/MeCN, 2 h (d) i: $SOCl_2$, $Et_3N$, DCM, 1.5, ii: $RuCl_3 \cdot H_2O$, $NaIO_4$, EtOAc/$H_2O$/MeCN, 2.5 h, 29% over 3 steps, (e) Pd/C, $H_2$, MeOH/THF, 5 h, 97%.

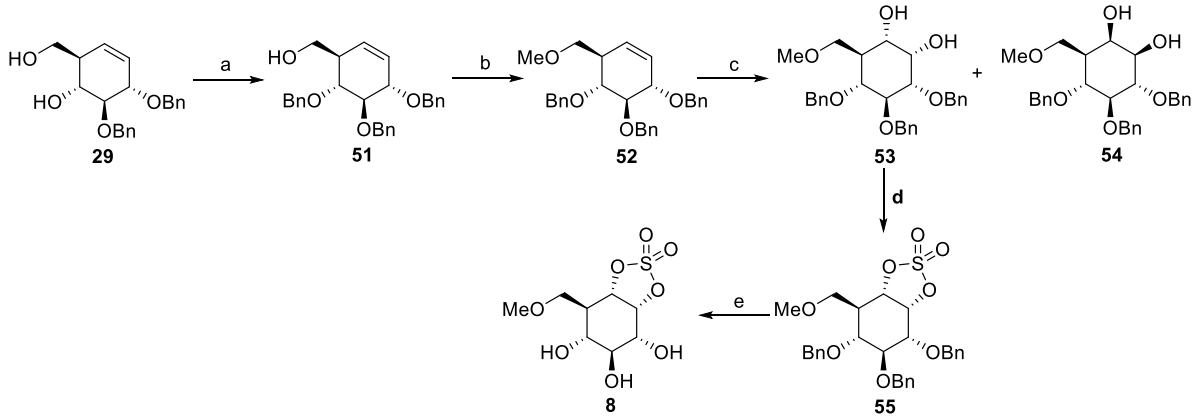


**Scheme S4**. Preparation of target compound **8**. Reagents and conditions: (a) i: TrtCl, DMAP, $Et_3N$, DMF, 18 h ii: BnBr, 60% NaH, TBAI, DMF, 6 h, iii: *p*-TsOH, DCM/MeOH, 4 h, 71% over 3 steps (b) MeI, 60% NaH, DMF, 2 h, 92% (c) $RuCl_3 \cdot H_2O$, $NaIO_4$, EtOAc/$H_2O$/MeCN, 2 h, 39% (**53**), 32% (**54**), (d) i: $SOCl_2$, $Et_3N$, DCM, 1.5 h, ii: $RuCl_3 \cdot H_2O$, $NaIO_4$, EtOAc/$H_2O$/MeCN, 2.5 h, 74% (e) Pd/C, $H_2$, MeOH/THF, 5 h, 93%.

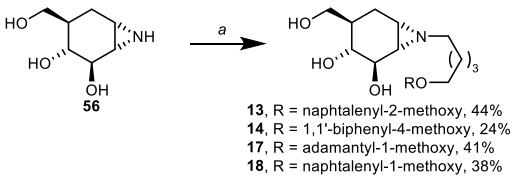


**Scheme S5**. Preparation of target compounds **13**, **14**, **17** and **18**. Reagents and conditions: (a) alkyl halogen, $K_2CO_3$, DMF, 3 h 100 ºC, 44% (**13**), 24% (**14**), 41% (**17**), 38% (**18**).

## Biochemical methods

### Cell culture/lysates

Fibroblast cell lines were cultured in HAMF12-DMEM medium supplied with 10% (v/v) FCS, 0.1% (w/v) penicillin/streptomycin, and 0.5% (w/v) sodium pyruvate, under 7% $CO_2$ at 37 °C. Confluent fibroblasts were cultured 1:3 each week. Cell pellets were stored at -80 °C until lysates were prepared. Cell lysates were prepared in potassium phosphate (KPi) lysis buffer (25 mM $K_2HPO_4/KH_2PO_4$, pH 6.5, supplemented with protease inhibitor cocktail (EDTA-free, Roche, Basel, Switzerland) and 0.1 % (v/v) triton X-100) via one Freeze-thaw cycle, followed by sonication on ice. Protein concentration was determined with the BCA Protein Assay Kit (ThermoFisher Pierce™) with 10x lysate dilution in KPi buffer (without protease inhibitor). Lysates were stored in aliquots at -80 °C until use.

### IC50

Enzymes used for $IC_{50}$ were obtained as follows: recombinant human GAA (Myozyme) were obtained from Genzyme, USA and fibroblast cell lysates were used for ER-II alpha-glucosidase. Apparent $IC_{50}$ values were determined throughout pre-incubation of 12.5 µL enzyme-mixture with 12.5 µL inhibitor for 30 minutes at 37 °C. GAA activity was measured with 47 nM enzyme (Myozyme) and 100 µL 3 mM 4-MU-α-D-glucopyranoside for 30 minutes at 37 °C. ER-II activity was measured using fibroblast cell lysates containing 10 µg protein (concentration was determined with BCA protein assay kit; Thermo Fisher) and 100 µL, 3 mM 4-MU α-D-glucopyranoside for 1 hour at 37 °C. After incubation with substrate mixture, the enzymatic reactions were quenched with 200 µL 1 M NaOH-Glycine (pH 10.3) and hydrolyzed 4-MU fluorescence is measured with a LS55 fluorescence spectrophotometer (Perkin Elmer: $\lambda_{EX}$ 366 nm, $\lambda_{EM}$ 445 nm). Background fluorescence (enzyme-mixture without substrate) is subtracted from the mean value, and normalized with maximal activity (without inhibitor). GAA is diluted in 150 mM McIlvain buffer pH 4.0 supplemented with 0.1% bovine serum albumin (BSA, w/v%) and 0.01% $NaN_3$ as bacteriostatic. ER-II is diluted in 150 mM McIlvain buffer pH 7.0 supplemented with 0.1% bovine serum albumin (BSA, w/v%) and 0.01% $NaN_3$ as bacteriostatic. Values plotted for concentration inhibitor are those in the final reaction mixture containing enzyme, inhibitor and substrate (125 µL total). The $IC_{50}$ value is the average of two-/triplicates from technical triplicates.

### Time-dependent inhibition

To study the type of inhibition, GAA and fibroblast cell lysates were pre-incubated for 5, 10, 15, 30, and 60 minutes with inhibitor (2x $IC_{50}$ value) at 37 °C. Thereafter, 100 µL of substrate mixture (3 mM 4-MU α-D-glucopyranoside pH 4.0 for GAA, pH 7.0 for ER-II alpha-glucosidase) was added and incubated for 30 minutes (GAA) or 60 minutes (ER-II alpha-glucosidase). Finally, stop buffer (1 M glycine-NaOH pH 10.3) was added to stop the reaction and hydrolyzed 4-MU fluorescence was measured. Background fluorescence (enzyme-mixture without substrate) was subtracted from the mean value, and normalized to maximal activity (without inhibitor). Time was plotted *vs* residual enzyme activity. either a straight line was observed or decreased activity over time, relating to non-covalent or covalent inhibition, respectively.

## Docking Method

The crystal structure co-ordinates of murine endoplasmic reticulum α-glucosidase II in complex with D-glucose (PDB: 5H9O) [5] were imported into Maestro software (Release 2024-1, Schrödinger, LLC, New York, NY, 2024) and prepared using the Protein Preparation module (pH = 7.4) [6]. A receptor grid was generated centred around the bound D-glucose molecule. The ligand was imported into the Maestro GUI and prepared using the LigPrep tool. Prepared ligands were docked into the generated receptor grid using the Glide module and the OPLS4 forcefield [7-11]. XP mode (extra precision) and flexible ligand

sampling were utilised, and epik state penalties were added to the docking scores [12]. Conformational, torsional and positional restraints were not used, except for stereochemical definitions in the ligand file. A maximum of 10 outputted poses was requested, and post-docking minimisation was carried out. Covalent docking was also performed using the covalent docking module of Glide [13]. The prepared ligand was docked into a receptor grid generated around the bound D-glucose molecule, and Asp564 was defined as the reactive residue. A custom reaction type for the aziridine and cyclic sulfate was created, allowing for attack of the aspartate residue at position 1 of the ligand definition (cyclic sulfate: [C][O][S]=[O]; aziridine [C][N][C]), and bond breakage between positions 1 and 2 of the ligand definition. A pre-defined reaction type was used for the epoxide. Docking was carried out in thorough 'pose prediction' mode, and MM-GBSA scoring was performed. Conformational, torsional and positional restraints were not used, except for stereochemical definitions in the ligand file.

The docking poses were exported as .pdb files and imported into ChimeraX, where figures were generated [14].

## Cytopathic Effect (CPE) reduction assay on H1299/ACE2

CPE reduction assays were performed as previously described [15]. Briefly, H1299/ACE2 cells were seeded in 96-well plates at a density of $1*10^4$ cells per well. The next day, cells were infected with SARS-CoV-2/Leiden0008 in the presence of 2-fold serial dilutions of compound. 2 days post infection the CellTiter 96 aqueous nonradioactive cell proliferation kit (Promega) was used to measure the cell viability of infected (protection) and non-infected cells (assessment of cytotoxicity). EC50 values reported are the mean values from three independent experiments and were calculated using GraphPad Prism 6.

**Fluorescent $IC_{50}$ assays on recombinant human GAA (Myozyme) and ER-II for compounds**

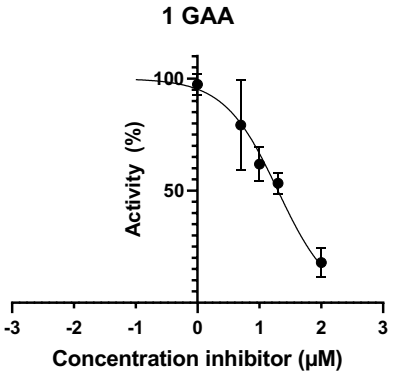


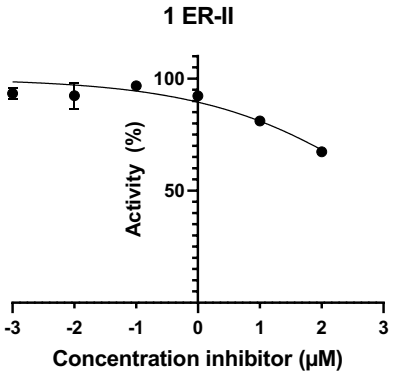


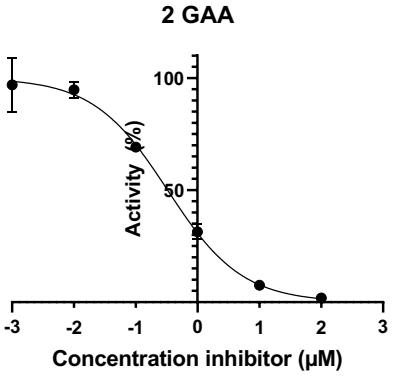


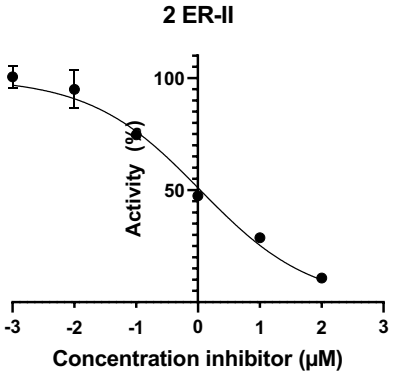


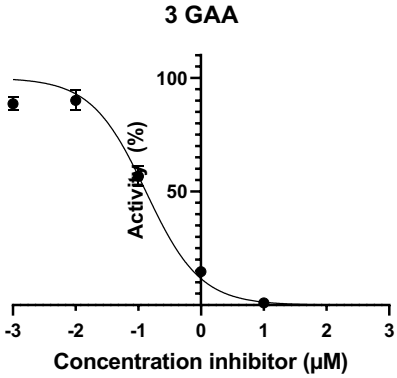


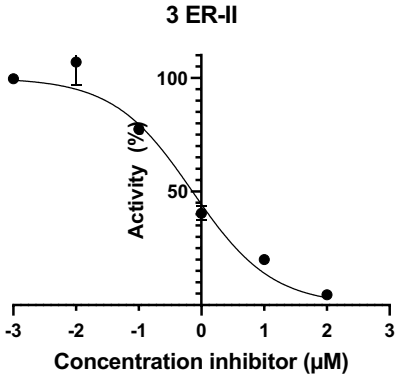


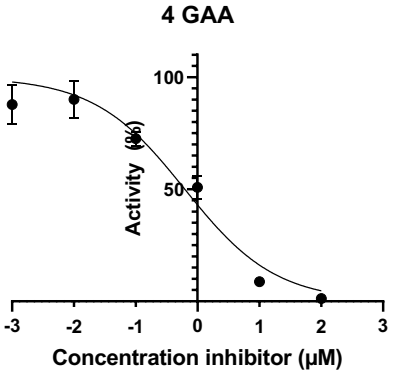


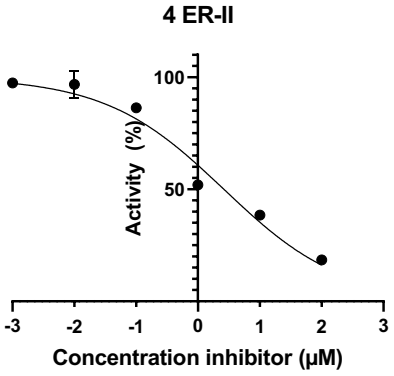

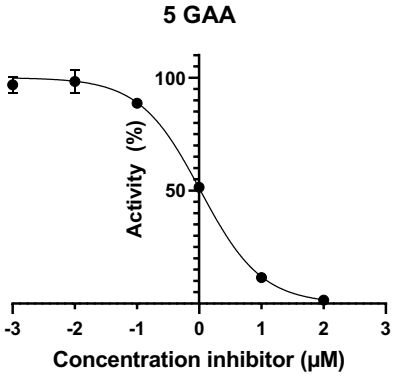
5 GAA
Activity (%)
100
50
-3
-2
-1
0
1
2
3
Concentration inhibitor (µM)

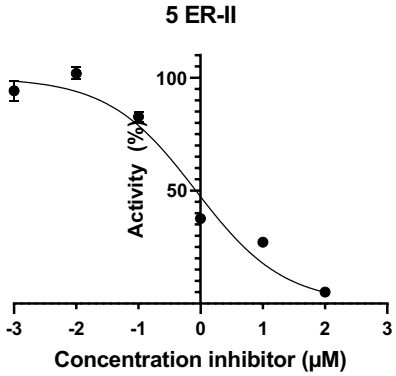
5 ER-II
Activity (%)
100
50
-3
-2
-1
0
1
2
3
Concentration inhibitor (µM)

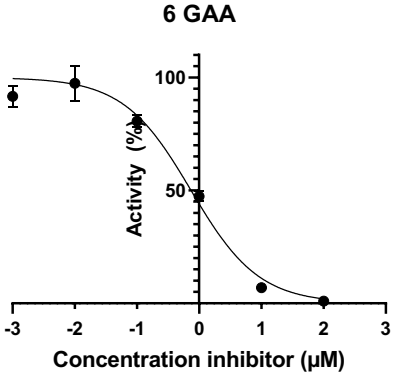
6 GAA
Activity (%)
100
50
-3
-2
-1
0
1
2
3
Concentration inhibitor (µM)

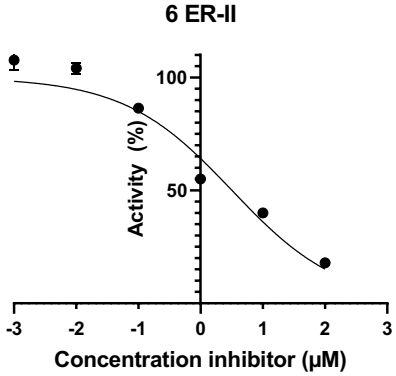
6 ER-II
Activity (%)
100
50
-3
-2
-1
0
1
2
3
Concentration inhibitor (µM)

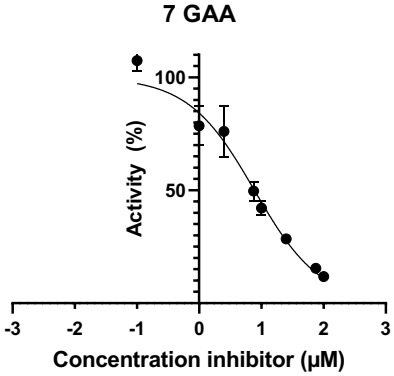
7 GAA
Activity (%)
100
50
-3
-2
-1
0
1
2
3
Concentration inhibitor (µM)

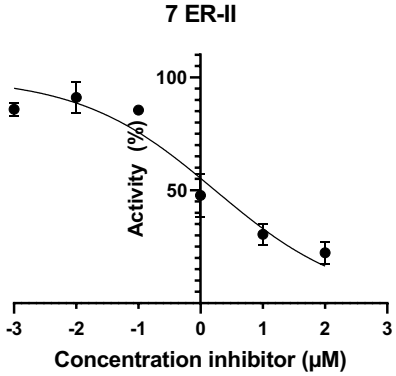
7 ER-II
Activity (%)
100
50
-3
-2
-1
0
1
2
3
Concentration inhibitor (µM)

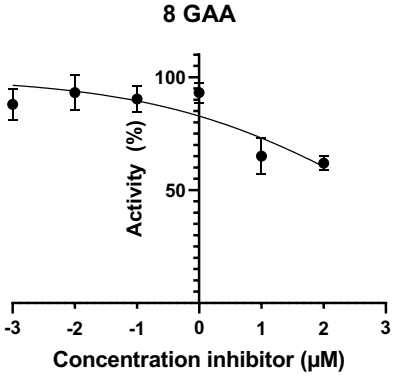
8 GAA
Activity (%)
100
50
-3
-2
-1
0
1
2
3
Concentration inhibitor (µM)

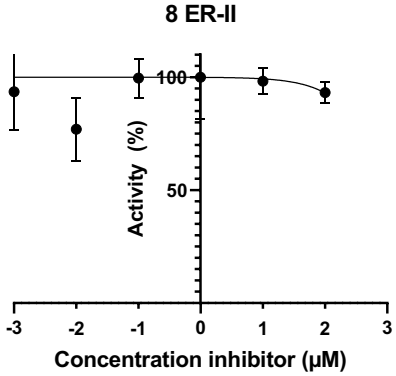
8 ER-II
Activity (%)
100
50
-3
-2
-1
0
1
2
3
Concentration inhibitor (µM)

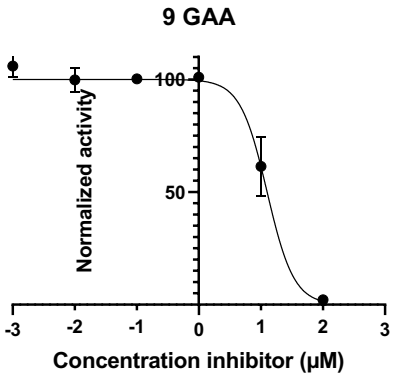
9 GAA
Normalized activity
100
50
-3
-2
-1
0
1
2
3
Concentration inhibitor (μM)

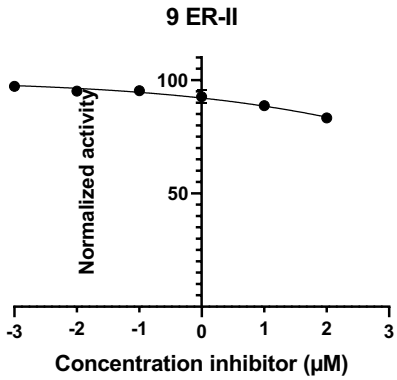
9 ER-II
Normalized activity
100
50
-3
-2
-1
0
1
2
3
Concentration inhibitor (μM)

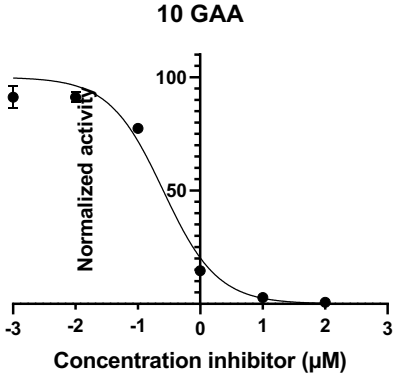
10 GAA
Normalized activity
100
50
-3
-2
-1
0
1
2
3
Concentration inhibitor (μM)

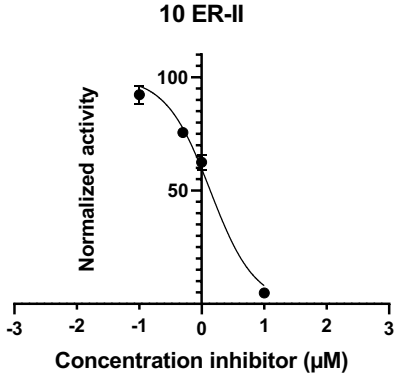
10 ER-II
Normalized activity
100
50
-3
-2
-1
0
1
2
3
Concentration inhibitor (μM)

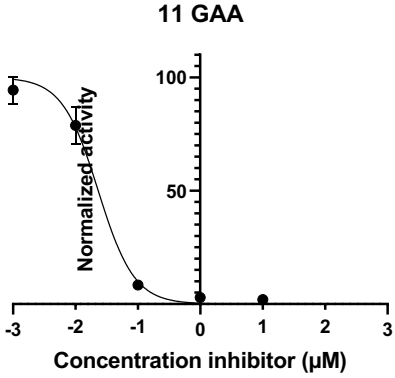
11 GAA
Normalized activity
100
50
-3
-2
-1
0
1
2
3
Concentration inhibitor (μM)

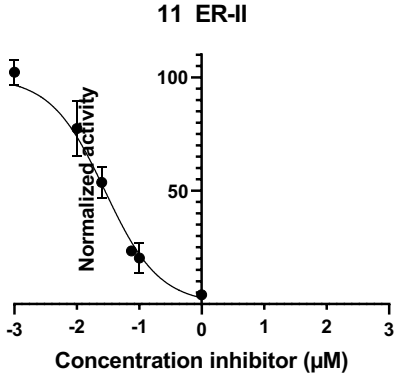
11 ER-II
Normalized activity
100
50
-3
-2
-1
0
1
2
3
Concentration inhibitor (μM)

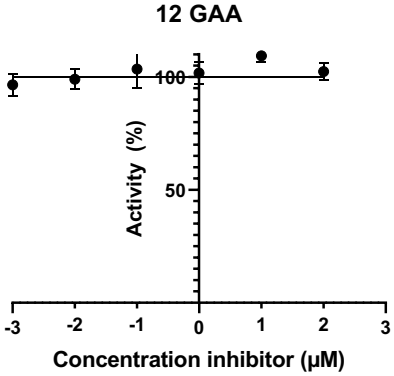
12 GAA
Activity (%)
100
50
-3
-2
-1
0
1
2
3
Concentration inhibitor (μM)

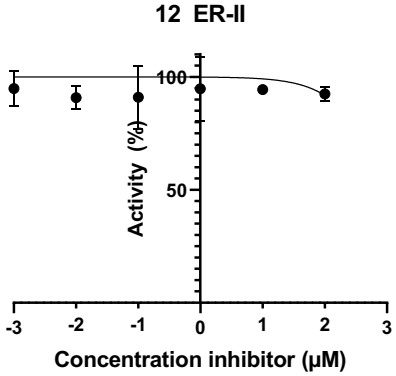
12 ER-II
Activity (%)
100
50
-3
-2
-1
0
1
2
3
Concentration inhibitor (μM)

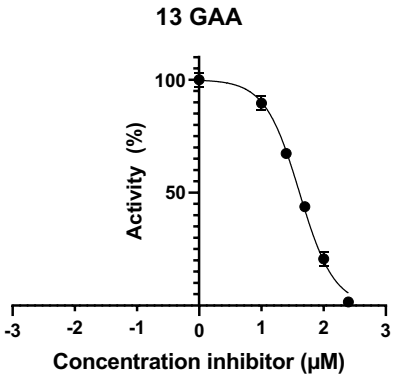
13 GAA
Activity (%)
100
50
-3
-2
-1
0
1
2
3
Concentration inhibitor (µM)

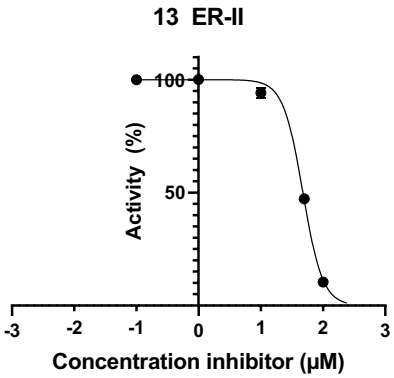
13 ER-II
Activity (%)
100
50
-3
-2
-1
0
1
2
3
Concentration inhibitor (µM)

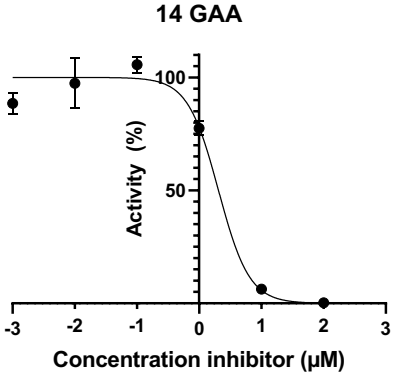
14 GAA
Activity (%)
100
50
-3
-2
-1
0
1
2
3
Concentration inhibitor (µM)

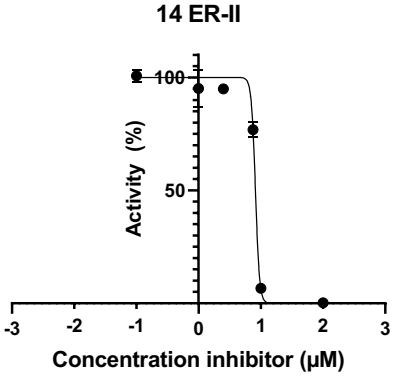
14 ER-II
Activity (%)
100
50
-3
-2
-1
0
1
2
3
Concentration inhibitor (µM)

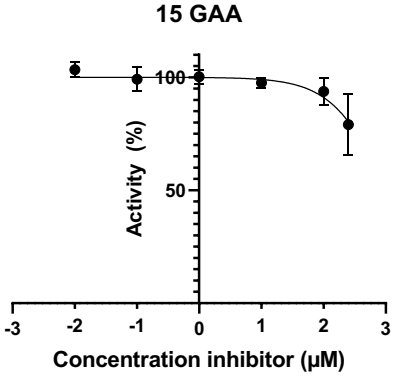
15 GAA
Activity (%)
100
50
-3
-2
-1
0
1
2
3
Concentration inhibitor (µM)

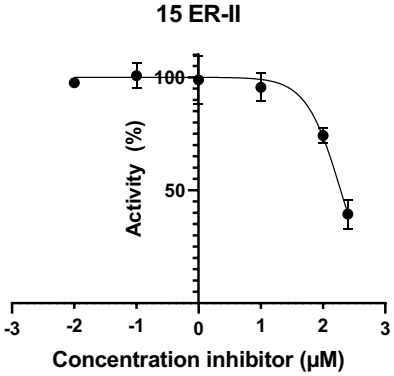
15 ER-II
Activity (%)
100
50
-3
-2
-1
0
1
2
3
Concentration inhibitor (µM)

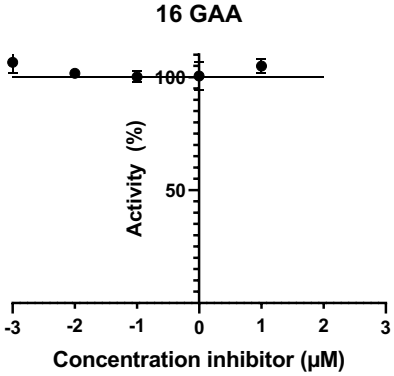
16 GAA
Activity (%)
100
50
-3
-2
-1
0
1
2
3
Concentration inhibitor (µM)

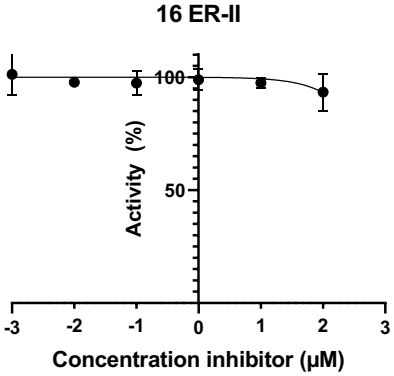
16 ER-II
Activity (%)
100
50
-3
-2
-1
0
1
2
3
Concentration inhibitor (µM)

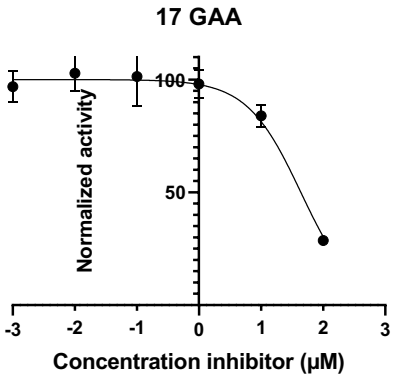
17 GAA
Normalized activity
100
50
-3
-2
-1
0
1
2
3
Concentration inhibitor (μM)

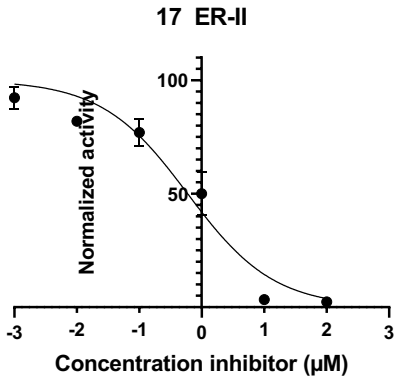
17 ER-II
Normalized activity
100
50
-3
-2
-1
0
1
2
3
Concentration inhibitor (μM)

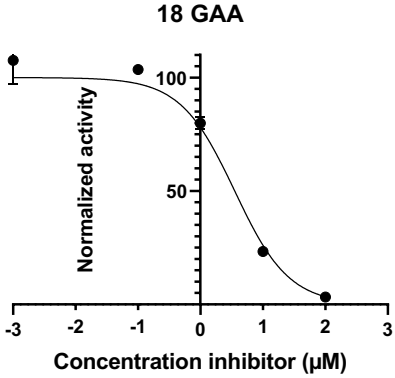
18 GAA
Normalized activity
100
50
-3
-2
-1
0
1
2
3
Concentration inhibitor (μM)

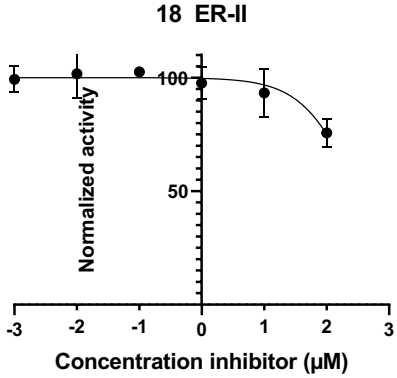
18 ER-II
Normalized activity
100
50
-3
-2
-1
0
1
2
3
Concentration inhibitor (μM)

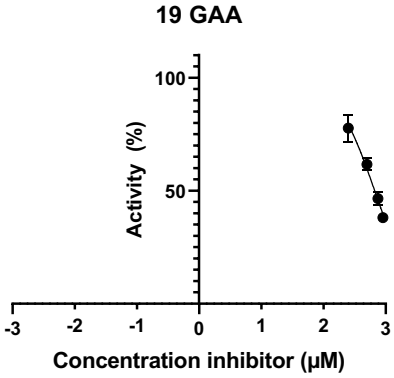
19 GAA
Activity (%)
100
50
-3
-2
-1
0
1
2
3
Concentration inhibitor (μM)

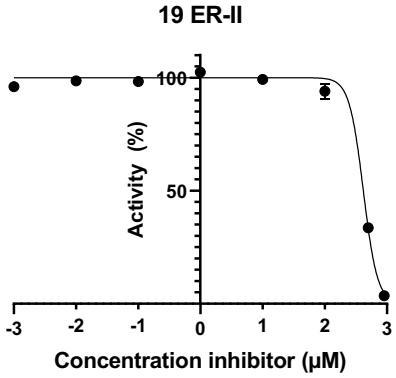
19 ER-II
Activity (%)
100
50
-3
-2
-1
0
1
2
3
Concentration inhibitor (μM)

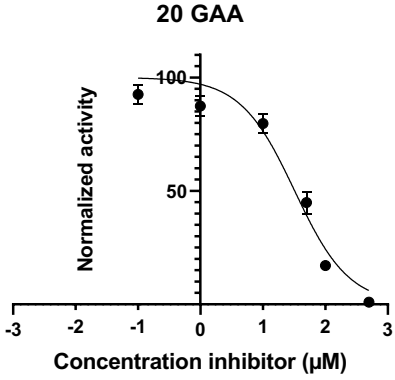
20 GAA
Normalized activity
100
50
-3
-2
-1
0
1
2
3
Concentration inhibitor (μM)

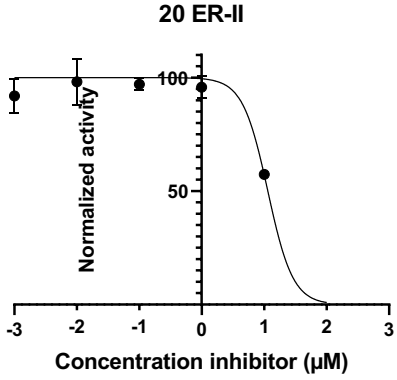
20 ER-II
Normalized activity
100
50
-3
-2
-1
0
1
2
3
Concentration inhibitor (μM)

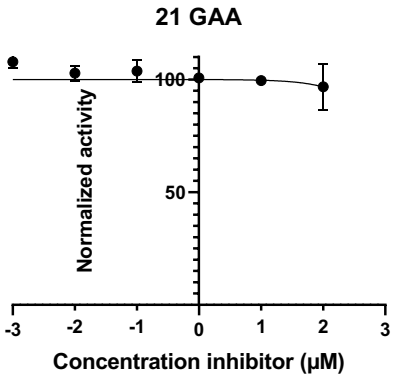
21 GAA
Normalized activity
100
50
-3
-2
-1
0
1
2
3
Concentration inhibitor (μM)

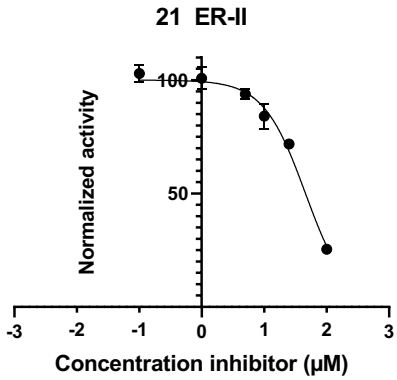
21 ER-II
Normalized activity
100
50
-3
-2
-1
0
1
2
3
Concentration inhibitor (μM)

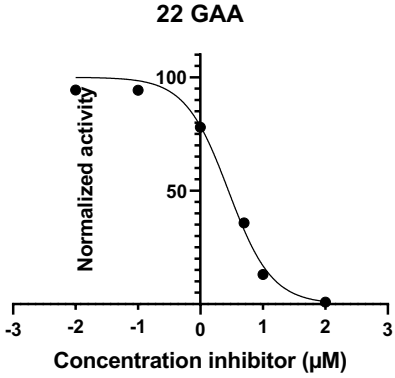
22 GAA
Normalized activity
100
50
-3
-2
-1
0
1
2
3
Concentration inhibitor (μM)

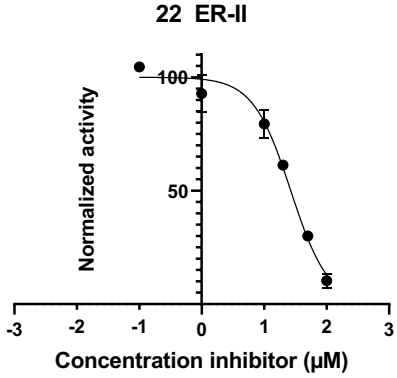
22 ER-II
Normalized activity
100
50
-3
-2
-1
0
1
2
3
Concentration inhibitor (μM)

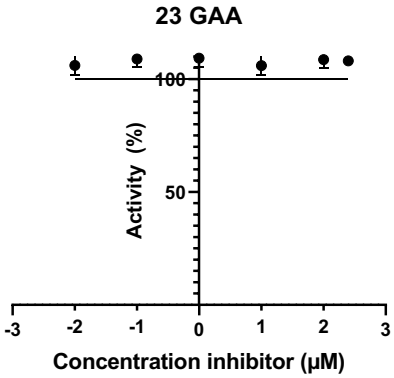
23 GAA
Activity (%)
100
50
-3
-2
-1
0
1
2
3
Concentration inhibitor (μM)

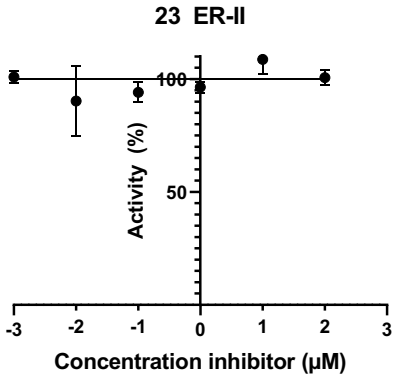
23 ER-II
Activity (%)
100
50
-3
-2
-1
0
1
2
3
Concentration inhibitor (μM)

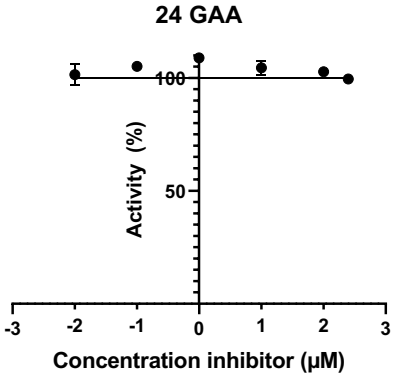
24 GAA
Activity (%)
100
50
-3
-2
-1
0
1
2
3
Concentration inhibitor (μM)

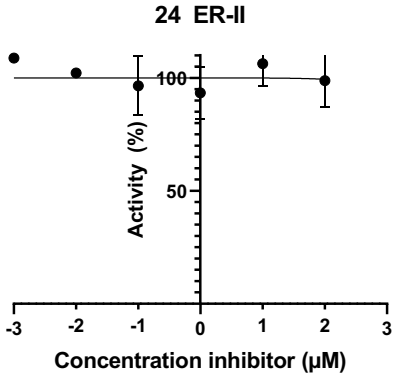
24 ER-II
Activity (%)
100
50
-3
-2
-1
0
1
2
3
Concentration inhibitor (μM)

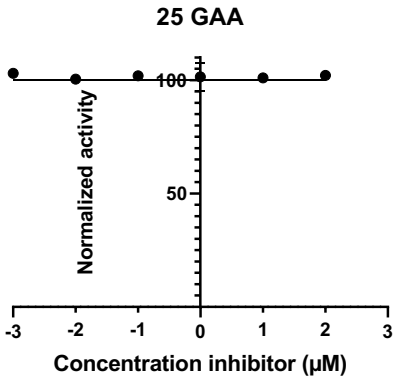
25 GAA
Normalized activity
100
50
-3
-2
-1
0
1
2
3
Concentration inhibitor (μM)

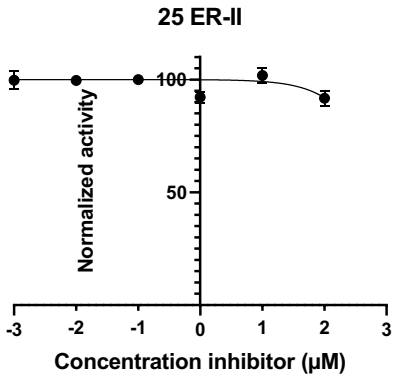
25 ER-II
Normalized activity
100
50
-3
-2
-1
0
1
2
3
Concentration inhibitor (μM)

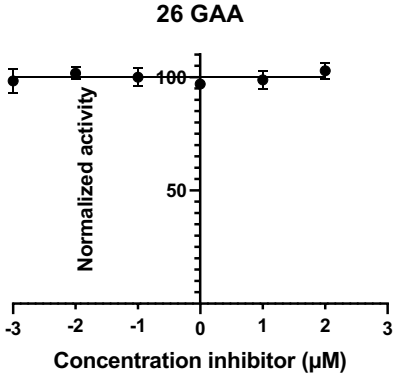
26 GAA
Normalized activity
100
50
-3
-2
-1
0
1
2
3
Concentration inhibitor (μM)

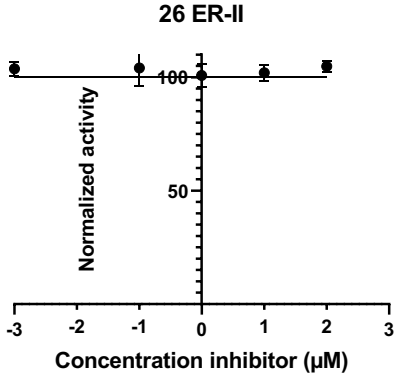
26 ER-II
Normalized activity
100
50
-3
-2
-1
0
1
2
3
Concentration inhibitor (μM)

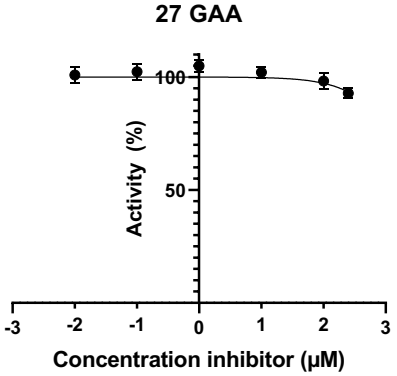
27 GAA
Activity (%)
100
50
-3
-2
-1
0
1
2
3
Concentration inhibitor (μM)

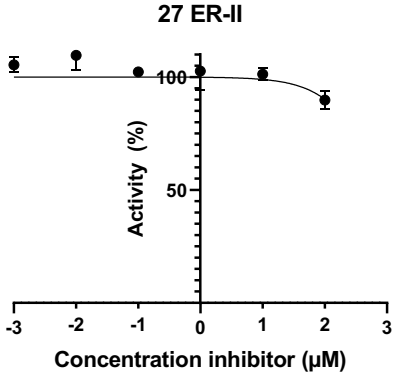
27 ER-II
Activity (%)
100
50
-3
-2
-1
0
1
2
3
Concentration inhibitor (μM)

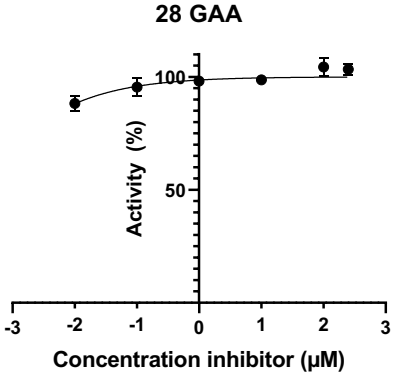
28 GAA
Activity (%)
100
50
-3
-2
-1
0
1
2
3
Concentration inhibitor (μM)

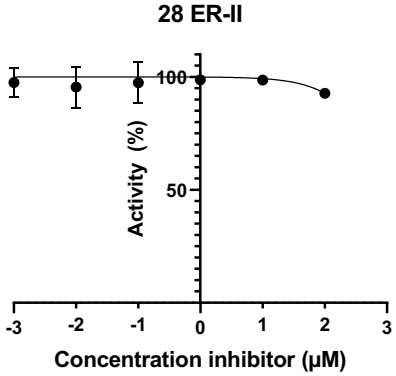
28 ER-II
Activity (%)
100
50
-3
-2
-1
0
1
2
3
Concentration inhibitor (μM)

## General experimental procedures

All chemicals were of commercial grade and were used as received unless stated otherwise. Solvents used in synthesis were dried and stored over 4Å molecular sieves. Deuterated chloroform was stored over activated 3 Å molecular rods (rods, size 1/16 in., Sigma Aldrich) and potassium carbonate. Flash column chromatography was performed on silica gel 60 Å (0.04 – 0.063 mm, Screening Devices B.V.). TLC analysis was performed on TLC Silica gel 60 (Kieselgel 60 F254, Merck) with UV detection (254 nm) and by spraying with a solution of $(NH_4)_6Mo_7O_{24}\cdot H_2O$ (25 g/L) and $(NH_4)_4Ce(SO_4)_4\cdot 2H_2O$ (10 g/L) in 10% sulfuric acid in water followed by charring at ± 200 °C. TLC-MS analysis was performed on a Camag TLC-MS Interface coupled with an API165 (SCIEX) mass spectrometer (eluted with *tert*-butylmethylether/EtOAc/MeOH, 5/4/1, v:v:v +0.1% formic acid, flow rate 0.12 mL/min). High-resolution mass spectra (HRMS) were recorded on a Waters Synapt G2-Si (TOF) equipped with an electrospray ion source in positive mode (source voltage 3.5 kV) and an internal lock mass LeuEnk ($M+H^+$ = 556.2771). $^1$H and $^{13}$C NMR spectra were recorded on a Bruker AV-400 NMR (400 and 101 MHz respectively) or a Bruker AV-500 NMR (500 and 126 MHz respectively). All samples were measured in $CDCl_3$, unless stated otherwise. Chemical shifts (δ) are given in ppm relative to tetramethyl silane as internal standard or the residual signal of the deuterated solvent. Coupling constants (*J*) are given in Hz. All given $^{13}$C APT spectra are proton decoupled. NMR peak assignment was accomplished using COSY, HSQC. Proton and carbon numbering for NMR peak assignment was done as followed: numbering was done similarly to their glucose counterparts and not their respective nomenclature. Numbering starts at the 'anomeric' center and progresses similarly as their glucose counterpart. 'H-7' or 'C-7' is used where the intramolecular oxygen is substituted for carbon.

## Synthetic procedures

**(1*R*,2*R*,3*S*,6*R*)-6-(hydroxymethyl)cyclohex-4-ene-1,2,3-triol (30)**

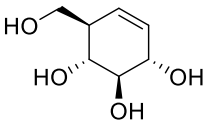


Cyclohexene **29** (0.85 g, 2.5 mmol, 1.0 eq) was dissolved in anhydrous DCM (17 mL), cooled to -78°C and $BCl_3$ (1M solution in DCM, 12.5 mmol, 5.0 eq) was added dropwise. The reaction was stirred at -78°C for 4 h and quenched with MeOH. The reaction mixture was concentrated *in vacuo* and the crude material was purified by silica gel flash column chromatography (0%→30% MeOH in EtOAc, silica prewashed with MeOH) to obtain **30** (0.35 g, 2.2 mmol, 89%) as a white solid. $^1$H NMR (400 MHz, MeOD) δ 5.63 (dt, *J* = 10.2, 1.7 Hz, 1H, H-1), 5.58 (dt, *J* = 10.1, 2.0 Hz, 1H, H-6), 4.04 (ddd, *J* = 7.7, 3.8, 2.0 Hz, 1H, H-2), 3.79 (dd, *J* = 10.6, 4.1 Hz, 1H, H-7b), 3.60 (dd, *J* = 10.7, 6.1 Hz, 1H, H-7a), 3.49 – 3.39 (m, 2H, H-3, H-4), 2.27 (ddq, *J* = 8.3, 4.3, 2.1 Hz, 1H, H-5). $^{13}$C NMR (101 MHz, MeOD) δ 128.9 (C-6), 126.5 (C-1), 76.8 (C-3), 71.5 (C-2), 69.9 (C-4), 61.3 (C-7), 45.6 (C-5). HRMS (ESI) m/z: $[M+Na^+]$ calcd for $C_7H_{12}O_4Na$ 183.0633, found 183.0634.

**(4a*R*,7*S*,8*R*,8a*R*)-2-phenyl-4a,7,8,8a-tetrahydro-4H-benzo[*d*][1,3]dioxine-7,8-diol (31)**

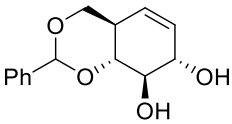


Cyclohexene **30** (80 mg, 0.5 mmol, 1.0 eq) was dissolved in an anhydrous 4:1 mixture of ACN/DMF (2.5 mL) and benzaldehyde dimethylacetal (0.19 mL, 1.25 mmol, 2.5 eq) was added. The pH of the mixture was adjusted to 2 with *p*TsOH and the reaction mixture was stirred on a rotary evaporator (rotavap) for 4 h at 60°C and 650 mbar. The reaction was quenched with $Et_3N$ and diluted with EtOAc. The organic layer was washed with sat. aq.

$NaHCO_3$ and brine, dried over $MgSO_4$, filtered and concentrated *in vacuo*. The crude product was purified by silica gel flash column chromatography (0%→10% MeOH in DCM) to obtain **31** (92 mg, 0.37 mmol, 73%) as a white solid. $^1$H NMR (400 MHz, $CDCl_3$) δ 7.56 – 7.43 (m, 2H, $CH_{Ar}$), 7.43 – 7.31 (m, 3H, $CH_{Ar}$), 5.62 (dt, *J* = 10.0, 2.8 Hz, 1H, H-6), 5.56 (s, 1H, H-8), 5.36 – 5.31 (m, 1H, H-1), 4.33 – 4.22 (m, 2H, H-2, H-7b), 3.88 (dd, *J* = 10.4, 7.3 Hz, 1H, H-3), 3.63 – 3.55 (m, 2H, H-4, H-7a), 2.62 (ddtd, *J* = 11.4, 6.6, 3.4, 1.6 Hz, 1H, H-5). $^{13}$C NMR (101 MHz, $CDCl_3$) δ 137.8 ($C_{qAr}$), 130.6 (C-6), 129.3, 128.4, 126.4 ($CH_{Ar}$), 124.3 (C-1), 102.3 (C-8), 80.8 (C-4), 75.7 (C-3), 73.9 (C-2), 70.0 (C-7), 38.6 (C-5). HRMS (ESI) m/z: [M+Na$^+$] calcd for $C_{14}H_{16}O_4Na$ 271.0946, found 271.0948.

**((((1*R*,2*R*,3*S*,6*R*)-6-((benzyloxy)methyl)-2-methoxycyclohex-4-ene-1,3-diyl)bis(oxy))bis(methylene))dibenzene (32)** Diol **31** (0.12 g, 0.5 mmol, 1.0 eq) was co-evaporated (3x) toluene and dissolved in anhydrous MeCN (2.5 mL). Subsequently, KI (83 mg, 0.5 mmol, 1.0 eq), $K_2CO_3$ (83 mg, 0.6 mmol, 1.2 eq) and 2-aminoethyl diphenylborinate (38 mg, 0.15 mmol, 0.3 eq) and BnBr (59 µL, 0.5 mmol, 1.0 eq) were added to the solution and the mixture was stirred at 60 °C for 18 h. The reaction was quenched with water and diluted with EtOAc. The organic layer was washed with sat. aq. $NaHCO_3$ and brine, dried over $MgSO_4$, filtered and concentrated *in vacuo*. The crude material was filtered over a silica plug. The filtered material was dissolved in DCM (2.5 mL) and cooled to 0 °C. Water (1 mL) and TFA (0.19 mL, 2.5 mmol, 5.0 eq) were added and the reaction was stirred for 1.5 h at rt after which TLC analysis indicated full conversion of the starting material. The solution was washed with sat. aq. $NaHCO_3$, $H_2O$ and brine, dried over $MgSO_4$, filtered and concentrated *in vacuo*. The crude material was dissolved in anhydrous DMF and cooled to 0°C. NaH (60% dispersion in mineral oil) was added and the reaction was stirred for 15 min at 0°C. Subsequently, MeI was added dropwise. The reaction was stirred for 2 h at rt, diluted with $Et_2O$ and quenched with MeOH at 0°C. The organic layer was washed with $H_2O$ and brine (2x), dried over $MgSO_4$, filtered and concentrated *in vacuo*. The crude material was purified by silica gel flash column chromatography (0%→15% EtOAc in pentane) to obtain **32** (80 mg, 0.18 mmol, 36% over 3 steps) as a colorless oil. $^1$H NMR (500 MHz, $CDCl_3$) δ 7.43 – 7.33 (m, 2H, $CH_{Ar}$), 7.31 – 7.23 (m, 13H, $CH_{Ar}$), 5.74 – 5.69 (m, 1H, H-6), 5.67 (dt, *J* = 10.2, 1.7 Hz, 1H, H-1), 4.91 (s, 1H, CH*H*Ph), 4.89 (s, 1H, CH*H*Ph), 4.71 (s, 1H, CH*H*Ph), 4.68 (s, 1H, CH*H*Ph), 4.56 – 4.52 (m, 1H, CH*H*Ph), 4.51 (d, *J* = 12.2 Hz, 1H, CH*H*Ph), 4.21 (ddd, *J* = 7.8, 3.5, 1.7 Hz, 1H, H-2), 3.74 (dd, *J* = 10.1, 7.8 Hz, 1H, H-3), 3.62 (dd, *J* = 9.0, 3.4 Hz, 1H, H-7b), 3.57 (dd, *J* = 9.0, 5.0 Hz, 1H, H-7a), 3.52 (s, 3H, $OCH_3$), 3.41 (t, *J* = 9.8 Hz, 1H, H-4), 2.51 – 2.43 (m, 1H, H-5). $^{13}$C NMR (126 MHz, $CDCl_3$) δ 139.5, 139.0, 138.6 (3x $C_{qAr}$), 129.6 (C-1), 128.5, 128.4, 128.1, 128.0, 127.9, 127.8, 127.7, 127.6 ($CH_{Ar}$), 127.2 (C-6), 85.7 (C-3), 81.2 (C-2), 80.9 (C-4), 75.6, 73.7, 72.8 (3x $CH_2Ph$), 70.1 (C-7), 59.1 ($OCH_3$), 45.1 (C-5). HRMS (ESI) m/z: [M+Na$^+$] calcd for $C_{29}H_{32}O_4Na$ 467.2198, found 467.2200.

**(3a*S*,4*R*,5*R*,6*S*,7*R*,7a*R*)-5-(benzyloxy)-4-((benzyloxy)methyl)-7-methoxy-6-(naphthalen-2-ylmethoxy)hexahydrobenzo[*d*][1,3,2]dioxathiole 2,2-dioxide (38)** A solution of $NaIO_4$ (0.13 g, 0.63 mmol, 2.5 eq) and $RuCl_3{\cdot}H_2O$ (3.7 mg, 18 µmol, 0.07 eq) in water (2.0 mL) was added dropwise to an ice-cooled and vigorously stirred solution of cyclohexene **32** (0.11 g, 0.25 mmol, 1.0 eq) in EtOAc/MeCN 1:1 (7.5 mL). The reaction was stirred for 2 h at 0°C after which TLC analysis indicated full conversion. The reaction was quenched with sat. aq. $Na_2S_2O_3$ and the aqueous layer was extracted with EtOAc (3x). The combined organic layers were washed with brine, dried over $MgSO_4$, filtered and concentrated *in vacuo*. The crude material was purified by silica gel flash column chromatography (5%→30% acetone in pentane) to obtain **34** as white solid. $SOCl_2$ (22 µL, 0.31 mmol, 3.5 eq) was added dropwise over 5 min to an ice- cooled solution of diol **34** (42 mg, 88 µmol, 1.0 eq) and $Et_3N$ (49 µL, 0.35 mmol, 4.0 eq) in DCM (1.0 mL). The reaction was stirred for 1,5 h at 0°C after which TLC analysis indicated full conversion of the starting material. The reaction mixture was diluted with cold $Et_2O$ and the organic layer was washed with cold water and brine, dried over $MgSO_4$, filtered and concentrated *in vacuo*. Final traces of $Et_3N$ were removed under high vacuum. The crude material was dissolved in EtOAc/ACN and a solution of $NaIO_4$ and $RuCl_3{\cdot}H_2O$ in water was added at 0°C. The reaction was stirred for 2,5 h at this temperature and subsequently diluted with EtOAc and quenched with sat. aq. $N_2S_2O_3$. The layers were separated and the aqueous layer was extracted with EtOAc. The combined organic layers were washed with water and brine, dried over $MgSO_4$, filtered and concentrated *in vacuo*. The crude product was purified by silica gel flash column chromatography (0%→15% EtOAc in pentane) to obtain cyclosulfate **38** (21 mg, 40 µmol, 46%) as a colorless oil. $^1$H NMR (500 MHz,

$CDCl_3$) δ 7.38 – 7.29 (m, 15H, $CH_{Ar}$), 5.09 – 5.02 (m, 2H, H-1, H-6), 4.77 – 4.71 (m, 4H, 4x CH*H*Ph), 4.54 (s, 2H, 2x CH*H*Ph), 3.86 – 3.80 (m, 2H, H-3, H-7b), 3.71 – 3.66 (m, 1H, H-2), 3.59 (dd, *J* = 9.5, 2.2 Hz, 1H, H-7a), 3.52 (s, 3H, $OCH_3$), 3.26 (dd, *J* = 11.7, 8.2 Hz, 1H, H-4), 2.44 (ddt, *J* = 11.6, 9.5, 2.2 Hz, 1H, H-5). $^{13}C$ NMR (126 MHz, $CDCl_3$) δ 138.4, 137.9, 137.5 (3x $C_{qAr}$), 128.9, 128.7, 128.6, 128.4, 128.2, 128.12, 128.08, 128.05, 128.0 ($CH_{Ar}$), 81.9 (C-3), 81.1 (C-1), 79.8 (C-6), 77.5 (C-4), 76.1 (C-2), 75.0, 74.1, 73.7 (3x $CH_2Ph$), 64.1 (C-7), 61.2 ($OCH_3$), 43.6 (C-5). HRMS (ESI) m/z: [M+$Na^+$] calcd for $C_{29}H_{32}O_8SNa$ 563.1716, found 563.1717.

**(3a*S*,4*R*,5*R*,6*S*,7*R*,7a*R*)-5,6-dihydroxy-4-(hydroxymethyl)-7-methoxyhexahydrobenzo[*d*][1,3,2]dioxathiole 2,2-dioxide (5)** Cyclosulfate **38** (15 mg, 28 µmol, 1.0 eq) was dissolved in MeOH/THF (1 mL) and purged with $N_2$. Pd/C (10 wt%, 12 mg, 11 µmol, 0.4 eq) was added to the solution and the reaction mixture was again purged with $N_2$. The reaction mixture was flushed for 5 min with $H_2$ before being left to stir under $H_2$ atmosphere for 5 h. The reaction mixture was flushed with $N_2$ and filtered over whatman filter paper. The filtrate was concentrated *in vacuo* and the crude material was purified by silica gel flash column chromatography (0%→20% MeOH in DCM, silica prewashed with MeOH) to obtain **5** (6.8 mg, 25 µmol, 91%) as a white solid. $^1H$ NMR (500 MHz, MeOD) δ 5.11 – 5.05 (m, 1H, H-1), 4.08 (dd, J = 11.1, 2.3 Hz, 1H, H-7B), 3.76 (dd, J = 10.9, 4.0 Hz, 1H, H-6), 3.69 (dd, J = 11.1, 2.8 Hz, 1H, H-7A), 3.63 – 3.54 (m, 2H, CH-2, H-3), 3.39 – 3.34 (m, 1H, H-4), 2.94 (s, 3H, $CH_3$), 1.98 (tt, J = 11.1, 2.6 Hz, 1H, H-5). $^{13}C$ NMR (126 MHz, MeOD) δ 85.3 (C-1), 74.6 (C-2/3), 70.9 (C-2/3), 68.8 (C-4), 62.7 (C-6), 57.1 (C-7), 47.1 (C-5), 37.3 ($CH_3$). HRMS (ESI) m/z: [M+$Na^+$] calcd for $C_8H_{14}O_8SNa$ 293.2418, found 293.2420.

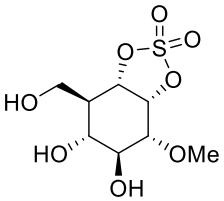


**((((1*R*,2*R*,3*S*,6*R*)-6-((benzyloxy)methyl)-2-methoxycyclohex-4-ene-1,3-diyl)bis(oxy))bis(methylene))dibenzene (33)** Diol **31** (0.12 g, 0.5 mmol, 1.0 eq) was co-evaporated (3x) toluene and dissolved in anhydrous MeCN (2.5 mL). Subsequently, KI (83 mg, 0.5 mmol, 1.0 eq), $K_2CO_3$ (83 mg, 0.6 mmol, 1.2 eq) and 2-aminoethyl diphenylborinate (38 mg, 0.15 mmol, 0.3 eq) and MeI (31 µL, 0.5 mmol, 1.0 eq) were added to the solution and the mixture was stirred at 60 °C for 18 h. The reaction was quenched with water and diluted with EtOAc. The organic layer was washed with sat. aq. $NaHCO_3$ and brine, dried over $MgSO_4$, filtered and concentrated *in vacuo*. The crude material was filtered over a silica plug. The filtered material was dissolved in DCM (2.5 mL) and cooled to 0 °C. Water (1 mL) and TFA (0.19 mL, 2.5 mmol, 5.0 eq) were added and the reaction was stirred for 1.5 h at rt after which TLC analysis indicated full conversion of the starting material. The solution was washed with sat. aq. $NaHCO_3$, $H_2O$ and brine, dried over $MgSO_4$, filtered and concentrated *in vacuo*. The crude material was dissolved in anhydrous DMF (10 mL) and cooled to 0°C. NaH (60% dispersion in mineral oil, 92 mg, 2.3 mmol, 4.5 eq) was added and the reaction was stirred for 15 min at 0°C. Subsequently, TBAI (9.2 mg, 25 µmol, 0.05 eq) and BnBr (0.21 mL, 1.8 mmol, 3.6 eq) were added. The reaction was stirred for 2 h at rt, diluted with $Et_2O$ and quenched with MeOH at 0°C. The organic layer was washed with $H_2O$ and brine (2x), dried over $MgSO_4$, filtered and concentrated *in vacuo*. The crude material was purified by silica gel flash column chromatography (0%→15% EtOAc in pentane) to obtain **33** (71 mg, 0.16 mmol, 31%) as a colorless oil. $^1H$ NMR (500 MHz, $CDCl_3$) δ 7.40 – 7.36 (m, 2H, $CH_{Ar}$), 7.35 – 7.26 (m, 13H, $CH_{Ar}$), 5.74 – 5.69 (m, 1H, H-6), 5.67 (dt, *J* = 10.2, 1.7 Hz, 1H, H-1), 4.93 (s, 1H, CH*H*Ph), 4.91 (s, 1H, CH*H*Ph), 4.72 (s, 1H, CH*H*Ph), 4.69 (s, 1H, CH*H*Ph), 4.59 – 4.55 (m, 1H, CH*H*Ph), 4.53 (d, *J* = 12.2 Hz, 1H, CH*H*Ph), 4.17 (ddd, *J* = 7.8, 3.5, 1.7 Hz, 1H, H-2), 3.75 (dd, *J* = 10.1, 7.8 Hz, 1H, H-3), 3.62 (dd, *J* = 9.0, 3.4 Hz, 1H, H-7b), 3.58 (dd, *J* = 9.0, 5.0 Hz, 1H, H-7a), 3.53 (s, 3H, $OCH_3$), 3.41 (t, *J* = 9.8 Hz, 1H, H-4), 2.51 – 2.46 (m, 1H, H-5). $^{13}C$ NMR (126 MHz, $CDCl_3$) δ 139.0, 138.9, 138.6 (3x $C_{qAr}$), 129.4 (C-1), 128.3, 128.2, 128.1, 128.0, 127.9, 127.8, 127.7, 127.6 ($CH_{Ar}$), 127.2 (C-6), 85.8 (C-3), 81.5 (C-2), 80.9 (C-4), 75.6, 73.5, 72.9 (3x $CH_2Ph$), 70.4 (C-7), 61.5 ($OCH_3$), 45.1 (C-5). HRMS (ESI) m/z: [M+$Na^+$] calcd for $C_{29}H_{32}O_4Na$ 467.2198, found 467.2200.

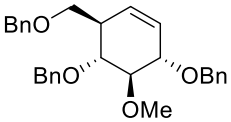


**(3a*R*,4*R*,5*S*,6*R*,7*R*,7a*S*)-4,6-bis(benzyloxy)-7-((benzyloxy)methyl)-5-methoxyhexahydrobenzo[*d*][1,3,2]dioxathiole 2,2-dioxide (39)** A solution of $NaIO_4$ (64 mg, 0.3 mmol, 2.5 eq)

and $RuCl_3 \cdot H_2O$ (1.7 mg, 8.4 µmol, 0.07 eq) in water was added dropwise to an ice-cooled and vigorously stirred solution of cyclohexene **33** (53 mg, 0.12 mmol, 1.0 eq)in EtOAc/MeCN 1:1 (6 mL). The reaction was stirred for

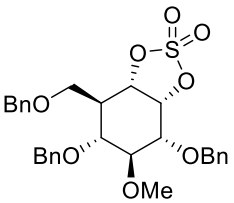


2 h at 0°C after which TLC analysis indicated full conversion. The reaction was quenched with sat. aq. $Na_2S_2O_3$ and the aqueous layer was extracted with EtOAc (3x). The combined organic layers were washed with brine, dried over $MgSO_4$, filtered and concentrated *in vacuo*. The crude material was purified by silica gel flash column chromatography (5%→30% acetone in pentane) to obtain diols **35** and **37**. $SOCl_2$ (14 µL, 0.19 mmol, 3.5 eq) was added dropwise over 5 min to an ice- cooled solution of diol **35** (26 mg, 54 µmol, 1.0 eq) and $Et_3N$ (67 µL, 0.48 mmol, 4.0 eq) in DCM (1.2 mL). The reaction was stirred for 1,5 h at 0°C after which TLC analysis indicated full conversion of the starting material. The reaction mixture was diluted with cold $Et_2O$ and the organic layer was washed with cold water and brine, dried over $MgSO_4$, filtered and concentrated *in vacuo*. Final traces of $Et_3N$ were removed under high vacuum. The crude material was dissolved in EtOAc/MeCN 1:1 (4.4 mL) and a solution of $NaIO_4$ (24 mg, 0.11 mmol, 2.0 eq) and $RuCl_3 \cdot H_2O$ (1.1 mg, 5.5 µmol, 0.1 eq) in water (2.2 mL) was added at 0°C. The reaction was stirred for 2,5 h at this temperature and subsequently diluted with EtOAc and quenched with sat. aq. $N_2S_2O_3$. The layers were separated and the aqueous layer was extracted with EtOAc. The combined organic layers were washed with water and brine, dried over $MgSO_4$, filtered and concentrated *in vacuo*. The crude product was purified by silica gel flash column chromatography (0%→15% EtOAc in pentane) to obtain cyclosulfate **39** (26 mg, 48 µmol, 40% over 3 steps) as a colorless oil. $^1$H NMR (500 MHz, $CDCl_3$) δ 7.34 – 7.27 (m, 15H, $CH_{Ar}$), 5.11 – 5.04 (m, 2H, H-1, H-6), 4.78 – 4.72 (m, 4H, 4x CH*H*Ph), 4.53 (s, 2H, 2x CH*H*Ph), 3.85 – 3.79 (m, 2H, H-3, H-7b), 3.71 – 3.66 (m, 1H, H-2), 3.56 (dd, *J* = 9.5, 2.2 Hz, 1H, H-7a), 3.52 (s, 3H, $OCH_3$), 3.28 (dd, *J* = 11.7, 8.2 Hz, 1H, H-4), 2.48 (ddt, *J* = 11.6, 9.5, 2.2 Hz, 1H, H-5). $^{13}$C NMR (126 MHz, $CDCl_3$) δ 138.5, 138.0, 137.6 (3x $C_{qAr}$), 128.7, 128.6, 128.5, 128.4, 128.3, 128.11, 128.08, 128.06, 128.0 ($CH_{Ar}$), 82.0 (C-3), 81.2 (C-1), 80.3 (C-6), 78.1 (C-4), 76.1 (C-2), 75.2, 73.9, 73.3 (3x $CH_2Ph$), 64.0 (C-7), 60.7 ($OCH_3$), 43.1 (C-5). HRMS (ESI) m/z: [M+Na$^+$] calcd for $C_{29}H_{32}O_8SNa$ 563.1716, found 563.1717.

**(3a*R*,4*R*,5*S*,6*R*,7*R*,7a*S*)-4,6-dihydroxy-7-(hydroxymethyl)-5-methoxyhexahydrobenzo[*d*][1,3,2]dioxathiole 2,2-dioxide (6)** Cyclosulfate **39** (21 mg, 39 µmol, 1.0 eq) was dissolved in MeOH/THF (1 mL) and purged with

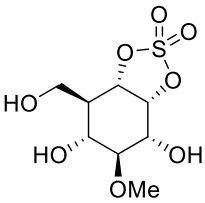


$N_2$. Pd/C (10 wt%, 17 mg, 16 µmol, 0.4 eq) was added to the solution and the reaction mixture was again purged with $N_2$. The reaction mixture was flushed for 5 min with $H_2$ before being left to stir under $H_2$ atmosphere for 5 h. The reaction mixture was flushed with $N_2$ and filtered over whatman filter paper. The filtrate was concentrated *in vacuo* and the crude material was purified by silica gel flash column chromatography (0%→20% MeOH in DCM, silica prewashed with MeOH) to obtain **6** (10 mg, 37 µmol, 94%) as a white solid. $^1$H NMR (500 MHz, MeOD) δ 4.91 (dd, J = 10.2, 5.3 Hz, 1H, H-6), 4.02 (dd, J = 11.2, 2.3 Hz, 1H, H-7A), 3.96 (dd, J = 5.3, 3.4 Hz, 1H, H-1), 3.69 (dd, J = 8.5, 2.7 Hz, 1H, H-7B), 3.68 – 3.65 (m, 1H, H-3), 3.61 (dd, J = 9.8, 3.4 Hz, 1H, H-2), 3.41 (dd, J = 11.2, 8.7 Hz, 1H, H-4), 2.97 (s, 3H, $CH_3$), 2.23 (tt, J = 10.3, 2.5 Hz, 1H, H-5). $^{13}$C NMR (126 MHz, MeOD) δ 80.1 (C-6), 76.2 (C-3), 72.9 (C-2), 70.1 (C-4), 65.3 (C-1), 57.8 (C-7), 47.9 (C-5), 35.1 ($CH_3$). HRMS (ESI) m/z: [M+Na$^+$] calcd for $C_8H_{14}O_8SNa$ 293.2418, found 293.2419.

**(4a*R*,7*S*,8*R*,8a*R*)-7,8-dimethoxy-2-phenyl-4a,7,8,8a-tetrahydro-4H-benzo[*d*][1,3]dioxine (40)**

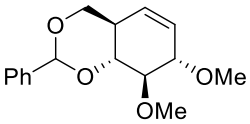


Compound **31** (62 mg, 0.25 mmol, 1.0 eq) was dissolved in anhydrous DMF (5 mL) and cooled to 0°C. NaH (60% dispersion in mineral oil, 30 mg, 0.75 mmol, 3.0 eq) was added and the reaction was stirred for 15 min at 0°C. Subsequently, MeI (39 µL, 0.63 mmol, 2.5 eq) was added dropwise to the solution. The reaction was stirred for 4 h at rt, diluted with $Et_2O$ and quenched with MeOH at 0°C. The organic layer was washed with $H_2O$ and brine (2x), dried over $MgSO_4$, filtered and concentrated *in vacuo*. The crude material was purified by silica gel flash column chromatography (10%→30% EtOAc in pentane) to obtain **40** (64 mg, 0.23 mmol, 91%) as a colorless oil. $^1$H NMR (400 MHz, $CDCl_3$) δ 7.55 – 7.49 (m, 2H, $CH_{Ar}$), 7.40 – 7.33 (m, 3H, $CH_{Ar}$), 5.75 (dt, *J* = 9.9, 3.0 Hz, 1H, H-1), 5.60 (s, 1H, H-8), 5.40 (dt, *J* = 9.9, 1.8 Hz, 1H, H-6), 4.28 (dd, *J* = 10.8, 4.6 Hz, 1H, H-7b), 3.97 (dtd, *J* = 6.4, 3.1, 1.8 Hz, 1H, H-2), 3.74 – 3.60 (m, 6H, H-3, H-4 , H-7a, $OCH_3$), 3.49 (s, 3H, $OCH_3$), 2.71 – 2.61 (m, 1H, H-5). $^{13}$C NMR (101 MHz, $CDCl_3$) δ 138.13 ($C_{qAr}$), 128.8, 128.3 ($CH_{Ar}$), 128.2 (C-1) 126.1 ($CH_{Ar}$), 125.4 (C-6), 101.6 (C-8), 83.1 (C-3), 82.2 (C-2/C-4), 82.1 (C-2/C-4), 70.0 (C-7),

60.5 ($OCH_3$), 57.2 ($OCH_3$), 38.4 (C-5). HRMS (ESI) m/z: [M+Na$^+$] calcd for $C_{16}H_{20}O_4Na$ 299.1259, found 299.1261.

**(1*R*,2*R*,5*S*,6*S*)-2-(hydroxymethyl)-5,6-dimethoxycyclohex-3-en-1-ol (41)** Compound **40** (55 mg, 0.2 mmol, 1.0 eq) was dissolved in DCM (1 mL) and cooled to 0 °C. Water (0.39 mL) and TFA (77 µL, 1.0 mmol, 5.0 eq) were added and the reaction was stirred for 1.5 h at rt after which TLC analysis indicated full conversion of the starting material. The solution was washed with sat. aq. $NaHCO_3$, $H_2O$ and brine, dried over $MgSO_4$, filtered and concentrated *in vacuo*. The crude product was purified by silica gel flash column chromatography (0%→10% MeOH in DCM) to obtain **41** (31 mg, 0.17 mmol, 83%) as a colorless oil. $^1$H NMR (400 MHz, MeOD) δ 5.73 – 5.65 (m, 2H, H-1, H-6), 3.83 – 3.76 (m, 2H, H-2, H-7b), 3.61 (s, 3H, $OCH_3$), 3.61 – 3.57 (m, 1H, H-7A), 3.51 (t, *J* = 9.7 Hz, 1H, H-4), 3.44 (s, 3H, $OCH_3$), 3.19 (dd, *J* = 10.1, 7.8 Hz, 1H, H-3), 2.29 – 2.23 (m, 1H, H-5). $^{13}$C NMR (101 MHz, MeOD) δ 129.7 (C-1/C-6), 127.5 (C-1/C-6), 86.9 (C-3), 83.1 (C-2), 71.6 (C-4), 63.2 (C-7), 60.8 ($OCH_3$), 57.0 ($OCH_3$), 47.7 (C-5). HRMS (ESI) m/z: [M+Na$^+$] calcd for $C_9H_{16}O_4Na$ 211.0946, found 211.0947.

**((((1*R*,4*S*,5*R*,6*R*)-6-(benzyloxy)-4,5-dimethoxycyclohex-2-en-1-yl)methoxy)methyl)benzene (42)** Compound **41** (28 mg, 0.15 mmol, 1.0 eq) was dissolved in anhydrous DMF (3 mL) and cooled to 0°C. NaH (60% dispersion in mineral oil, 18 mg, 0.45 mmol, 3.0 eq) was added and the reaction was stirred for 15 min at 0°C. Subsequently, TBAI (3 mg, 7.5 µmol, 0.05 eq) was added followed by dropwise addition of BnBr (45 µL, 0.38 mmol, 2.5 eq). The reaction was stirred for 5 h at rt, diluted with $Et_2O$ and quenched with MeOH at 0°C. The organic layer was washed with $H_2O$ and brine (2x), dried over $MgSO_4$, filtered and concentrated *in vacuo*. The crude material was purified by silica gel flash column chromatography (5%→25% EtOAc in pentane) to obtain **42** (52 mg, 0.14 mmol, 94%) as a colorless oil. $^1$H NMR (400 MHz, $CDCl_3$) δ 7.38 – 7.23 (m, 10H, $CH_{Ar}$), 5.71 – 5.64 (m, 2H, H-1, H-6), 4.89 (d, *J* = 10.9 Hz, 1H, CH*H*Ph), 4.49 – 4.38 (m, 3H, 3x CH*H*Ph), 3.91 (ddd, *J* = 7.8, 3.2, 1.8 Hz, 1H, H-2), 3.68 (s, 3H, $OCH_3$), 3.57 (t, *J* = 9.8 Hz, 1H, H-4), 3.51 (dd, *J* = 4.1, 1.6 Hz, 2H, H-7a, H-7b), 3.48 (s, 3H, $OCH_3$), 3.42 (dd, *J* = 10.1, 7.8 Hz, 1H, H-3), 2.47 (dddd, *J* = 9.1, 5.6, 2.8, 1.0 Hz, 1H, H-5). $^{13}$C NMR (101 MHz, $CDCl_3$) δ 138.8, 138.4 (2x $C_{qAr}$), 129.4, 128.5, 128.3, 127.9, 127.78, 127.76, 126.5 ($CH_{Ar}$), 86.8 (C-3), 82.5 (C-2), 78.5 (C-4), 75.3, 73.2 (2x $CH_2Ph$), 69.2 (C-7), 60.9 ($OCH_3$), 57.2 ($OCH_3$), 44.3 (C-5). HRMS (ESI) m/z: [M+Na$^+$] calcd for $C_{23}H_{28}O_4Na$ 391.1885, found 391.1887.

**(1*S*,2*S*,3*S*,4*R*,5*S*,6*S*)-4-(benzyloxy)-3-((benzyloxy)methyl)-5,6-dimethoxycyclohexane-1,2-diol (43) and (1*R*,2*R*,3*S*,4*R*,5*S*,6*S*)-4-(benzyloxy)-3-((benzyloxy)methyl)-5,6-dimethoxycyclohexane-1,2-diol (44)** A solution of $NaIO_4$ (39 mg, 0.18 mmol, 1.5 eq) and $RuCl_3{\cdot}H_2O$ (1.7 mg, 8.4 µmol, 0.07 eq) in water (1.0 mL) was added dropwise to an ice-cooled and vigorously stirred solution of cyclohexene **42** (44 mg, 0.12 mmol, 1.0 eq) in EtOAc/MeCN 1:1 (3.6 mL). The reaction was stirred for 2 h at 0°C after which TLC analysis indicated full conversion. The reaction was quenched with sat. aq. $Na_2S_2O_3$ and the aqueous layer was extracted with EtOAc (3x). The combined organic layers were washed with brine, dried over $MgSO_4$, filtered and concentrated *in vacuo*. The crude material was purified by silica gel flash column chromatography (5%→30% acetone in pentane) to obtain **43** (19 mg, 47 µmol, 39%) and **44** (14 mg, 35 µmol, 29%) as white solids.

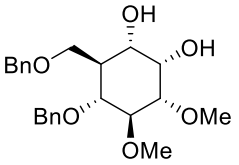


(**43**): $^1$H NMR (400 MHz, $CDCl_3$) δ 7.37 – 7.24 (m, 10H, C*H*$_{Ar}$), 4.85 (d, *J* = 10.8 Hz, 1H, CH*H*Ph), 4.54 – 4.43 (m, 3H, 3x CH*H*Ph), 4.19 (t, *J* = 2.8 Hz, 1H, H-1), 3.85 (dd, *J* = 9.0, 2.7 Hz, 1H, H-7b), 3.63 (s, 5H, H-6, H-7a, OC*H*$_3$), 3.58 (t, *J* = 9.4 Hz, 1H, h-3), 3.51 (s, 3H, OC*H*$_3$), 3.25 (dd, *J* = 11.0, 9.2 Hz, 1H, H-4), 3.22 – 3.16 (s, 1H, OH), 3.05 (dd, *J* = 9.6, 2.8 Hz, 1H, H-2), 2.51 (s, 1H, OH), 2.20 – 2.12 (m, 1H, H-5). $^{13}$C NMR (101 MHz, $CDCl_3$) δ 138.6, 138.1 (2x $C_{qAr}$), 128.7, 128.6, 128.5, 128.23, 128.20, 128.1, 127.91, 127.87, 127.8 (*C*H$_{Ar}$), 84.6 (C-3), 82.3 (C-2), 77.8 (C-4), 75.2 (*C*H$_2$Ph), 73.5 (*C*H$_2$Ph), 70.0 (C-6), 69.6 (C-1), 68.4 (C-7), 61.2 (O*C*H$_3$), 58.2 (O*C*H$_3$), 43.0 (C-5). HRMS (ESI) m/z: [M+H$^+$] calcd for $C_{23}H_{31}O_6$ 403.2121, found 403.2122.

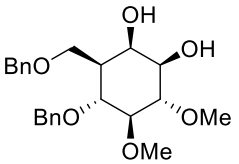


(**44**): $^1$H NMR (400 MHz, $CDCl_3$) δ 7.38 – 7.24 (m, 10H, C*H*$_{Ar}$), 4.87 (d, *J* = 10.7 Hz, 1H, CH*H*Ph), 4.53 – 4.44 (m, 3H, 3x CH*H*Ph), 4.24 (t, *J* = 2.5 Hz, 1H, H-6), 3.88 (dd, *J* = 9.0, 5.5 Hz, 1H, H-7b), 3.78 (dd, *J* = 11.4, 9.1 Hz, 1H, H-4), 3.71 (dd, *J* = 9.0, 3.1 Hz, 1H, H-7a), 3.68 (s, 3H, OC*H*$_3$), 3.66 (s, 3H, OC*H*$_3$), 3.51 – 3.42 (m, 1H, H-2), 3.42 – 3.37 (m, 1H, H-1), 3.34 (s, 1H, 6-OH), 3.16 (t, *J* = 9.0 Hz, 1H, H-3), 2.50 (d, *J* = 4.9 Hz, 1H, 1-OH), 1.67 (dddd, *J* = 10.9, 5.4, 3.1, 2.0 Hz, 1H, H-5). $^{13}$C NMR (101 MHz, $CDCl_3$) δ 138.6, 137.7 (2x $C_{qAr}$), 128.7, 128.6, 128.2, 128.1, 127.91, 127.89 (*C*H$_{Ar}$), 88.8 (C-3), 83.9 (C-2), 77.3 (C-4), 75.5 (*C*H$_2$Ph), 74.4 (C-1), 73.7 (*C*H$_2$Ph), 71.0 (C-6), 69.0 (C-7), 61.3 (O*C*H$_3$), 61.0 (O*C*H$_3$), 43.3 (C-5). HRMS (ESI) m/z: [M+H$^+$] calcd for $C_{23}H_{31}O_6$ 403.2121, found 403.2123.

**(3a*S*,4*R*,5*R*,6*S*,7*R*,7a*R*)-5-(benzyloxy)-4-((benzyloxy)methyl)-6,7-dimethoxyhexahydrobenzo[*d*][1,3,2]dioxathiole 2,2-dioxide (45)** $SOCl_2$ (9.4 µL, 0.13 mmol, 3.5 eq) was added dropwise over 5 min to a ice- cooled solution of diol **43** (15 mg, 37 µmol, 1.0 eq) and $Et_3N$ (21 µL, 0.15 mmol, 4.0 eq) in DCM. The reaction was stirred for 1,5 h at 0°C after which TLC analysis indicated full conversion of the starting material. The reaction mixture was diluted with cold $Et_2O$ and the organic layer was washed with cold water and brine, dried over $MgSO_4$, filtered and concentrated *in vacuo*. Final traces of $Et_3N$ were removed under high vacuum. The crude material was dissolved in EtOAc/ACN 1:1 (3 mL) and a solution of $NaIO_4$ (16 mg, 74 µmol, 2.0 eq) and $RuCl_3{\cdot}H_2O$ (1.0 mg, 3.7 µmol, 0.1 eq) in water (1.5 mL) was added at 0°C. The reaction was stirred for 2,5 h at this temperature and subsequently diluted with EtOAc and quenched with sat. aq. $N_2S_2O_3$. The layers were separated and the aqueous layer was extracted with EtOAc. The combined organic layers were washed with water and brine, dried over $MgSO_4$, filtered and concentrated *in vacuo*. The crude product was purified by silica gel flash column chromatography (0%→15% EtOAc in pentane) to obtain cyclosulfate **45** (13 mg, 27 µmol, 73%) as a colorless oil. $^1$H NMR (400 MHz, $CDCl_3$) δ 7.37 – 7.24 (m, 10H, C*H*$_{Ar}$), 5.21 (dd, *J* = 5.1, 3.4 Hz, 1H, H-1), 5.11 (dd, *J* = 10.0, 5.1 Hz, 1H, H-6), 4.83 (d, *J* = 10.9 Hz, 1H, CH*H*Ph), 4.51 (d, *J* = 10.8 Hz, 1H, CH*H*Ph), 4.49 – 4.45 (m, 1H, CH*H*Ph), 4.42 (d, *J* = 11.7 Hz, 1H, CH*H*Ph), 3.86 (dd, *J* = 9.4, 2.2 Hz, 1H, H-7b), 3.60 (s, 3H, OC*H*$_3$), 3.59 – 3.54 (m, 5H, H-3, H-7a, OC*H*$_3$), 3.49 – 3.44 (m, 1H, H-4), 3.44 – 3.40 (m, 1H, H-2), 2.45 (ddt, *J* = 12.1, 10.1, 2.2 Hz, 1H, H-5). $^{13}$C NMR (101 MHz, $CDCl_3$) δ 138.2, 137.7 (2x $C_{qAr}$), 128.7, 128.6, 128.1, 128.04, 128.02 (*C*H$_{Ar}$), 83.6 (C-3), 80.4 (C-1), 80.2 (C-6), 78.6 (C-4), 75.4 (C-2), 75.2, 73.5 (2x CH*H*Ph), 64.1 (C-7), 60.7 (O*C*H$_3$), 59.6 (O*C*H$_3$), 43.4 (C-5). HRMS (ESI) m/z: [M+Na$^+$] calcd for $C_{23}H_{28}O_8SNa$ 487.1403, found 487.1404.

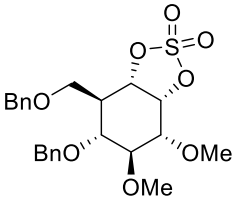

**(3a*S*,4*R*,5*R*,6*S*,7*R*,7a*R*)-5-hydroxy-4-(hydroxymethyl)-6,7-dimethoxyhexahydrobenzo[*d*][1,3,2]dioxathiole 2,2-dioxide (9)** Cyclosulfate **45** (10 mg, 22 µmol, 1.0 eq) was dissolved in MeOH/THF 3:1 (1.0 mL) and purged with $N_2$. Pd/C (10 wt%, 9.4 mg, 8.8 µmol, 0.4 eq) was added to the solution and the reaction mixture was again purged with $N_2$. The reaction mixture was flushed for 5 min with $H_2$ before being left to stir under $H_2$ atmosphere for 4 h. The reaction mixture was flushed with $N_2$ and filtered over whatman filter paper. The filtrate was concentrated *in vacuo* and the crude material was purified by silica gel flash column chromatography (0%→15% MeOH in DCM) to obtain **9** (5.8 mg, 20 µmol, 93%) as a white solid. $^1$H NMR (500 MHz, MeOD) δ 5.45 (dd, *J* = 4.6, 3.4 Hz, 1H, H-1), 5.15 (dd, *J* = 10.2, 4.6 Hz, 1H, H-6), 4.03 (dd, *J* = 11.2, 2.4 Hz, 1H, H-7b), 3.65 (dd, *J* = 10.9, 2.4 Hz, 1H, H-7a), 3.62 (s, 3H, OC*H*$_3$), 3.55 (s, 3H, OC*H*$_3$), 3.49 (dd, *J* = 9.3, 3.4 Hz, 1H, H-2), 3.45 (dd, *J* = 11.6, 9.0 Hz, 1H, H-4), 3.29 (d, *J* = 9.1 Hz, 1H, H-3), 2.13 (ddt, *J* = 11.4, 10.1, 2.5 Hz, 1H, H-5). $^{13}$C NMR (126 MHz, MeOD) δ 84.6 (C-3), 82.8 (C-1), 82.6 (C-6), 79.6 (C-2), 68.2 (C-4), 61.4 (O*C*H$_3$), 59.0 (O*C*H$_3$), 57.0 (C-7), 46.6 (C-5). HRMS (ESI) m/z: [M+Na$^+$] calcd for $C_9H_{16}O_8SNa$ 307.0464, found 307.0465.

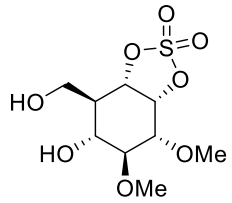


**((1*R*,4*S*,5*S*,6*R*)-4,5-bis(benzyloxy)-6-methoxycyclohex-2-en-1-yl)methanol (46)** Cyclohexene **29** (0.17 g, 0.5 mmol, 1.0 eq) was dissolved in anhydrous DMF (5 mL) and TrtCl (0.17 g, 0.6 mmol, 1.2 eq) were added and the reaction mixture was stirred overnight rt. The reaction mixture was diluted with $Et_2O$ and the organic layer was washed with sat. aq. $NaHCO_3$, water and brine, dried over $Na_2SO_4$ and concentrated *in vacuo*. Final traces of $Et_3N$ were removed under high vacuum and the crude material was used without further purification. The obtained oil was dissolved in anhydrous DMF (10 mL) and cooled to 0°C. NaH (60% dispersion in mineral oil, 30 mg, 0.75 mmol, 1.5 eq) was added and the solution was stirred for 15 min at 0°C. MeI (37 µL, 0.6 mmol, 1.2 eq) was added dropwise and the reaction was stirred for 3 h at rt. The reaction was diluted with $Et_2O$ and quenched with MeOH at 0°C. The organic layer was washed with water and brine (2x), dried over $MgSO_4$, filtered and concentrated *in vacuo*. The obtained crude oil was dissolved in DCM/MeOH 1:3 (2.5 mL) and *p*-TsOH (29 mg, 0.15 mmol, 0.3 eq) was added. The reaction was stirred for 4 h at rt and quenched with $Et_3N$ until pH 6-7 was reached. The reaction mixture was diluted with DCM and the organic layer was washed with sat. aq. $NaHCO_3$ and brine. The crude material was purified by silica gel flash column chromatography (5%→25 EtOAc in pentane) to obtain **46** (0.11 g, 0.31 mmol, 62% over 3 steps) as a colorless oil. $^1$H NMR (500 MHz, $CDCl_3$) δ 7.41 – 7.37 (m, 2H, CH$_{Ar}$), 7.36 – 7.26 (m, 8H, CH$_{Ar}$), 5.74 (ddd, *J* = 10.2, 2.9, 2.2 Hz, 1H, H-6), 5.53 (dt, *J* = 10.1, 2.1 Hz, 1H, H-1), 4.88 (s, 2H, 2x CH*H*Ph), 4.71 – 4.64 (m, 2H, 2x CH*H*Ph), 4.18 (ddt, *J* = 7.6, 3.4, 2.1 Hz, 1H, H-2), 3.78 – 3.71 (m, 3H, H-7a, H-7b, H-3), 3.62 (s, 3H, OCH$_3$), 3.39 (dd, *J* = 10.0, 9.2 Hz, 1H, H-4), 2.46 (dddd, *J* = 11.4, 7.0, 3.2, 1.5 Hz, 1H, H-5), 2.08 (s, 1H, 7-OH). $^{13}$C NMR (126 MHz, $CDCl_3$) δ 138.9, 138.5 (2x C$_{qAr}$), 128.53 (C-6), 128.49, 128.4, 128.1, 128.0, 127.82, 127.78 (CH$_{Ar}$), 127.7 (C-1), 84.8 (C-3), 82.0 (C-4), 80.6 (C-2), 75.2, 72.2 (2x *C*H$_2$Ph), 64.0 (C-7), 61.0 (O*C*H$_3$), 45.7 (C-5). HRMS (ESI) m/z: [M+Na$^+$] calcd for $C_{22}H_{26}O_4Na$ 377.1729, found 377.1731.

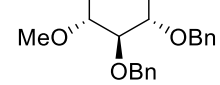


**((((1*S*,2*S*,5*R*,6*R*)-5-((benzyloxy)methyl)-6-methoxycyclohex-3-ene-1,2-diyl)bis(oxy))bis(methylene))dibenzene (47)** Compound **46** (0.1 g, 0.28 mmol, 1.0 eq) was dissolved in anhydrous DMF (5.6 mL) and cooled to 0°C. NaH (60% dispersion in mineral oil, 17 mg, 0.42 mmol, 1.5 eq) was added and the reaction was stirred for 15 min at 0°C. Subsequently, TBAI (5.2 mg, 14 µmol, 0.05 eq) was added followed by dropwise addition of BnBr (40 µL, 0.34 mmol, 1.2 eq). The reaction was stirred for 2 h at rt, diluted with $Et_2O$ and quenched with MeOH at 0°C. The organic layer was washed with $H_2O$ and brine (2x), dried over $MgSO_4$, filtered and concentrated *in vacuo*. The crude material was purified by silica gel flash column chromatography (5%→15% EtOAc in pentane) to obtain **47** (0.12 g, 0.27 mmol, 95%) as a colorless oil. $^1$H NMR (500 MHz, $CDCl_3$) δ 7.41 – 7.37 (m, 2H, CH$_{Ar}$), 7.37 – 7.24 (m, 13H, CH$_{Ar}$), 5.72 – 5.68 (m, 1H, H-6), 5.66 (dt, *J* = 10.2, 1.7 Hz, 1H, H-1), 4.88 (s, 1H, CH*H*Ph), 4.88 (s, 1H, CH*H*Ph), 4.68 (s, 1H, CH*H*Ph), 4.68 (s, 1H, CH*H*Ph), 4.58 – 4.54 (m, 1H, CH*H*Ph), 4.49 (d, *J* = 12.2 Hz, 1H, CH*H*Ph), 4.19 (ddd, *J* = 7.8, 3.5, 1.7 Hz, 1H, H-2), 3.71 (dd, *J* = 10.1, 7.8 Hz, 1H, H-3), 3.58 (dd, *J* = 9.0, 3.4 Hz, 1H, H-7b), 3.55 (dd, *J* = 9.0, 5.0 Hz, 1H, H-7a), 3.50 (s, 3H, OCH$_3$), 3.38 (t, *J* = 9.8 Hz, 1H, H-4), 2.48 – 2.42 (m, 1H, H-5).

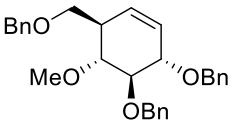

$^{13}$C NMR (126 MHz, $CDCl_3$) δ 139.1, 138.7, 138.4 (3x $C_{qAr}$), 129.2 (C-1), 128.48, 128.45, 128.1, 128.0, 127.9, 127.8, 127.7, 127.6 ($CH_{Ar}$), 127.0 (C-6), 85.3 (C-3), 80.8 (C-2), 80.6 (C-4), 75.3, 73.3, 72.2 (3x $CH_2Ph$), 69.5 (C-7), 61.1 ($OCH_3$), 44.5 (C-5). HRMS (ESI) m/z: [M+Na$^+$] calcd for $C_{29}H_{32}O_4Na$ 467.2198, found 467.2200.

**(3a*R*,4*R*,5*S*,6*R*,7*R*,7a*S*)-4,5-bis(benzyloxy)-7-((benzyloxy)methyl)-6-methoxyhexahydrobenzo[*d*][1,3,2]dioxathiole 2,2-dioxide (50)** A solution of $NaIO_4$ (0.13 g, 0.63 mmol, 2.5 eq) and $RuCl_3{\cdot}H_2O$ (3.7 mg, 18 µmol, 0.07 eq) in water (2.0 mL) was added dropwise to an ice-cooled and vigorously stirred solution of cyclohexene **47** (0.11 g, 0.25 mmol, 1.0 eq) in EtOAc/MeCN 1:1 (7.5 mL). The reaction was stirred for 2 h at 0°C after which TLC analysis indicated full conversion. The reaction was quenched with sat. aq. $Na_2S_2O_3$ and the aqueous layer was extracted with EtOAc (3x). The combined organic layers were washed with brine, dried over $MgSO_4$, filtered and concentrated *in vacuo*. The crude material was purified by silica gel flash column chromatography (5%→30% acetone in pentane) to obtain **48** as white solid. $SOCl_2$ (25 µL, 0.35 mmol, 3.5 eq) was added dropwise over 5 min to an ice- cooled solution of diol **48** (48 mg, 0.1 mmol, 1.0 eq) and $Et_3N$ (56 mg, 0.4 mmol, 4.0 eq) in DCM (5 mL). The reaction was stirred for 1,5 h at 0°C after which TLC analysis indicated full conversion of the starting material. The reaction mixture was diluted with cold $Et_2O$ and the organic layer was washed with cold water and brine, dried over $MgSO_4$, filtered and concentrated *in vacuo*. Final traces of $Et_3N$ were removed under high vacuum. The crude material was dissolved in EtOAc/MeCN 1:1 (8.0 mL) and a solution of $NaIO_4$ (43 mg, 0.2 mmol, 2.0 eq) and $RuCl_3{\cdot}H_2O$ (2.1 mg, 10 µmol, 0.1 eq) in water (4.0 mL) was added at 0°C. The reaction was stirred for 2,5 h at this temperature and subsequently diluted with EtOAc and quenched with sat. aq. $N_2S_2O_3$. The layers were separated and the aqueous layer was extracted with EtOAc. The combined organic layers were washed with water and brine, dried over $MgSO_4$, filtered and concentrated *in vacuo*. The crude product was purified by silica gel flash column chromatography (0%→15% EtOAc in pentane) to obtain cyclosulfate **50** (39 mg, 73 µmol, 29% over 3 steps) as a colorless oil. $^1$H NMR (500 MHz, $CDCl_3$) δ 7.37 – 7.26 (m, 15H, $CH_{Ar}$), 5.07 – 5.02 (m, 2H, H-1, H-6), 4.75 – 4.70 (m, 4H, 4x CH*H*Ph), 4.51 (s, 2H, 2x CH*H*Ph), 3.83 – 3.77 (m, 2H, H-3, H-7b), 3.68 – 3.64 (m, 1H, H-2), 3.57 (dd, *J* = 9.5, 2.2 Hz, 1H, H-7a), 3.48 (s, 3H, $OCH_3$), 3.23 (dd, *J* = 11.7, 8.2 Hz, 1H, H-4), 2.41 (ddt, *J* = 11.6, 9.5, 2.2 Hz, 1H, H-5). $^{13}$C NMR (126 MHz, $CDCl_3$) δ 138.0, 137.8, 137.1 (3x $C_{qAr}$), 128.8, 128.62, 128.61, 128.4, 128.3, 128.11, 128.09, 128.05, 128.0 ($CH_{Ar}$), 81.8 (C-3), 81.0 (C-1), 80.1 (C-6), 77.3 (C-4), 75.7 (C-2), 75.0, 73.8, 73.5 (3x $CH_2Ph$), 64.2 (C-7), 60.9 ($OCH_3$), 43.4 (C-5). HRMS (ESI) m/z: [M+Na$^+$] calcd for $C_{29}H_{32}O_8SNa$ 563.1716, found 563.1717.

**(3a*R*,4*R*,5*R*,6*R*,7*R*,7a*S*)-4,5-dihydroxy-7-(hydroxymethyl)-6-methoxyhexahydrobenzo[*d*][1,3,2]dioxathiole 2,2-dioxide (7)** Cyclosulfate **50** (35 mg, 65 µmol, 1.0 eq) was dissolved in MeOH/THF 4:1 (1.0 mL) and purged with $N_2$. Pd/C (10 wt%, 28 mg, 26 µmol, 0.4 eq) was added to the solution and the reaction mixture was again purged with $N_2$. The reaction mixture was flushed for 5 min with $H_2$ before being left to stir under $H_2$ atmosphere for 5 h. The reaction mixture was flushed with $N_2$ and filtered over whatman filter paper. The filtrate was concentrated *in vacuo* and the crude material was purified by silica gel flash column chromatography (0%→20% MeOH in DCM, silica prewashed with MeOH) to obtain **50** (17 mg, 63 µmol, 97%) as a white solid. $^1$H NMR (500 MHz, MeOD) δ 5.26 (dd, *J* = 4.5, 2.9 Hz, 1H, H-1), 5.18 (dd, *J* = 10.2, 4.5 Hz, 1H, H-6), 3.91 (dd, *J* = 11.1, 2.3 Hz, 1H, H-7b), 3.73 – 3.64 (m, 3H, H-2, H-3, H-7a), 3.60 (s, 3H, $OCH_3$), 3.10 (ddd, *J* = 11.4, 7.8, 1.1 Hz, 1H, H-4), 2.08 (ddt, *J* = 11.4, 10.2, 2.3 Hz, 1H, H-5). $^{13}$C NMR (126 MHz, MeOD) δ 85.8 (C-1), 82.8 (C-6), 78. (C-5), 74.8 (C-3), 70.5 (C-2), 61.0 ($OCH_3$), 56.8 (C-7), 46.1 (C-5). HRMS (ESI) m/z: [M+Na$^+$] calcd for $C_8H_{14}O_8SNa$ 293.2418, found 293.2419.

**((1*R*,4*S*,5*R*,6*R*)-4,5,6-tris(benzyloxy)cyclohex-2-en-1-yl)methanol (51)**

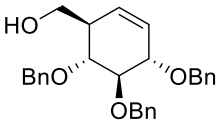


Cyclohexene **29** (0.17 g, 0.5 mmol, 1.0 eq) was dissolved in anhydrous DMF (5 mL) and $Et_3N$ (0.14 mL, 1.0 mmol, 2.0 eq). Subsequently, DMAP (12 mg, 0.1 mmol, 0.1 eq) and TrtCl (0.17 g, 0.6 mmol, 1.2 eq) were added and the reaction mixture was stirred overnight rt. The reaction mixture was diluted with $Et_2O$ and the organic layer was washed with sat. aq. $NaHCO_3$, water and brine, dried over $Na_2SO_4$ and concentrated *in vacuo*. Final traces of $Et_3N$ were removed under high vacuum and the crude material was used without further purification. The obtained oil was dissolved in anhydrous DMF (10 mL) and cooled to 0°C. NaH (60% dispersion in mineral oil, 30 mg, 0.75 mmol 1.5 eq) was added and the solution was stirred for 15 min at 0°C. TBAI (9.2 mg, 25 µmol, 0.05 eq) was added followed by dropwise addition of BnBr (71 µL, 0.6 mmol, 1.2 eq) and the reaction was stirred for 6 h at rt. The reaction was diluted with $Et_2O$ and quenched with MeOH at 0°C. The organic layer was washed with water and brine (2x), dried over $MgSO_4$, filtered and concentrated *in vacuo*. The obtained crude oil was dissolved in DCM/MeOH 1:3 2.5 mL and *p*TsOH (29 mg, 0.15 mmol, 0.3 eq) was added. The reaction was stirred for 4 h at rt and quenched with $Et_3N$ until pH6-7 was reached. The reaction mixture was diluted with DCM and the organic layer was washed with sat. aq. $NaHCO_3$ and brine. The crude material was purified by silica gel flash column chromatography (5%→25 EtOAc in pentane) to obtain cyclohexene **51** (0.15 g, 0.36 mmol, 71% over 3 steps) as a colorless oil. $^1$H NMR (500 MHz, $CDCl_3$) δ 7.39 – 7.24 (m, 15H, $CH_{Ar}$), 5.75 (ddd, *J* = 10.2, 2.9, 2.2 Hz, 1H, H-6), 5.54 (dt, *J* = 10.1, 2.0 Hz, 1H, H-1), 4.99 (d, *J* = 11.2 Hz, 1H, CH*H*Ph), 4.94 (d, *J* = 11.1 Hz, 1H, CH*H*Ph), 4.91 (d, *J* = 11.1 Hz, 1H, CH*H*Ph), 4.71 – 4.62 (m, 3H, 3x CH*H*Ph), 4.23 (ddt, *J* = 7.6, 3.4, 2.0 Hz, 1H, H-2), 3.84 (dd, *J* = 10.1, 7.7 Hz, 1H, H-3), 3.69 – 3.59 (m, 3H, H-4, H-7A, H-7B), 2.52 – 2.43 (m, 1H, H-5), 1.62 (d, *J* = 39.7 Hz, 1H, 7-OH). $^{13}$C NMR (126 MHz, $CDCl_3$) δ 138.9, 138.5, 138.4 (3x $C_{qAr}$), 128.6, 128.53, 128.49, 128.4 ($CH_{Ar}$), 128.30 (C-1/C-6), 128.25 (C-1/C-6), 128.02, 127.98, 127.8, 127.7 ($CH_{Ar}$), 85.2 (C-3), 80.9 (C-2), 78.7 (C-4), 75.3, 75.2, 72.2 (3x $CH_2Ph$), 63.3 (C-7), 45.9 (C-5). HRMS (ESI) m/z: [M+Na$^+$] calcd for $C_{28}H_{30}O_4Na$ 453.2042, found 453.2043.

**((((1*R*,2*R*,3*S*,6*R*)-6-(methoxymethyl)cyclohex-4-ene-1,2,3-triyl)tris(oxy))tris(methylene))tribenzene (52)**

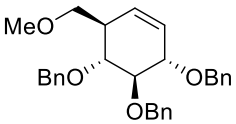


Cyclohexene **51** (0.13 g, 0.3 mmol, 1.0 eq) was dissolved in anhydrous DMF (6 ml) and cooled to 0°C. NaH (60% dispersion in mineral oil, 18 mg, 0.45 mmol, 1.5 eq) was added and the reaction was stirred for 15 min at 0°C. Subsequently, MeI (22 µL, 0.36 mmol, 1.2 eq) was added dropwise. The reaction was stirred for 2 h at rt, diluted with $Et_2O$ and quenched with MeOH at 0°C. The organic layer was washed with $H_2O$ and brine (2x), dried over $MgSO_4$, filtered and concentrated *in vacuo*. The crude material was purified by silica gel flash column chromatography (5%→15% EtOAc in pentane) to obtain **52** (0.12 g, 0.28 mmol, 92%) as a colorless oil. $^1$H NMR (500 MHz, $CDCl_3$) δ 7.38 – 7.24 (m, 15H, $CH_{Ar}$), 5.72 (ddd, *J* = 10.2, 2.8, 2.1 Hz, 1H, H-6), 5.63 (dt, *J* = 10.1, 2.0 Hz, 1H, H-1), 4.96 (d, *J* = 11.1 Hz, 1H, CH*H*Ph), 4.92 (s, 2H, 2x CH*H*Ph), 4.69 (s, 2H, 2x CH*H*Ph), 4.59 (d, *J* = 11.1 Hz, 1H, CH*H*Ph), 4.25 (ddt, *J* = 7.6, 3.7, 2.0 Hz, 1H, H-2), 3.81 (dd, *J* = 10.1, 7.8 Hz, 1H, H-3), 3.66 (t, *J* = 9.9 Hz, 1H, H-4), 3.43 (d, *J* = 3.9 Hz, 2H, H-7a, H-7b), 3.24 (s, 3H, $OCH_3$), 2.53 – 2.47 (m, 1H, H-5). $^{13}$C NMR (126 MHz, $CDCl_3$) δ 139.0, 138.8, 138.6 (3x $C_{qAr}$), 129.2 (C-1), 128.51, 128.49, 128.4, 128.2, 128.01, 127.98, 127.8, 127.7, 127.6 ($CH_{Ar}$), 127.2 (C-6), 85.5 (C-3), 80.9 (C-2), 78.3 (C-4), 75.5, 75.4, 72.2 (3x $CH_2Ph$), 72.0 (C-7), 59.1 ($OCH_3$), 44.5 (C-5). HRMS (ESI) m/z: [M+Na$^+$] calcd for $C_{29}H_{32}O_4Na$ 467.2198, found 467.2199.

**(1*S*,2*S*,3*S*,4*S*,5*R*,6*S*)-3,4,5-tris(benzyloxy)-6-(methoxymethyl)cyclohexane-1,2-diol (53) and (1*R*,2*R*,3*S*,4*S*,5*R*,6*S*)-3,4,5-tris(benzyloxy)-6-(methoxymethyl)cyclohexane-1,2-diol (54)**

A solution of $NaIO_4$ (0.13 g, 0.63 mmol, 2.5 eq) and $RuCl_3{\cdot}H_2O$ (3.7 mg, 18 µmol, 0.07 eq) in water (2.0 mL) was added dropwise to an ice-cooled and vigorously stirred solution of cyclohexene **52** (0.11 g, 0.25 mmol, 1.0 eq) in EtOAc/MeCN 1:1 (7.5 mL). The reaction was stirred for 2 h at 0°C after which TLC analysis indicated full conversion. The reaction was quenched with sat. aq. $Na_2S_2O_3$ and the aqueous layer was extracted with EtOAc (3x). The combined organic layers were washed with brine, dried over $MgSO_4$, filtered and concentrated *in vacuo*. The crude material was purified by silica gel flash column chromatography (5%→30% acetone in pentane) to obtain diols **53** (47 mg, 98 µmol, 39%) and **54** (38 mg, 80 µmol, 32%) as white solids.

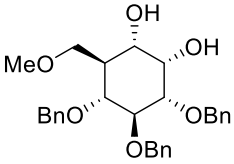

(**53**): $^1$H NMR (400 MHz, $CDCl_3$) δ 7.39 – 7.26 (m, 15H, $CH_{Ar}$), 4.89 (d, *J* = 10.8 Hz, 1H, CH*H*Ph), 4.81 (d, *J* = 10.8 Hz, 1H, CH*H*Ph), 4.70 (s, 1H, CH*H*Ph), 4.70 (s, 1H, CH*H*Ph), 4.56 (d, *J* = 11.8 Hz, 1H, CH*H*Ph), 4.51 (d, *J* = 11.8 Hz, 1H, CH*H*Ph), 4.12 (t, *J* = 2.8 Hz, 1H, H-1), 3.90 – 3.81 (m, 2H, H-3, H-7b), 3.69 (dd, *J* = 9.0, 5.2 Hz, 1H, H-7a), 3.66 – 3.60 (m, 1H, H-6), 3.50 (s, 3H, $OCH_3$), 3.36 (dd, *J* = 9.6, 2.8 Hz, 1H, H-2), 3.11 (dd, *J* = 11.0, 9.3 Hz, 1H, H-4), 3.05 (d, *J* = 6.2 Hz, 1H, 6-OH), 2.59 (s, 1H, 1-OH), 2.10 (tdd, *J* = 10.9, 5.2, 2.6 Hz, 1H, H-5). $^{13}$C NMR (101 MHz, $CDCl_3$) δ 138.9, 138.1, 138.0 (3x $C_{qAr}$), 128.5, 128.43, 128.37, 128.0, 127.93, 127.89, 127.7, 127.64, 127.57 ($CH_{Ar}$), 82.7 (C-3), 79.9 (C-2), 79.6 (C-4), 75.6, 73.4, 72.6 (3x $CH_2Ph$), 70.4 (C-1), 69.4 (C-6), 67.9 (C-7), 60.9 ($OCH_3$), 43.2 (C-5). HRMS (ESI) m/z: [M+Na$^+$] calcd for $C_{29}H_{34}O_6Na$ 501.2253, found 467.2254.

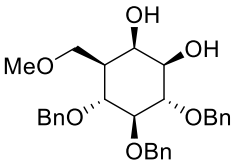

(**54**): $^1$H NMR (500 MHz, $CDCl_3$) δ 7.39 – 7.26 (m, 15H, $CH_{Ar}$), 4.93 (d, *J* = 11.2 Hz, 1H, CH*H*Ph), 4.87 (s, 2H, 2x CH*H*Ph), 4.76 (d, *J* = 11.2 Hz, 1H, CH*H*Ph), 4.57 (d, *J* = 11.8 Hz, 1H, CH*H*Ph), 4.54 (d, *J* = 11.8 Hz, 1H, CH*H*Ph), 4.23 (t, *J* = 2.5 Hz, 1H, H-6), 3.90 (dd, *J* = 9.0, 5.8 Hz, 1H, H-7b), 3.80 – 3.72 (m, 2H, H-2, H-7a), 3.61 (dd, *J* = 11.3, 9.1 Hz, 1H, H-4), 3.51 (s, 3H, $OCH_3$), 3.49 (d, *J* = 10.2 Hz, 1H, H-1), 3.45 (t, *J* = 9.3 Hz, 1H, H-3), 3.23 (s, 1H, 6-OH), 2.38 (s, 1H, 1-OH), 1.66 (dddd, *J* = 11.2, 5.6, 3.1, 2.1 Hz, 1H, H-5). $^{13}$C NMR (126 MHz, $CDCl_3$) δ 138.83, 138.80, 137.8 (3x $C_{qAr}$), 128.69, 128.67, 128.5, 128.14, 128.05, 128.0, 127.9, 127.8, 127.7 ($CH_{Ar}$), 86.5 (C-3), 82.3 (C-2), 79.4 (C-4), 75.8, 75.6 (2x $CH_2Ph$), 74.6 (C-1), 73.7 ($CH_2Ph$), 70.9 (C-6), 68.9 (C-7), 61.2 ($OCH_3$), 43.6 (C-5). HRMS (ESI) m/z: [M+Na$^+$] calcd for $C_{29}H_{34}O_6Na$ 501.2253, found 467.2254.

**(3a*R*,4*R*,5*S*,6*R*,7*R*,7a*S*)-4,5,6-tris(benzyloxy)-7-(methoxymethyl)hexahydrobenzo[*d*][1,3,2]dioxathiole 2,2-dioxide (55)** $SOCl_2$ (21 µL, 0.29 mmol, 3.5 eq) was added dropwise over 5 min to an ice- cooled solution of diol **53** (40 mg, 84 µg, 1.0 eq) and $Et_3N$ (47 µL, 0.34 mmol, 4.0 eq) in DCM (4.2 mL). The reaction was stirred for 1,5 h at 0°C after which TLC analysis indicated full conversion of the starting material. The reaction mixture was diluted with cold $Et_2O$ and the organic layer was washed with cold water and brine, dried over $MgSO_4$, filtered and concentrated *in vacuo*. Final traces of $Et_3N$ were removed under high vacuum. The crude material was dissolved in EtOAc/MeCN 1:1 (6.7 mL) and a solution of $NaIO_4$ (36 mg, 0.17 mmol, 2.0 eq) and $RuCl_3{\cdot}H_2O$ (1.7 mg, 8.4 µmol, 0.1 eq) in water was added at 0°C. The reaction was stirred for 2,5 h at this temperature and subsequently diluted with EtOAc and quenched with sat. aq. $N_2S_2O_3$. The layers were separated and the aqueous layer was extracted with EtOAc. The combined organic layers were washed with water and brine, dried over $MgSO_4$, filtered and concentrated *in vacuo*. The crude product was purified by silica gel flash column chromatography (0%→15% EtOAc in pentane) to obtain cyclosulfate **55** (34 mg, 62 µmol, 74%) as a colorless oil. $^1$H NMR (400 MHz, $CDCl_3$) δ 7.39 – 7.26 (m, 15H, $CH_{Ar}$), 5.08 – 5.00 (m, 2H, H-1, H-6), 4.82 (d, *J* = 11.0 Hz, 1H, CH*H*Ph), 4.79 – 4.73 (m, 3H, 3x CH*H*Ph), 4.71 (d, *J* = 10.9 Hz, 1H, CH*H*Ph), 4.54 (d, *J* = 11.0 Hz, 1H, CH*H*Ph), 3.91 (t, *J* = 7.9 Hz, 1H, H-3), 3.72 (dq, *J* = 7.6, 2.6 Hz, 2H, H-2, H-7b), 3.50 – 3.45 (m, 1H, H-4)), 3.45 – 3.41 (m, 1H, H-7a), 3.27 (s, 3H, $OCH_3$), 2.49 (ddt, *J* = 11.7, 9.5, 2.2 Hz, 1H, H-5). $^{13}$C NMR (101 MHz, $CDCl_3$) δ 138.0, 137.8, 137.0 ($C_{qAr}$), 128.7, 128.52, 128.49, 128.3, 128.2, 127.97, 127.95, 127.89, 127.85 ($CH_{Ar}$), 81.8 (C-3), 80.9 (C-1), 79.8 (C-6), 75.6 (C-2), 75.3 (C-4), 75.1, 74.9, 73.7 (3x $CH_2Ph$), 66.3 (C-7), 58.9 ($OCH_3$), 43.3 (C-5). HRMS (ESI) m/z: [M+Na$^+$] calcd for $C_{29}H_{34}O_8SNa$ 563.1716, found 563.1717.

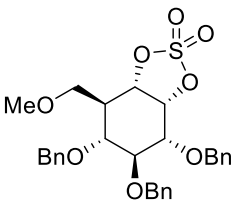

**(3a*R*,4*R*,5*S*,6*R*,7*R*,7a*S*)-4,5,6-trihydroxy-7-(methoxymethyl)hexahydrobenzo[*d*][1,3,2]dioxathiole 2,2-dioxide (8)** Cyclosulfate **55** (30 mg, 55 µmol, 1.0 eq) was dissolved in MeOH/THF 3:1 (2 mL) and purged with $N_2$. Pd/C (10 wt%, 23 mg, 22 µmol, 0.4 eq) was added to the solution and the reaction mixture was again purged with $N_2$. The reaction mixture was flushed for 5 min with $H_2$ before being left to stir under $H_2$ atmosphere for 5 h. The reaction mixture was flushed with $N_2$ and filtered over whatman filter paper. The filtrate was concentrated *in vacuo* and the crude material was purified by silica gel flash column chromatography (0%→20% MeOH in DCM, silica prewashed with MeOH) to obtain **8** (14 mg, 51 µmol, 93%) as a white solid. $^1$H NMR (500 MHz, MeOD) δ 5.28 – 5.24 (m, 1H, H-1), 5.17 (dd, *J* = 10.2, 4.4 Hz, 1H, H-6), 3.81 (dd, *J* = 9.5, 2.5 Hz, 1H, H-7b), 3.66 (dd, *J* = 9.9,

3.5 Hz, 1H, H-2), 3.56 (dd, $J$ = 9.9, 9.2 Hz, 1H, H-3), 3.48 (dd, $J$ = 9.5, 2.5 Hz, 1H, H-7a), 3.38 (s, 3H, $OCH_3$), 3.36 – 3.34 (m, 1H, H-4), 2.16 (ddt, $J$ = 11.3, 10.1, 2.5 Hz, 1H, H-5). $^{13}$C NMR (126 MHz, MeOD) δ 86.2 (C-1), 83.3 (C-6), 74.7 (C-3), 70.4 (C-2), 68.9 (C-4), 67.7 (C-7), 59.4 ($OCH_3$), 45.8 (C-5). HRMS (ESI) m/z: [M+Na$^+$] calcd for $C_8H_{14}O_8SNa$ 293.2418, found 293.2419.

***N*-(Naphtalenyl-2-methoxy)-pentyl-1,2-Dideoxy-1,2-azabicyclo[4.1.0]-carba-α-D-glucose (13).**

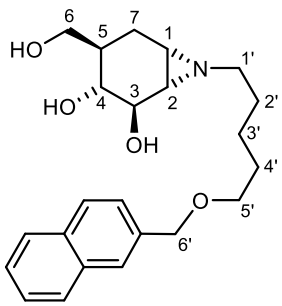

Compound **56** (16 mg, 0.1 mmol), prepared according to literature procedures[1–4], was dissolved in anhydrous DMF (2.0 mL, 0.05 M) followed by the addition of naphtalenyl-2-methoxypentyl iodide (71 mg, 0.2 mmol, 2.0 eq.), prepared according to literature procedures[3,4], and $K_2CO_3$ (138 mg, 0.3 mmol, 3.0 eq.). The reaction was stirred for 3 hours at 100 °C under protective atmosphere. Upon full conversion was observed ($R_f$ 0.7 (MeOH:DCM, 2:8, v:v), the reaction mixture was concentrated and purified by flash column chromatography (2:98 MeOH:DCM → 8:92 MeOH:DCM). A second flash column purification (40:60 acetone:DCM → 60:40 acetone:DCM) yielded the title compound (17.0 mg, 44 µmol, 44%) as a colorless oil. $^1$H NMR (500 MHz, MeOD, HH-COSY, HSQC): δ 7.86 – 7.78 (m, 4H, $CH_{arom}$), 7.51 – 7.43 (m, 3H, $CH_{arom}$), 4.65 (d, $J$ = 0.8 Hz, 2H, H-6'), 3.60 – 3.50 (m, 5H, H-3, H-6, H-5'), 3.07 (dd, $J$ = 10.9, 8.2 Hz, 1H, H-4), 2.32 (dt, $J$ = 11.7, 7.3 Hz, 1H, H-1'), 2.21 (dt, $J$ = 11.7, 7.4 Hz, 1H, H-1'), 2.04 (ddd, $J$ = 14.0, 4.4, 1.2 Hz, 1H, H-7), 1.75 (ddd, $J$ = 6.4, 3.4, 1.2 Hz, 1H, H-2), 1.69 – 1.53 (m, 6H, H-1, H-7, H-2', H-4'), 1.52 – 1.40 (m, 3H, H-5, H-3'); $^{13}$C NMR (126 MHz, MeOD, HSQC): δ 137.4, 134.8, 134.5 ($C_{q\text{-arom}}$), 129.1, 128.9, 128.7, 127.5, 127.2, 126.9 ($CH_{arom}$), 76.3 (C-4), 74.9 (C-3), 74.0 (C-6'), 71.3, 64.5 (C-6, C-5'), 61.6 (C-1'), 45.6 (C-1), 40.9 (C-2), 37.5 (C-5), 30.7, 30.3 (C-2', C-4'), 28.2 (C-7), 25.1 (C-3'); HRMS (ESI) m/z: [M+Na$^+$] calcd for $C_{23}H_{31}NO_4Na$ 408.2151, found 408.2153.

***N*-(Biphenyl-4-methoxy)-pentyl-1,2-Dideoxy-1,2-azabicyclo[4.1.0]-carba-α-D-glucose (14).**

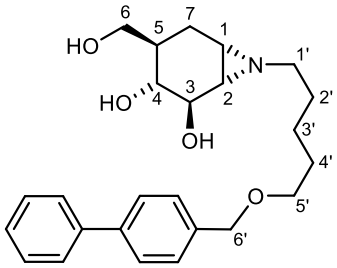

Compound **56** (16 mg, 0.1 mmol), prepared according to literature procedures[1–4], was dissolved in anhydrous DMF (2.0 mL, 0.05 M) followed by the addition of 1,1'-biphenyl-4-methoxypentyl iodide (76 mg, 0.2 mmol, 2.0 eq.), prepared according to literature procedures[3,4], and $K_2CO_3$ (138 mg, 0.3 mmol, 3.0 eq.). The reaction was stirred for 3 hours at 100 °C under protective atmosphere. Upon full conversion was observed ($R_f$ 0.7 (MeOH:DCM, 2:8, v:v), the reaction mixture was concentrated and purified by flash column chromatography (2:98 MeOH:DCM → 8:92 MeOH:DCM). A second flash column purification (40:60 acetone:DCM → 60:40 acetone:DCM) yielded the title compound (10.0 mg, 24 µmol, 24%) as a colorless oil. $^1$H NMR (500 MHz, MeOD, HH-COSY, HSQC): δ 7.64 – 7.57 (m, 4H, $CH_{arom}$), 7.45 – 7.38 (m, 4H, $CH_{arom}$), 7.35 – 7.30 (m, 1H, $CH_{arom}$), 4.54 (s, 2H, H-6'), 3.60 – 3.57 (m, 2H, H-6/H-5'), 3.55 – 3.50 (m, 3H, H-3, H-6/H-5'), 3.07 (dd, $J$ = 10.9, 8.2 Hz, 1H, H-4), 2.33 (dt, $J$ = 11.7, 7.3 Hz, 1H, H-1'), 2.24 (dt, $J$ = 11.7, 7.3 Hz, 1H, H-1'), 2.06 (ddd, $J$ = 14.1, 4.4, 1.3 Hz, 1H, H-7), 1.78 (ddd, $J$ = 6.4, 3.4, 1.2 Hz, 1H, H-1), 1.68 – 1.55 (m, 6H, H-2, H-7, H-2', H-4'), 1.53 – 1.41 (m, 3H, H-5, H-3'); $^{13}$C NMR (126 MHz, MeOD, HSQC): δ 142.1, 141.8, 139.0 ($C_{q\text{-arom}}$), 129.9, 129.4, 128.3, 128.0 ($CH_{arom}$), 76.3 (C-4), 74.9 (C-3), 73.6 (C-6'), 71.3, 64.5 (C-6, C-5'), 61.6 (C-1'), 45.6 (C-2), 40.9 (C-1), 37.5 (C-5), 30.7, 30.3 (C-2', C-4'), 28.2 (C-7), 25.1 (C-3'); HRMS (ESI) m/z: [M+Na$^+$] calcd for $C_{25}H_{33}NO_4Na$ 434.2307, found 434.2308.

***N*-(Adamantly-1-methoxy)-pentyl-1,2-Dideoxy-1,2-azabicyclo[4.1.0]-carba-α-D-glucose (17).**

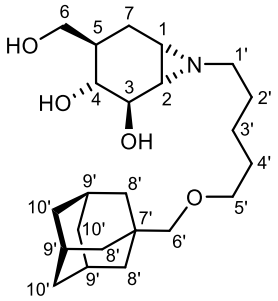

Compound **56** (16 mg, 0.1 mmol), prepared according to literature procedures[1–4], was dissolved in anhydrous DMF (2.0 mL, 0.05 M) followed by the addition of adamantyl-1-methoxypentyl iodide (72 mg, 0.2 mmol, 2.0 eq.), prepared according to literature procedures[3,4], and $K_2CO_3$ (138 mg, 0.3 mmol, 3.0 eq.). The reaction was stirred for 3 hours at 100 °C under protective atmosphere. Upon full conversion was observed ($R_f$ 0.8 (MeOH:DCM, 2:8, v:v), the reaction mixture was concentrated and purified by flash column chromatography (2:98 MeOH:DCM → 8:92 MeOH:DCM) yielded the title compound (16.3 mg, 41 µmol, 41%) as a colorless oil. $^1$H NMR (500 MHz, MeOD, HH-COSY, HSQC): δ 3.59 (d, *J* = 4.9 Hz, 2H, H-6), 3.53 (d, *J* = 8.2 Hz, 1H, H-3), 3.39 (t, *J* = 6.4 Hz, 2H, H-5'), 3.09 – 3.07 (m, 1H, H-4), 2.97 (s, 2H, H-6'), 2.36 (dt, *J* = 11.7, 7.2 Hz, 1H, H-1'), 2.23 (dt, *J* = 11.7, 7.4 Hz, 1H, H-1'), 2.07 (ddd, *J* = 14.2, 4.5, 1.3 Hz, 1H, H-7), 1.95 (p, *J* = 3.1 Hz, 3H, H-9', H-9', H-9'), 1.82 – 1.73 (m, 4H, H-10', H-10', H-10', H-1/H-2), 1.71 – 1.66 (m, 4H, H-10', H-10', H-10'), 1.63 – 1.54 (m, 12H, H-1/H-2, H-7, H-2', H-4', H-8', H-8', H-8'), 1.53 – 1.47 (m, 1H, H-5), 1.44 – 1.38 (m, 2H, H-3'); $^{13}$C NMR (126 MHz, MeOD, HSQC): δ 83.1 (C-6'), 76.3 (C-4), 74.9 (C-3), 72.5 (C-5'), 64.5 (C-6), 61.7 (C-1'), 45.6, 40.9 (C-1, C-2), 40.9 (C-2'/C-4'/C-8'), 38.4 (C-10'), 37.5 (C-5), 35.2 (C-7'), 30.7 (C-2'/C-4'/C-8'), 30.4 (C-2'/C-4'/C-8'), 30.2 (C-9'), 28.2 (C-7), 25.2 (C-3'); HRMS (ESI) m/z: [M+Na$^+$] calcd for $C_{23}H_{39}NO_4Na$ 416.2777, found 416.2778.

***N*-(Naphtalenyl-1-methoxy)-pentyl-1,2-Dideoxy-1,2-azabicyclo[4.1.0]-carba-α-D-glucose (18).**

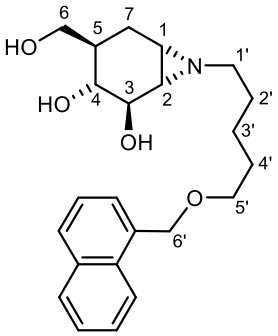

Compound **56** (16 mg, 0.1 mmol), prepared according to literature procedures[1–4], was dissolved in anhydrous DMF (2.0 mL, 0.05 M) followed by the addition of naphtalenyl-1-methoxypentyl bromide (61 mg, 0.2 mmol, 2.0 eq.), prepared according to literature procedures[3,4], and $K_2CO_3$ (138 mg, 0.3 mmol, 3.0 eq.). The reaction was stirred for 3 hours at 100 °C under protective atmosphere. Upon full conversion was observed ($R_f$ 0.7 (MeOH:DCM, 2:8, v:v), the reaction mixture was concentrated and purified by flash column chromatography (2:98 MeOH:DCM → 8:92 MeOH:DCM). A second flash column purification (40:60 acetone:DCM → 70:30 acetone:DCM) yielded the title compound (14.5 mg, 38 µmol, 38%) as a colorless oil. $^1$H NMR (500 MHz, MeOD, HH-COSY, HSQC): δ 8.14 – 8.11 (m, 1H, $CH_{arom}$), 7.90 – 7.81 (m, 2H, $CH_{arom}$), 7.55 – 7.41 (m, 4H, $CH_{arom}$), 4.94 (d, *J* = 1.9 Hz, 2H, H-6'), 3.59 – 3.55 (m, 4H, H-6, H-5'), 3.51 (d, *J* = 8.2 Hz, 1H, H-3), 3.06 (dd, *J* = 10.9, 8.2 Hz, 1H, H-4), 2.28 (dt, *J* = 11.7, 7.2 Hz, 1H, H-1'), 2.14 (dt, *J* = 11.7, 7.4 Hz, 1H, H-1'), 2.01 (ddd, *J* = 14.0, 4.5, 1.2 Hz, 1H, H-7), 1.73 – 1.68 (m, 1H, H-2, H-2'/H-4'), 1.67 – 1.57 (m, 2H), 1.57 – 1.36 (m, 7H, H-1, H-5, H-7, H-3', H-2'/H-4'); $^{13}$C NMR (126 MHz, MeOD, HSQC): δ 135.3, 135.2, 133.2 ($C_{q\text{-}arom}$), 129.7, 129.5, 127.7, 127.1, 126.8, 126.2, 125.2 ($CH_{arom}$), 76.3 (C-4), 74.9 (C-3), 72.4 (C-6'), 71.1, 64.5 (C-6, C-5'), 61.5 (C-1'), 45.6 (C-1), 40.9 (C-2), 37.5 (C-5), 30.7, 30.2 (C-2', C-4'), 28.2 (C-7), 25.0 (C-3'); HRMS (ESI) m/z: [M+Na$^+$] calcd for $C_{23}H_{31}NO_4Na$ 408.2151, found 408.2152.

# NMR Data; spectra of new and selected compounds

$^{1}$H NMR, 400MHz, MeOD of **30**

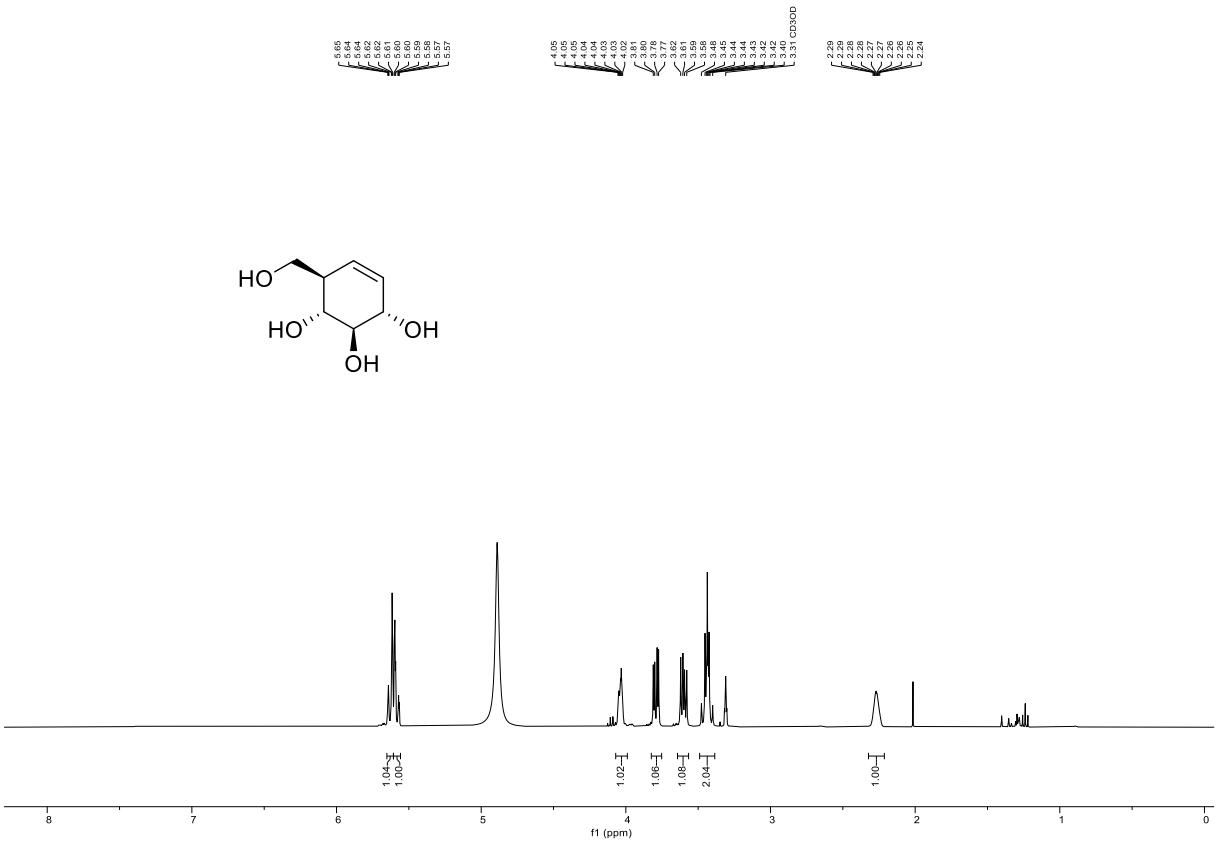


$^{13}$C NMR, 101MHz, MeOD of **30**

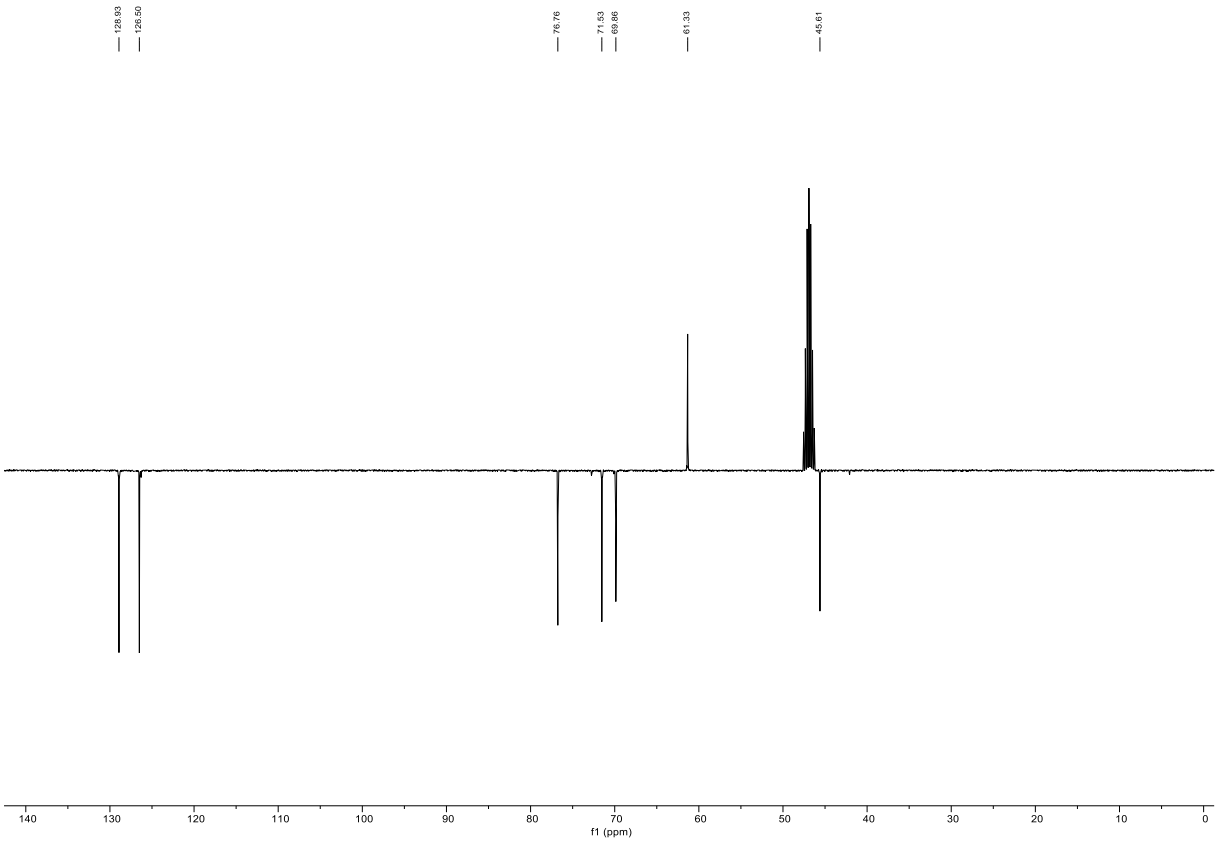

HH-COSY NMR, MeOD of **30**

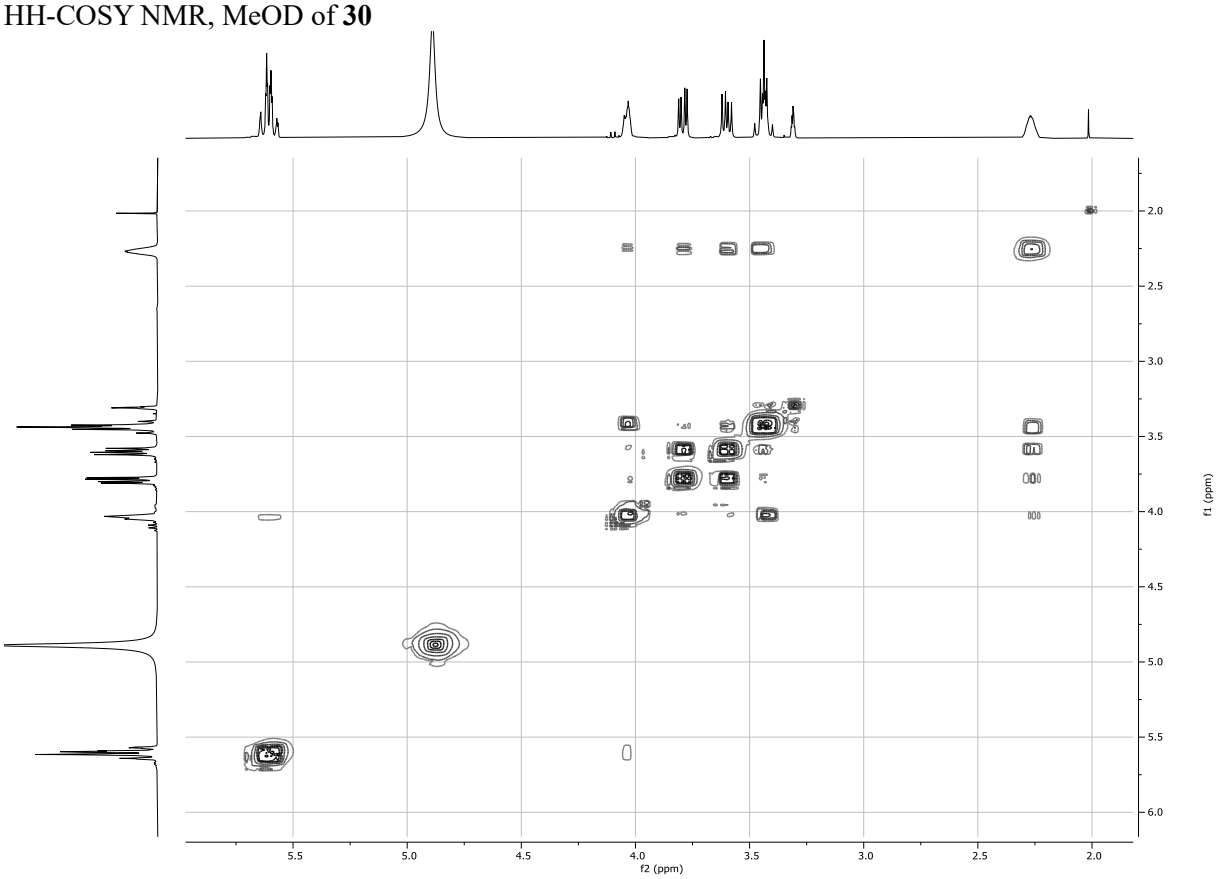


HSQC NMR, MeOD of **30**

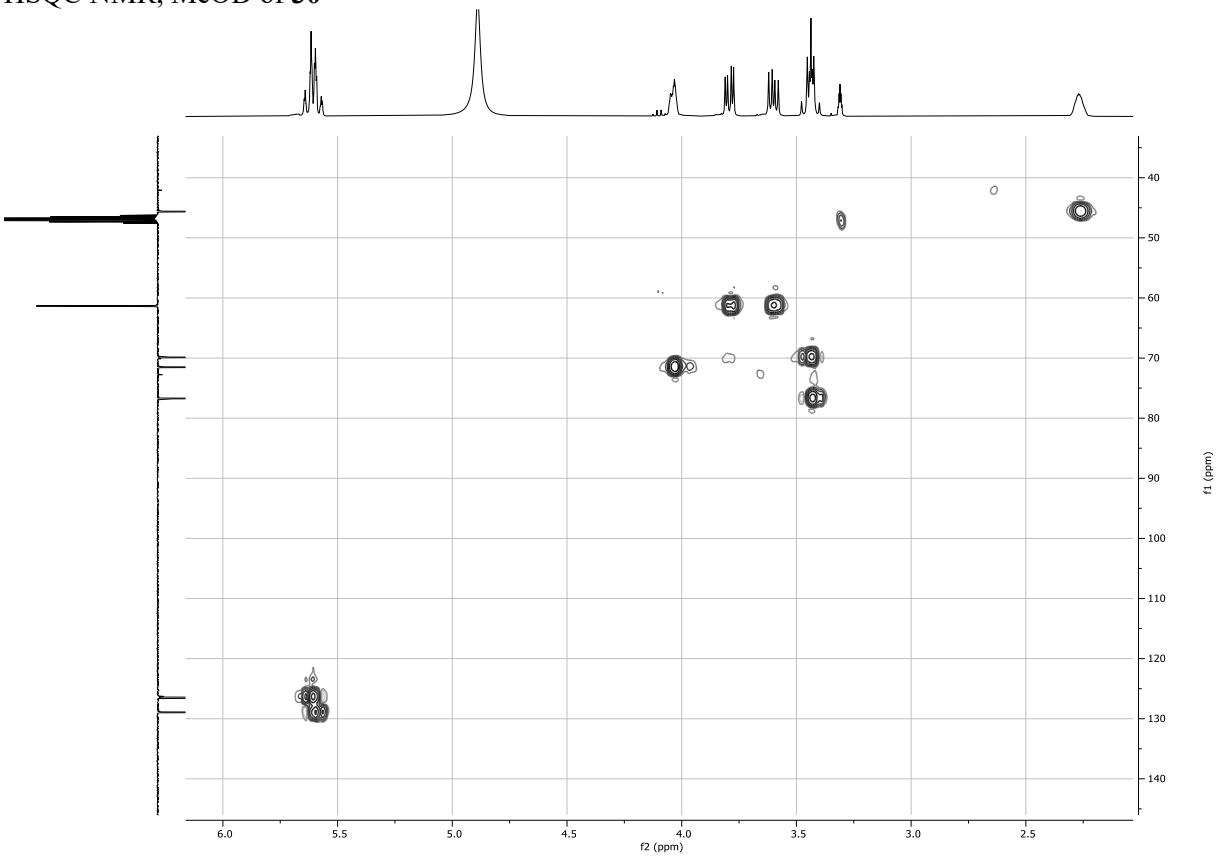

$^{1}$H NMR, 400MHz, $CDCl_3$ of **31**

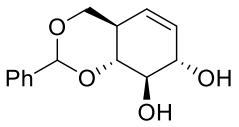


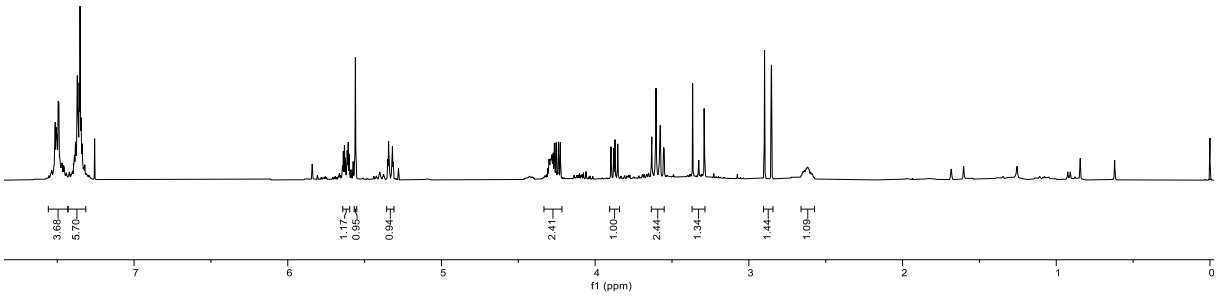


$^{13}$C NMR, 101MHz, $CDCl_3$ of **31**

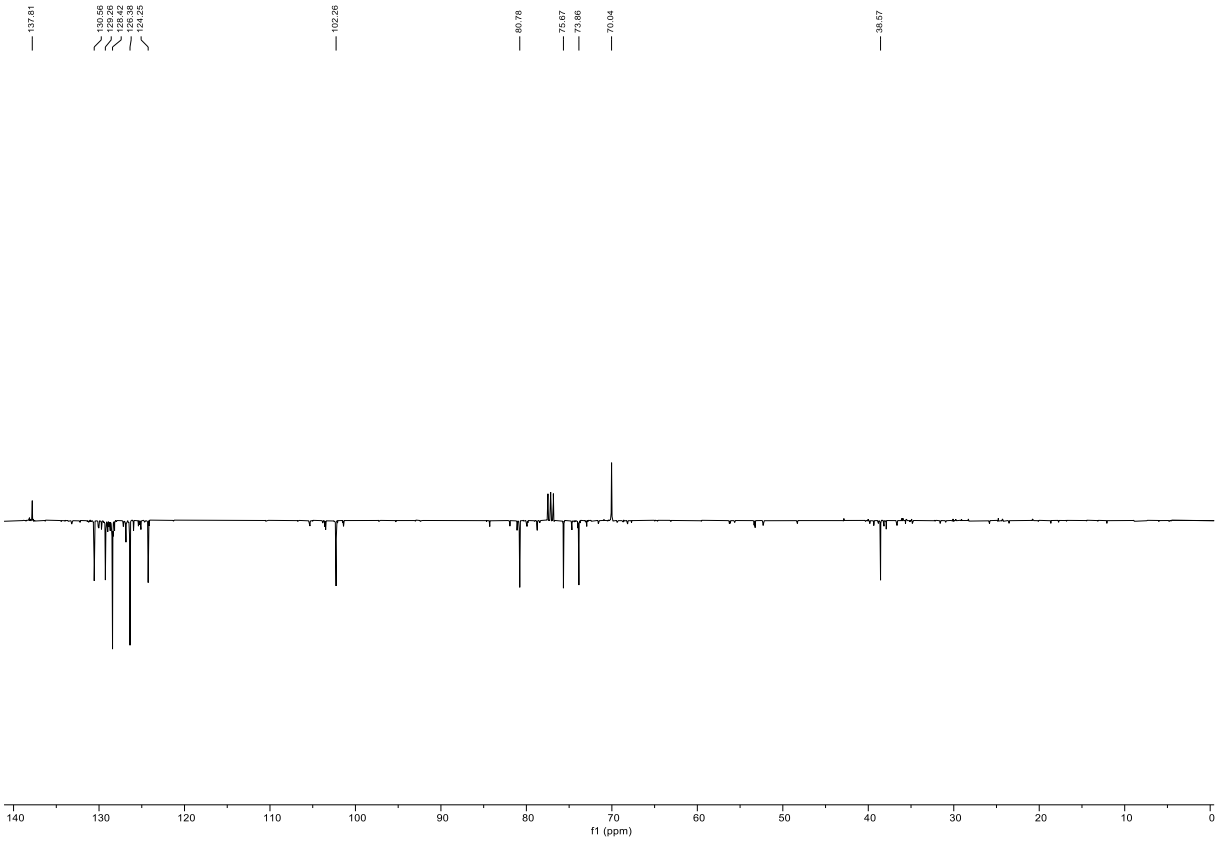

HH-COSY NMR, $CDCl_3$ of **31**

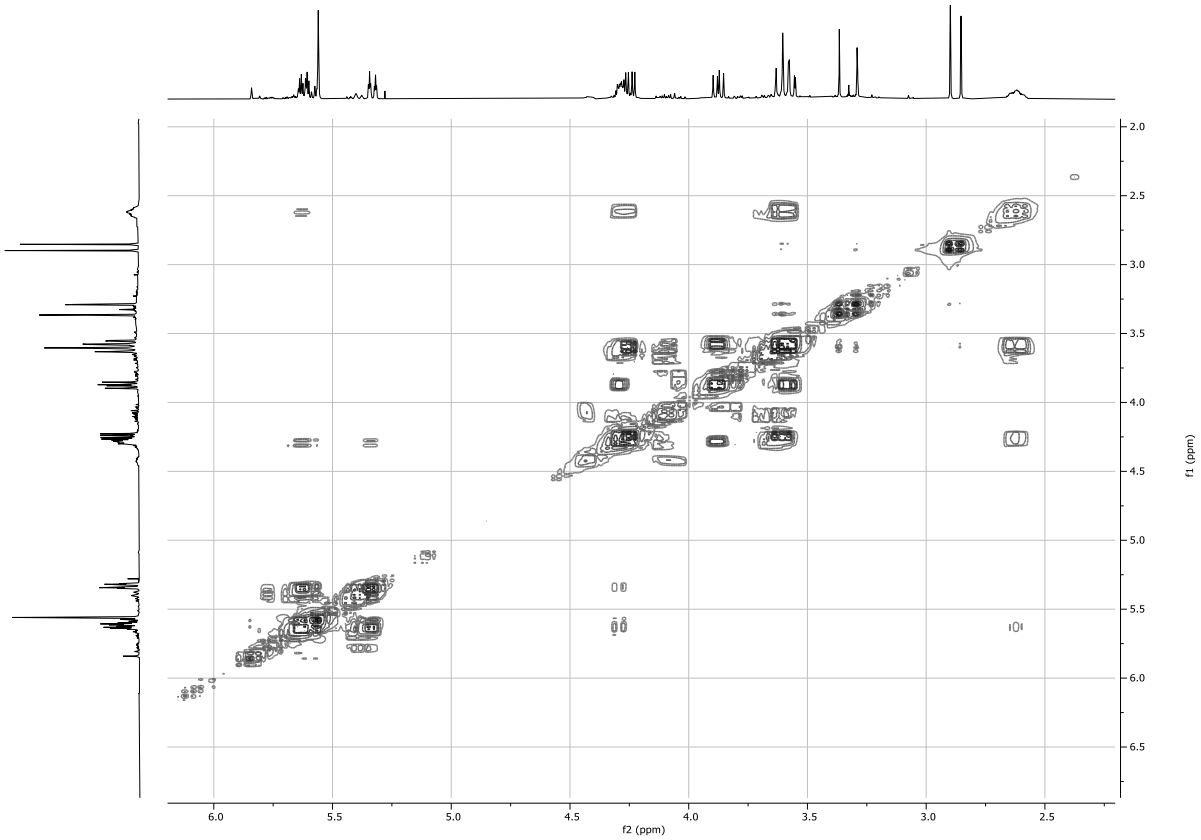


HSQC NMR, $CDCl_3$ of **31**

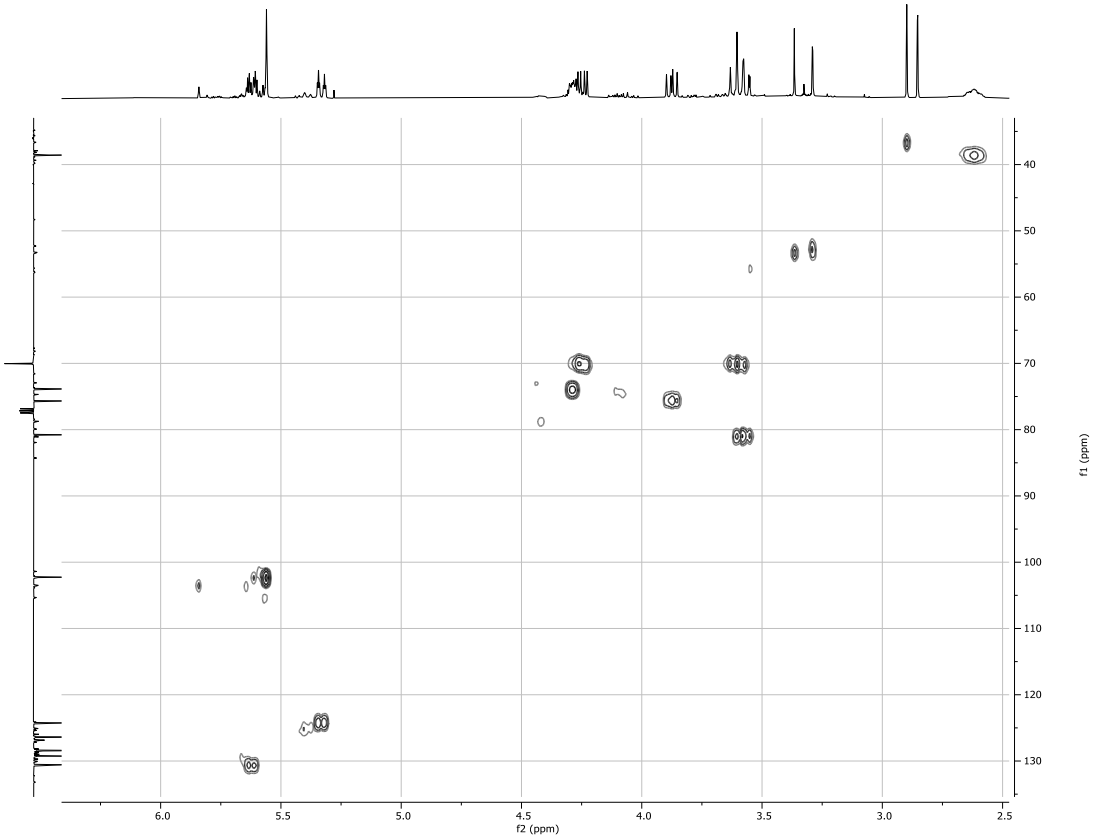

$^{1}$H NMR, 500MHz, $CDCl_3$ of **32**

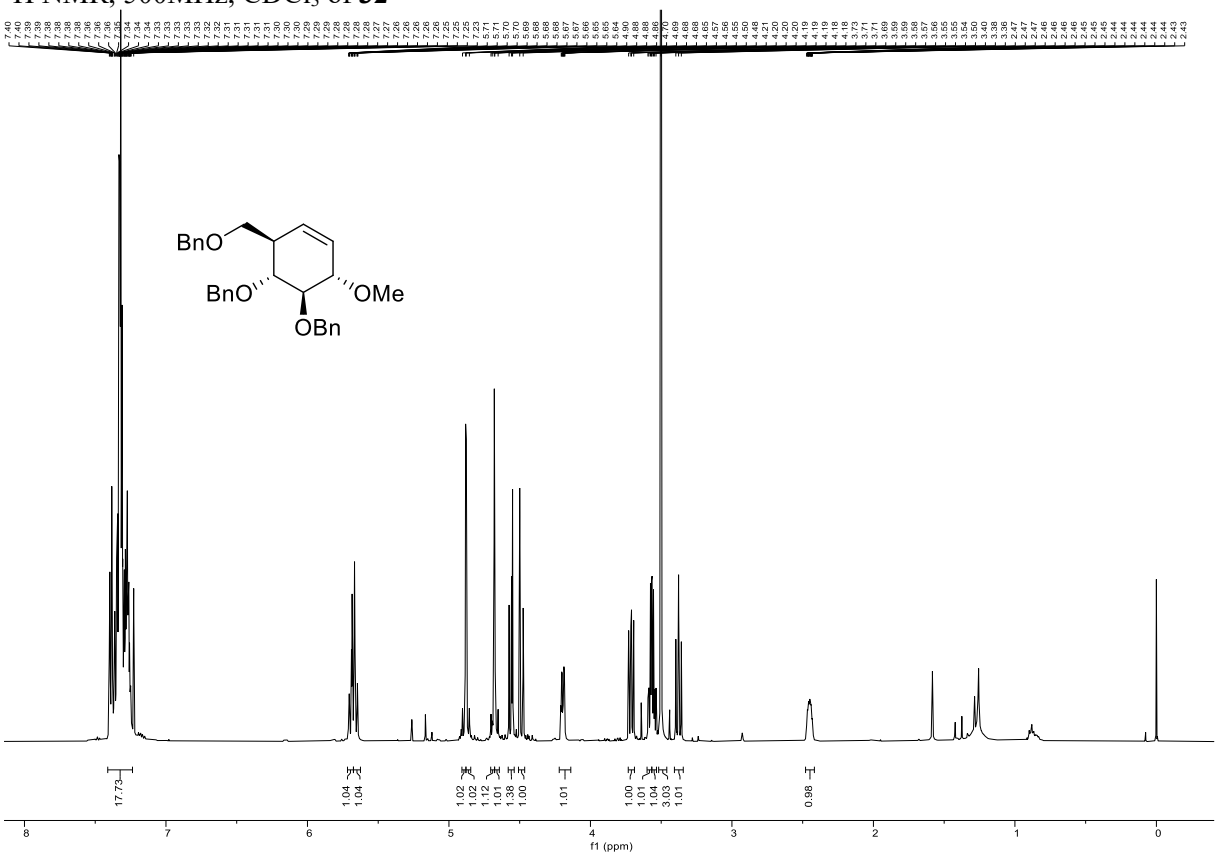


$^{13}$C NMR, 126MHz, $CDCl_3$ of **32**

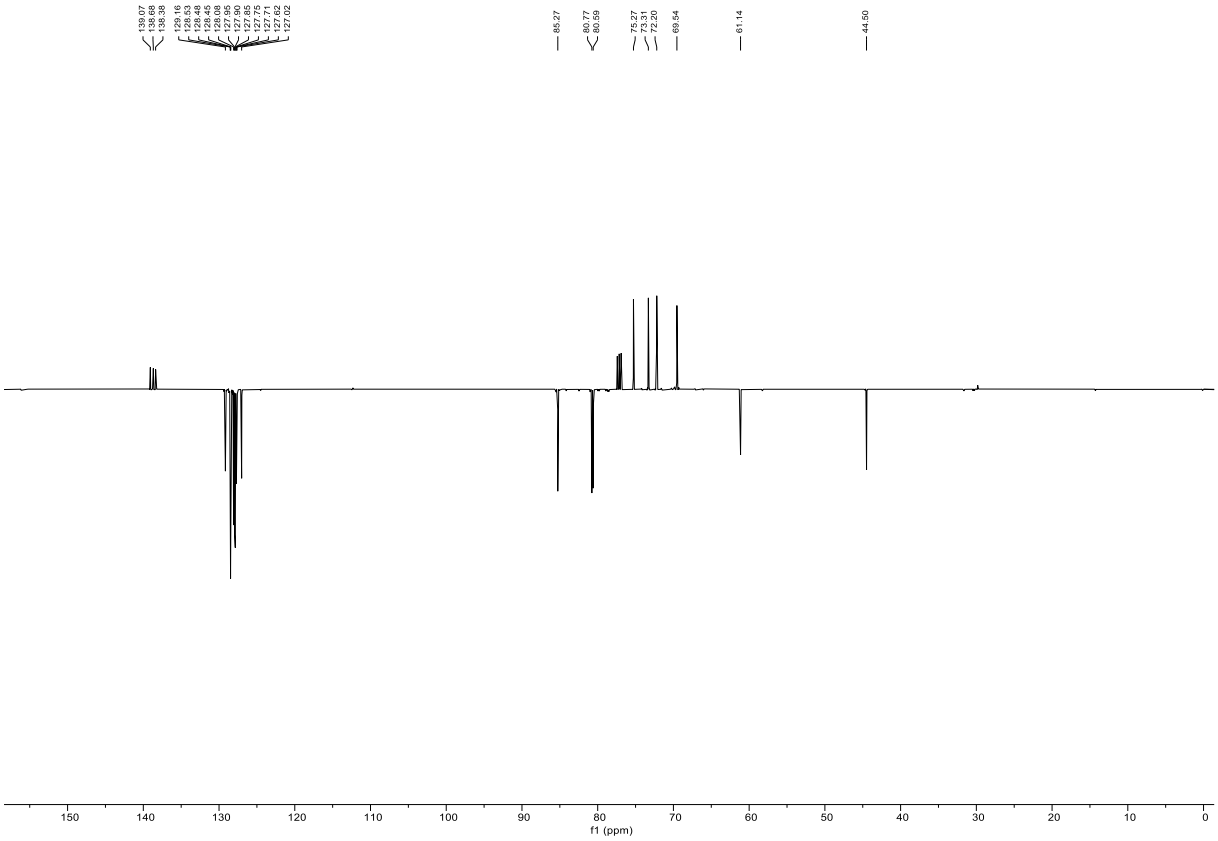

HH-COSY NMR, $CDCl_3$ of **32**

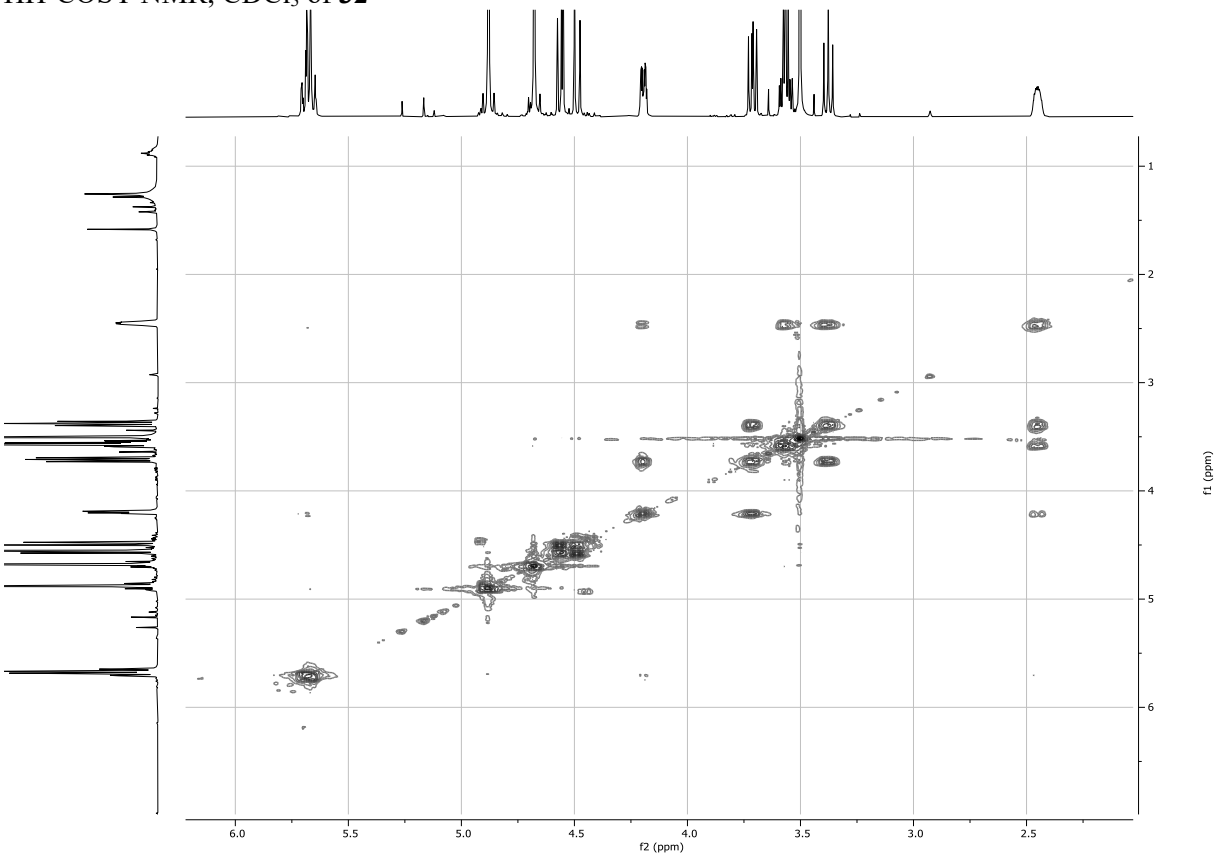


HSQC NMR, $CDCl_3$ of **32**

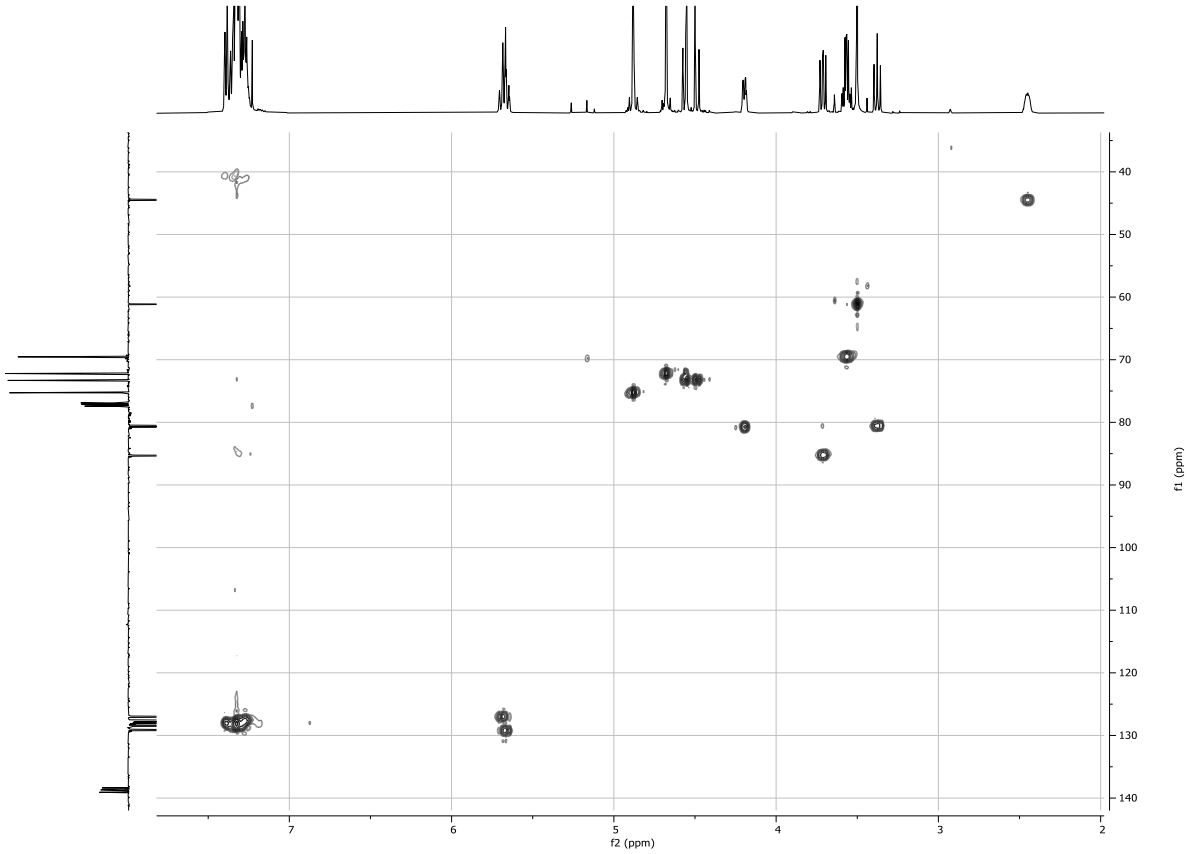

$^{1}$H NMR, 500MHz, $CDCl_3$ of **38**

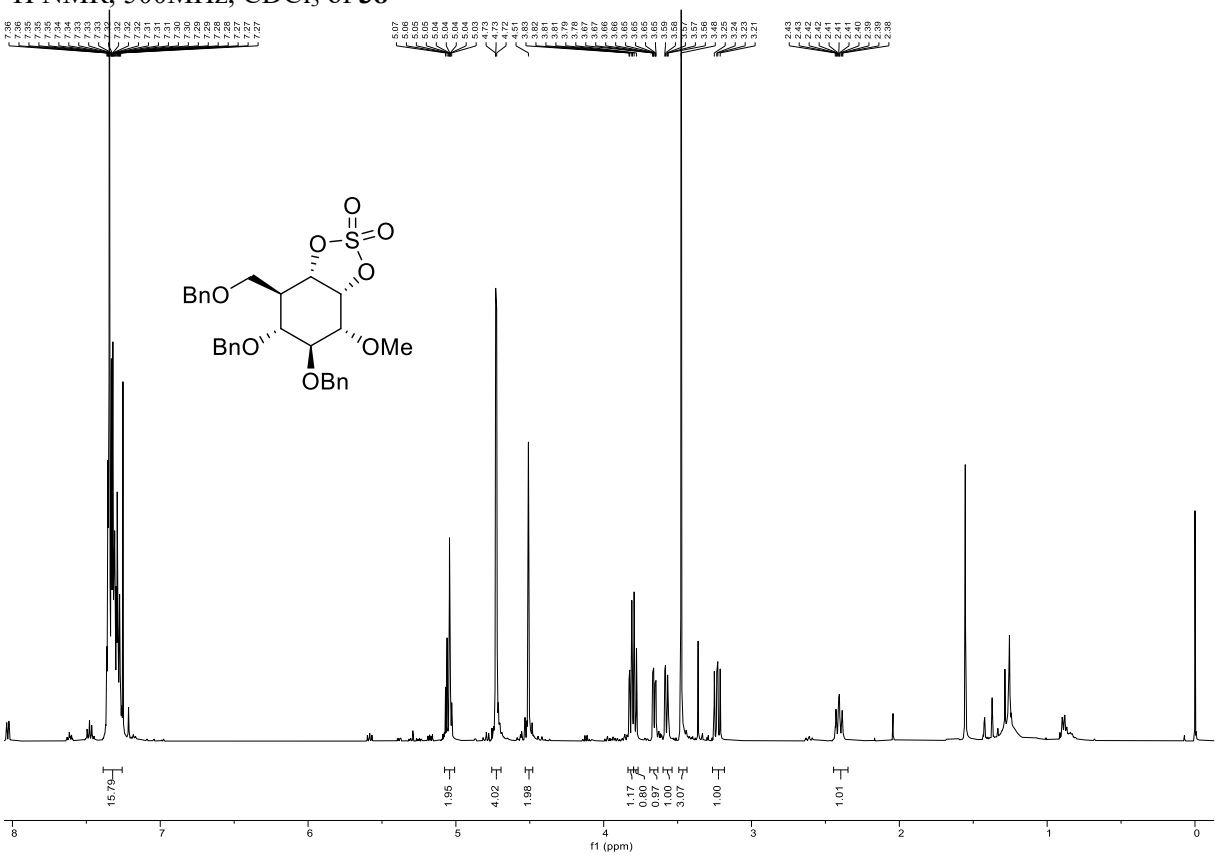


$^{13}$C NMR, 126MHz, $CDCl_3$ of **38**

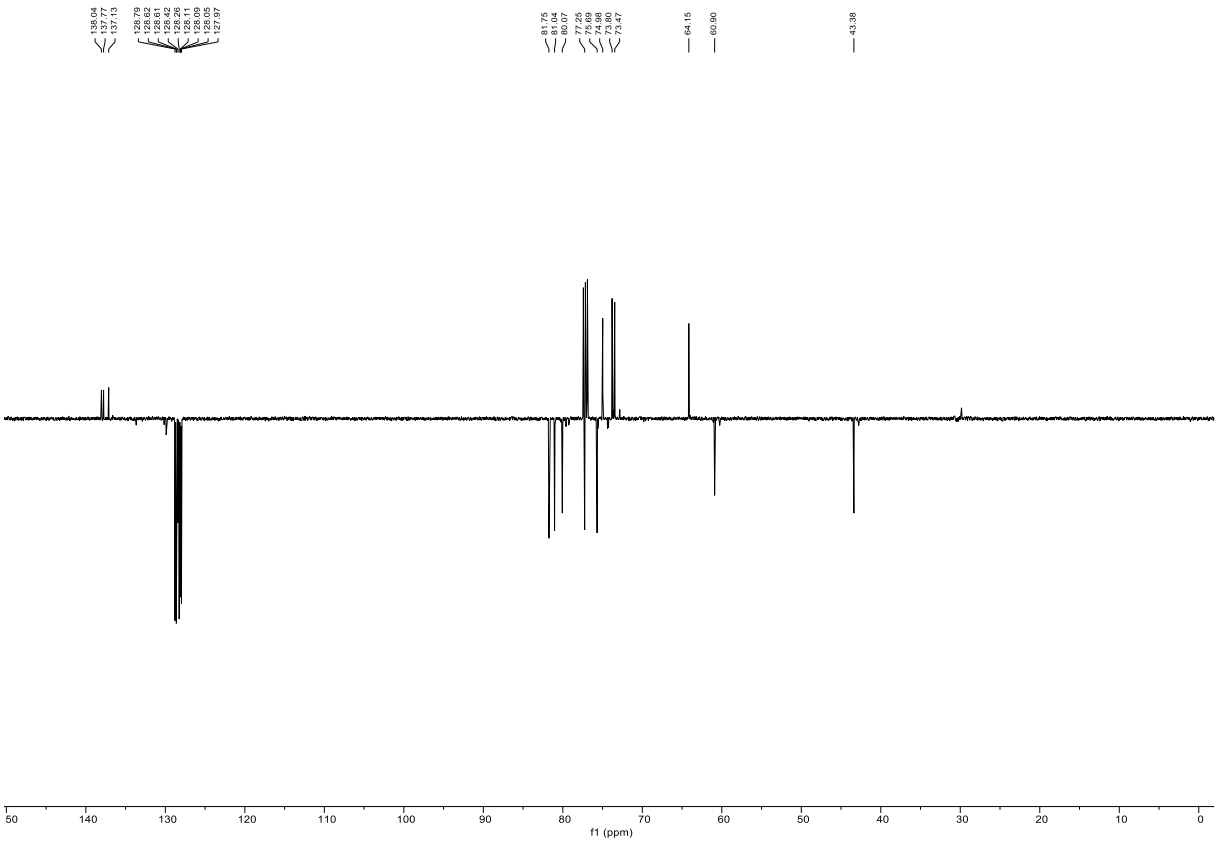

HH-COSY NMR, $CDCl_3$ of **38**

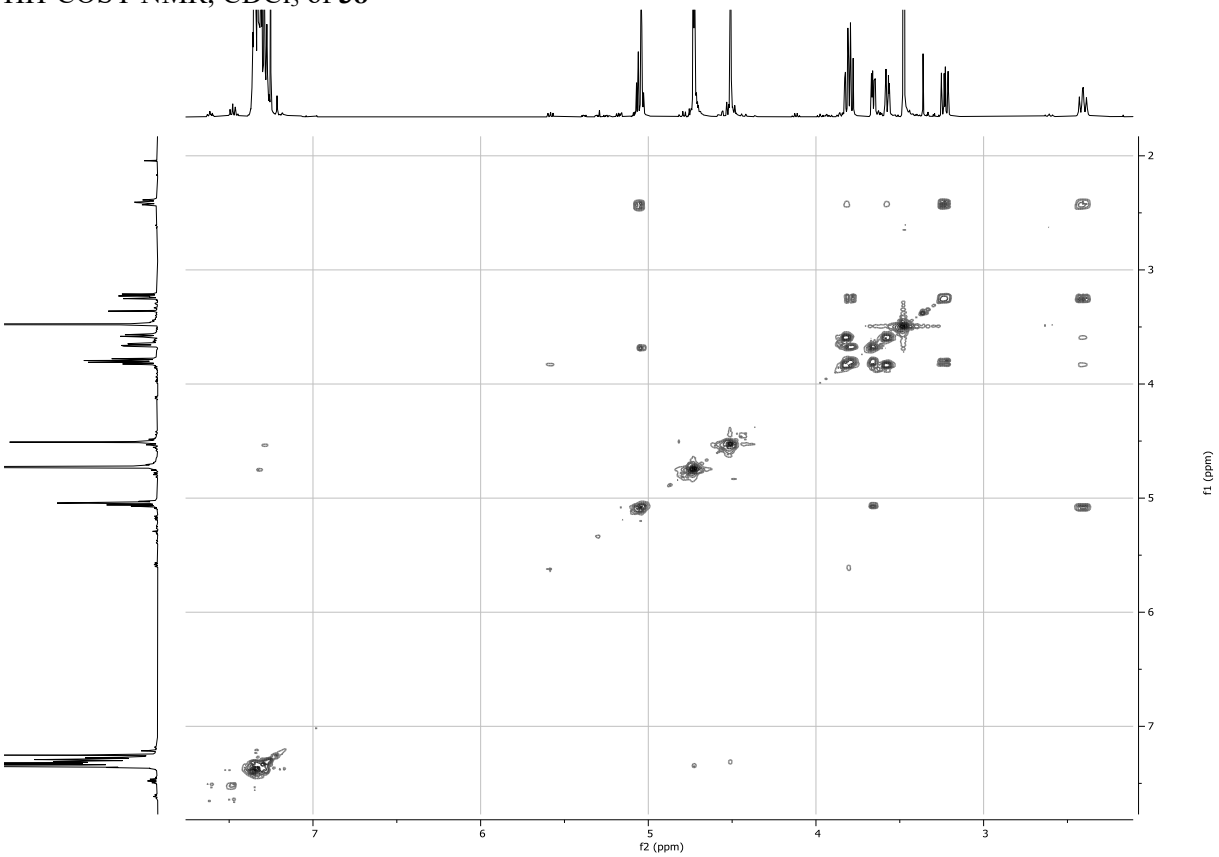


HSQC NMR, $CDCl_3$ of **38**

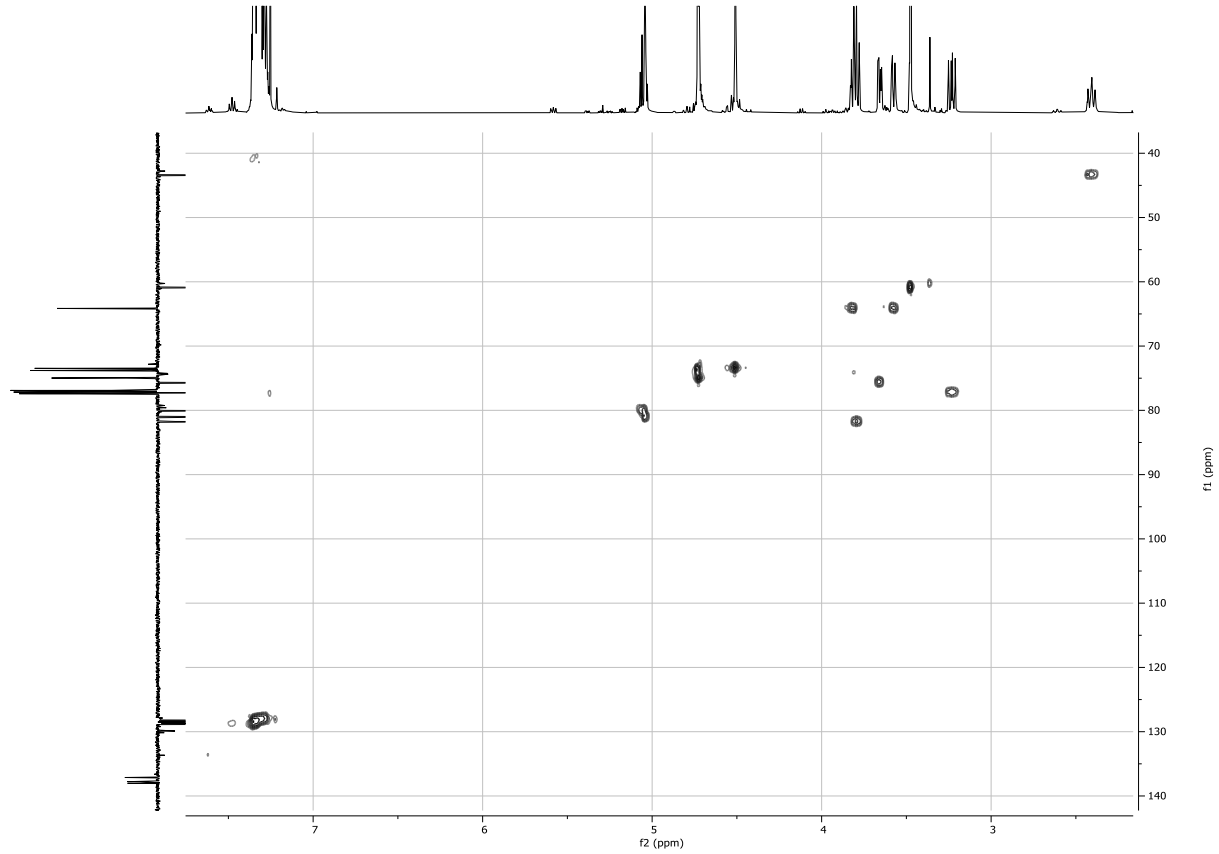

$^{1}$H NMR, 500MHz, MeOD of **5**

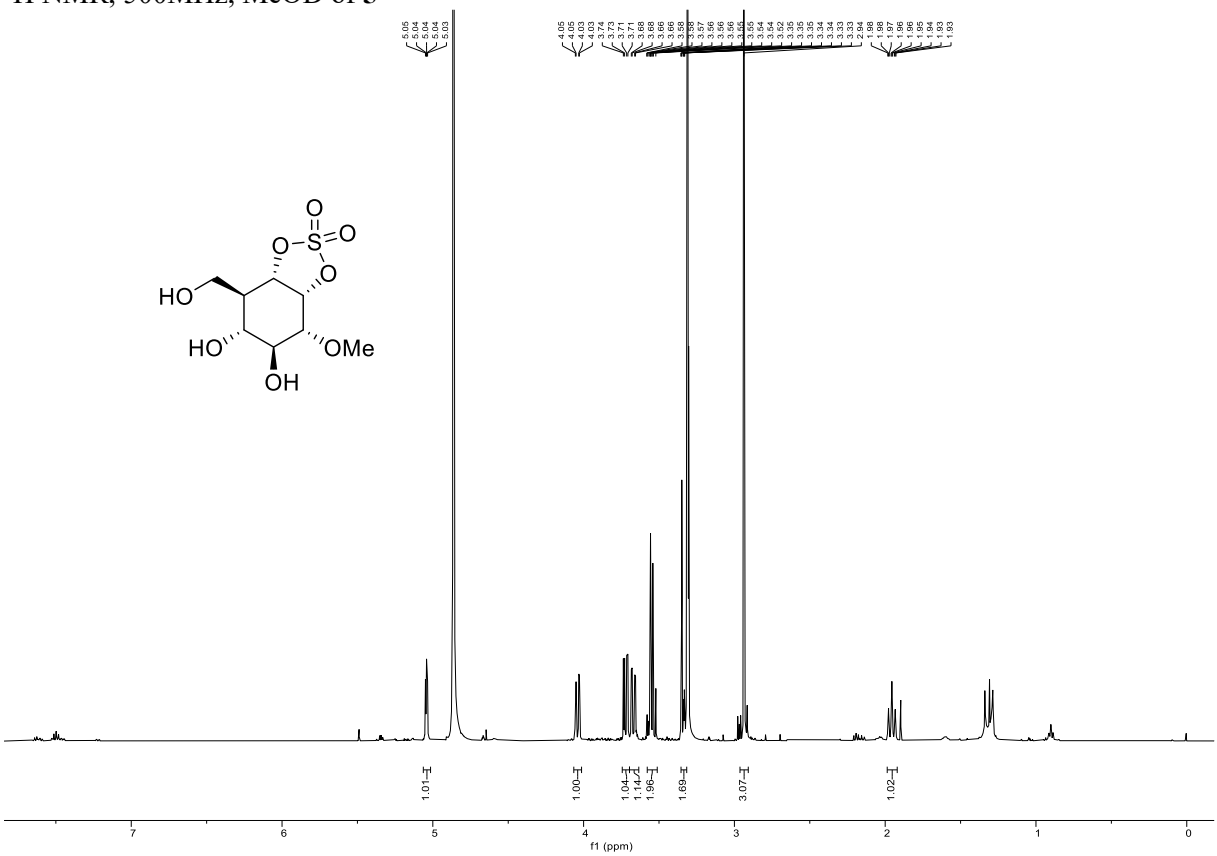


$^{13}$C NMR, 126MHz, MeOD of **5**

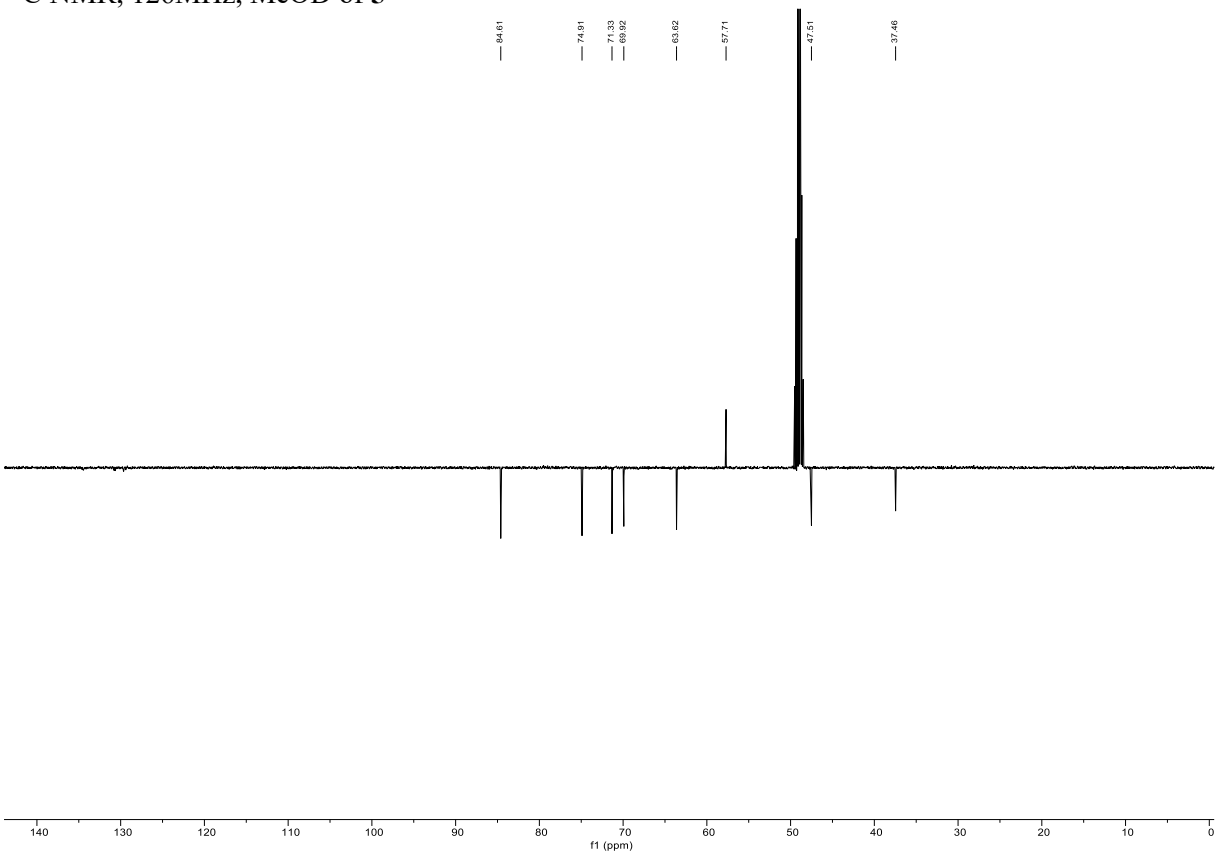

HH-COSY NMR, MeOD of **5**

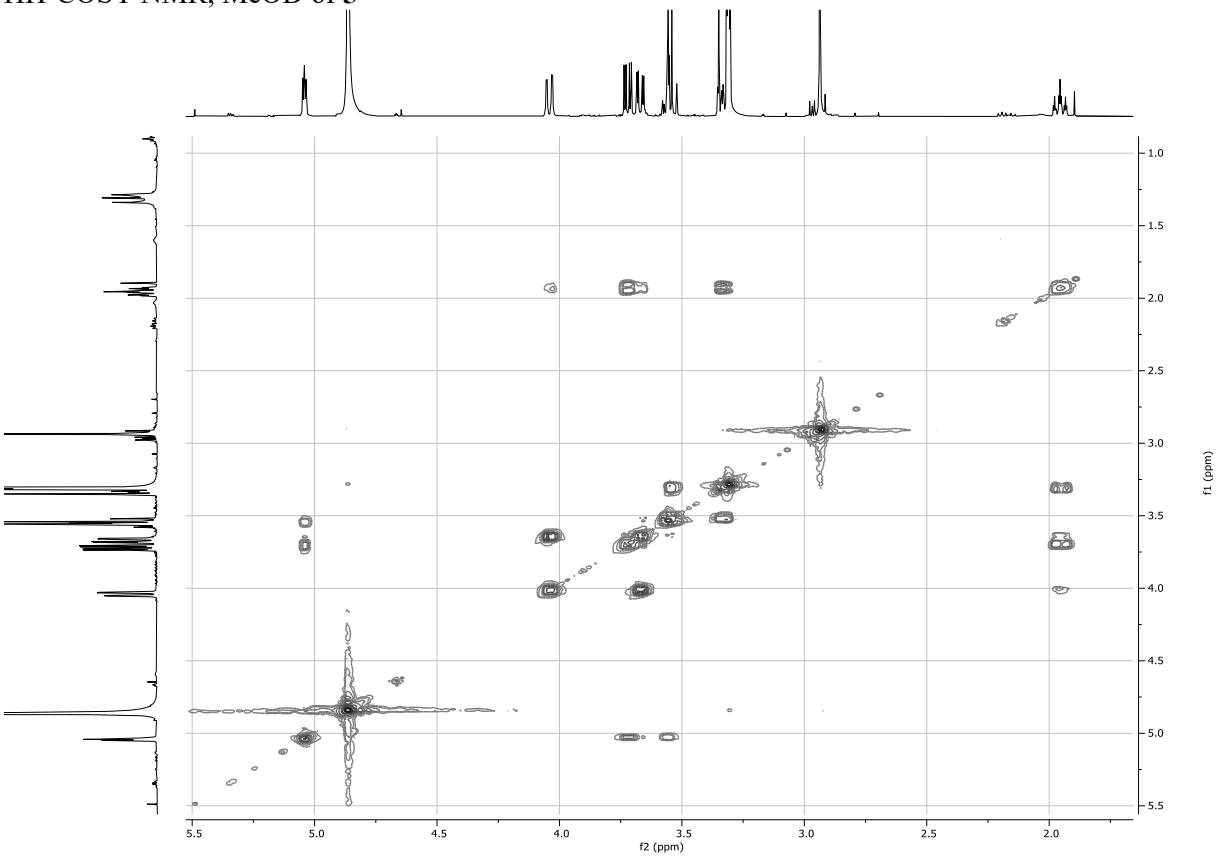


HSQC NMR, MeOD of **5**

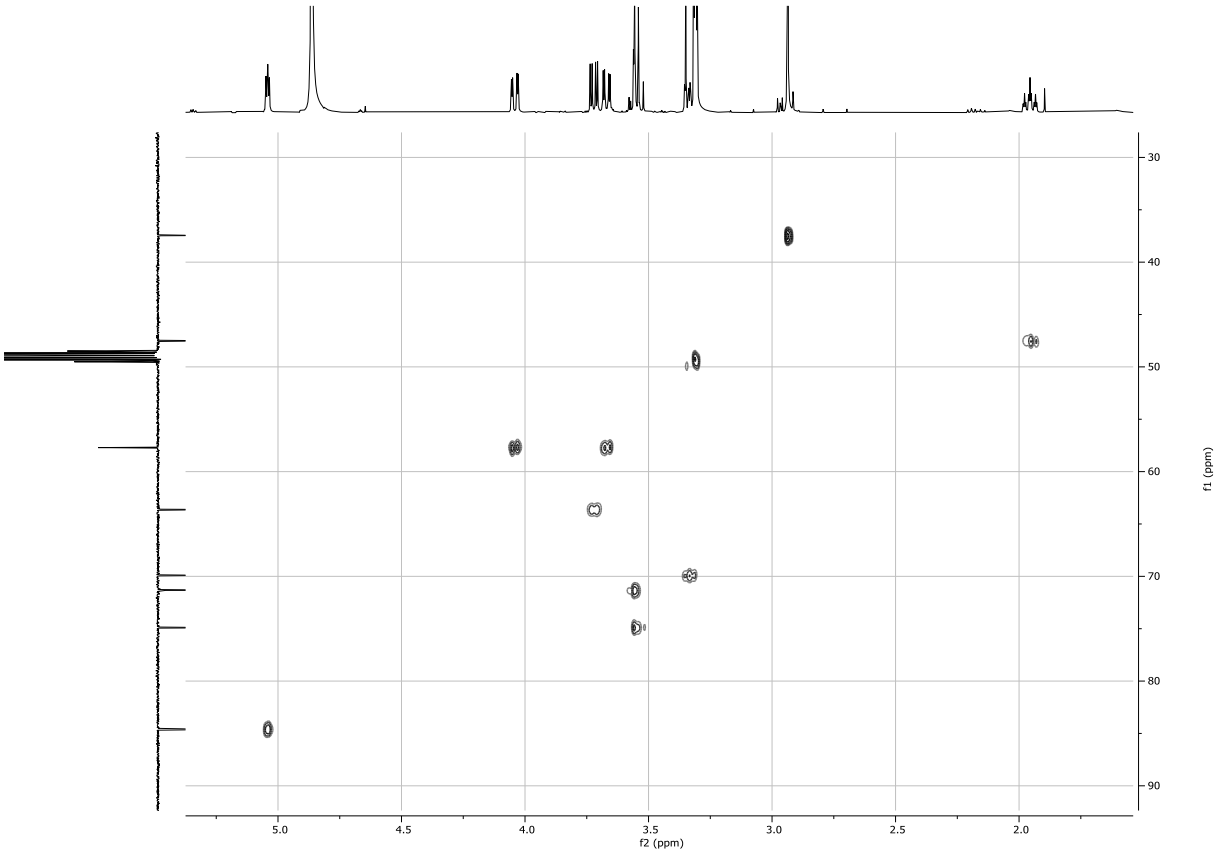

$^{1}$H NMR, 500MHz, $CDCl_3$ of **33**

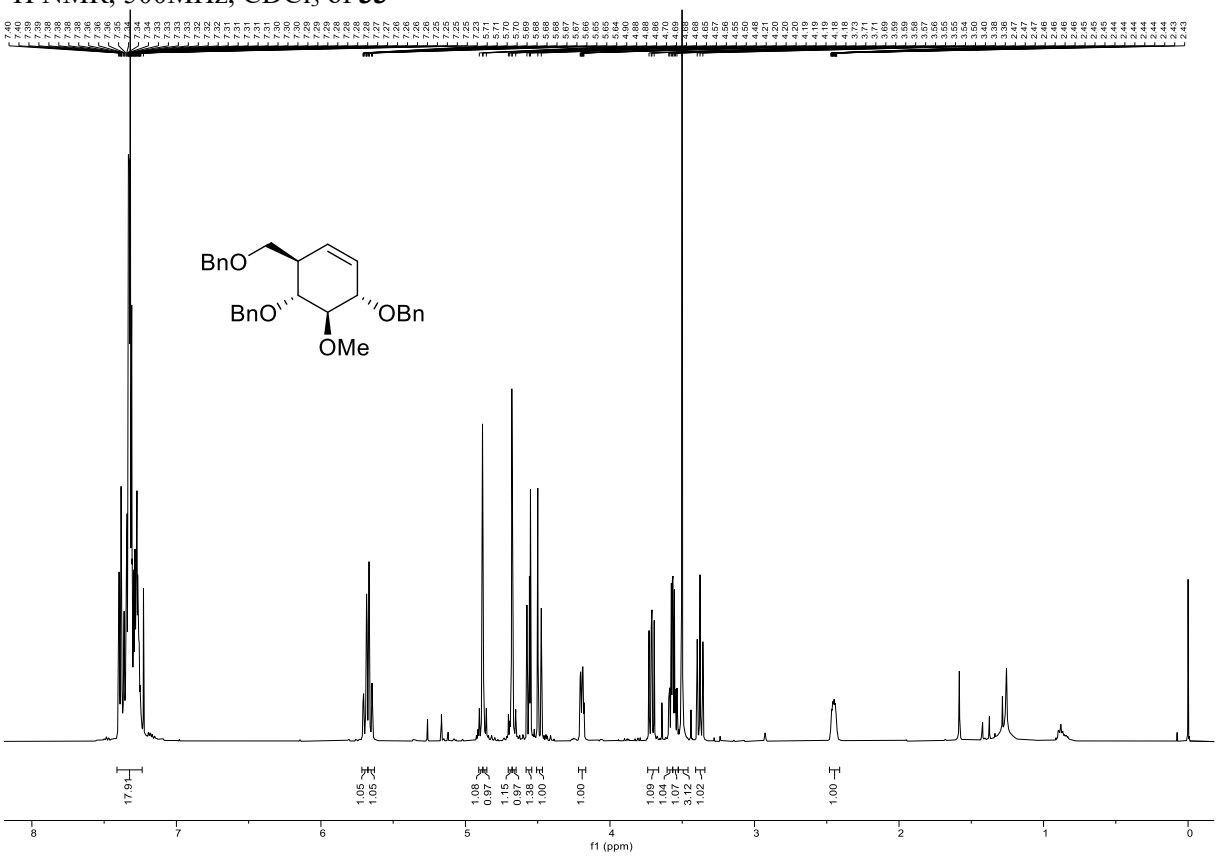


$^{13}$C NMR, 126MHz, $CDCl_3$ of **33**

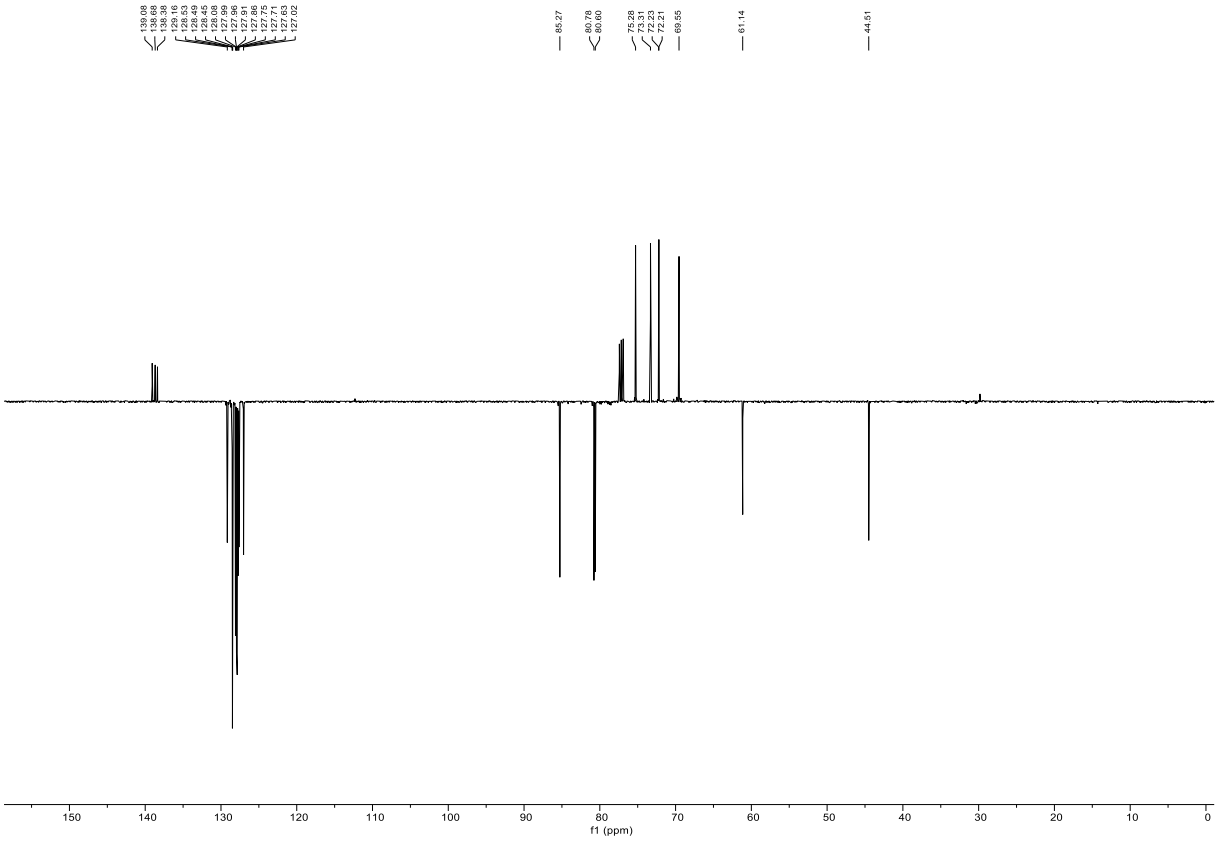

HH-COSY NMR, $CDCl_3$ of **33**

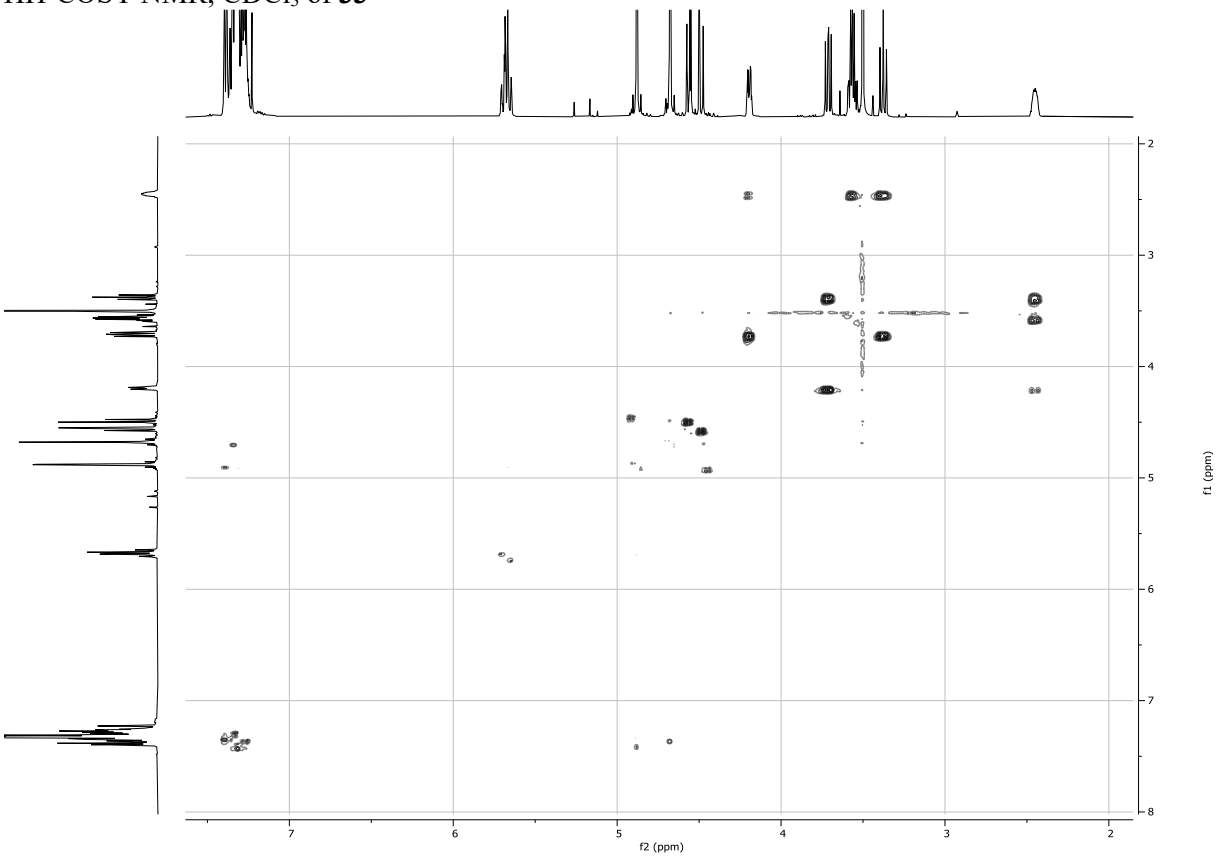


HSQC NMR, $CDCl_3$ of **33**

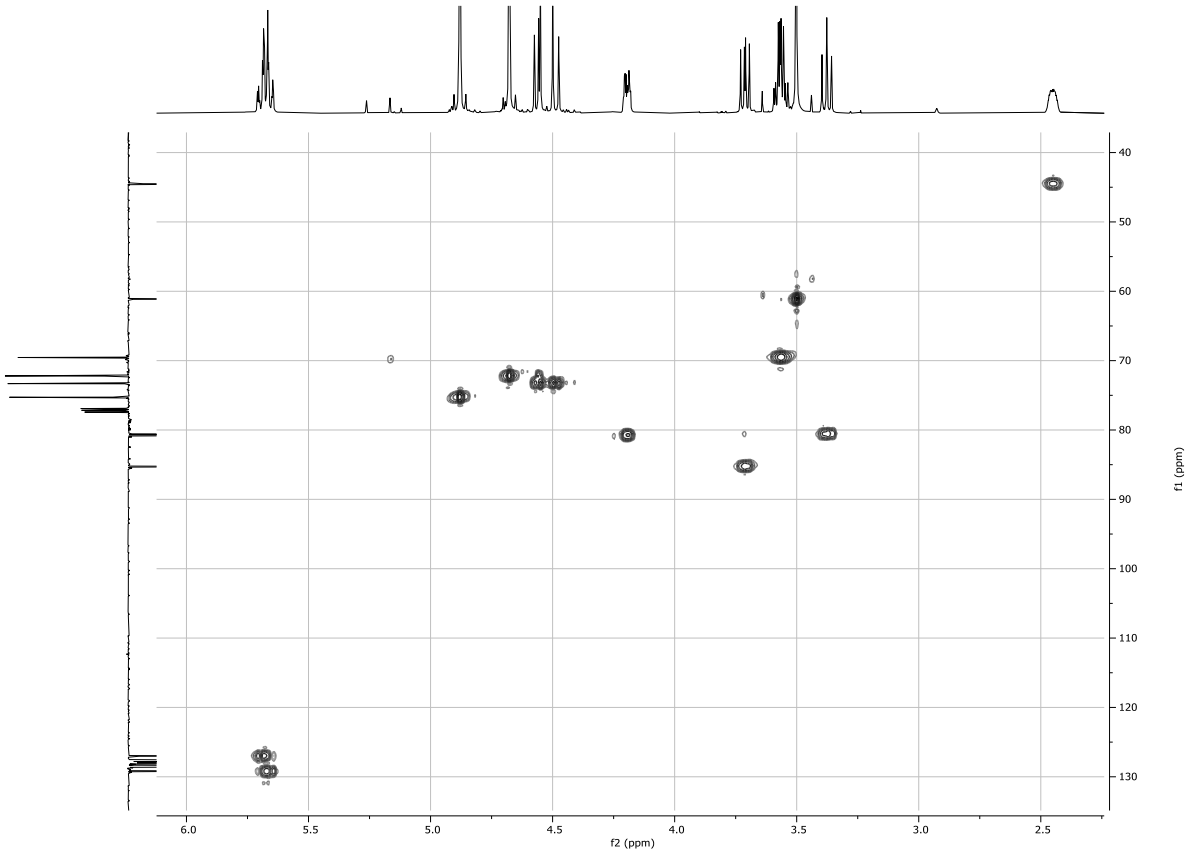

$^{1}$H NMR, 500MHz, $CDCl_3$ of **39**

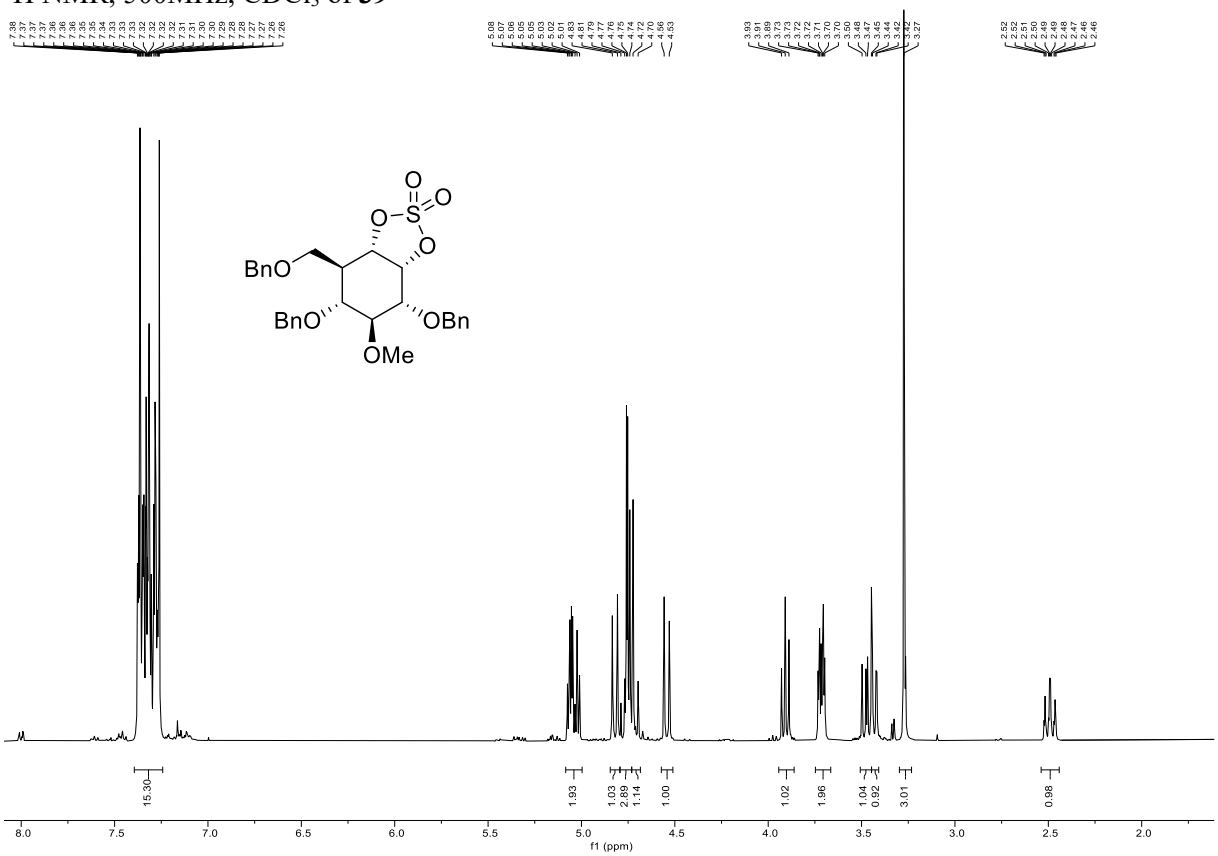


$^{13}$C NMR, 126MHz, $CDCl_3$ of **39**

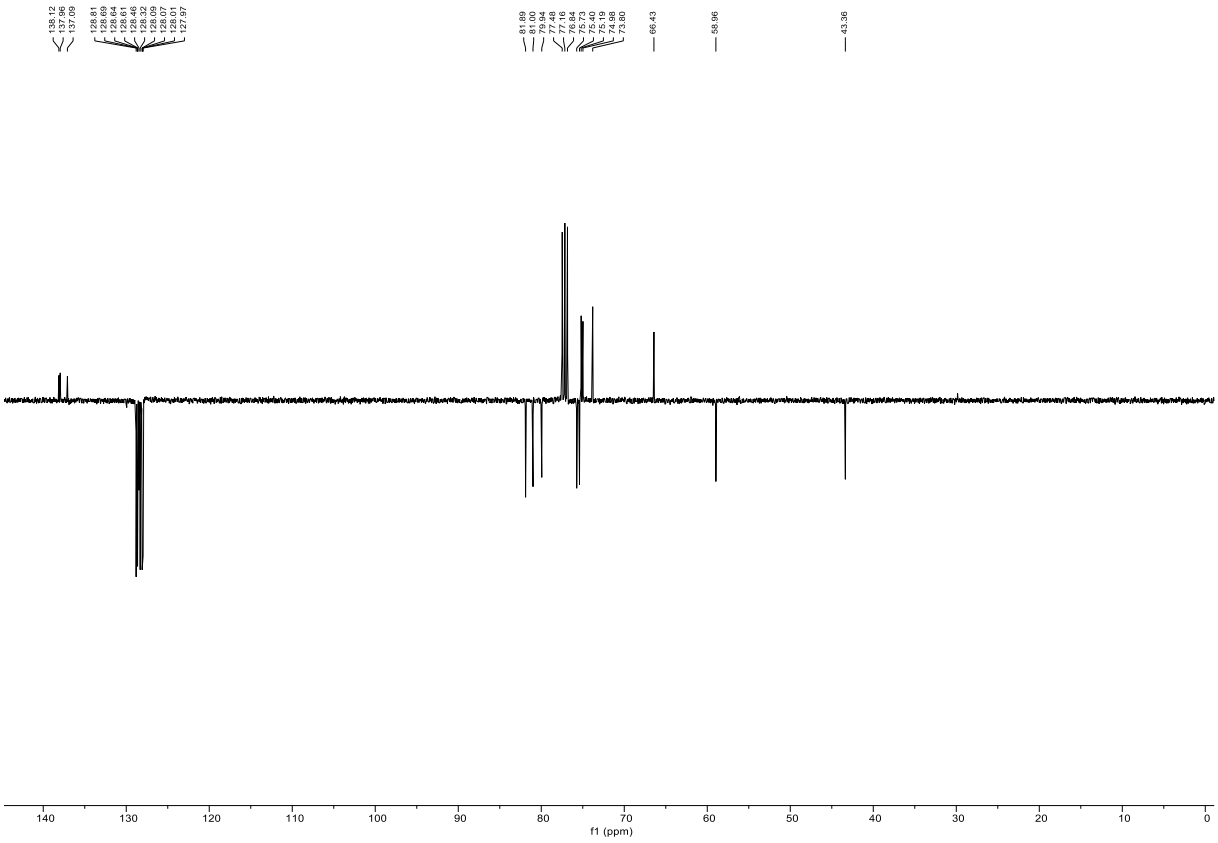

HH-COSY NMR, $CDCl_3$ of **39**

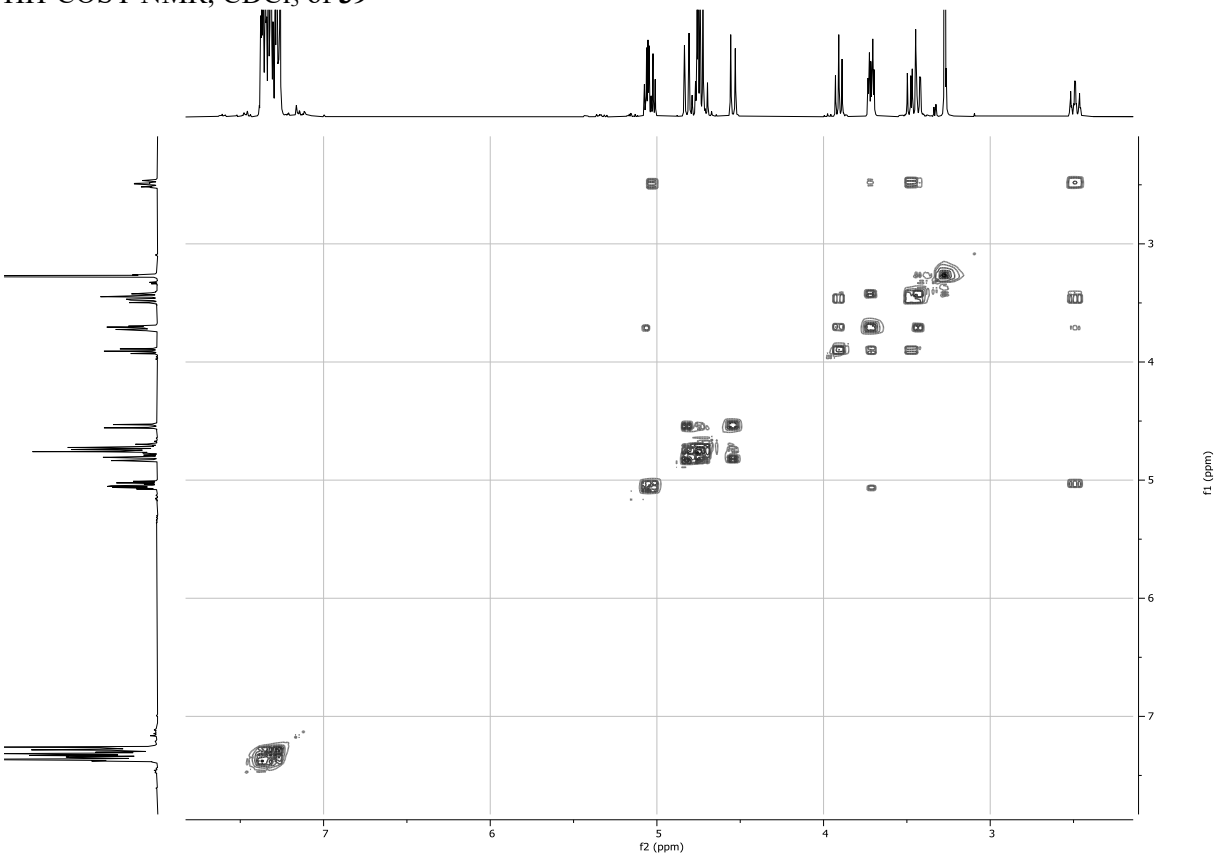


HSQC NMR, $CDCl_3$ of **39**

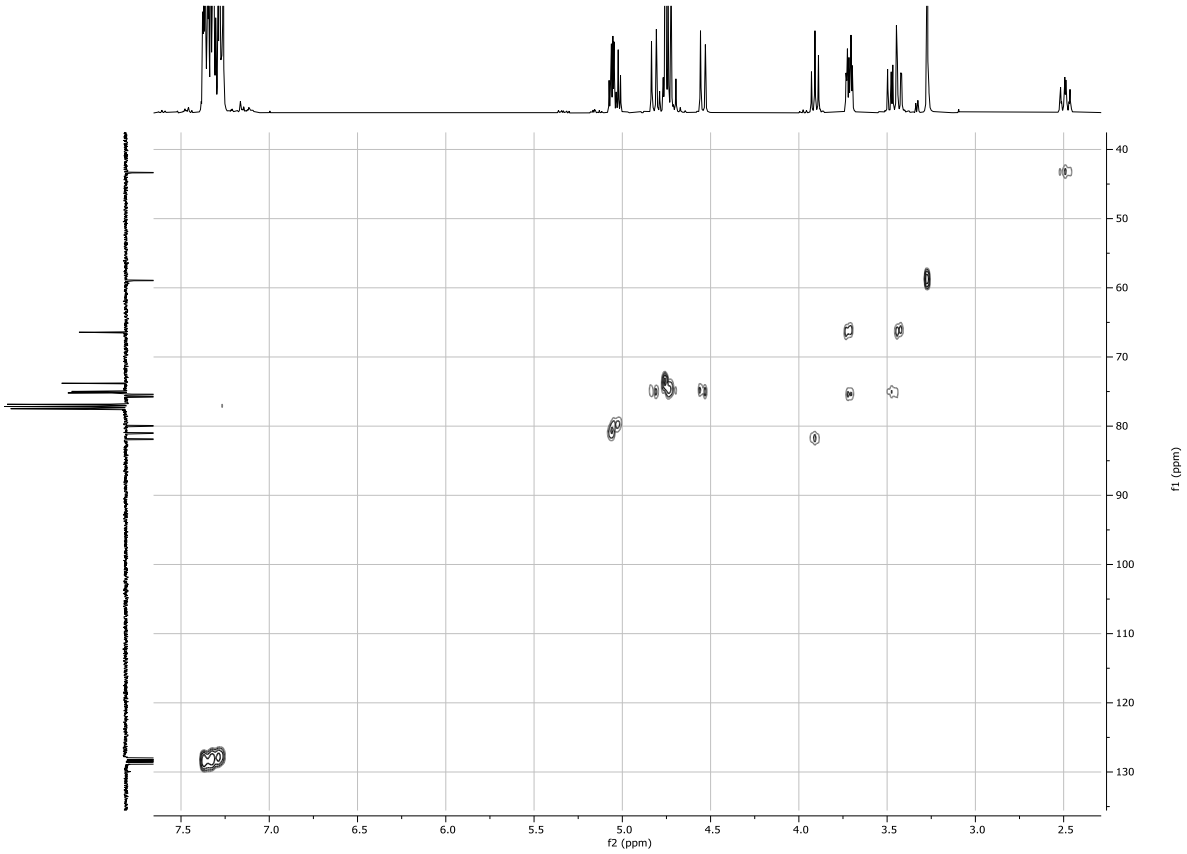

$^{1}$H NMR, 500MHz, MeOD of **6**

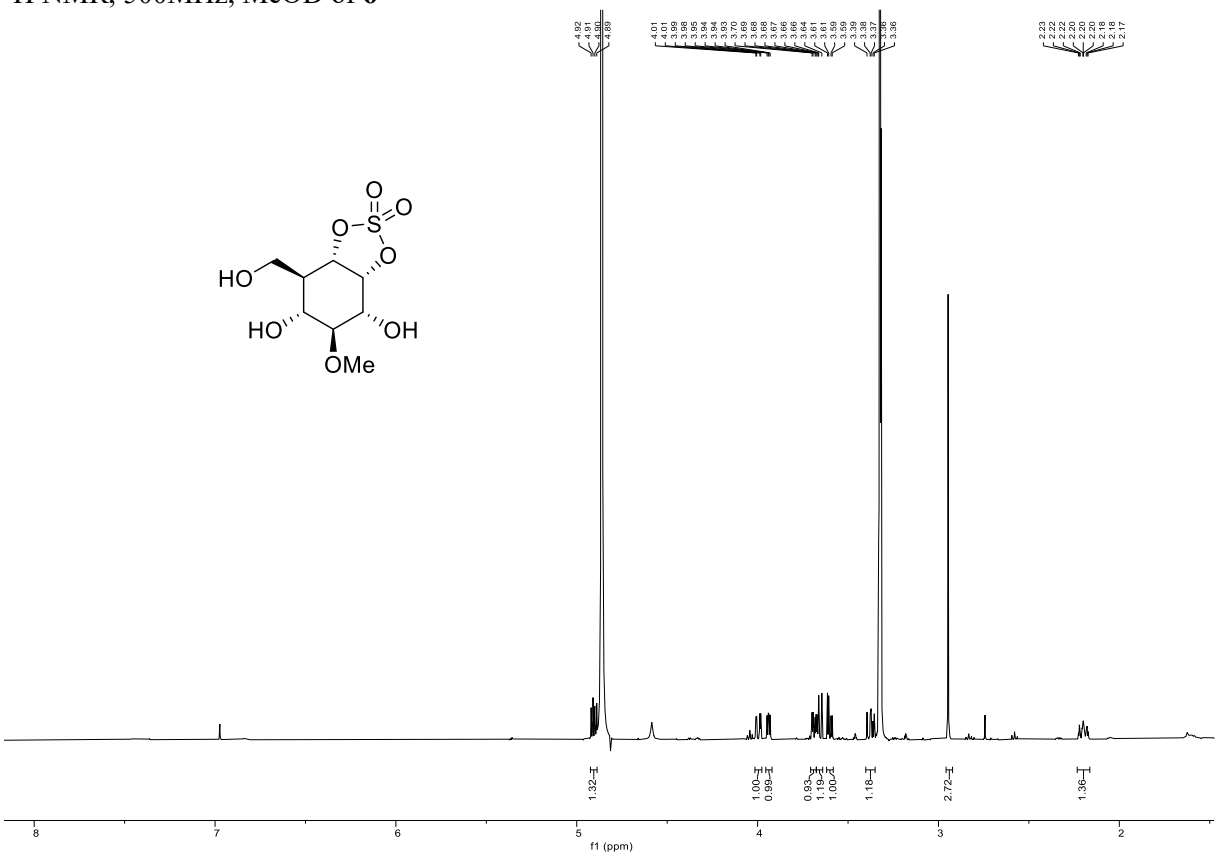


$^{13}$C NMR, 126MHz, MeOD of **6**

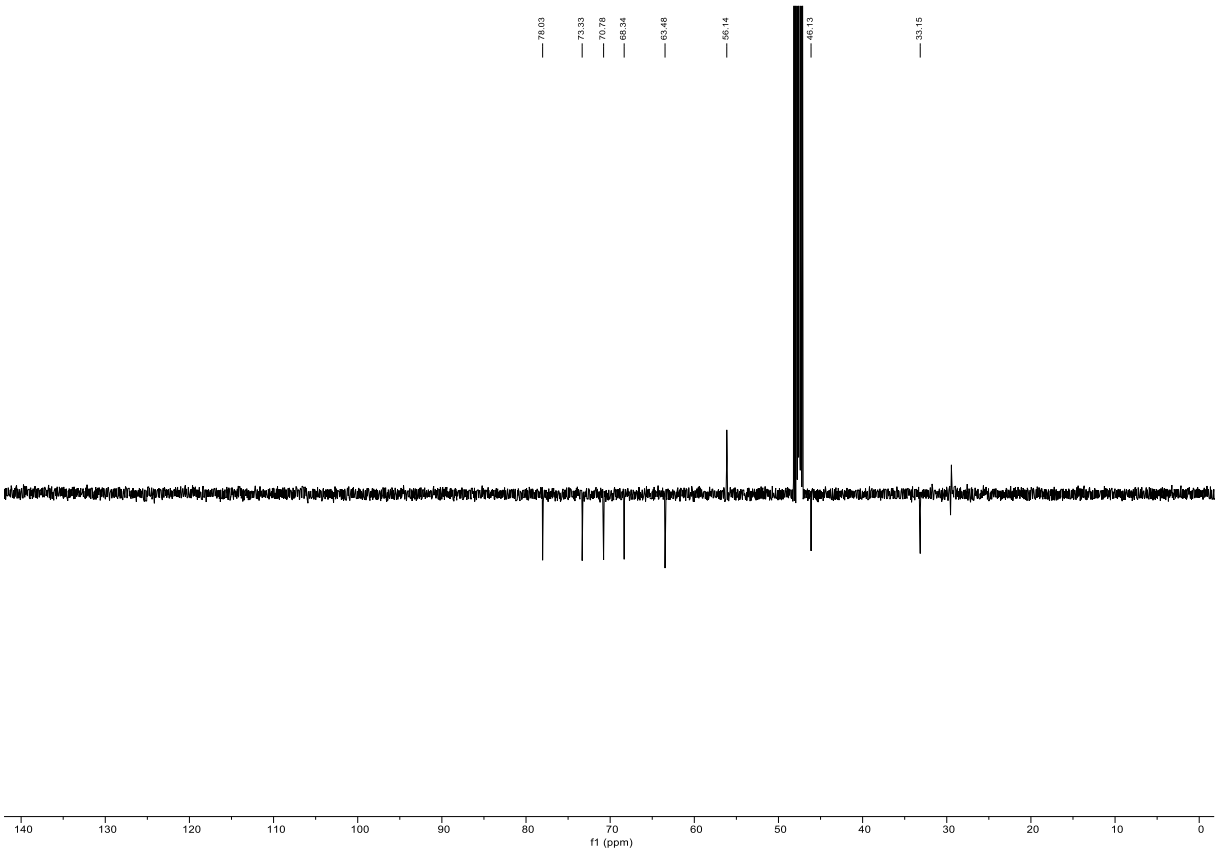

HH-COSY NMR, MeOD of **6**

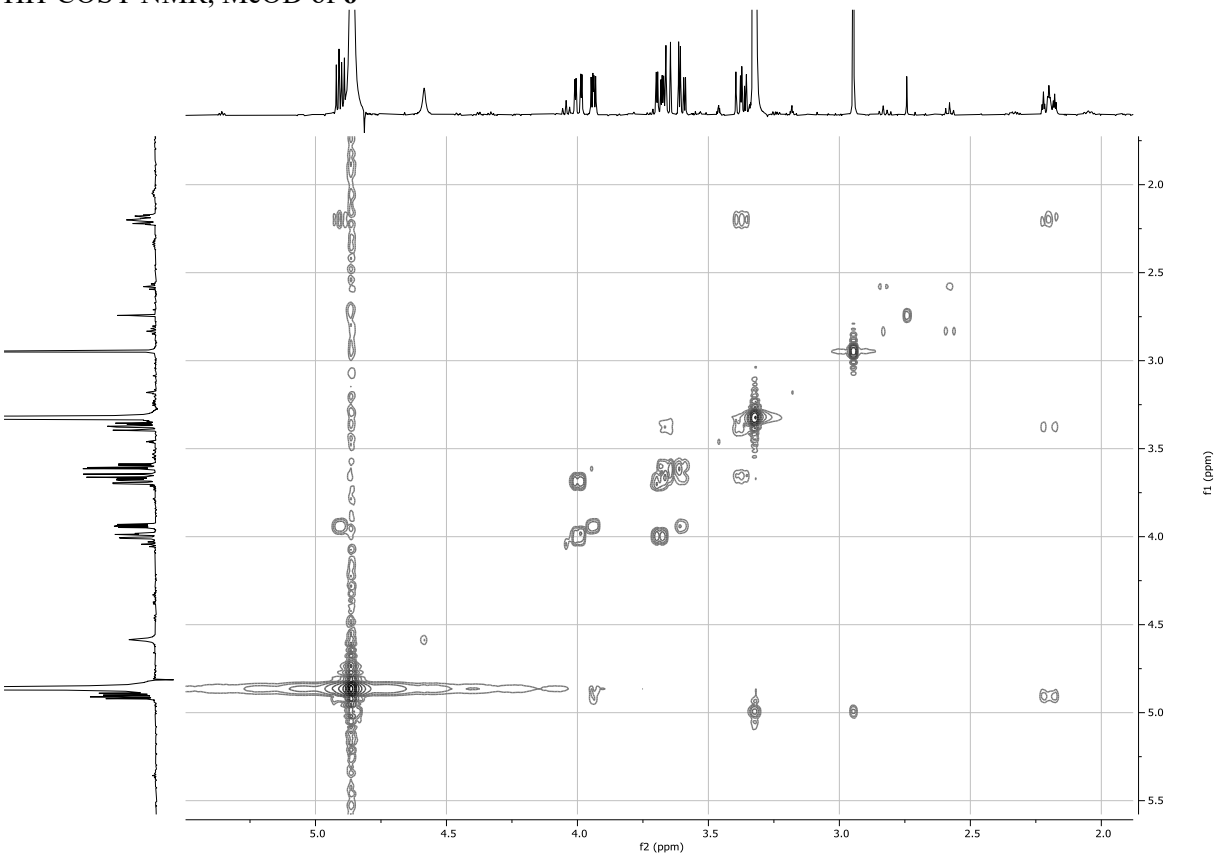


HSQC NMR, MeOD of **6**

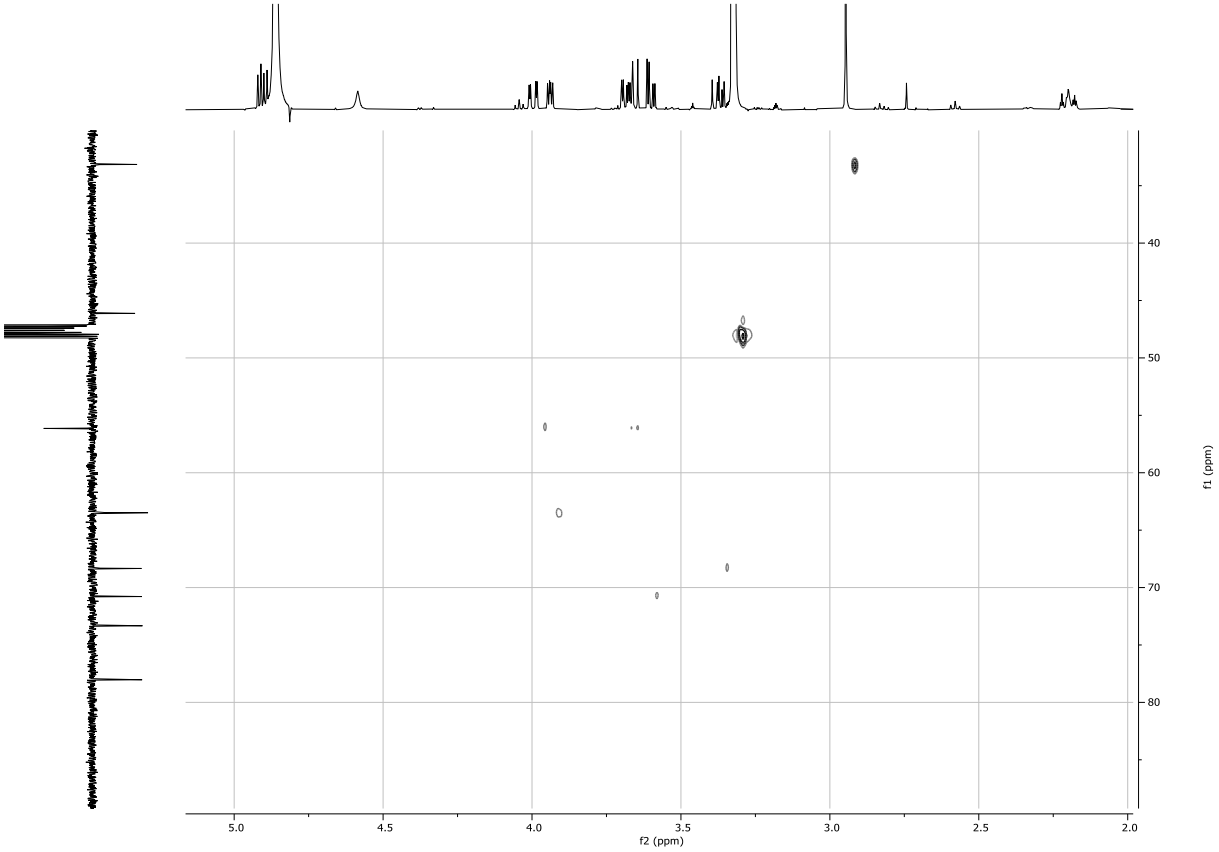

$^{1}$H NMR, 400MHz, $CDCl_3$ of **40**

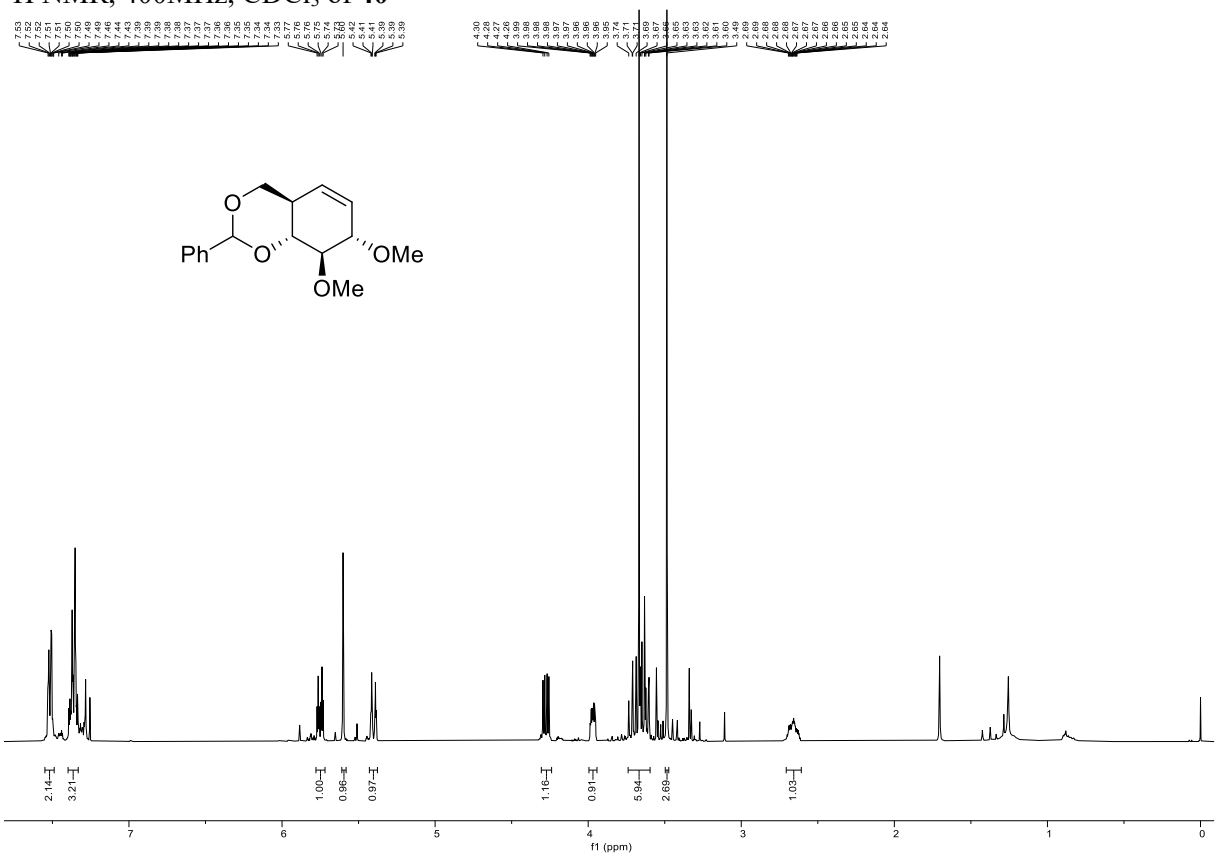


$^{13}$C NMR, 101MHz, $CDCl_3$ of **40**

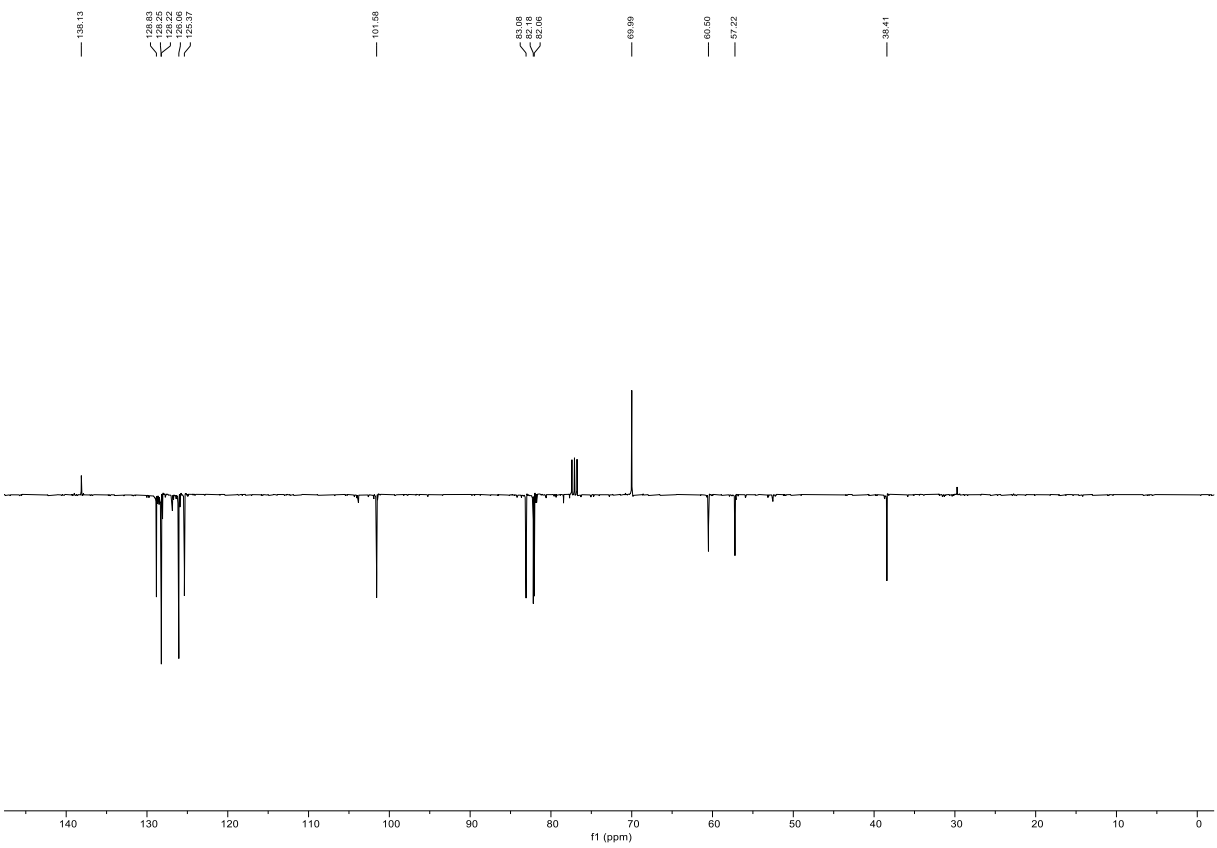

HH-COSY NMR, $CDCl_3$ of **40**

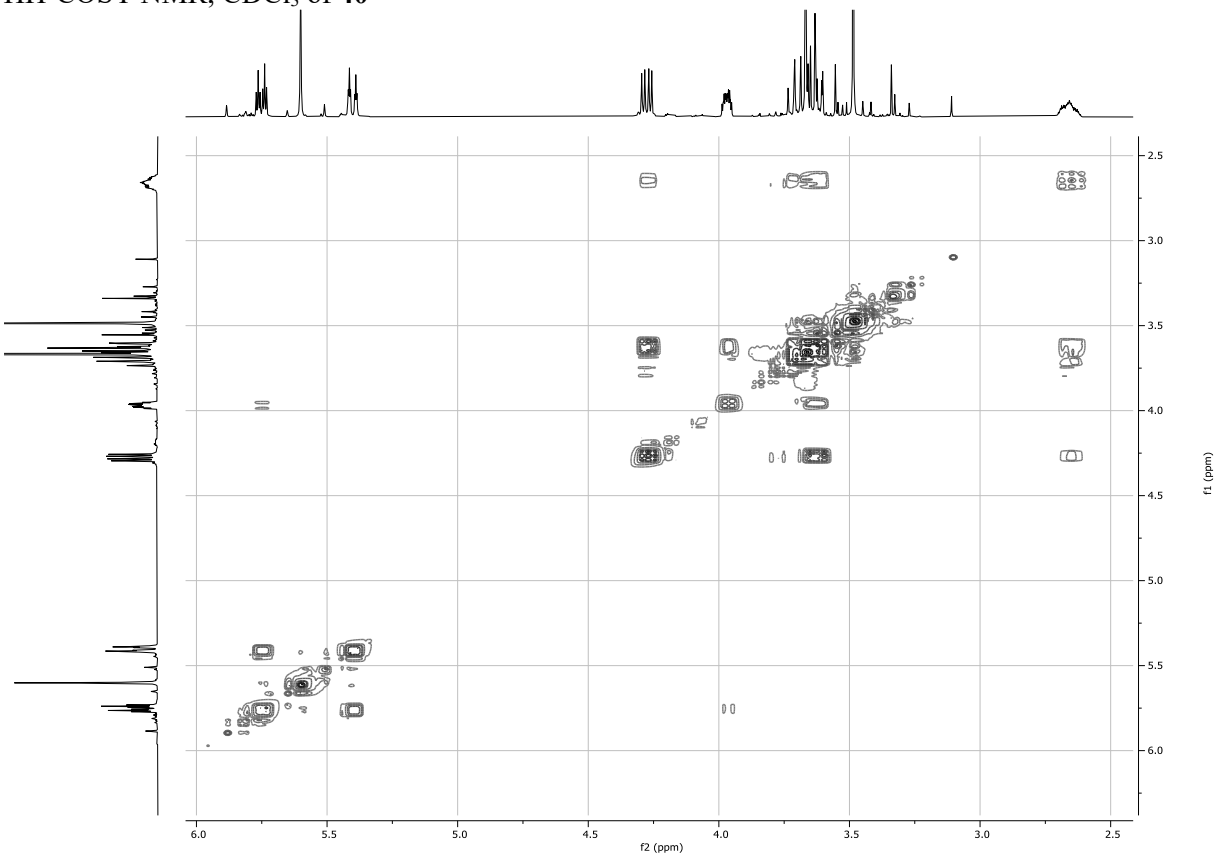


HSQC NMR, $CDCl_3$ of **40**

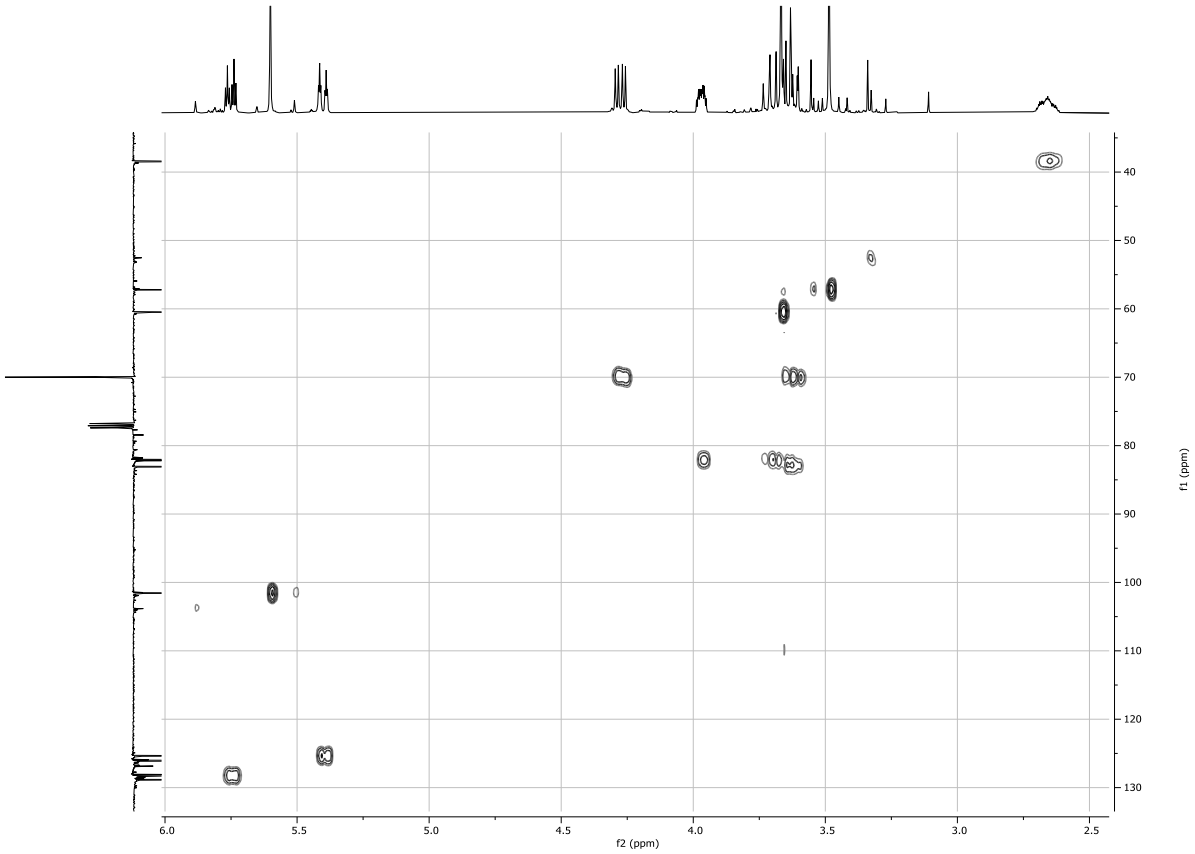

$^{1}$H NMR, 400MHz, MeOD of **41**

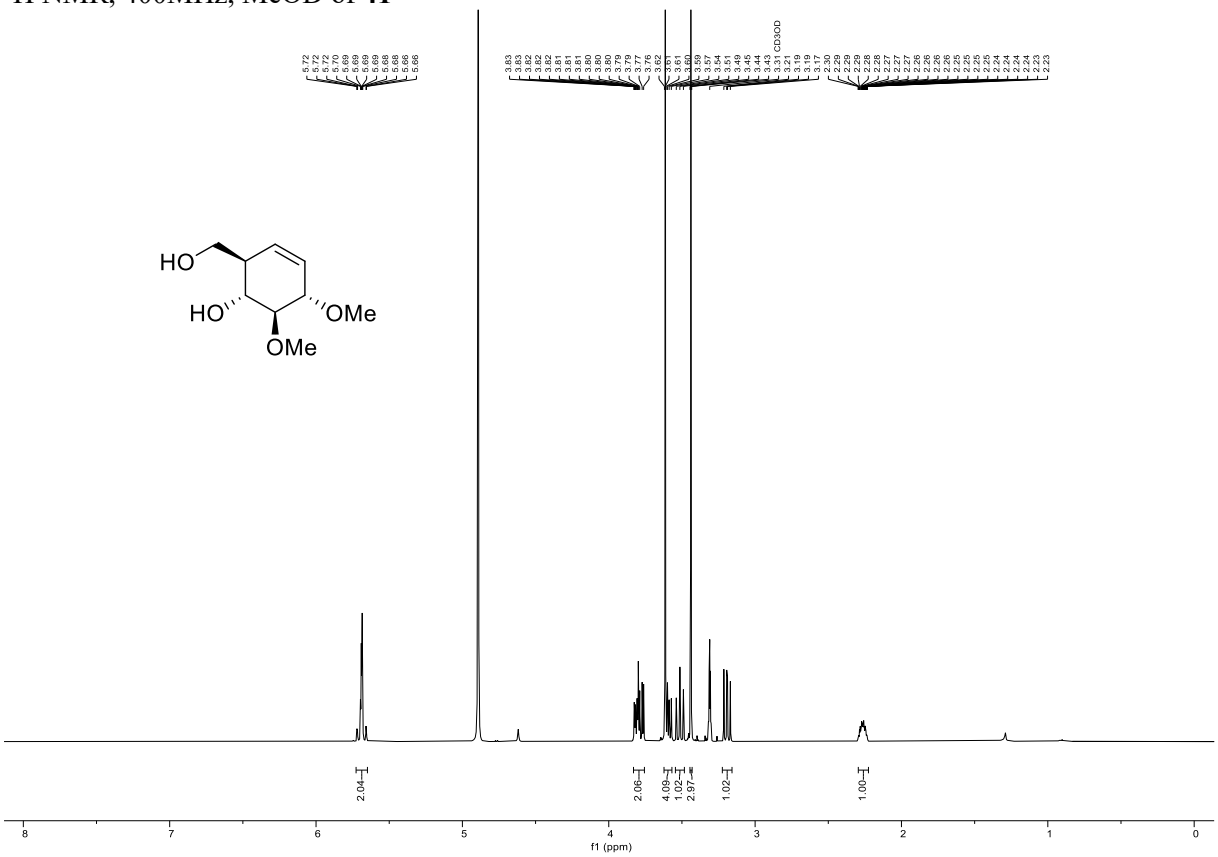


$^{13}$C NMR, 101MHz, MeOD of **41**

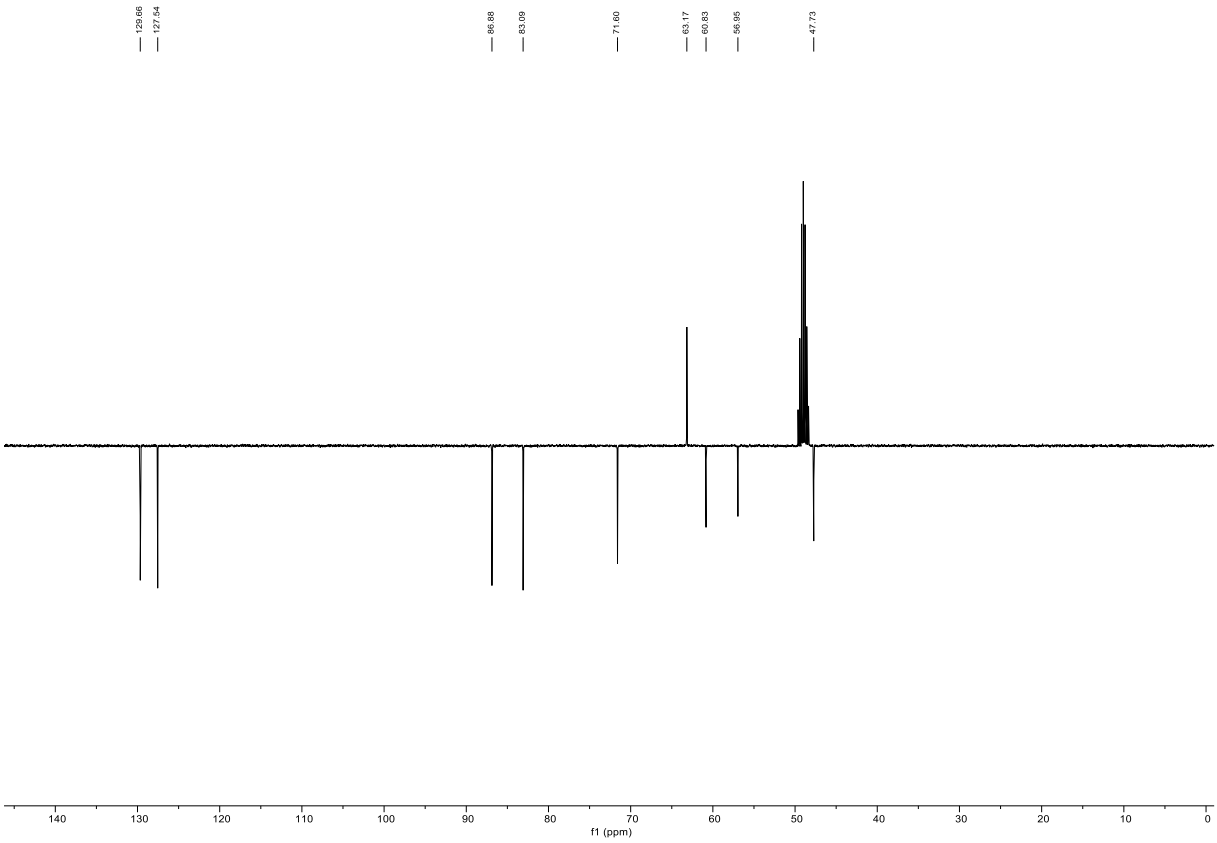

HH-COSY NMR, MeOD of **41**

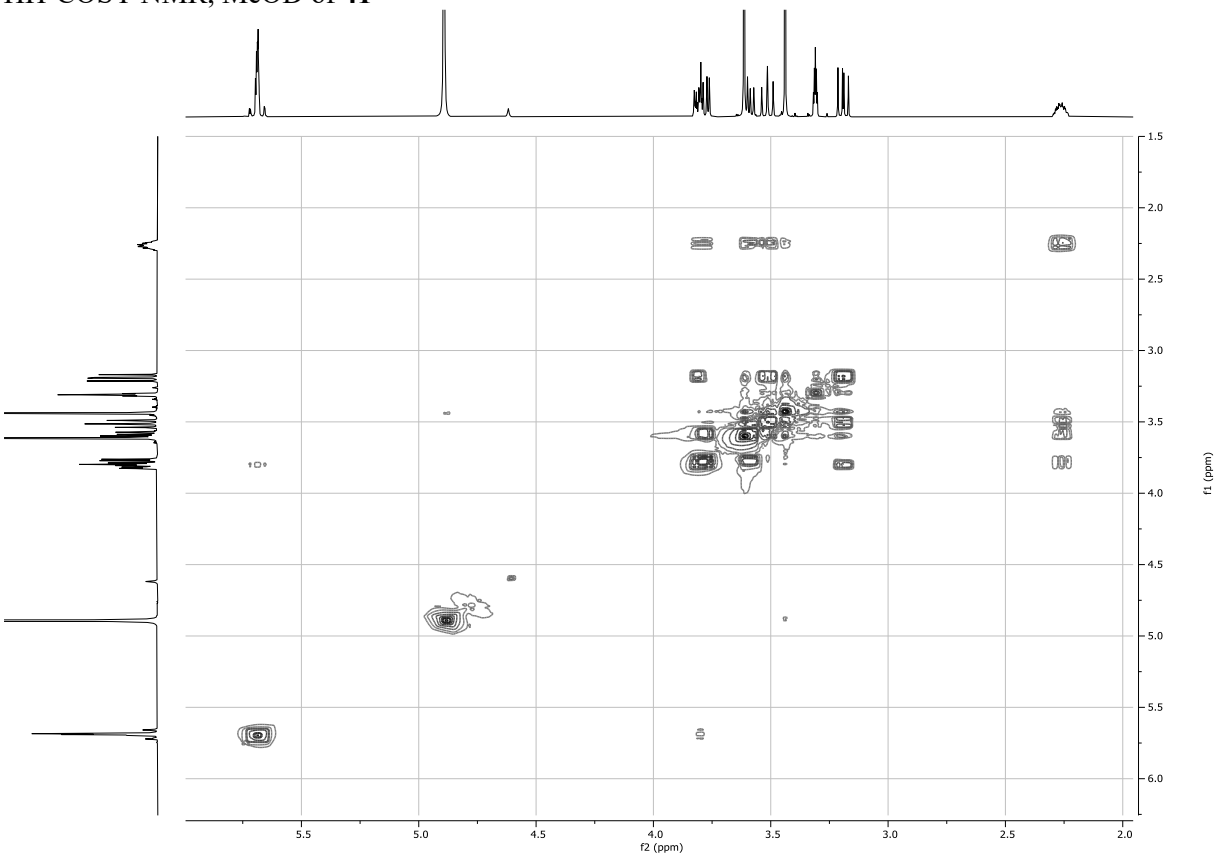


HSQC NMR, MeOD of **41**

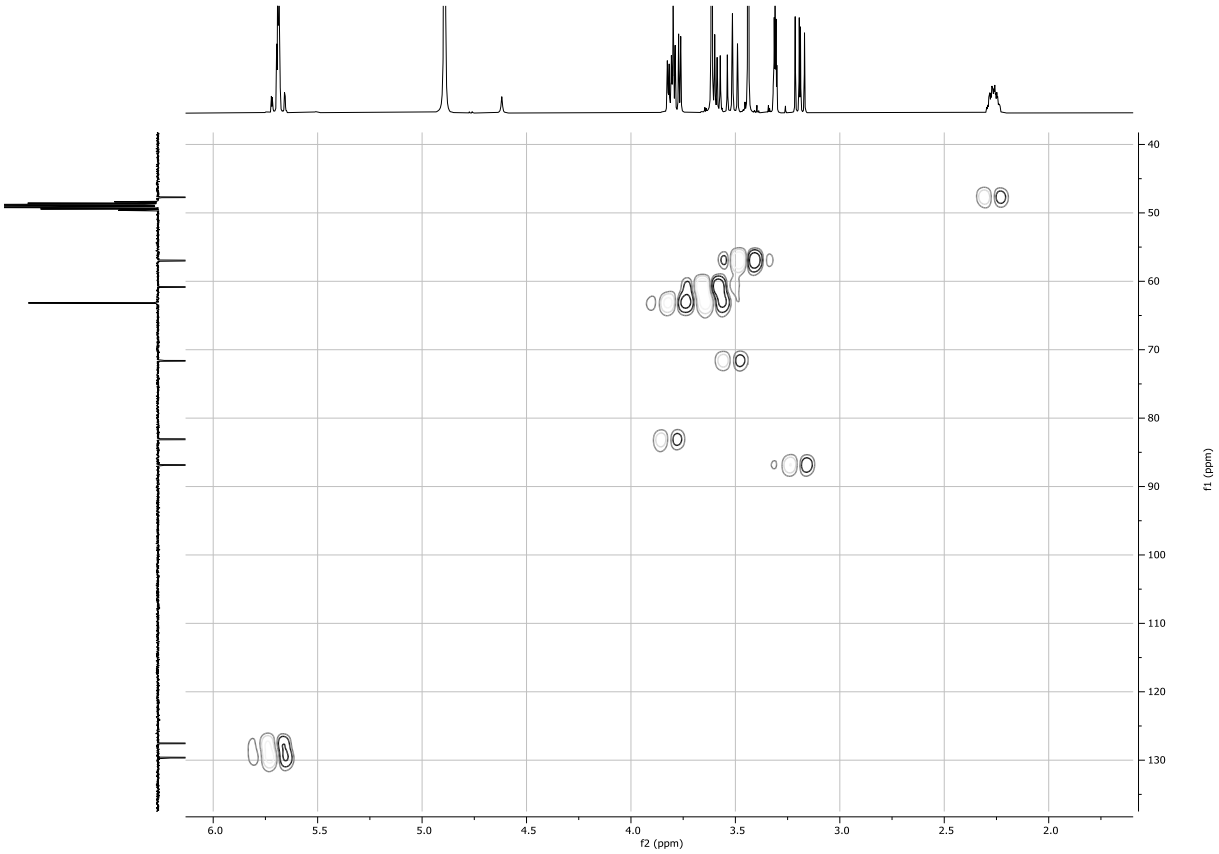

$^{1}$H NMR, 400MHz, $CDCl_3$ of **42**

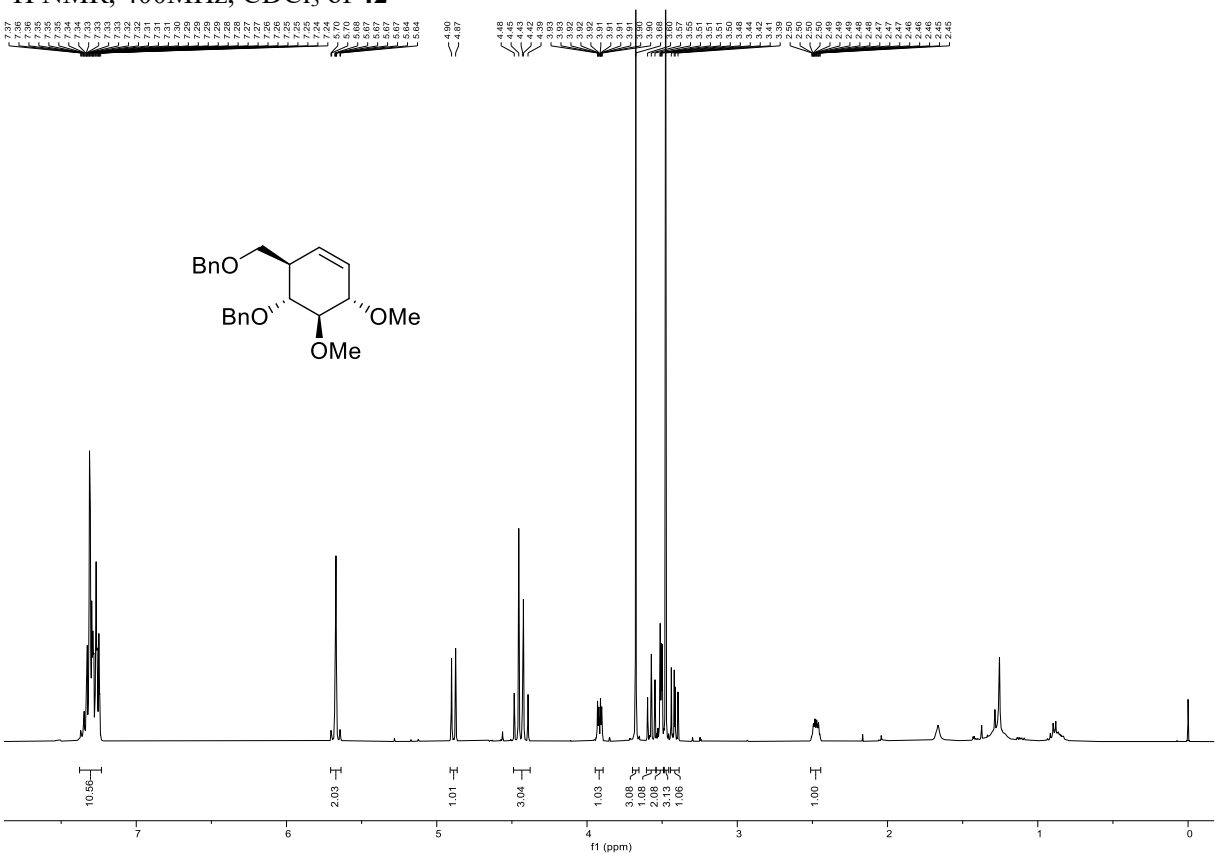


$^{13}$C NMR, 101MHz, $CDCl_3$ of **42**

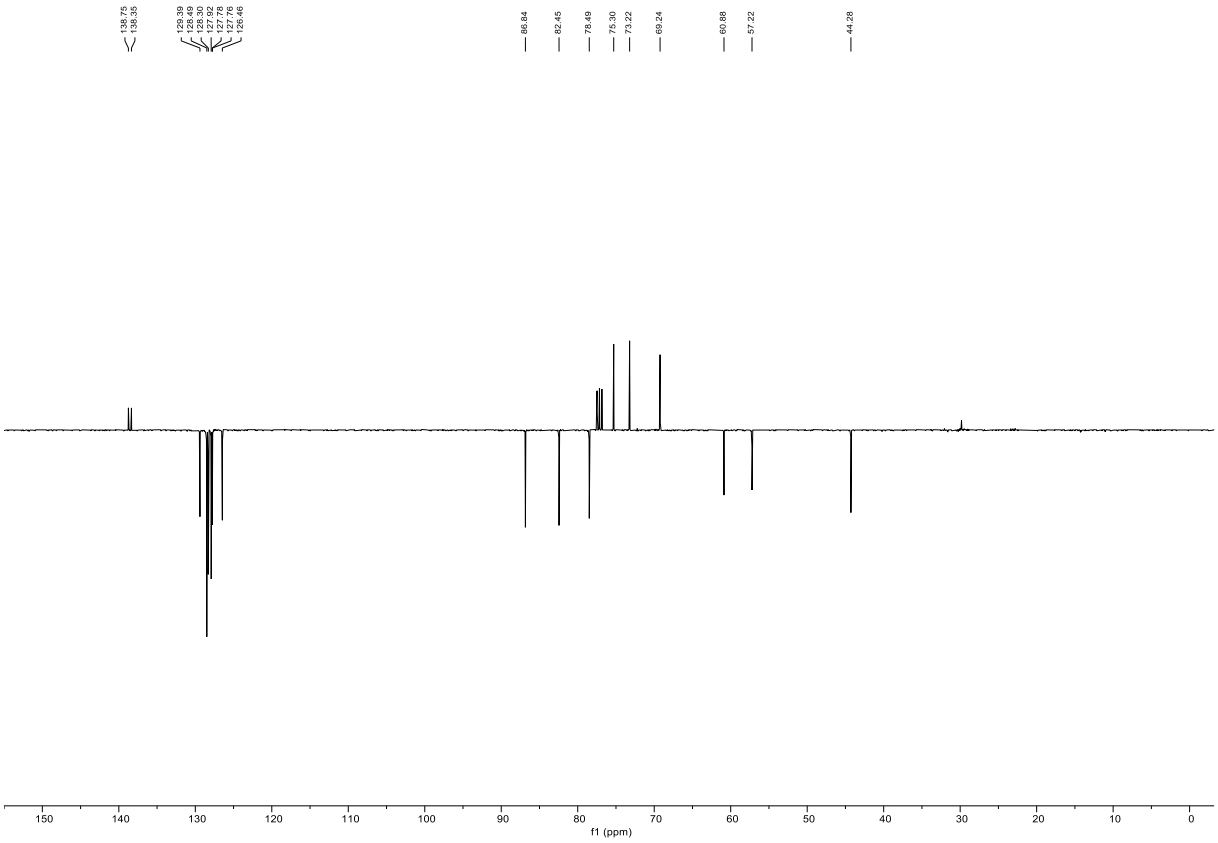

HH-COSY NMR, $CDCl_3$ of **42**

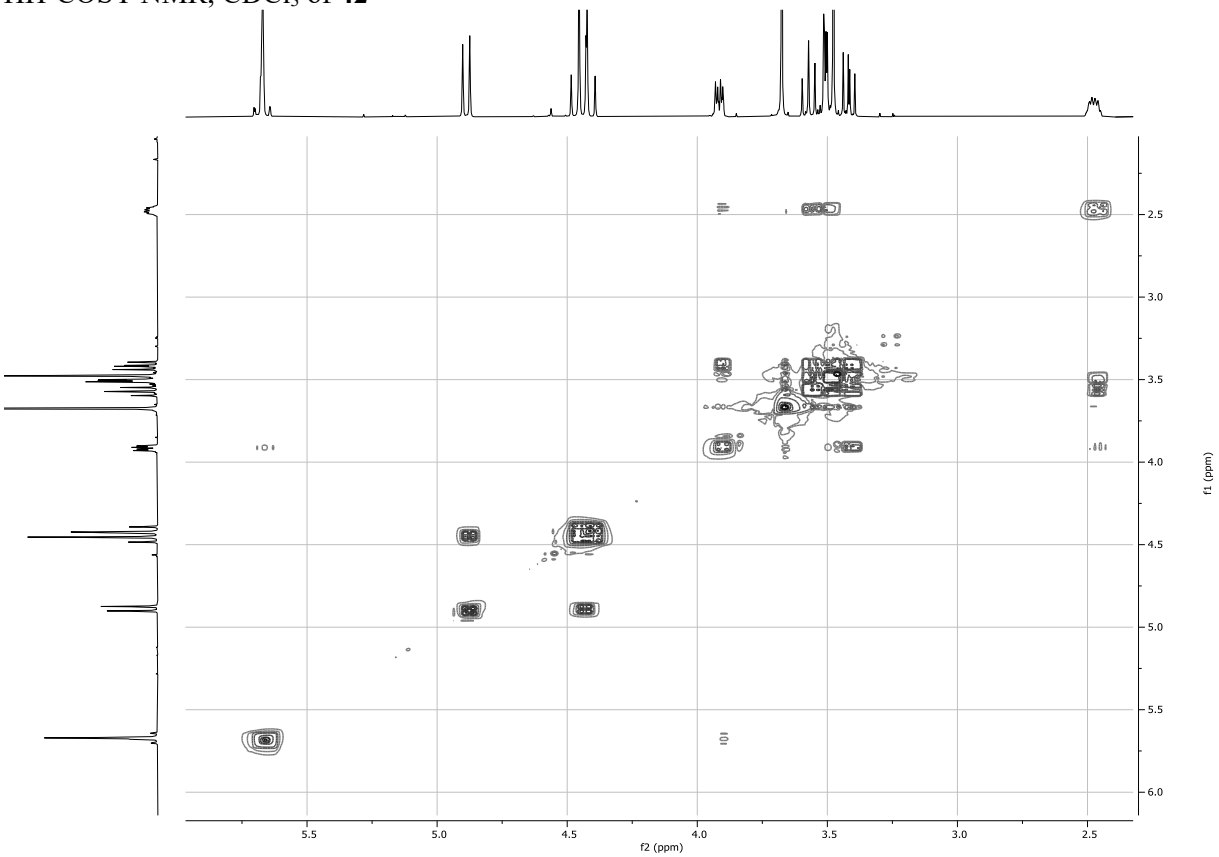


HSQC NMR, $CDCl_3$ of **42**

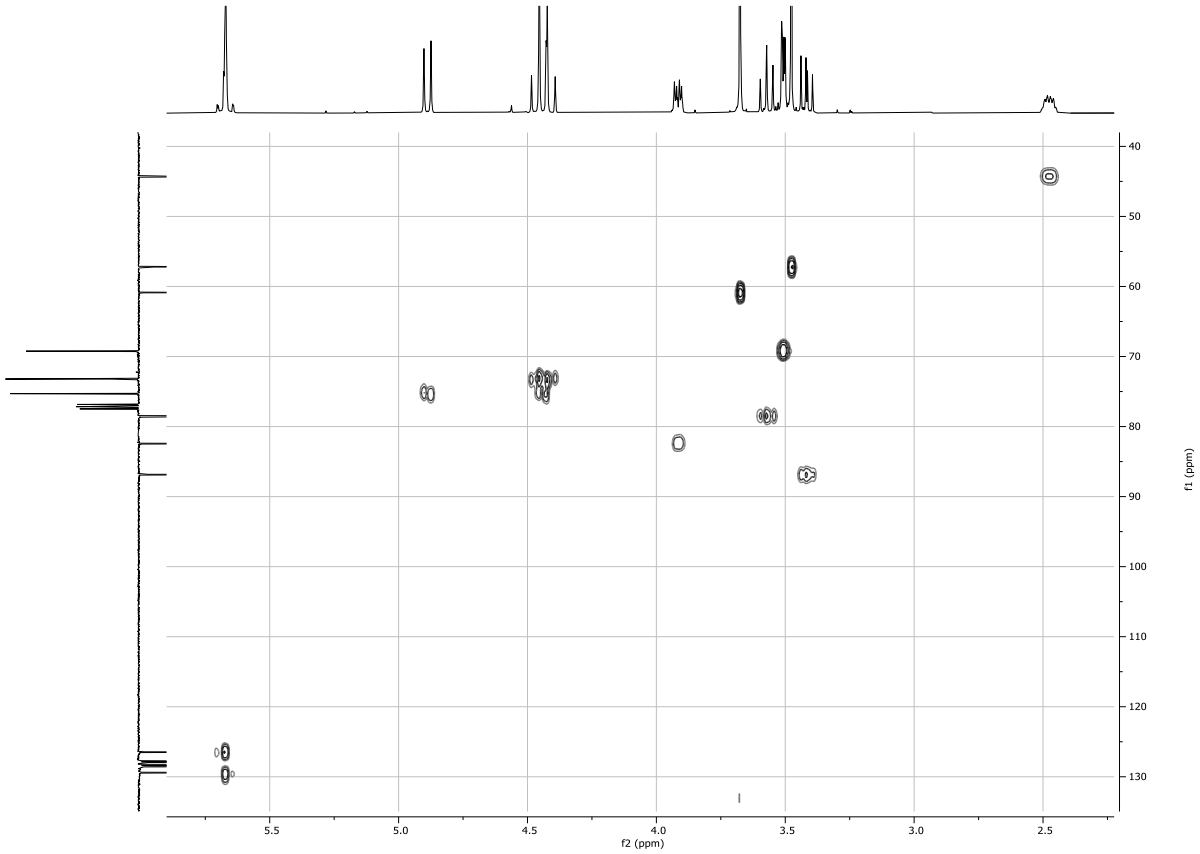

$^{1}$H NMR, 400MHz, $CDCl_3$ of **43**

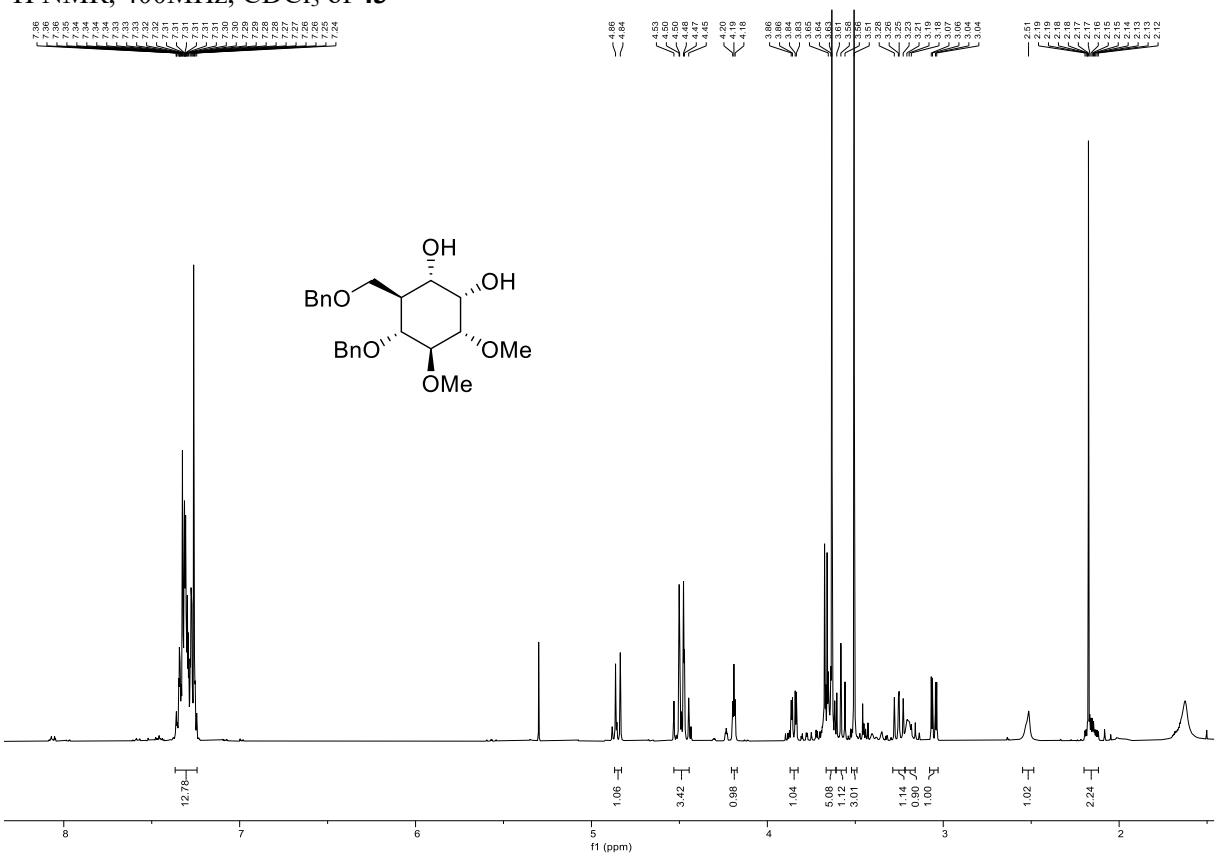


$^{13}$C NMR, 101MHz, $CDCl_3$ of **43**

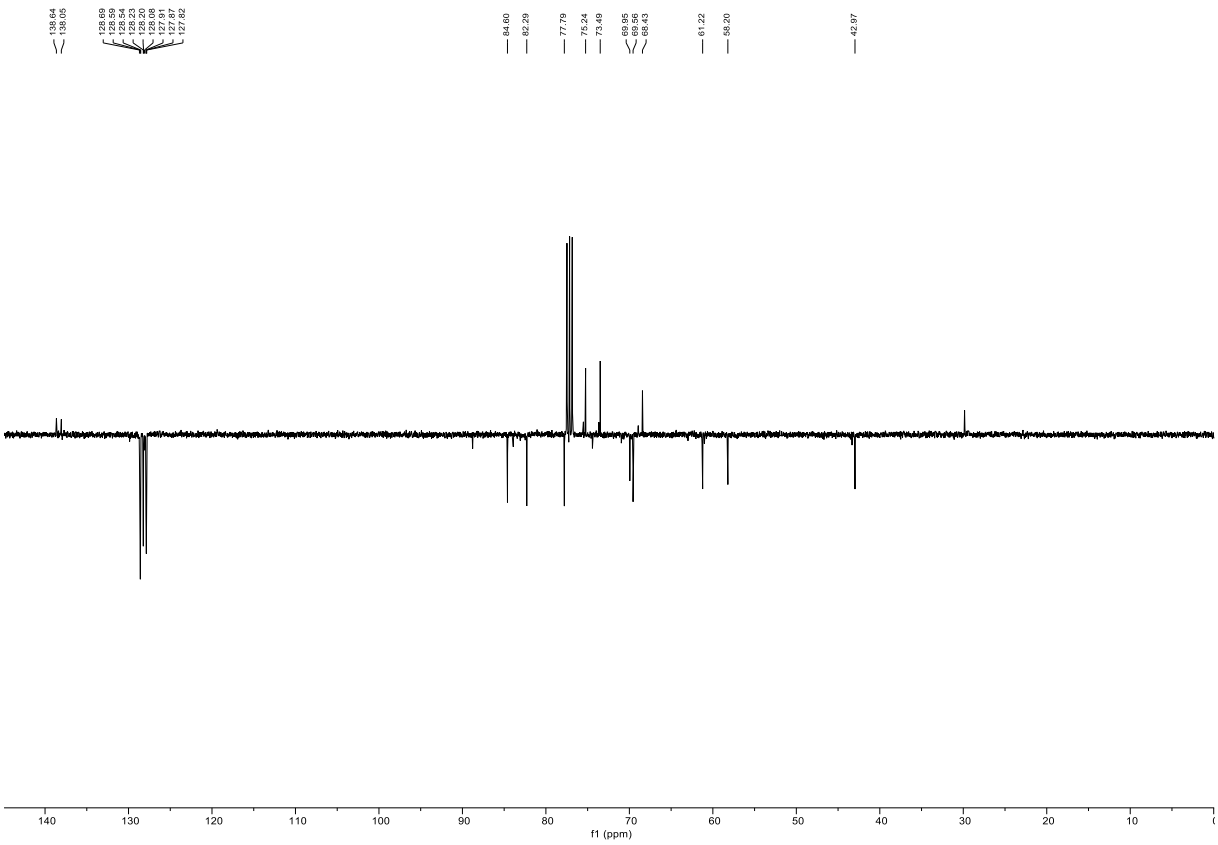

HH-COSY NMR, $CDCl_3$ of **43**

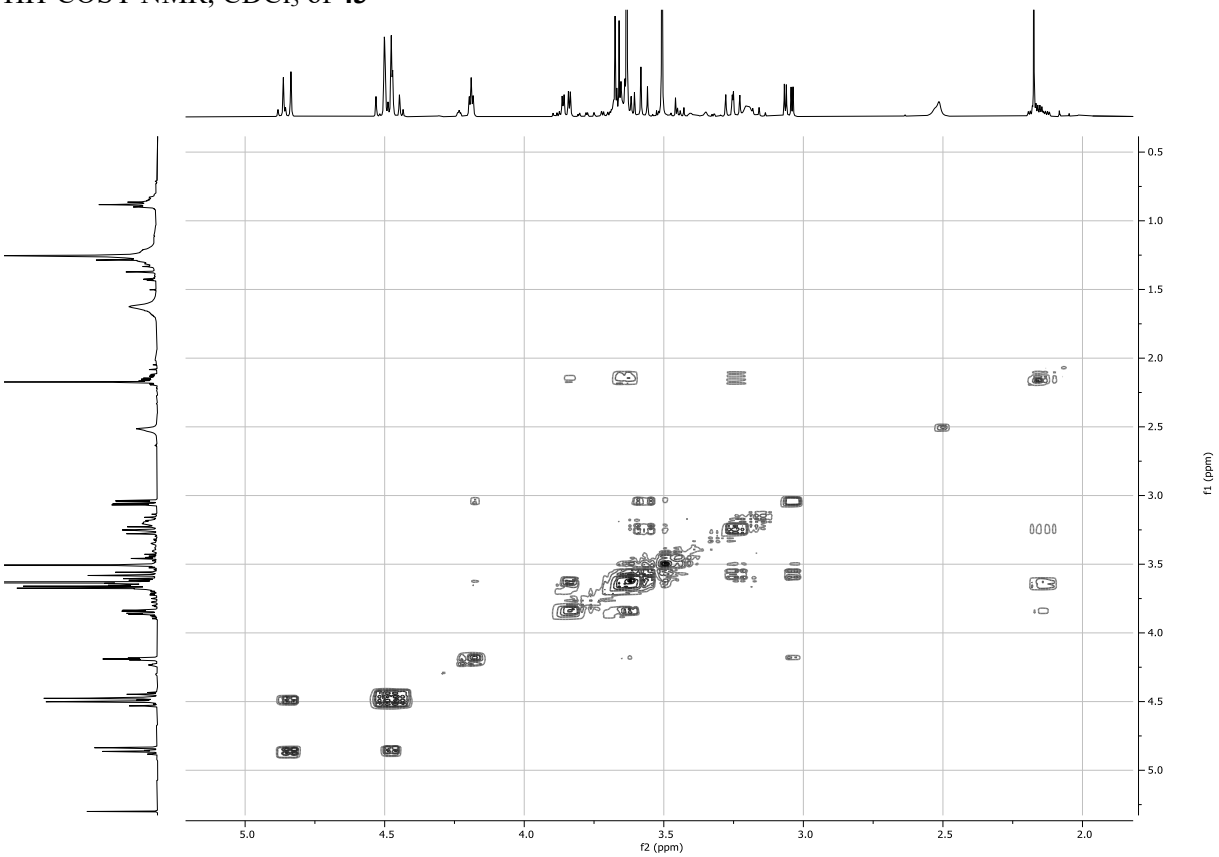


HSQC NMR, $CDCl_3$ of **43**

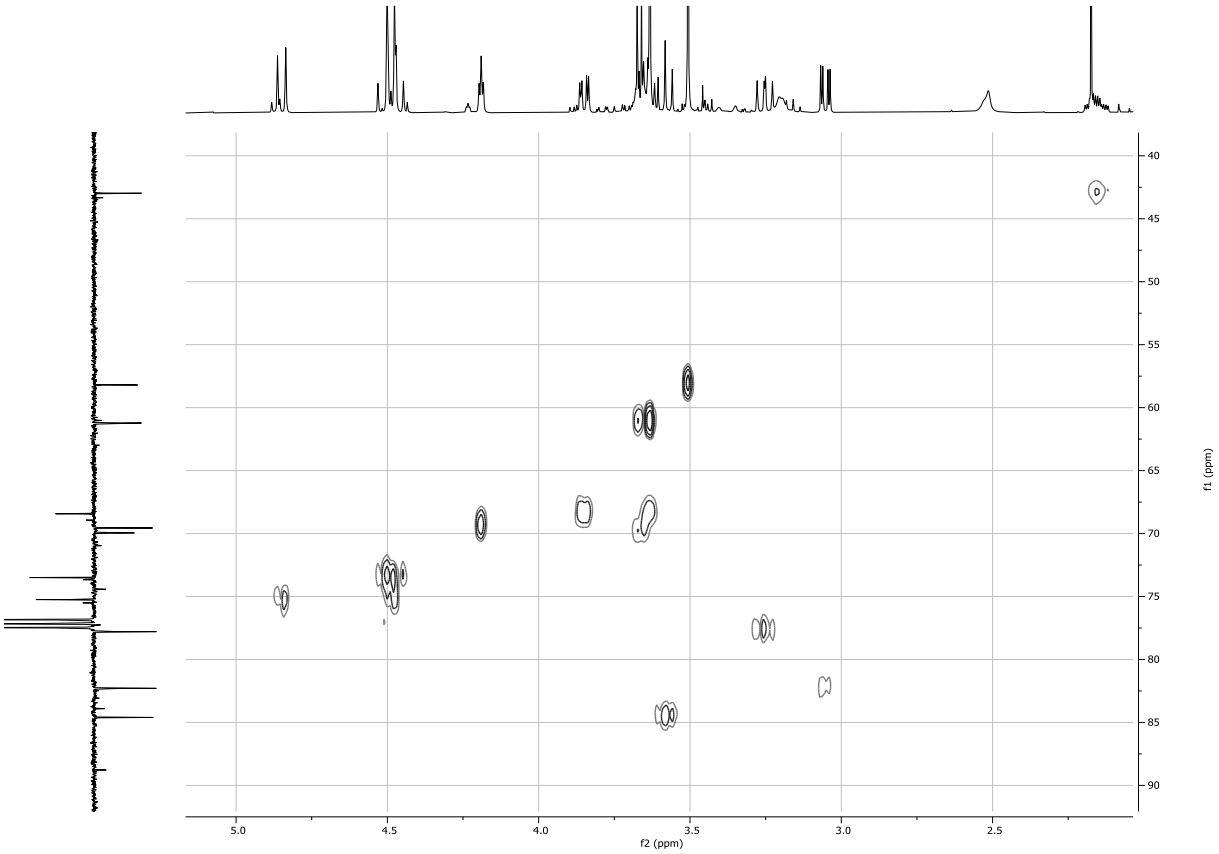

$^{1}$H NMR, 400MHz, $CDCl_3$ of **44**

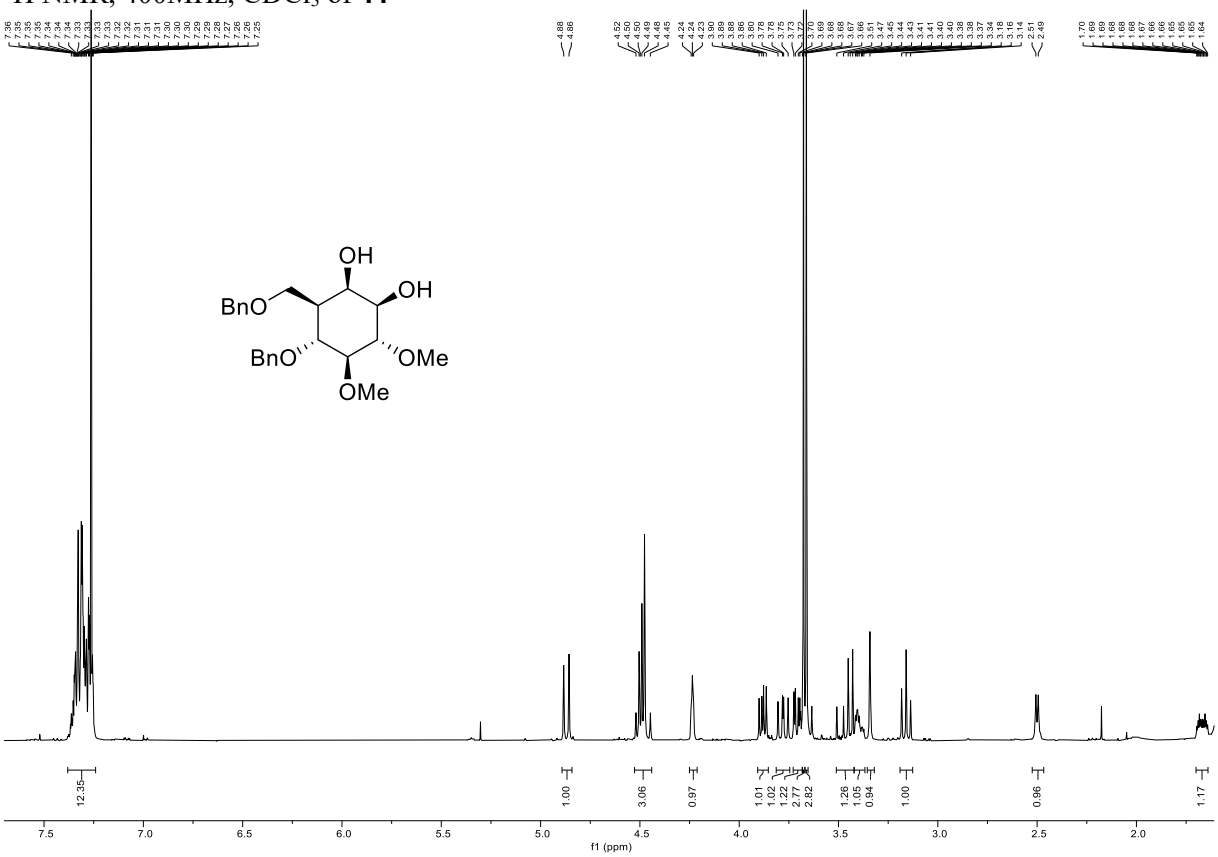


$^{13}$C NMR, 101MHz, $CDCl_3$ of **44**

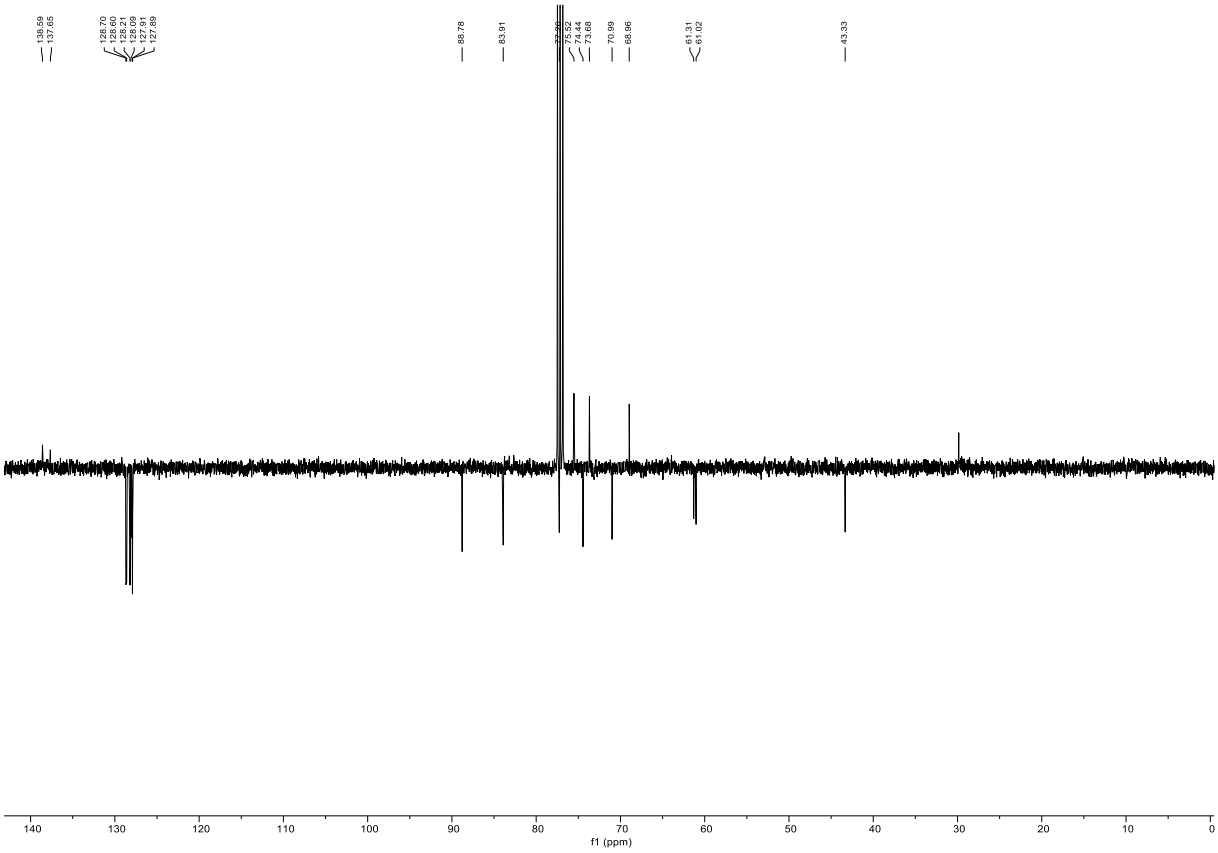

HH-COSY NMR, $CDCl_3$ of **44**

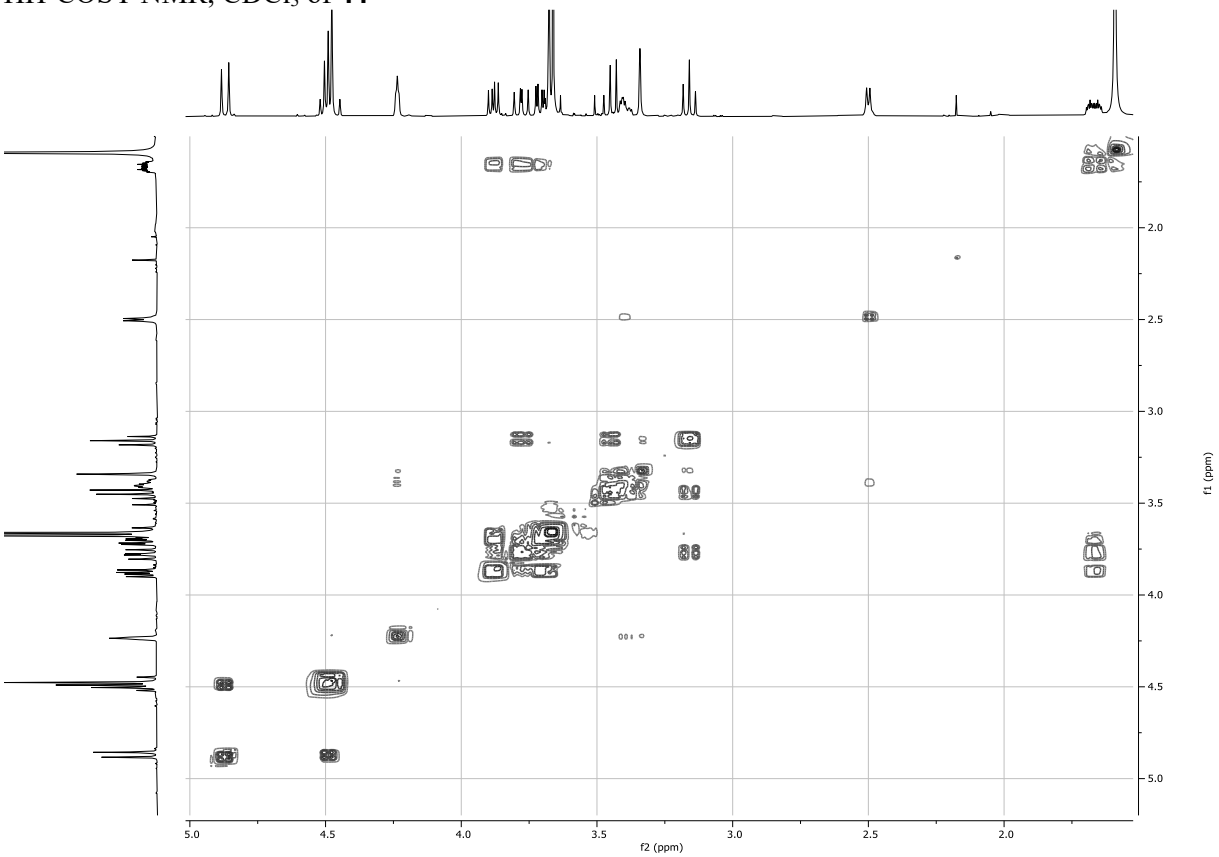


HSQC NMR, $CDCl_3$ of **44**

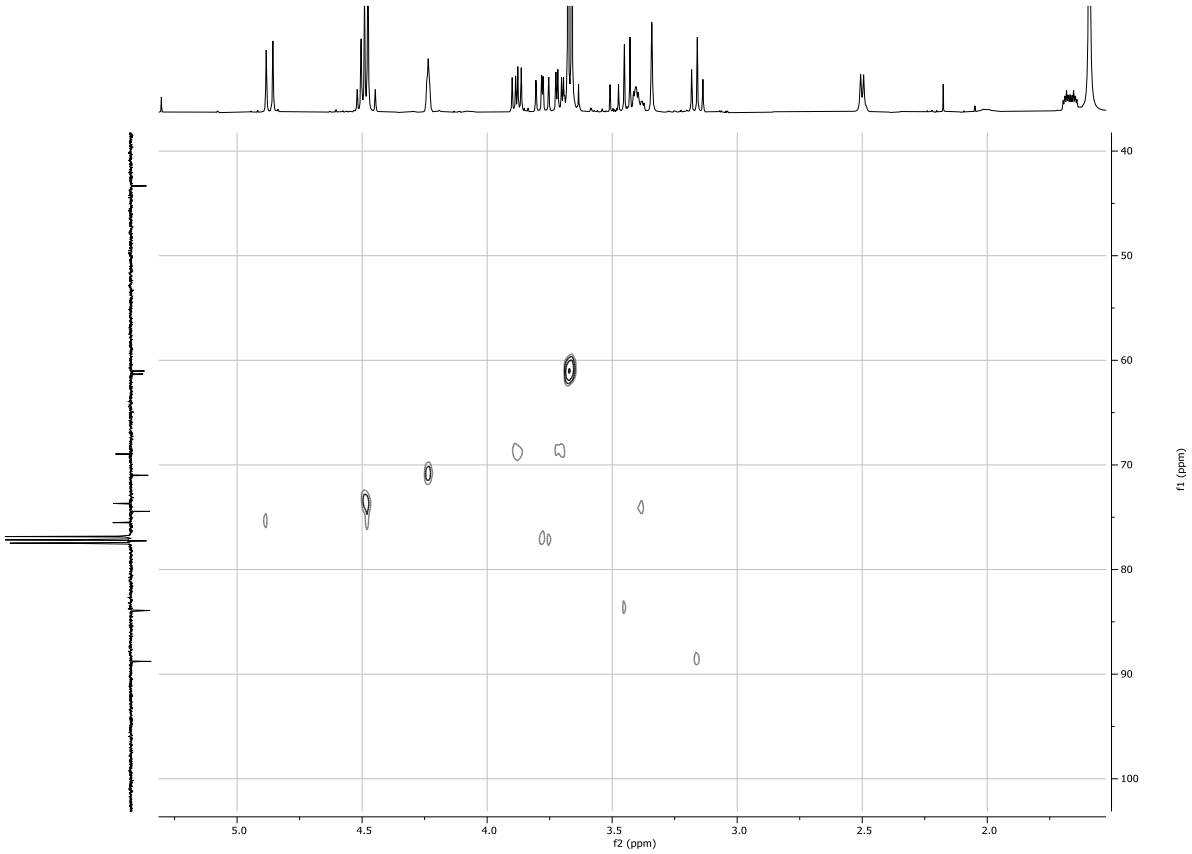

$^{1}$H NMR, 400MHz, $CDCl_3$ of **45**

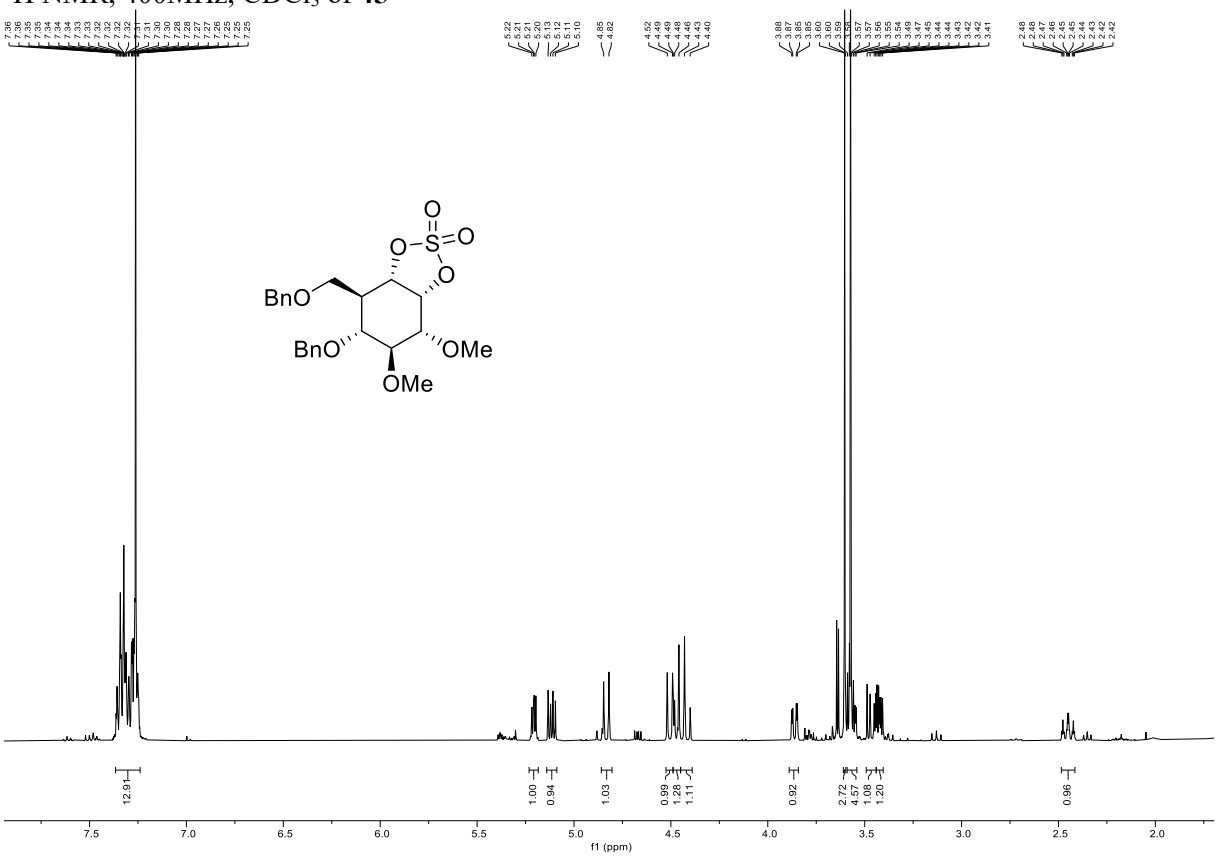


$^{13}$C NMR, 101MHz, $CDCl_3$ of **45**

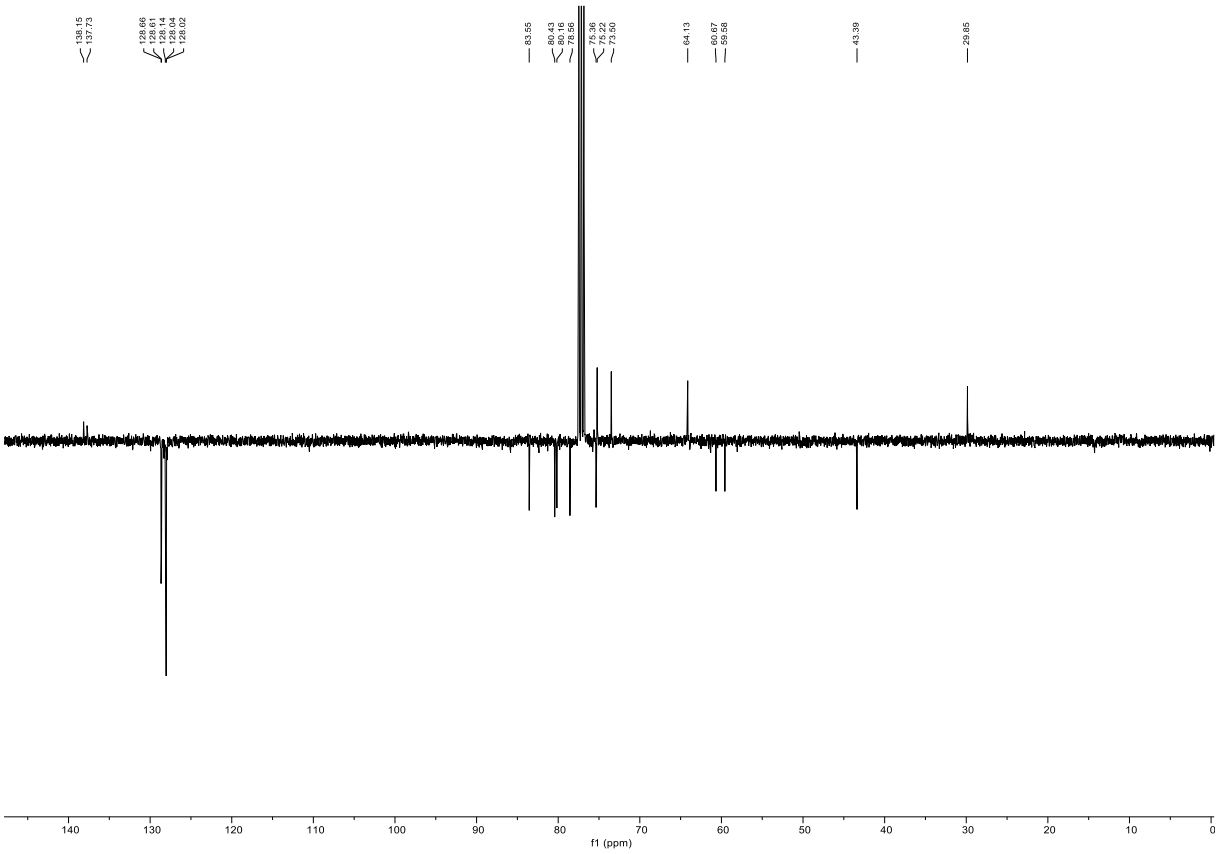

HH-COSY NMR, $CDCl_3$ of **45**

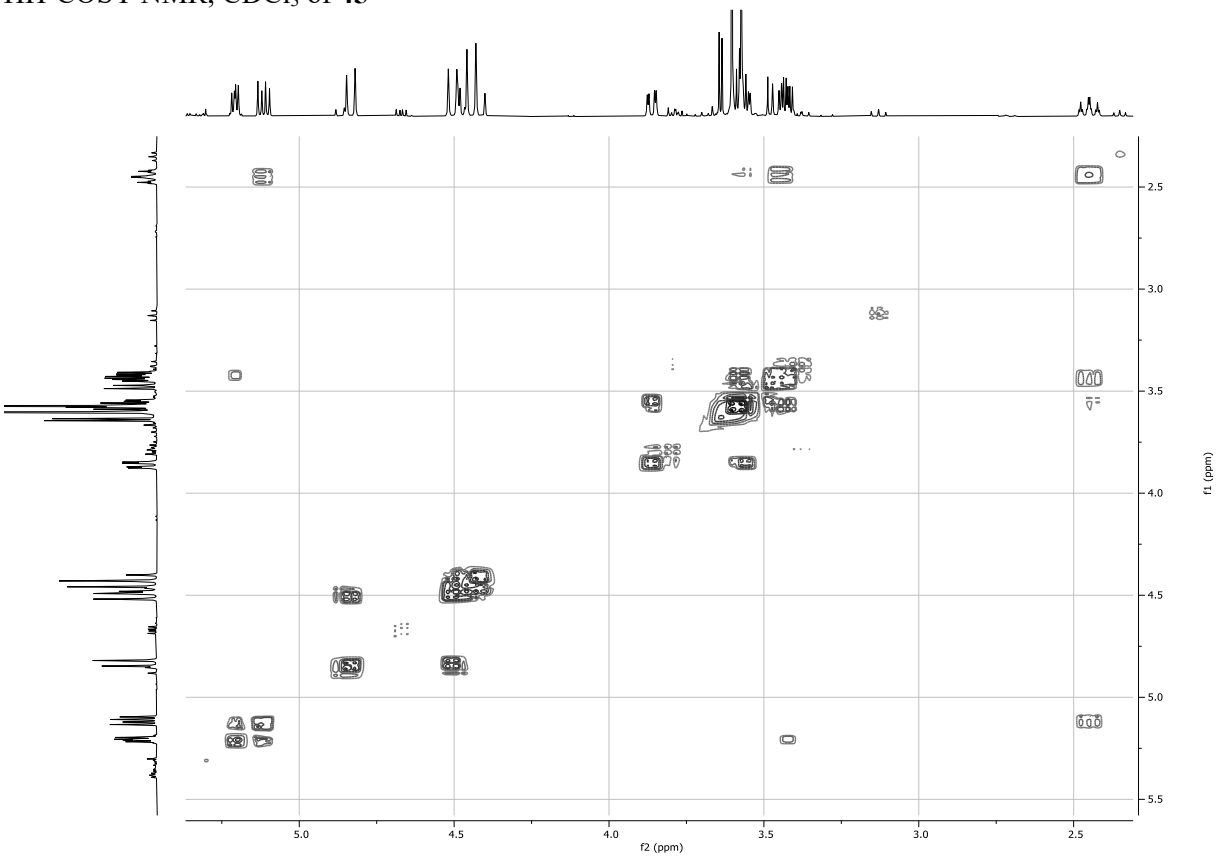


HSQC NMR, $CDCl_3$ of **45**

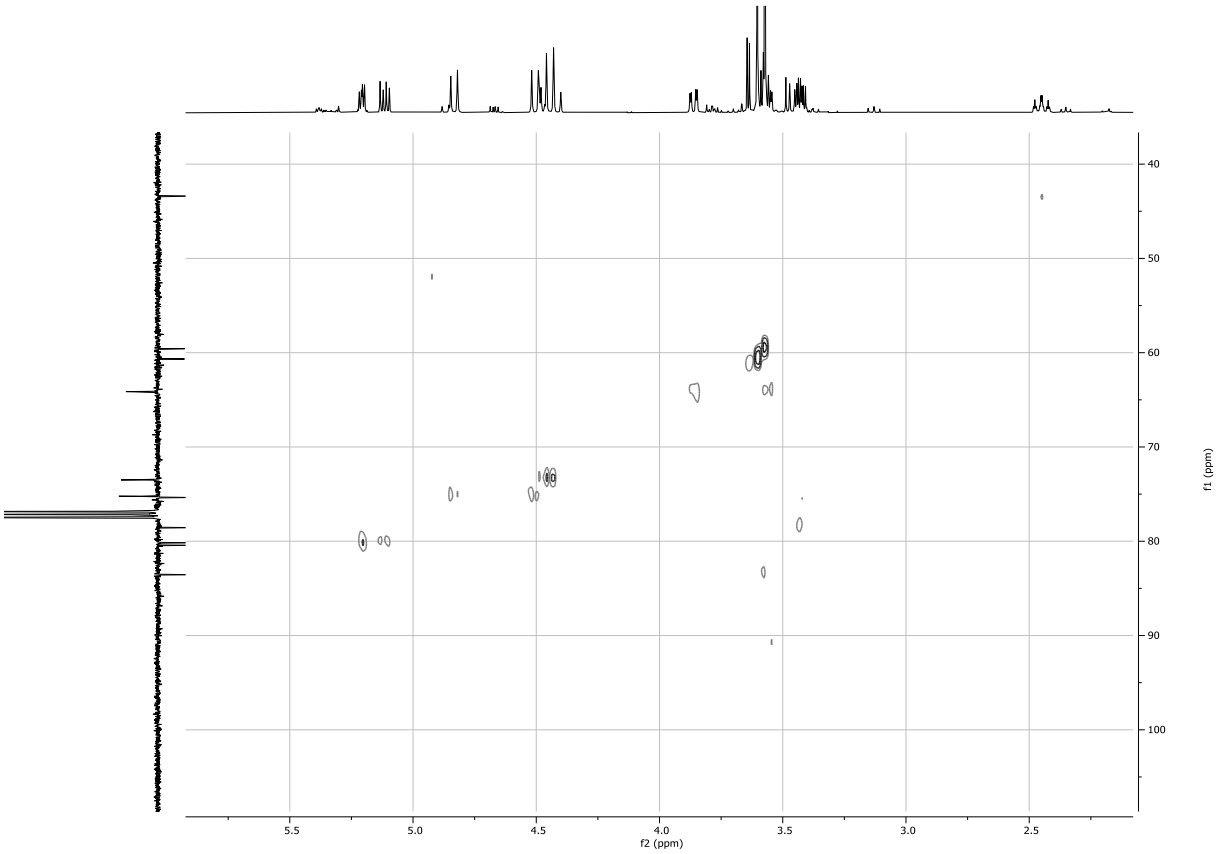

$^{1}$H NMR, 500MHz, MeOD of **9**

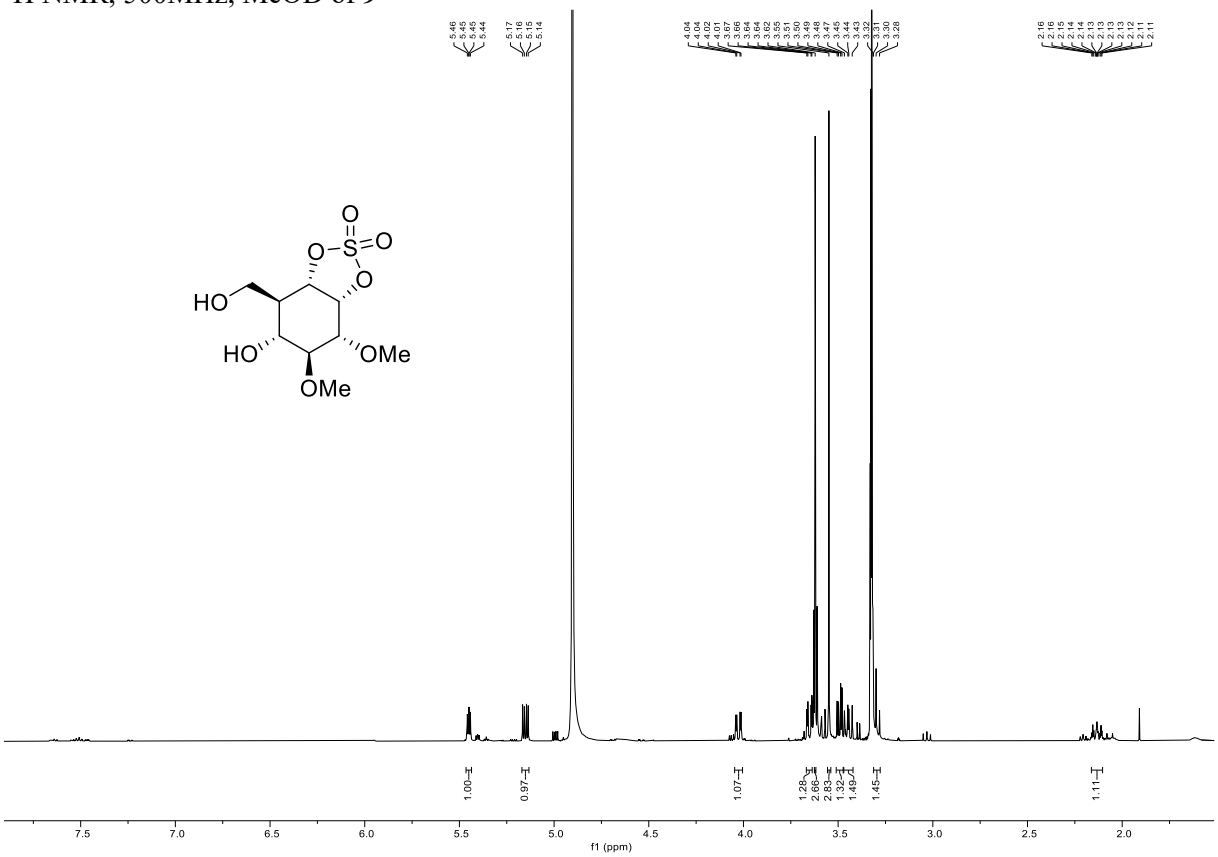


$^{13}$C NMR, 126MHz, MeOD of **9**

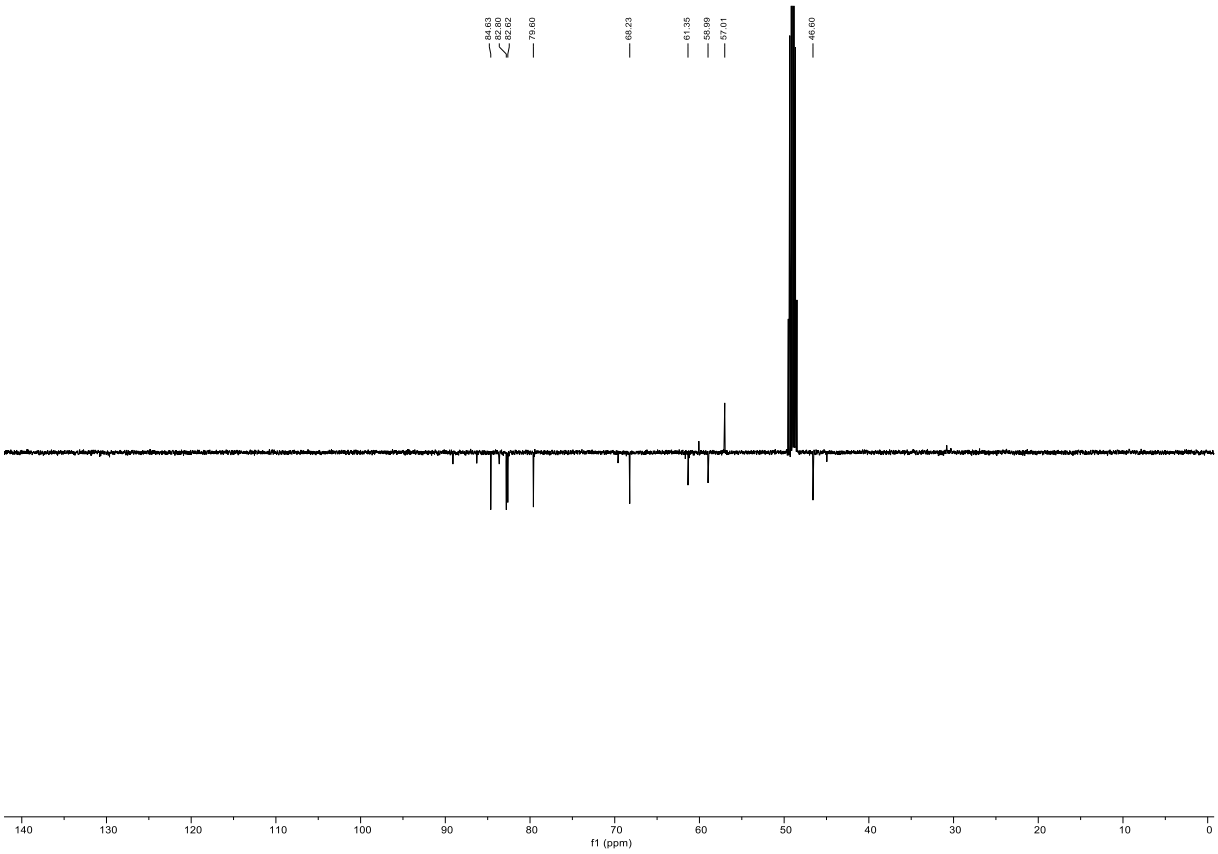

HH-COSY NMR, MeOD of **9**

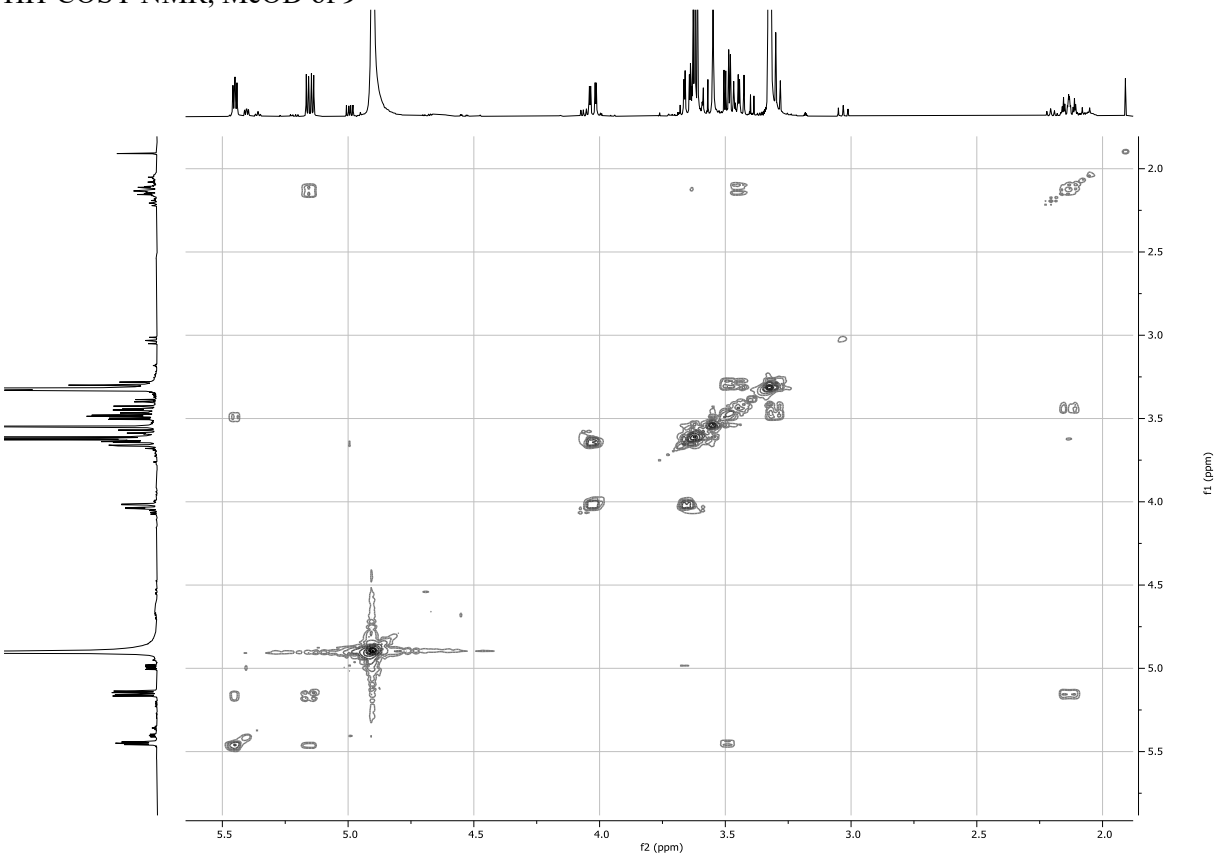


HSQC NMR, MeOD of **9**

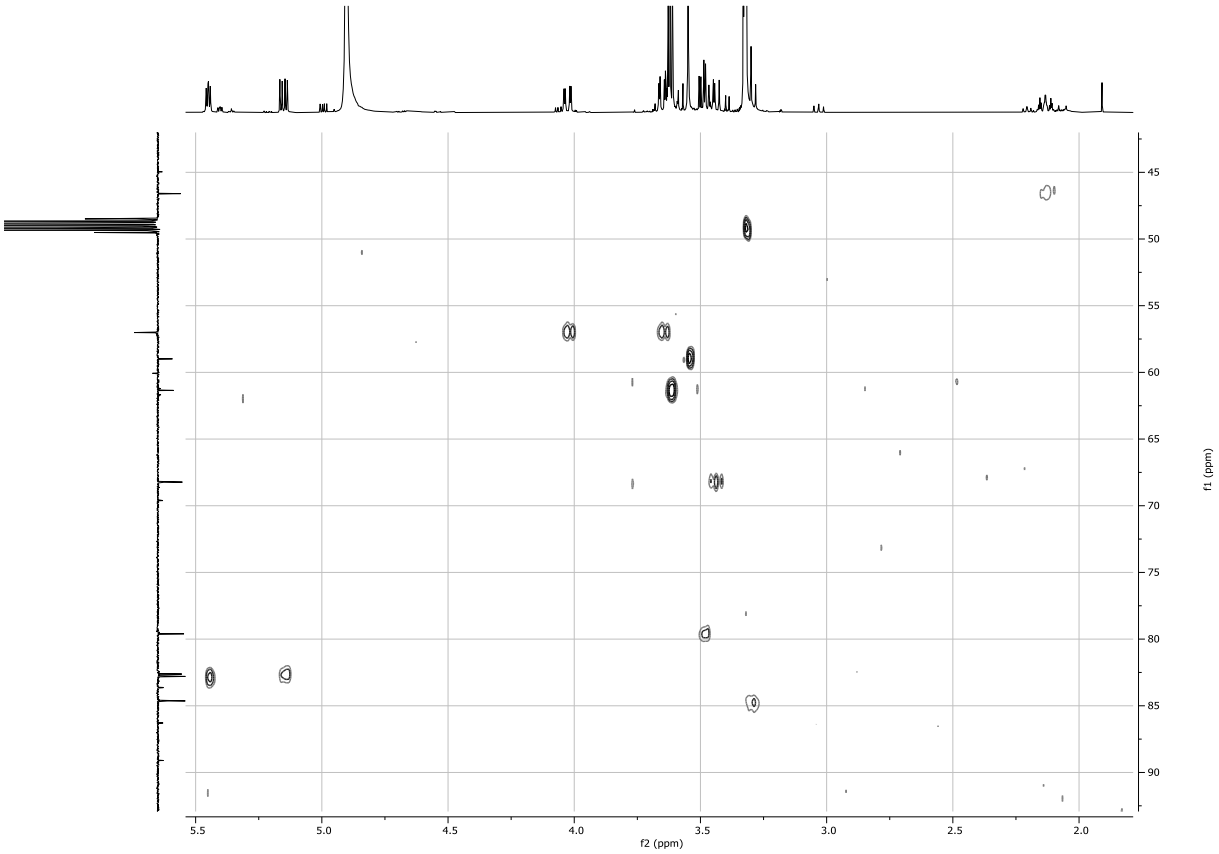

$^{1}$H NMR, 500MHz, $CDCl_3$ of **46**

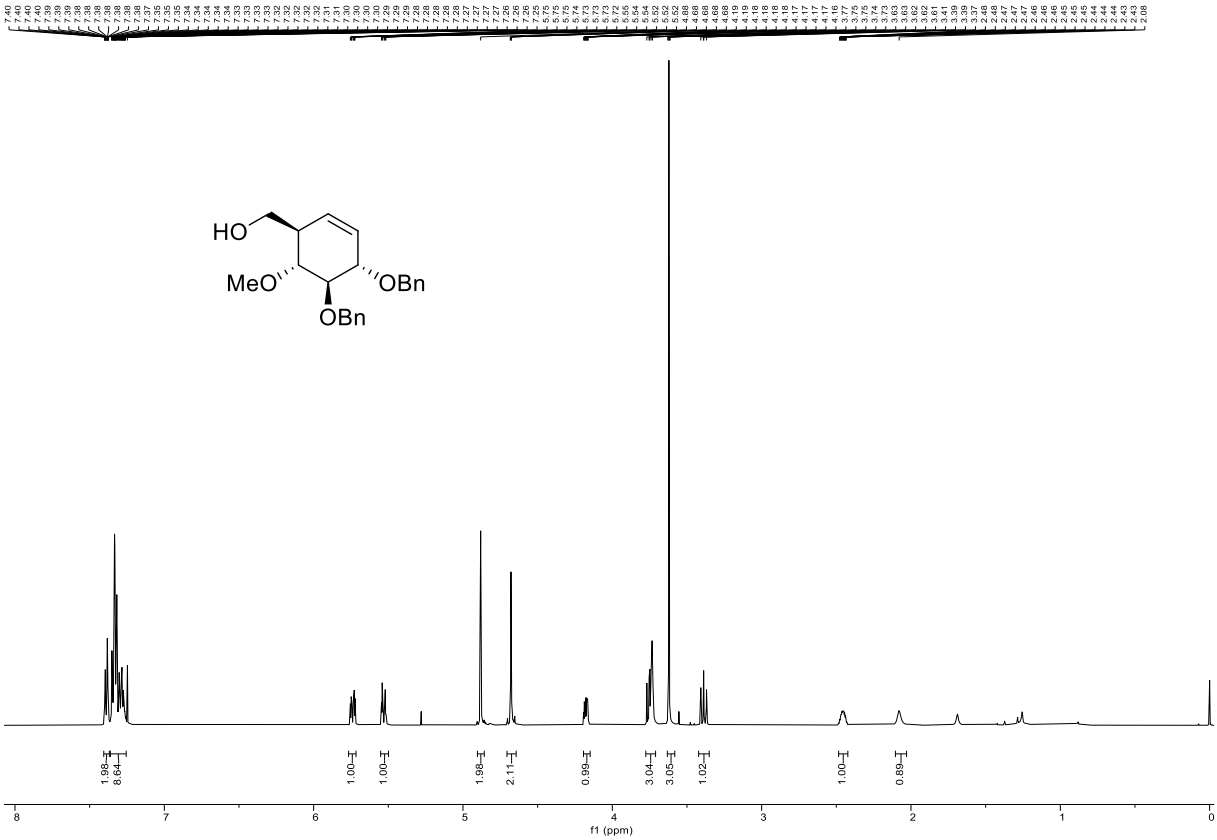


$^{13}$C NMR, 126MHz, $CDCl_3$ of **46**

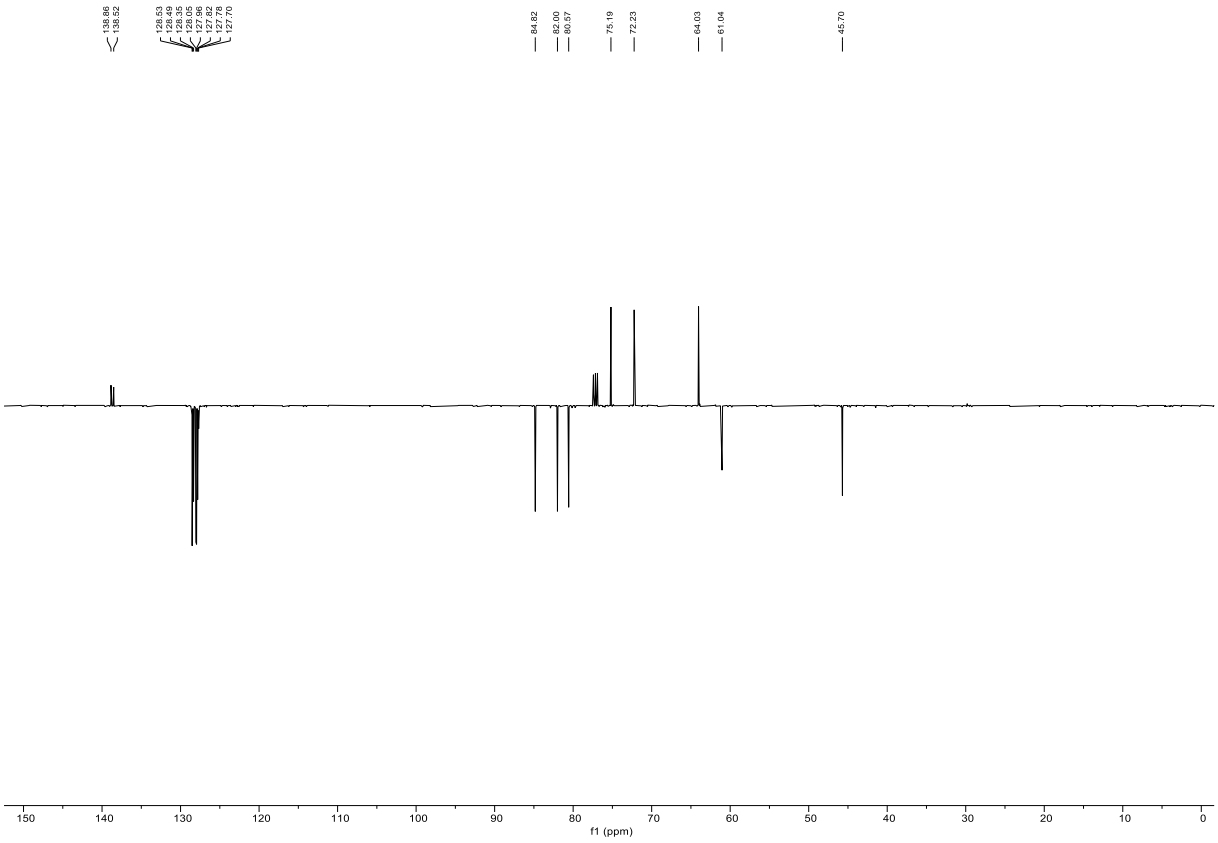


HH-COSY NMR, $CDCl_3$ of **46**

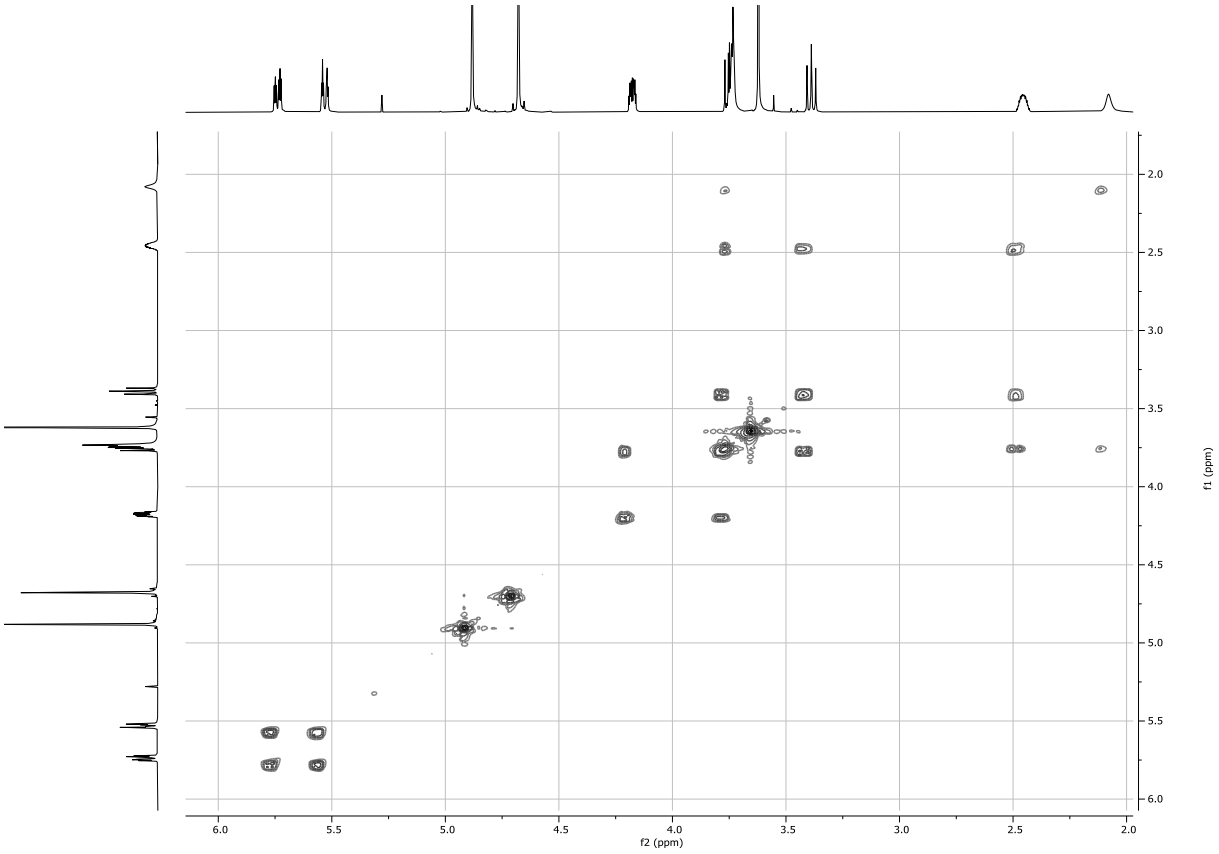


HSQC NMR, $CDCl_3$ of **46**

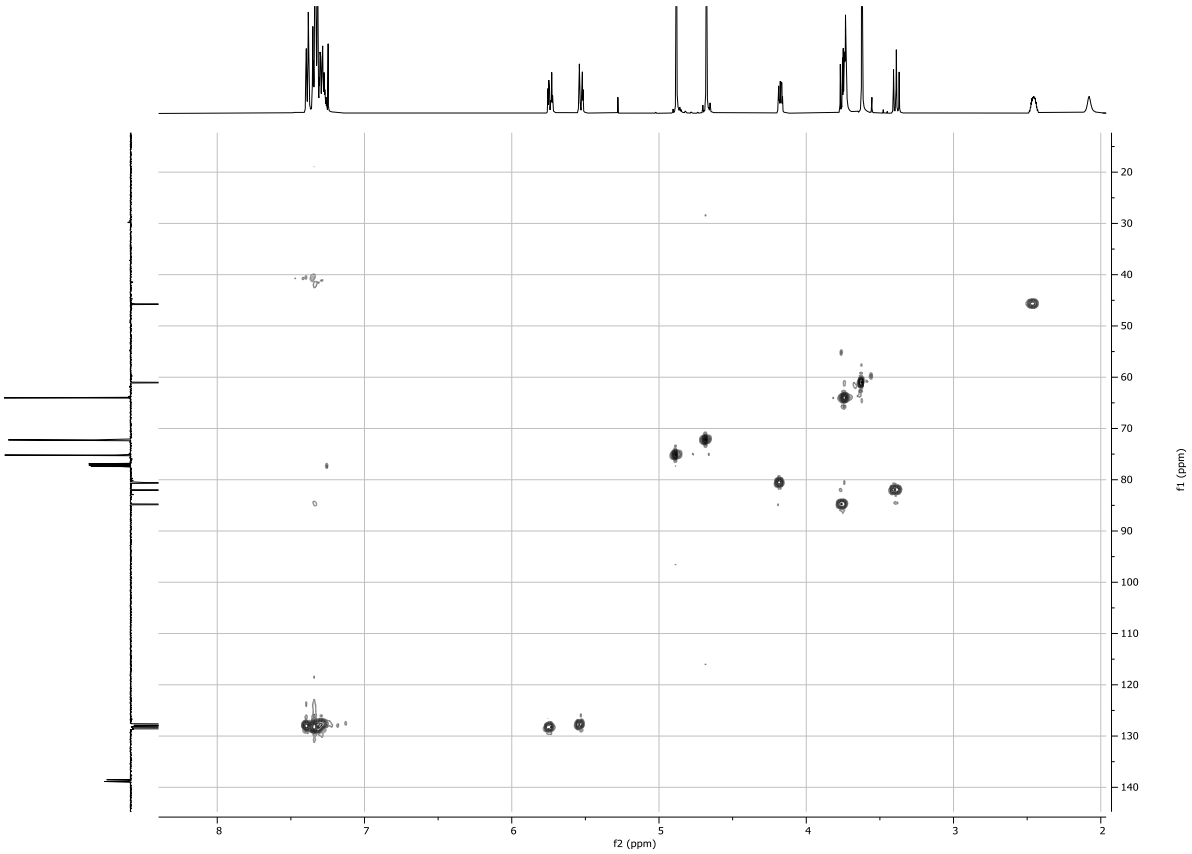


$^1H$ NMR, 500MHz, $CDCl_3$ of **47**

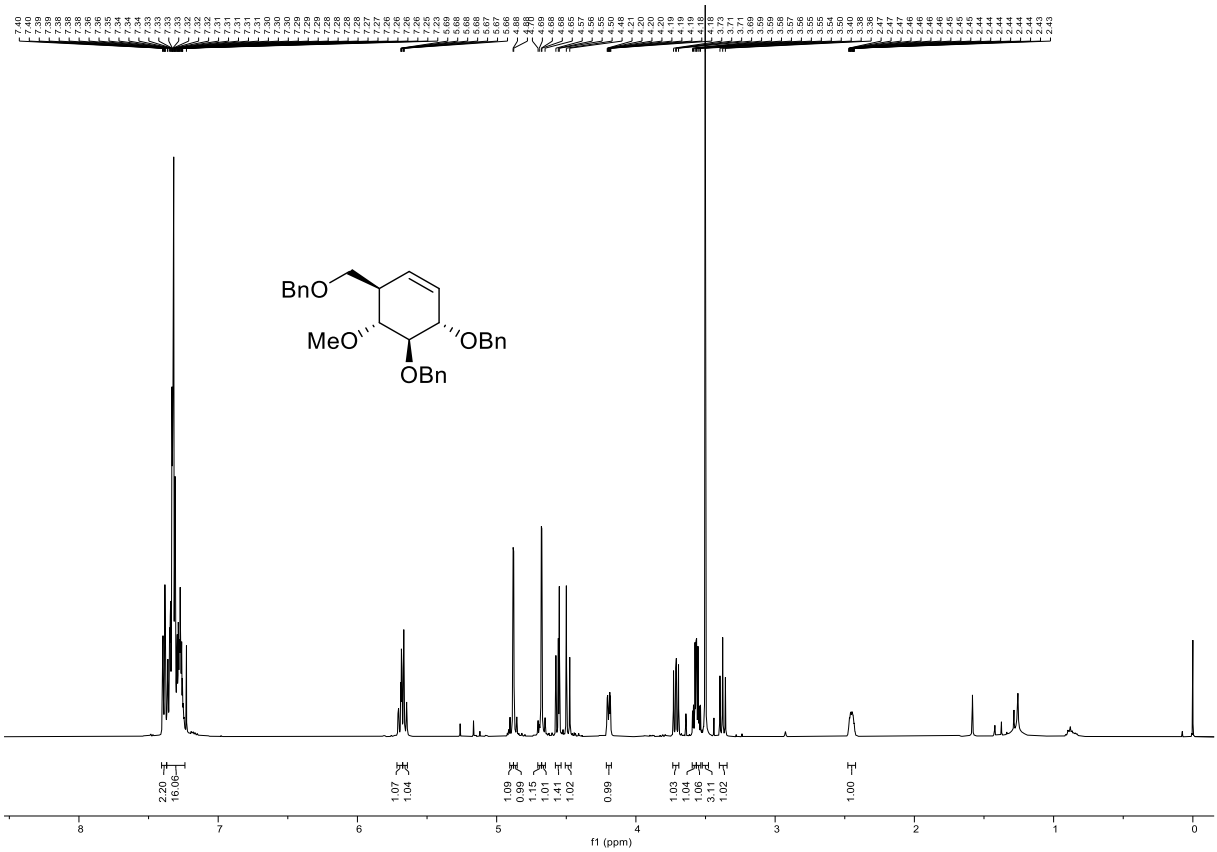


$^{13}$C NMR, 126MHz, $CDCl_3$ of **47**

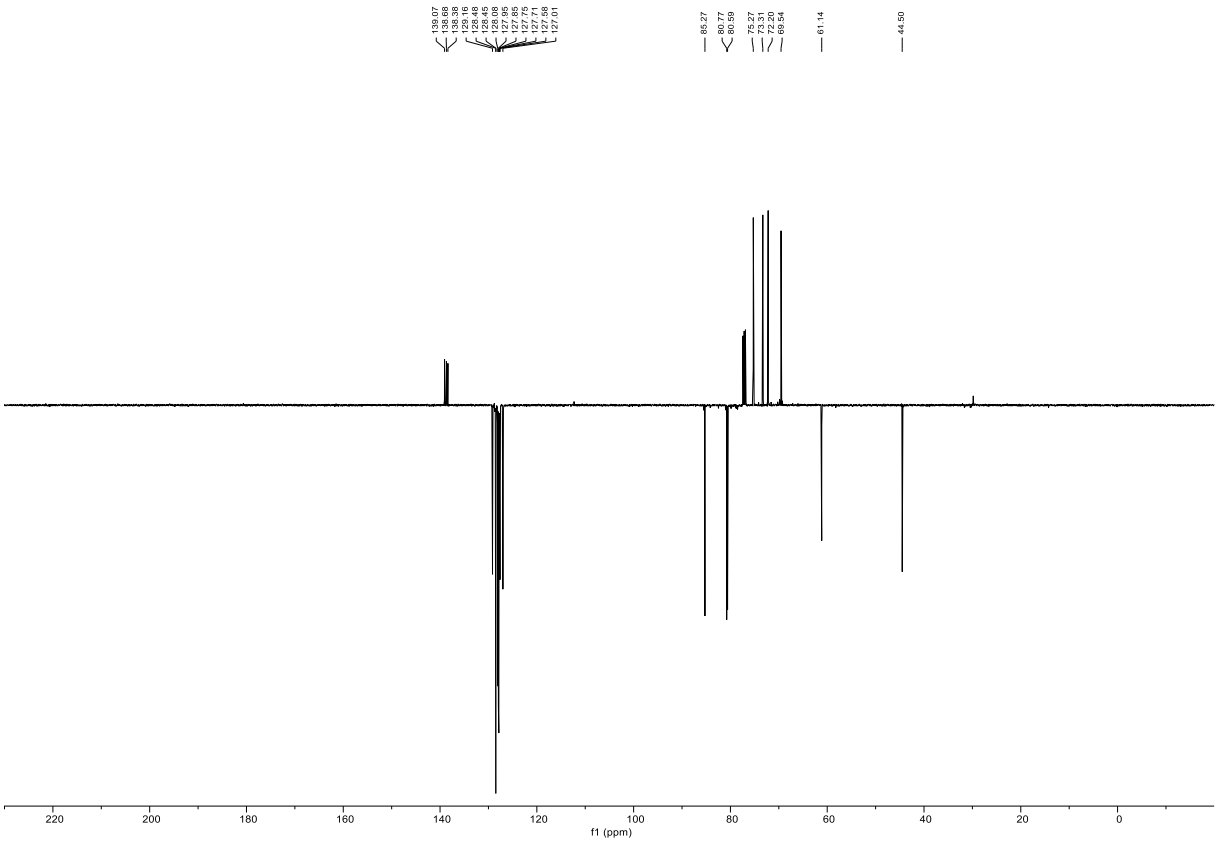


HH-COSY NMR, $CDCl_3$ of **47**

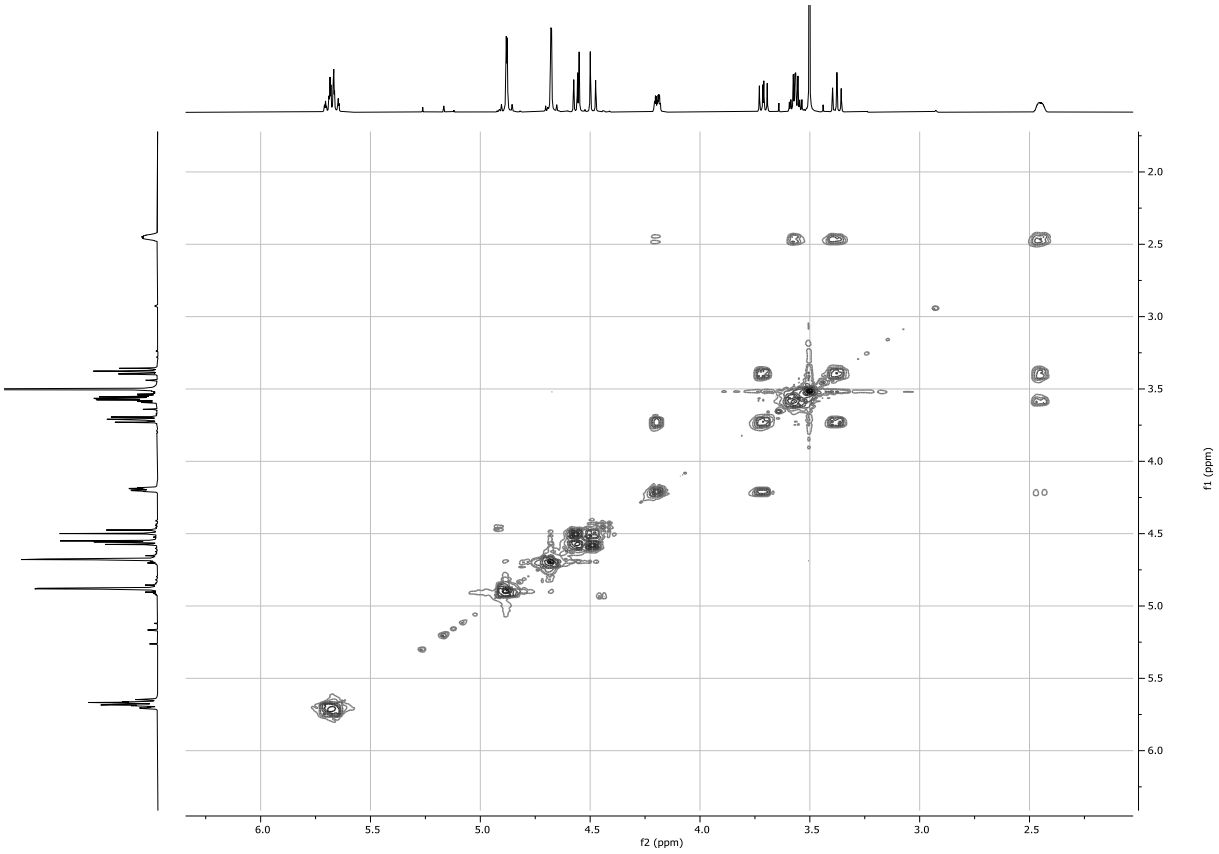


HSQC NMR, $CDCl_3$ of **47**

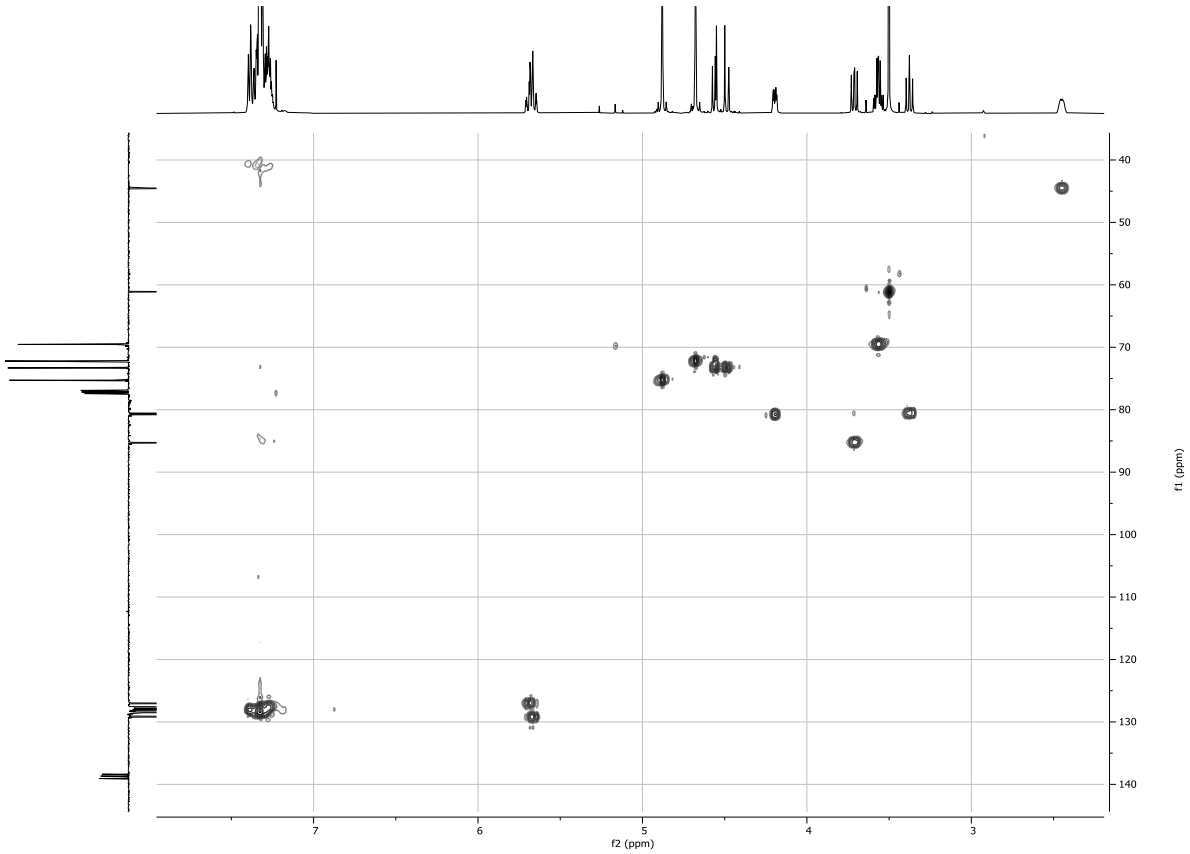

$^{1}$H NMR, 500MHz, $CDCl_3$ of **50**

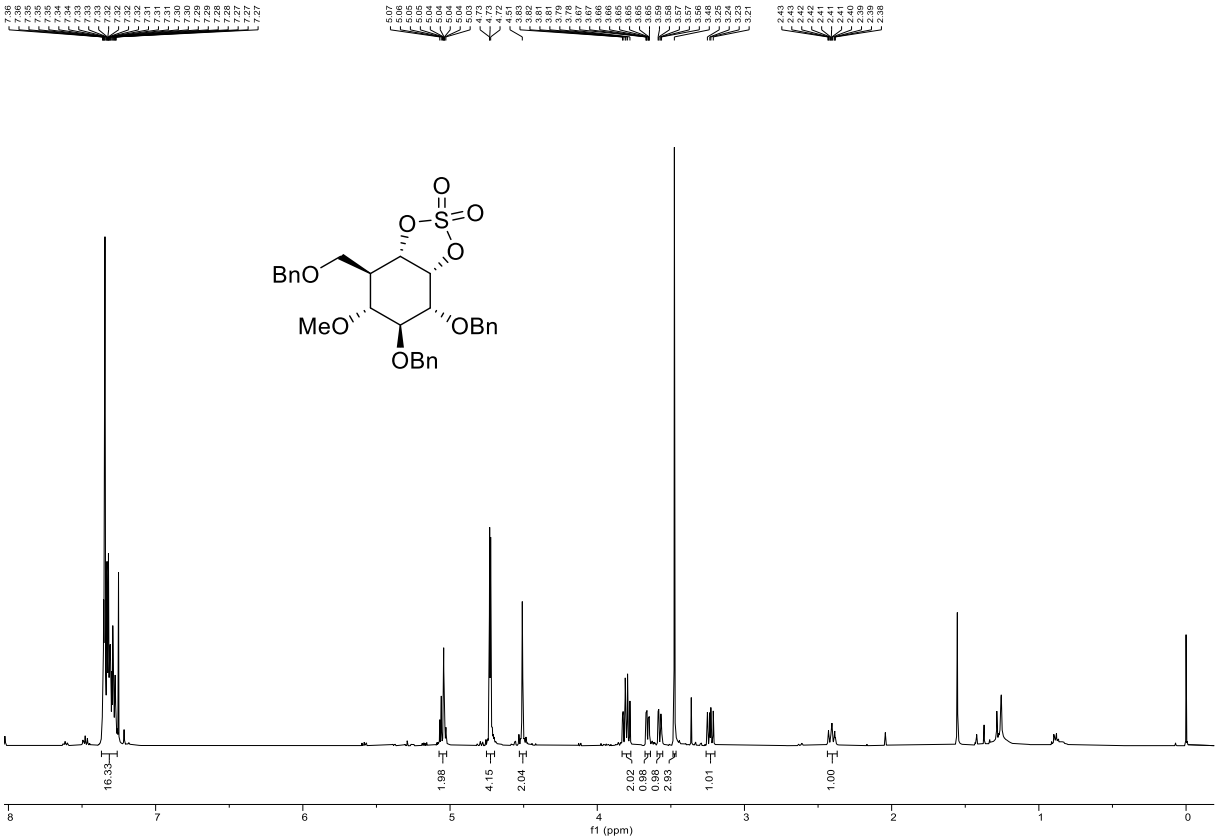


$^{13}$C NMR, 126MHz, $CDCl_3$ of **50**

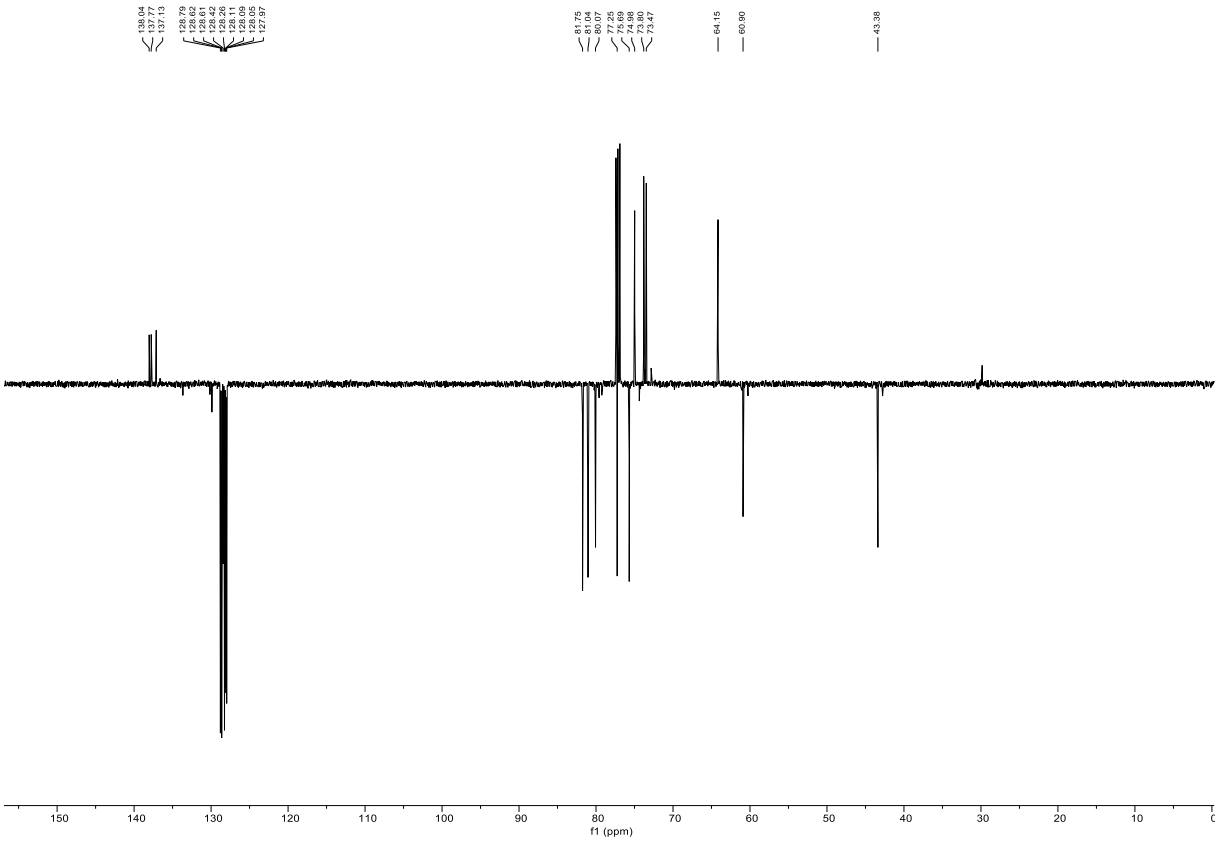

HH-COSY NMR, $CDCl_3$ of **50**

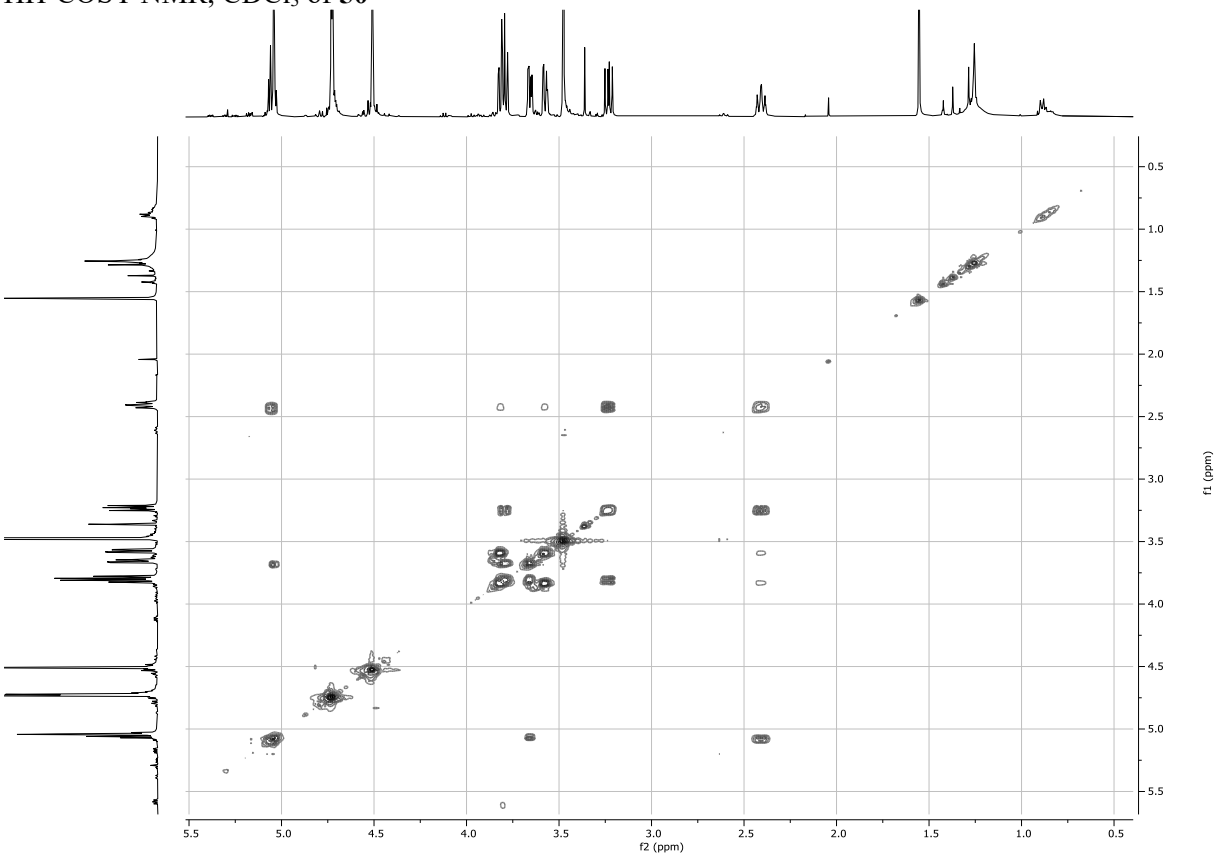


HSQC NMR, $CDCl_3$ of **50**

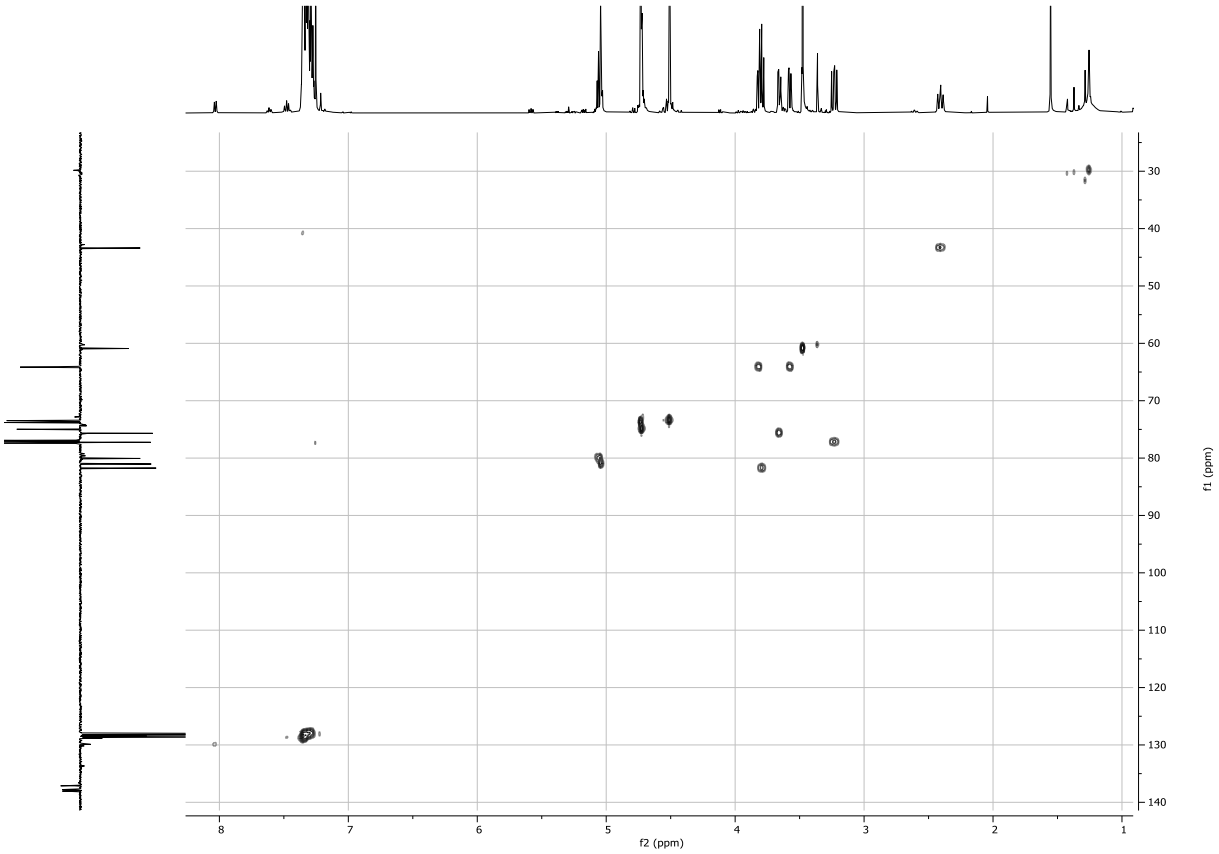

$^{1}$H NMR, 500MHz, MeOD of **7**

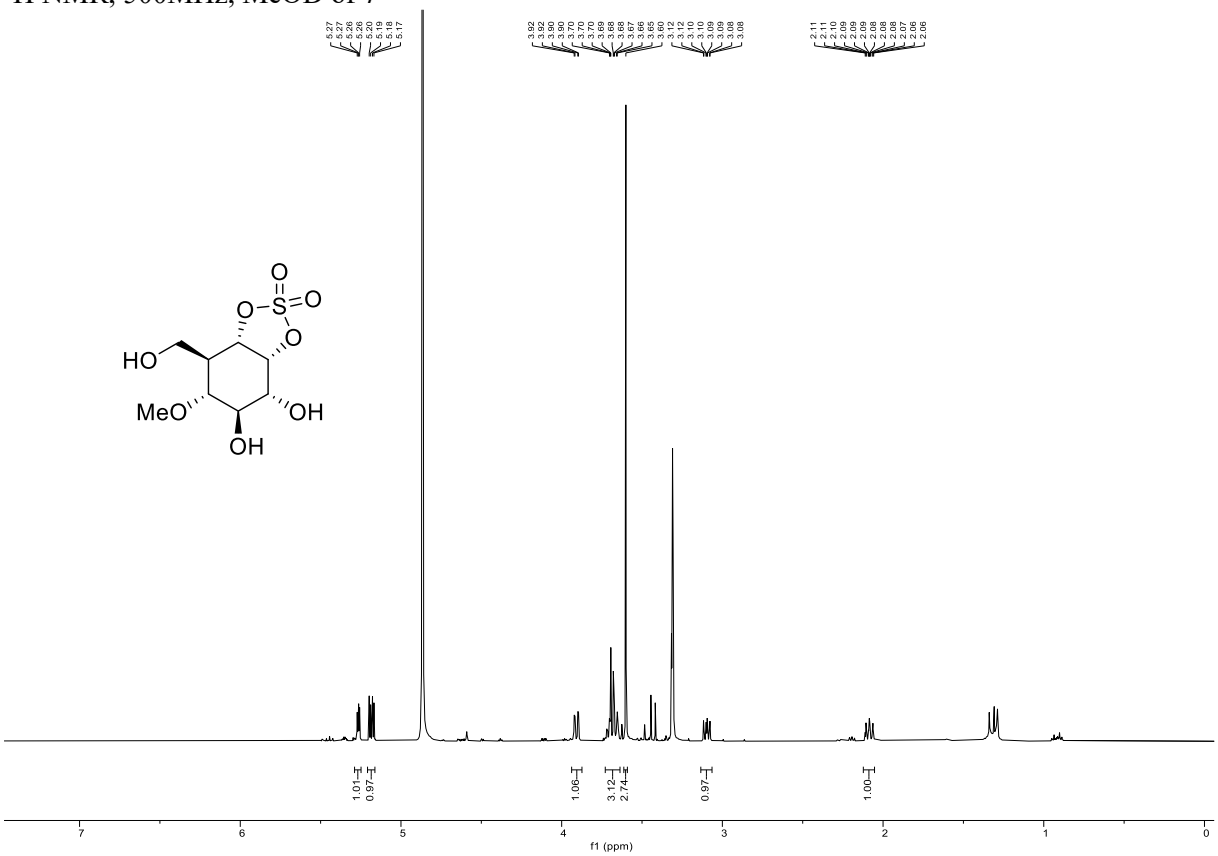


$^{13}$C NMR, 126MHz, MeOD of **7**

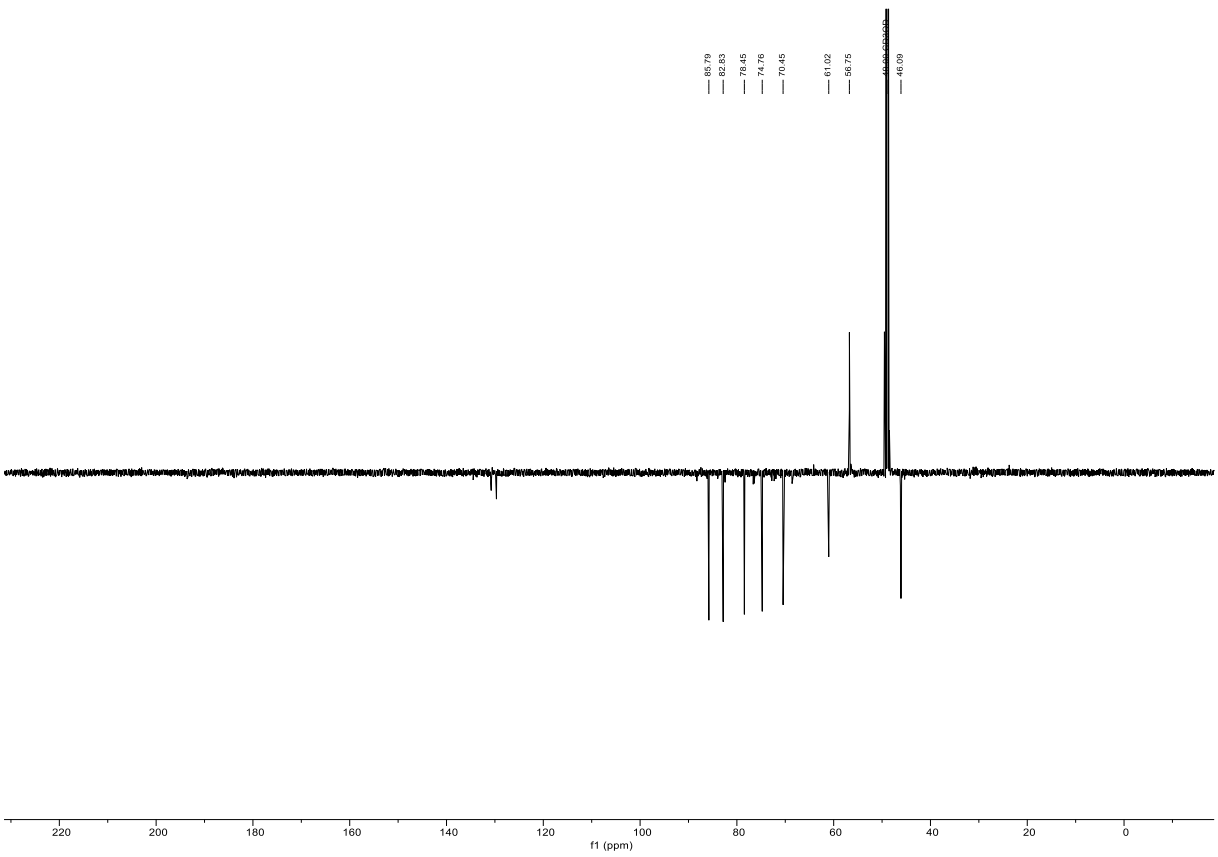


HH-COSY NMR, MeOD of **7**

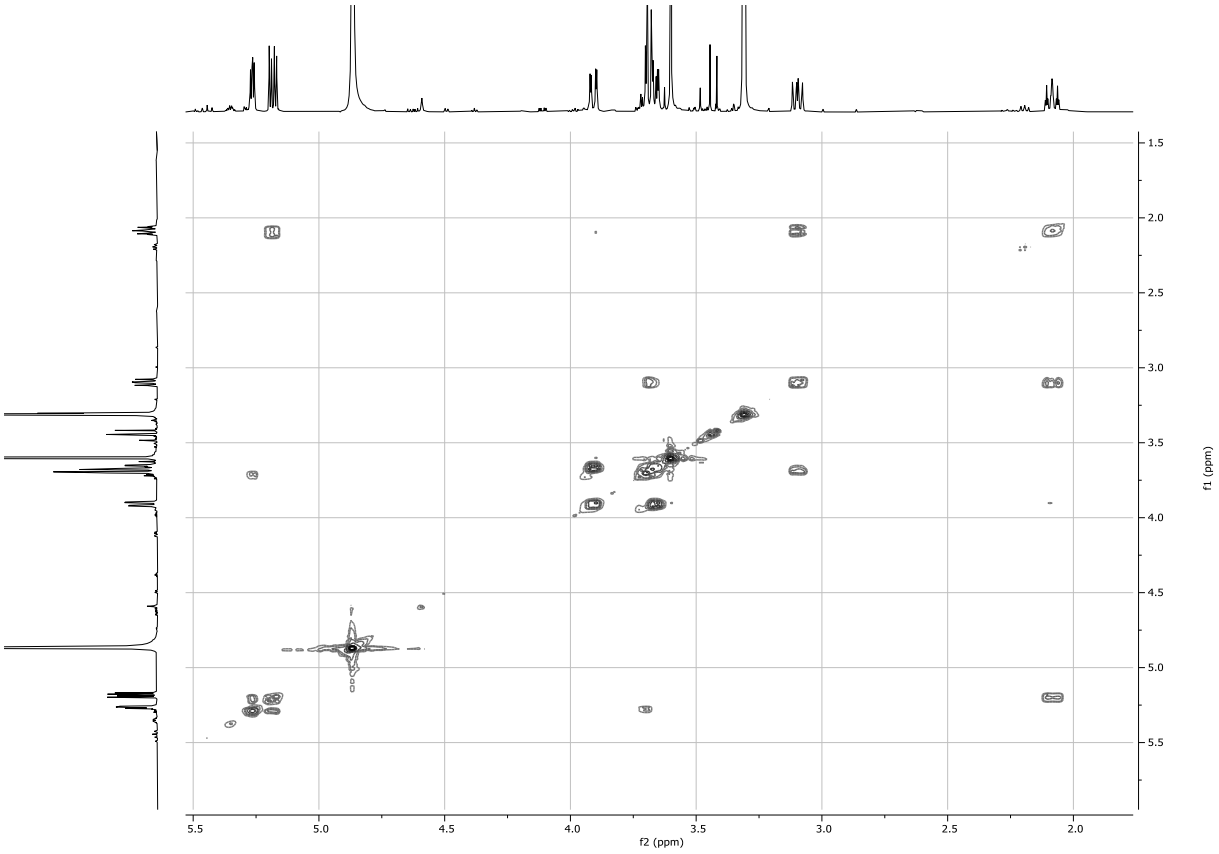


HSQC NMR, MeOD of **7**

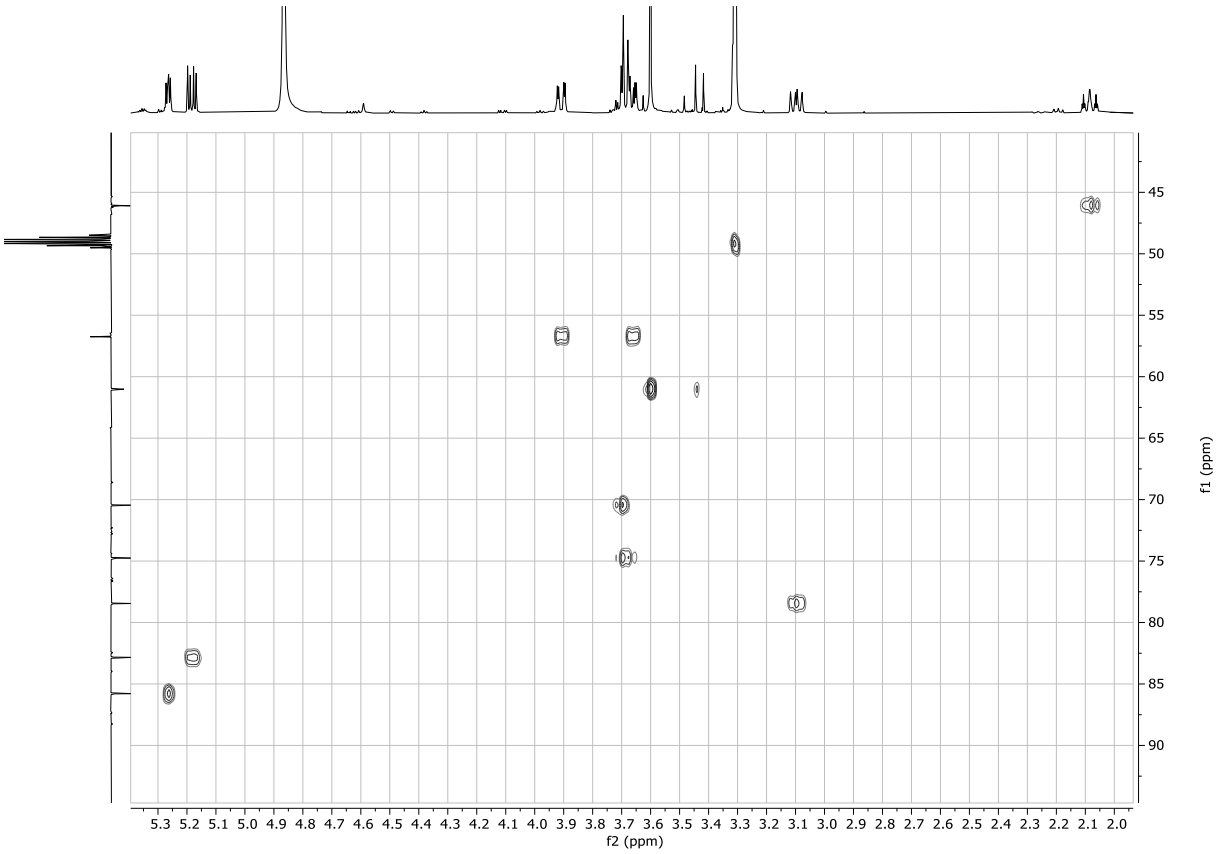

$^{1}$H NMR, 500MHz, $CDCl_3$ of **51**

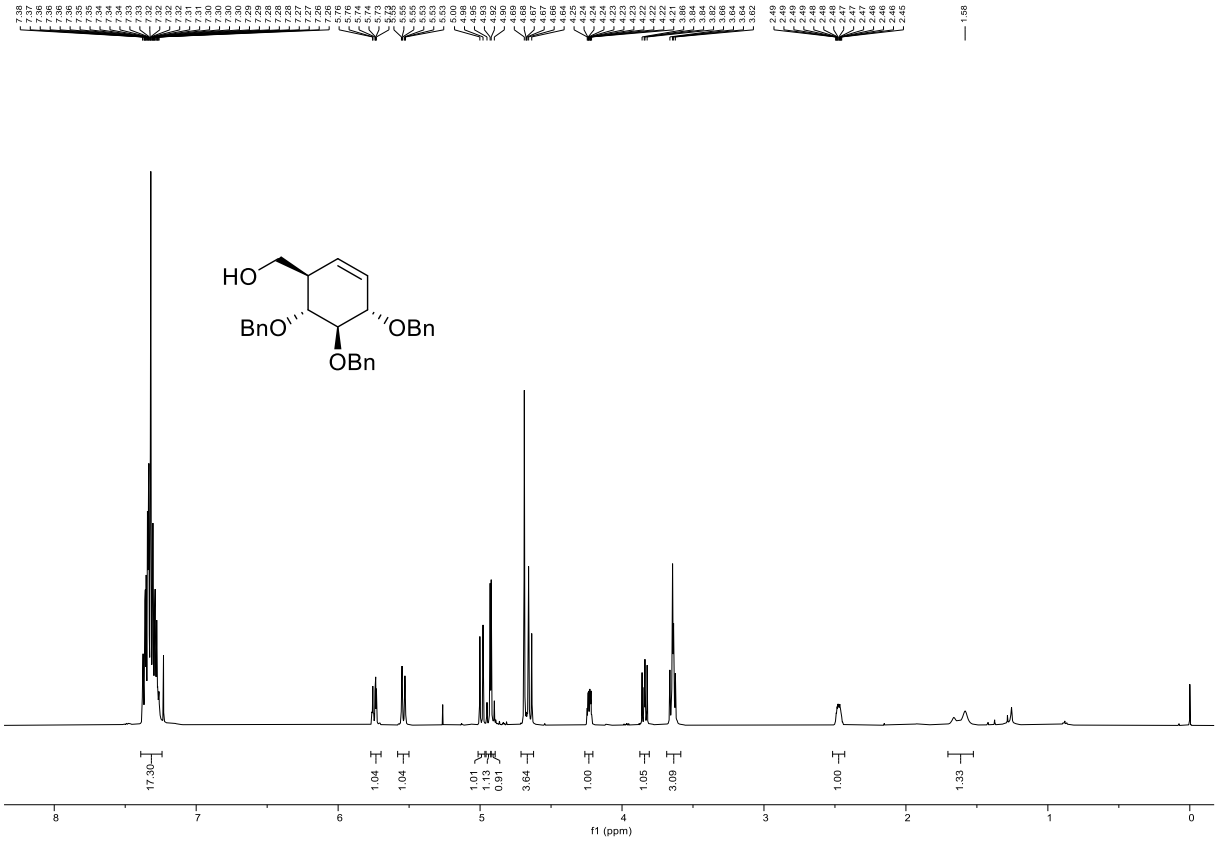


$^{13}$C NMR, 126MHz, $CDCl_3$ of **51**

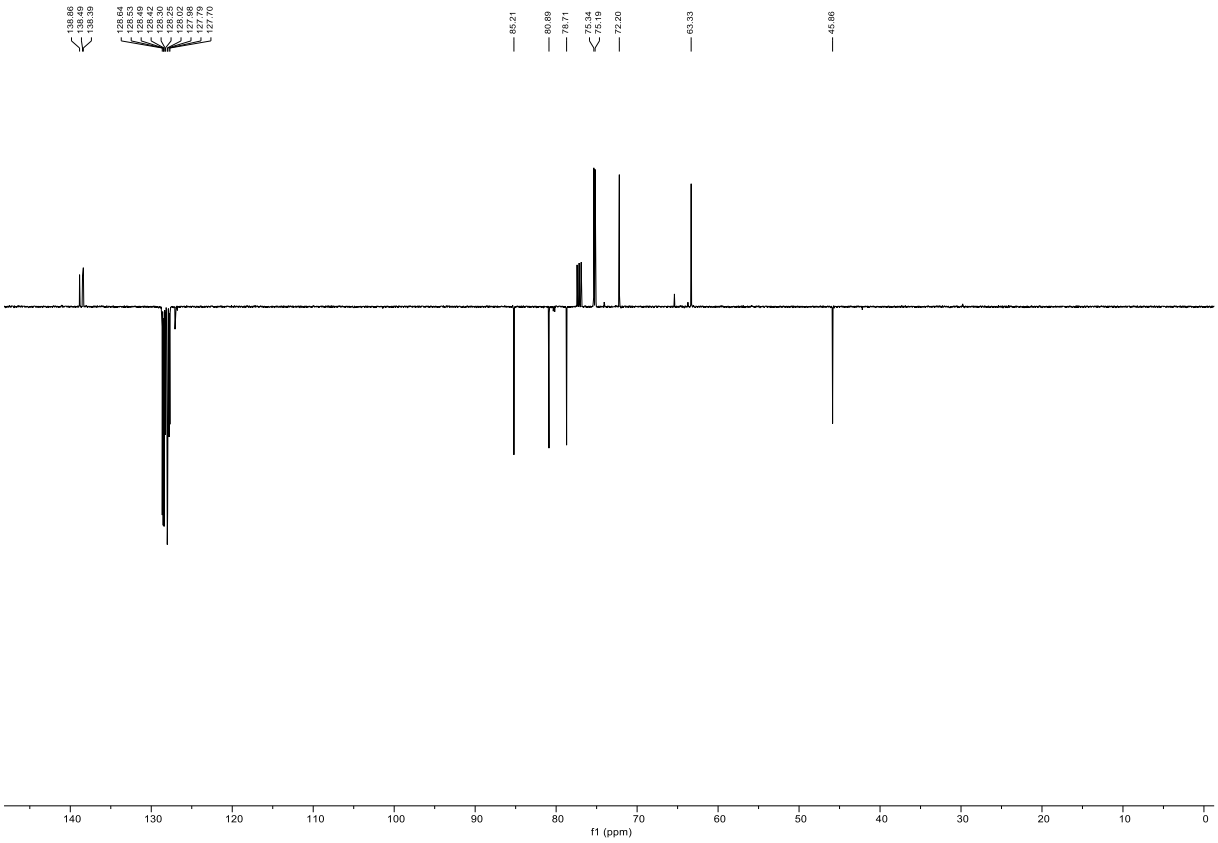

HH-COSY NMR, $CDCl_3$ of **51**

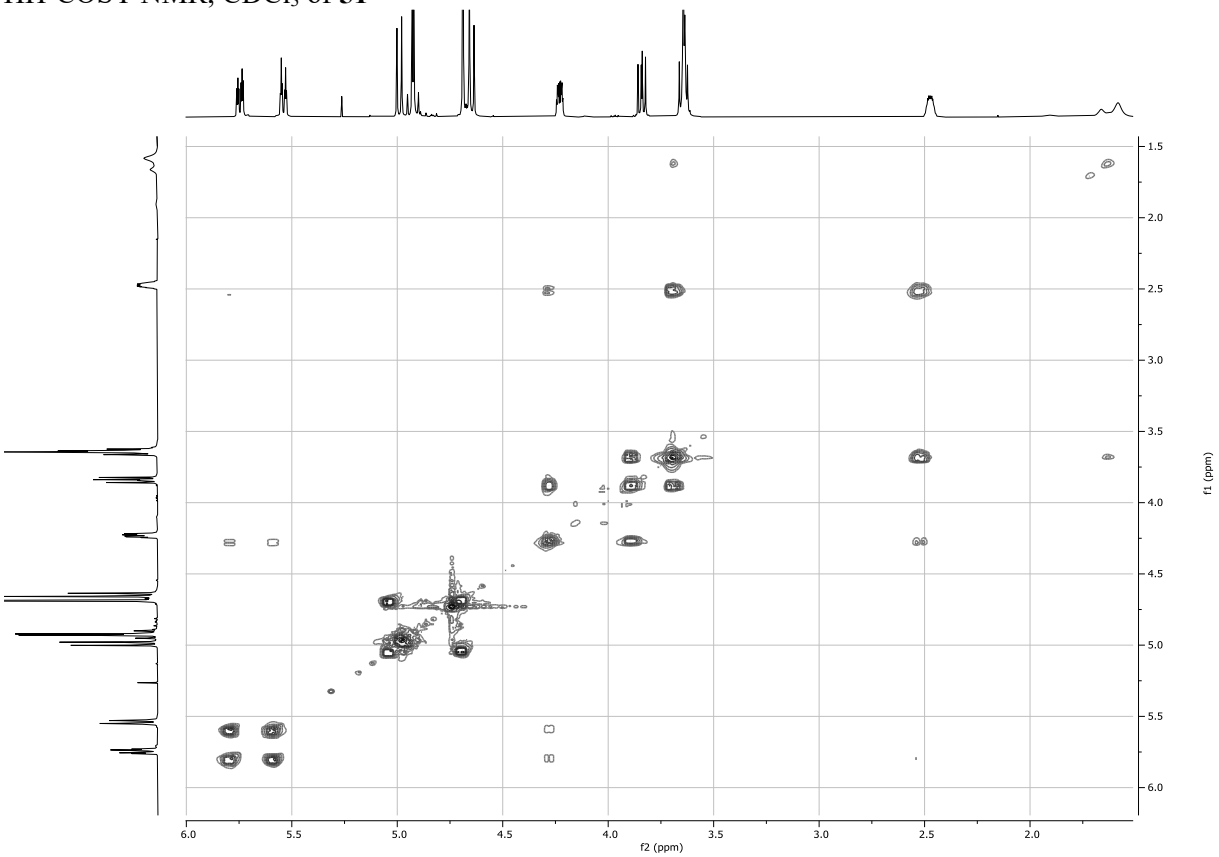


HSQC NMR, $CDCl_3$ of **51**

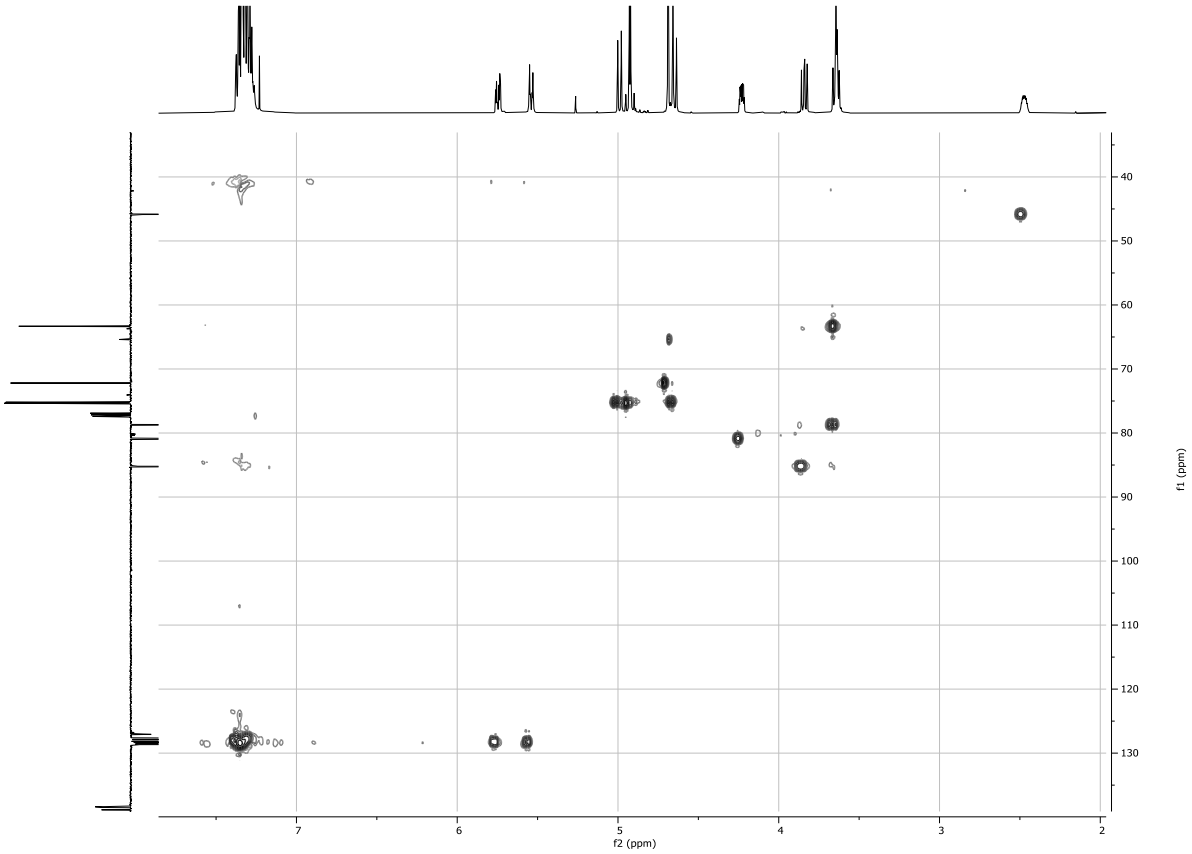

$^{1}$H NMR, 500MHz, $CDCl_3$ of **52**

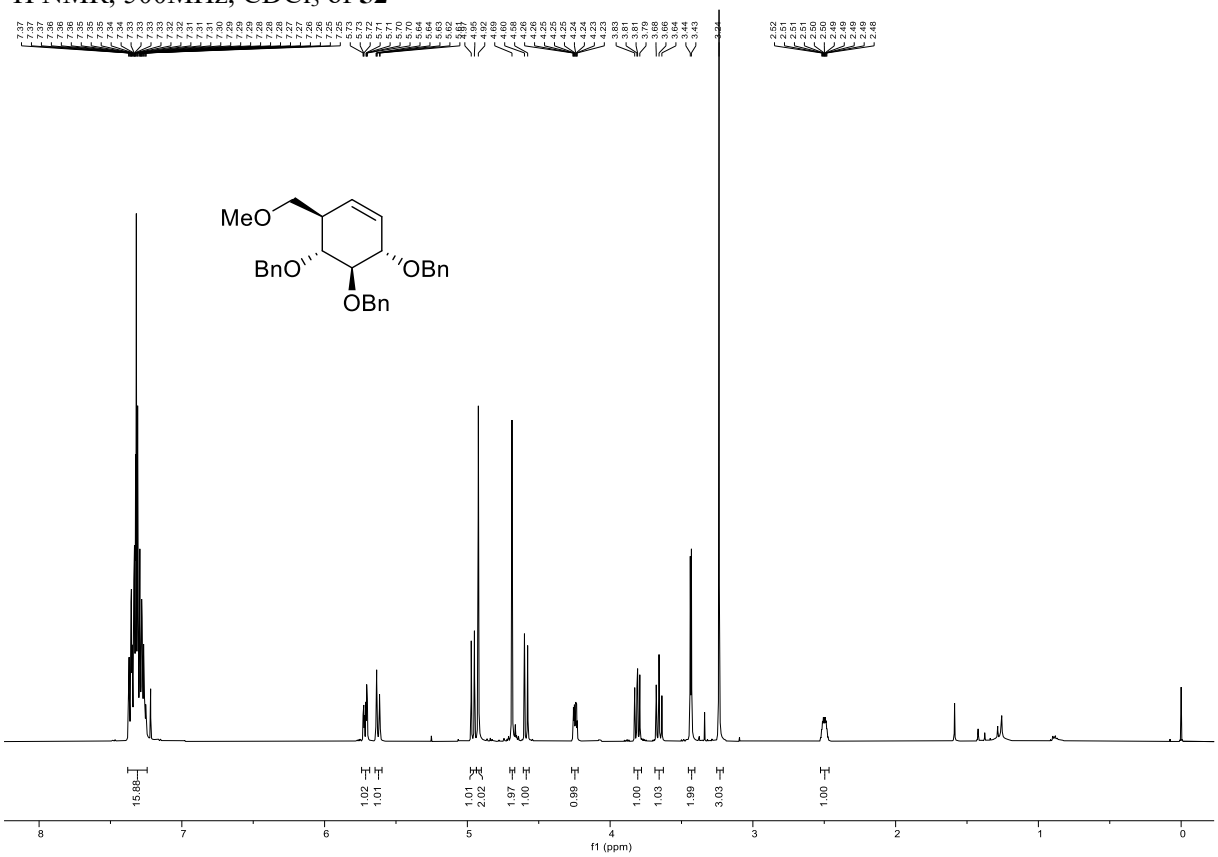


$^{13}$C NMR, 126MHz, $CDCl_3$ of **52**

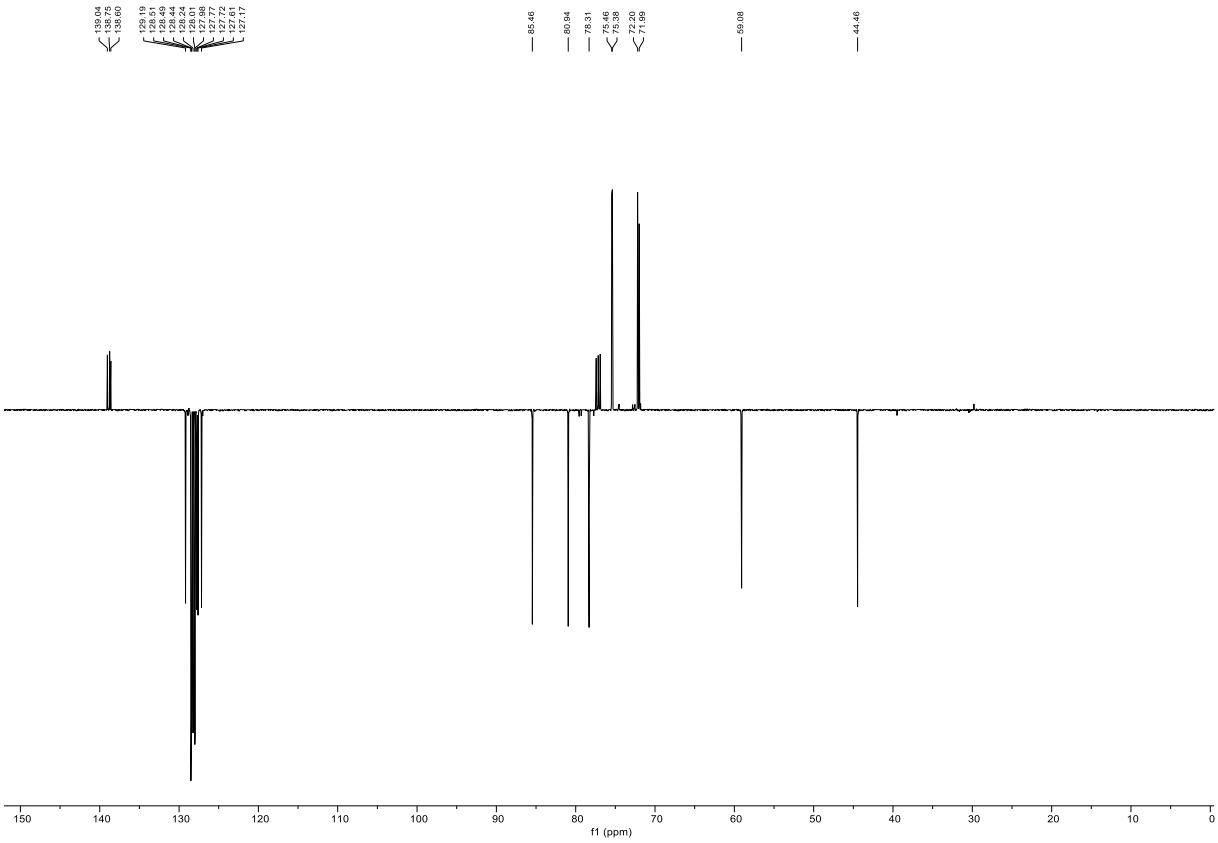

HH-COSY NMR, $CDCl_3$ of **52**

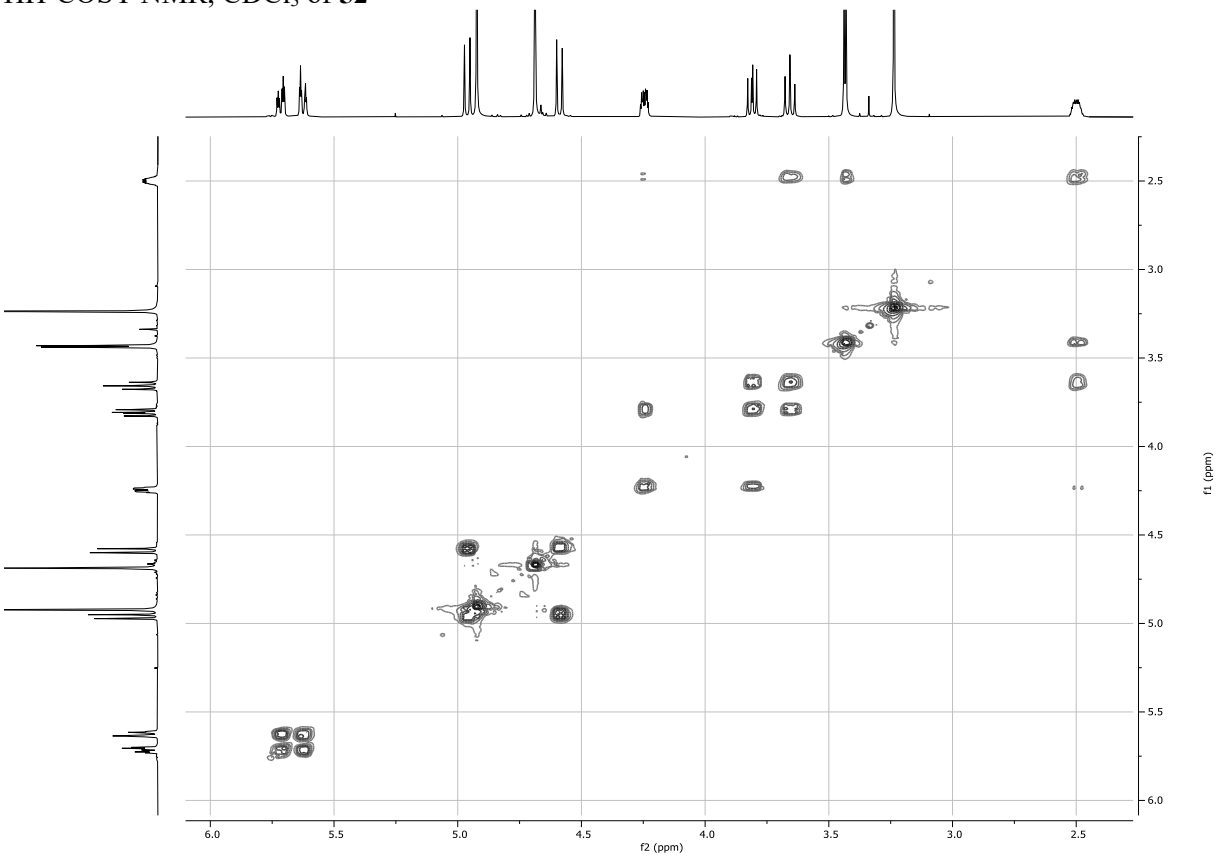


HSQC NMR, $CDCl_3$ of **52**

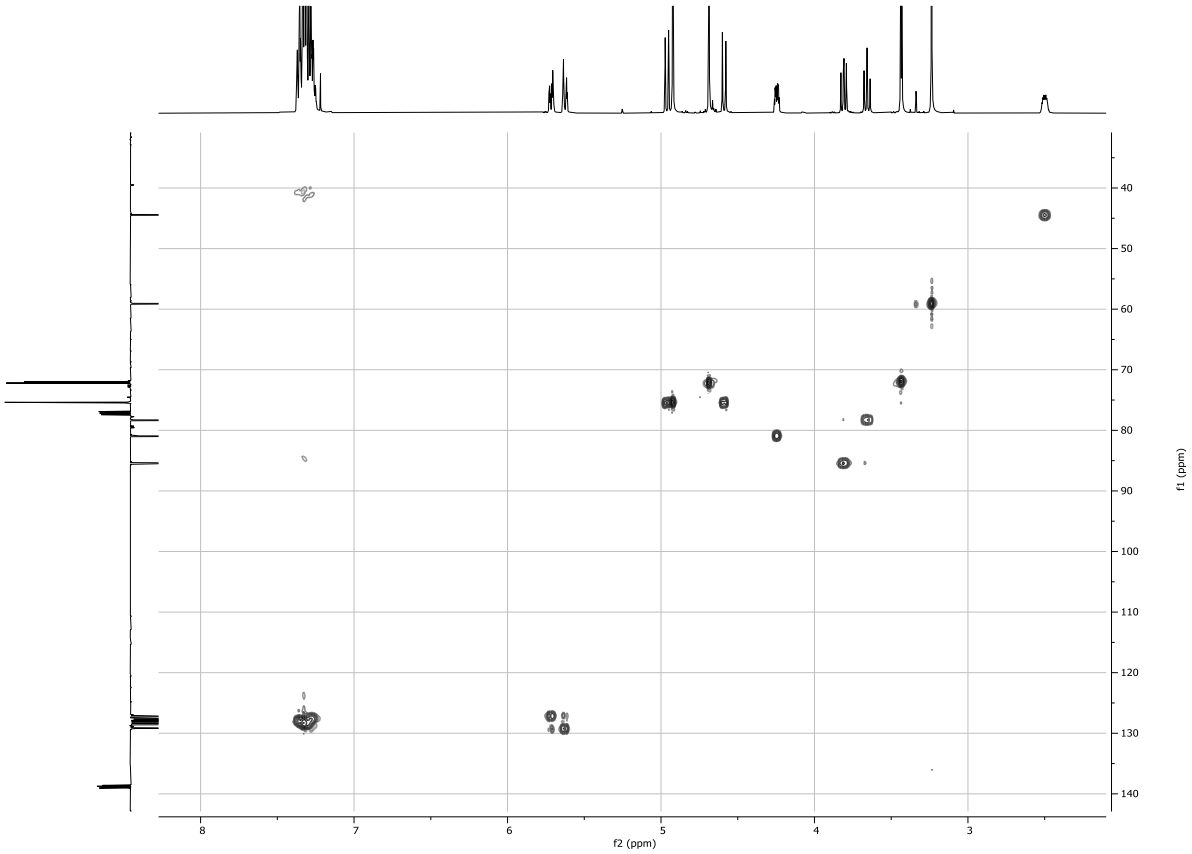

$^{1}$H NMR, 400MHz, $CDCl_3$ of **53**

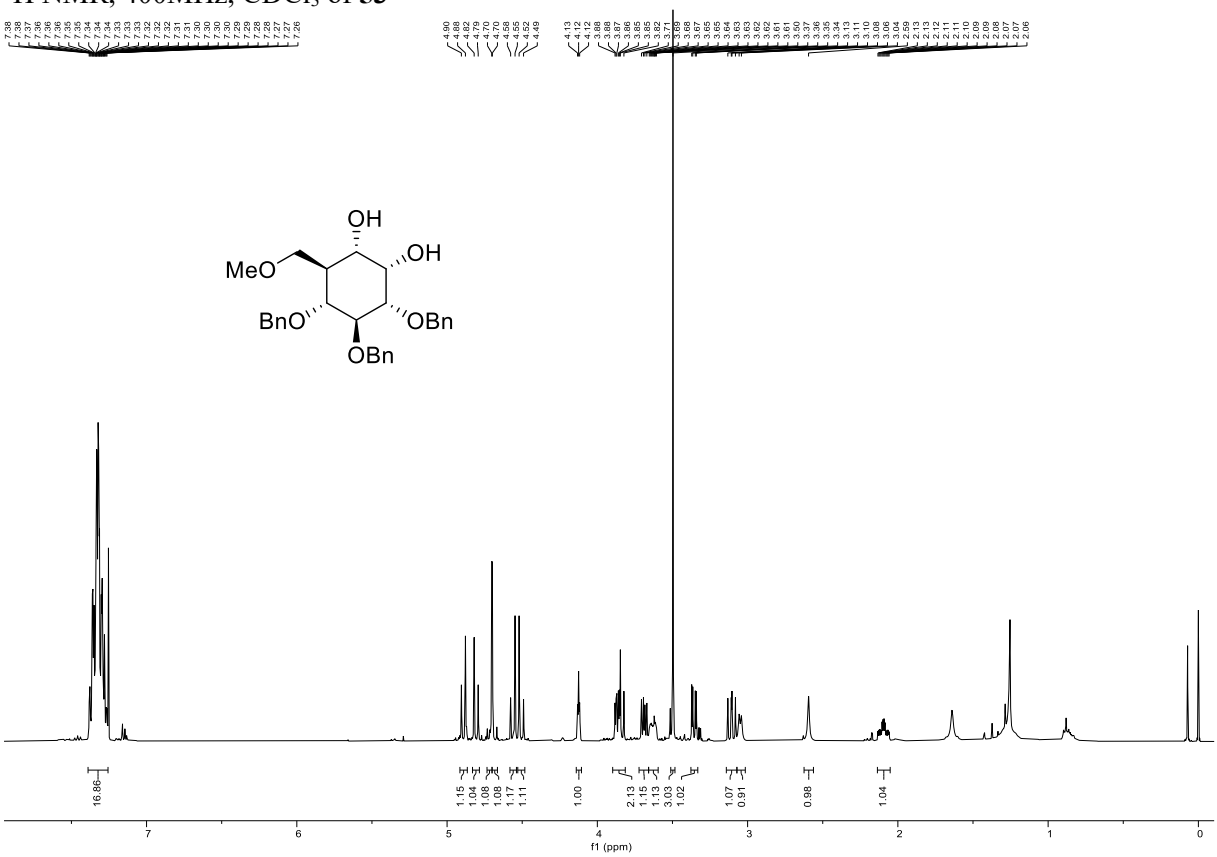


$^{13}$C NMR, 101MHz, $CDCl_3$ of **53**

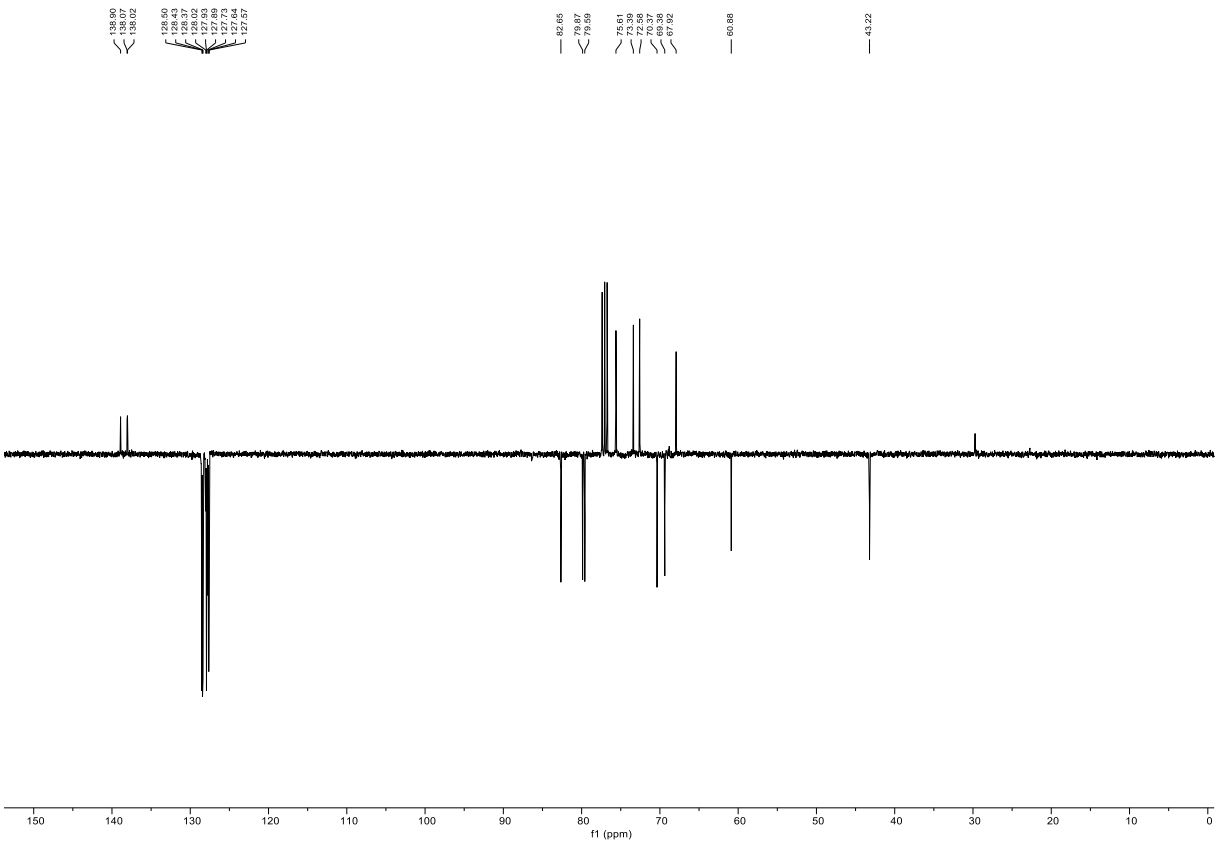

HH-COSY NMR, $CDCl_3$ of **53**

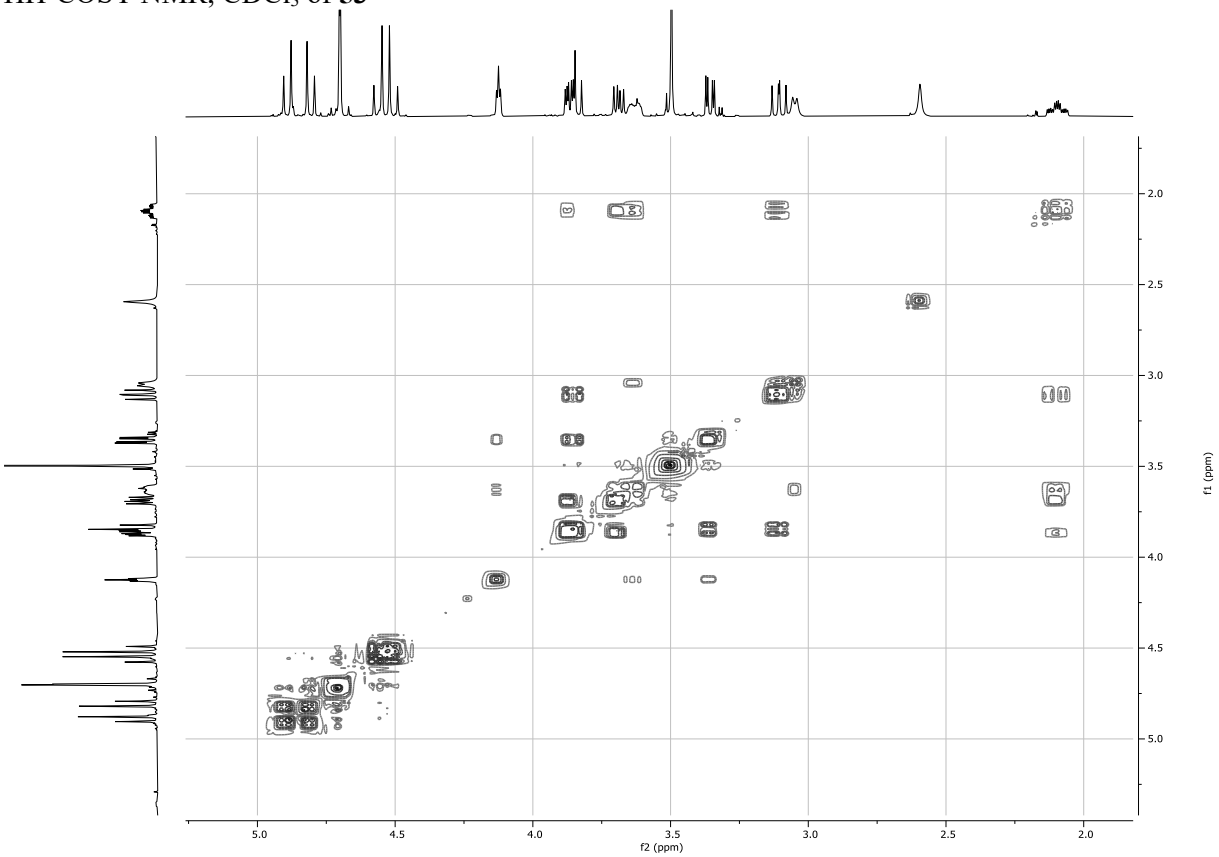


HSQC NMR, $CDCl_3$ of **53**

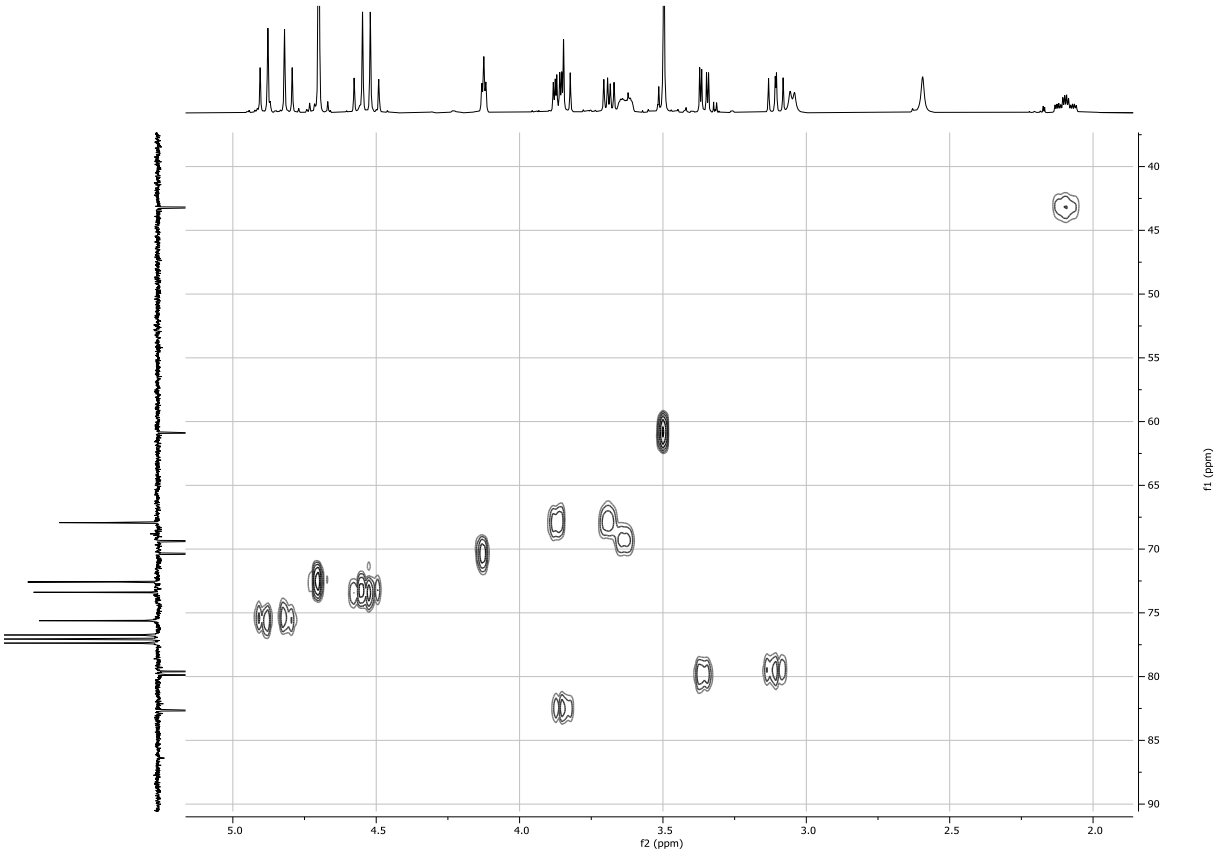

$^{1}$H NMR, 500MHz, $CDCl_3$ of **54**

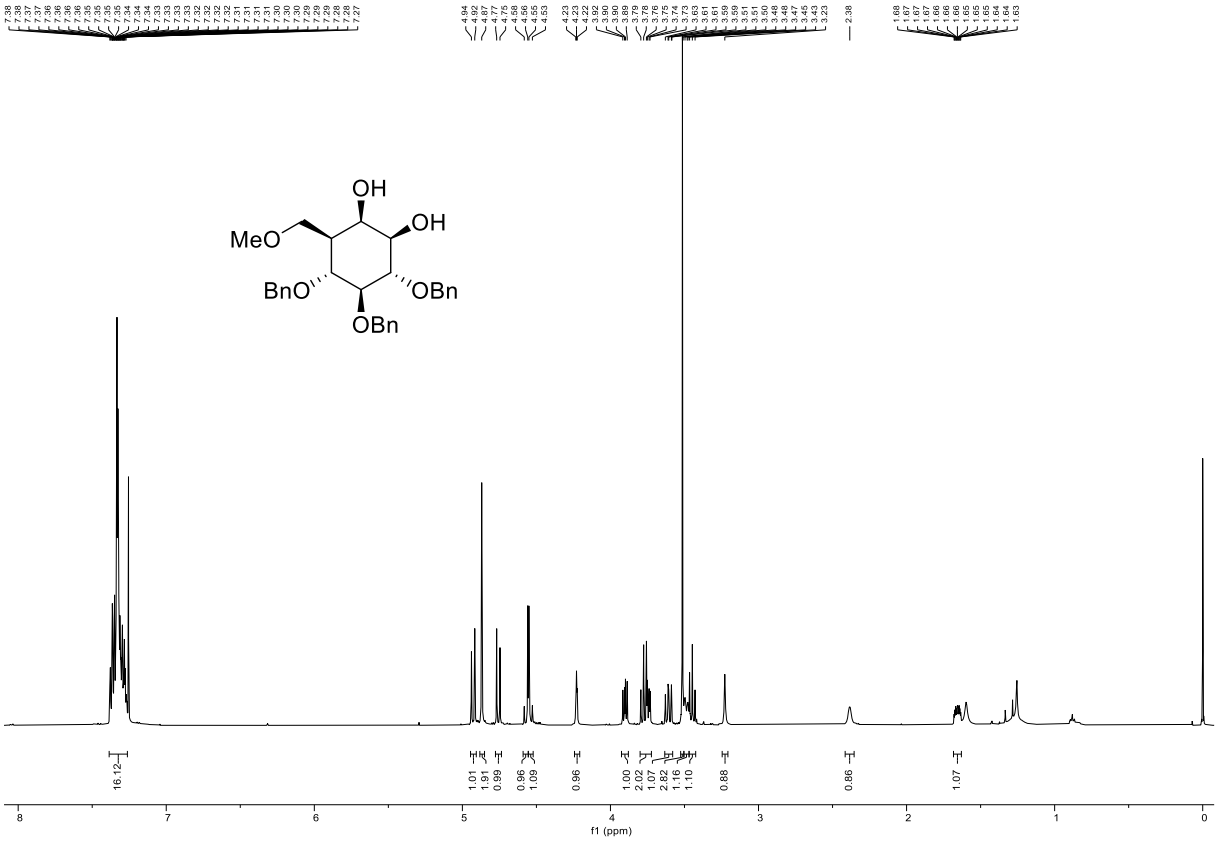


$^{13}$C NMR, 126MHz, $CDCl_3$ of **54**

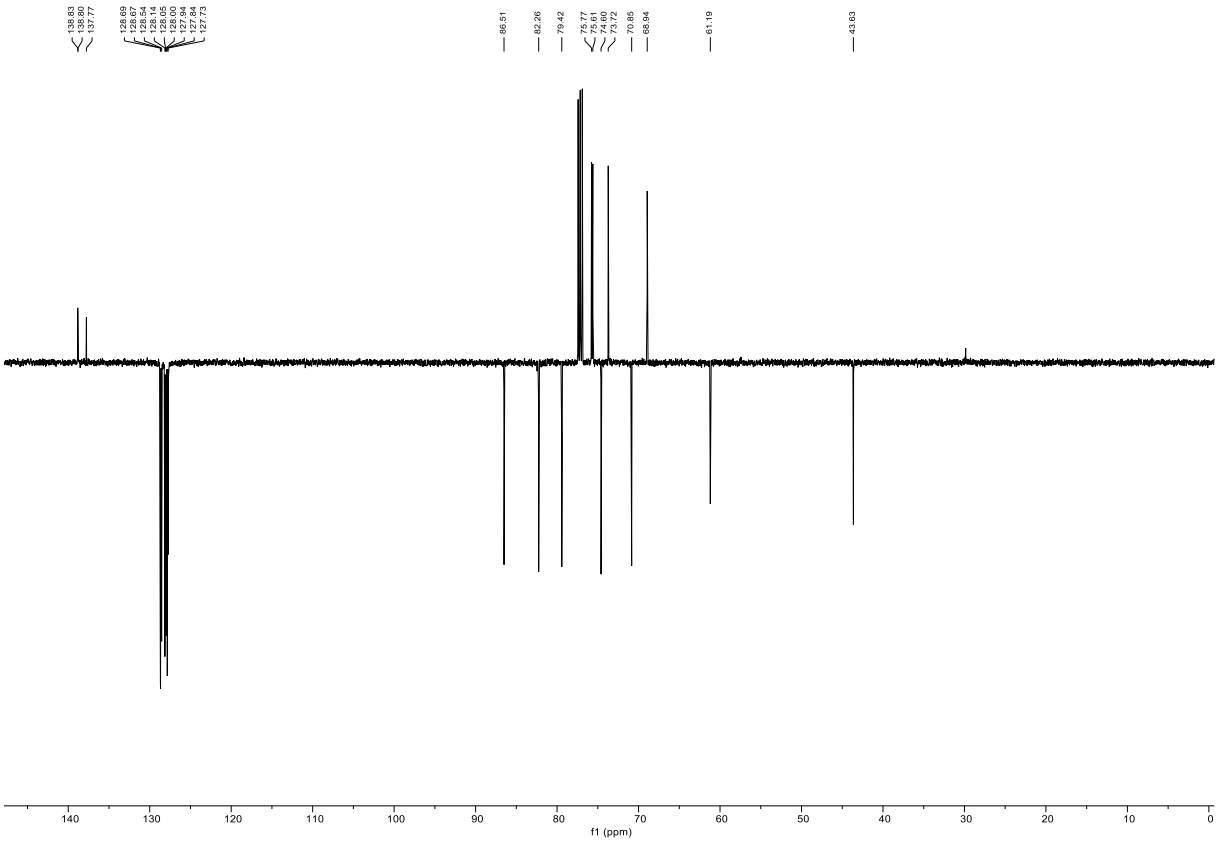

HH-COSY NMR, $CDCl_3$ of **54**

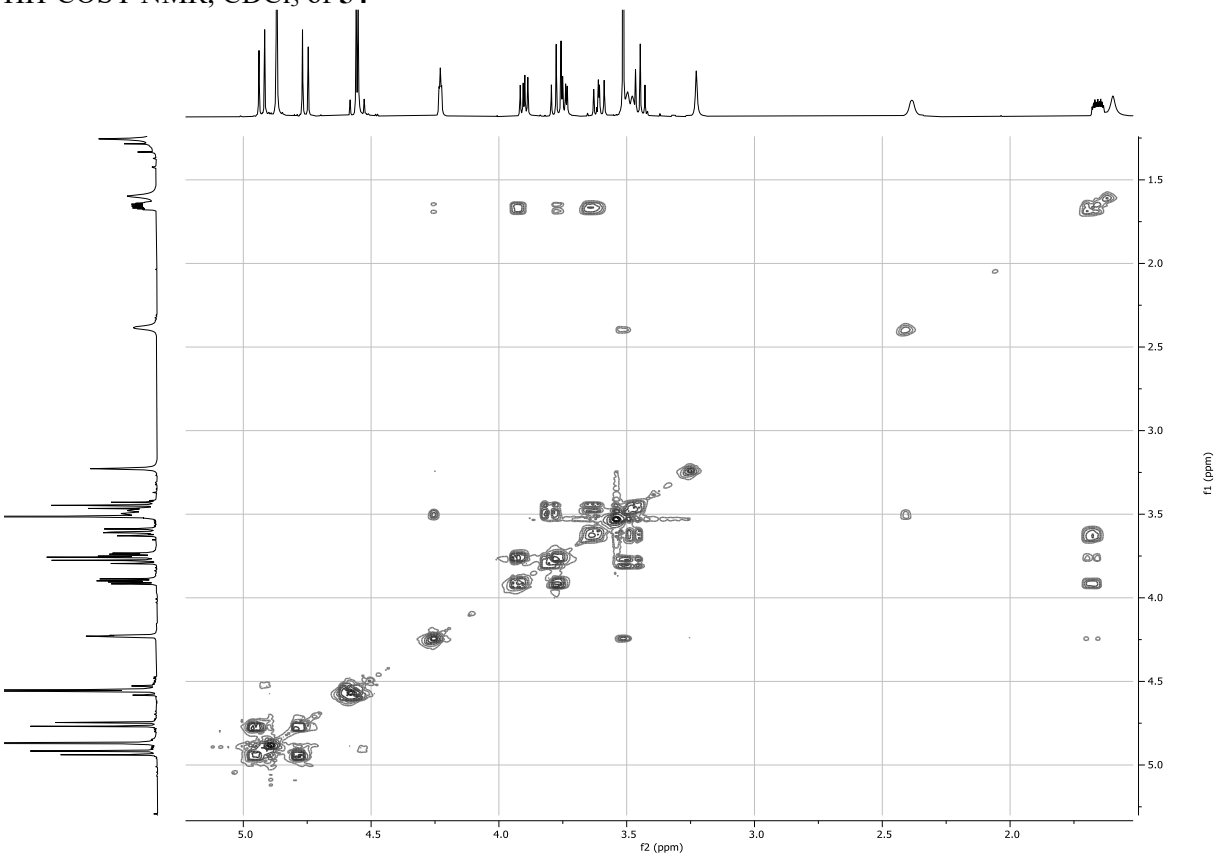


HSQC NMR, $CDCl_3$ of **54**

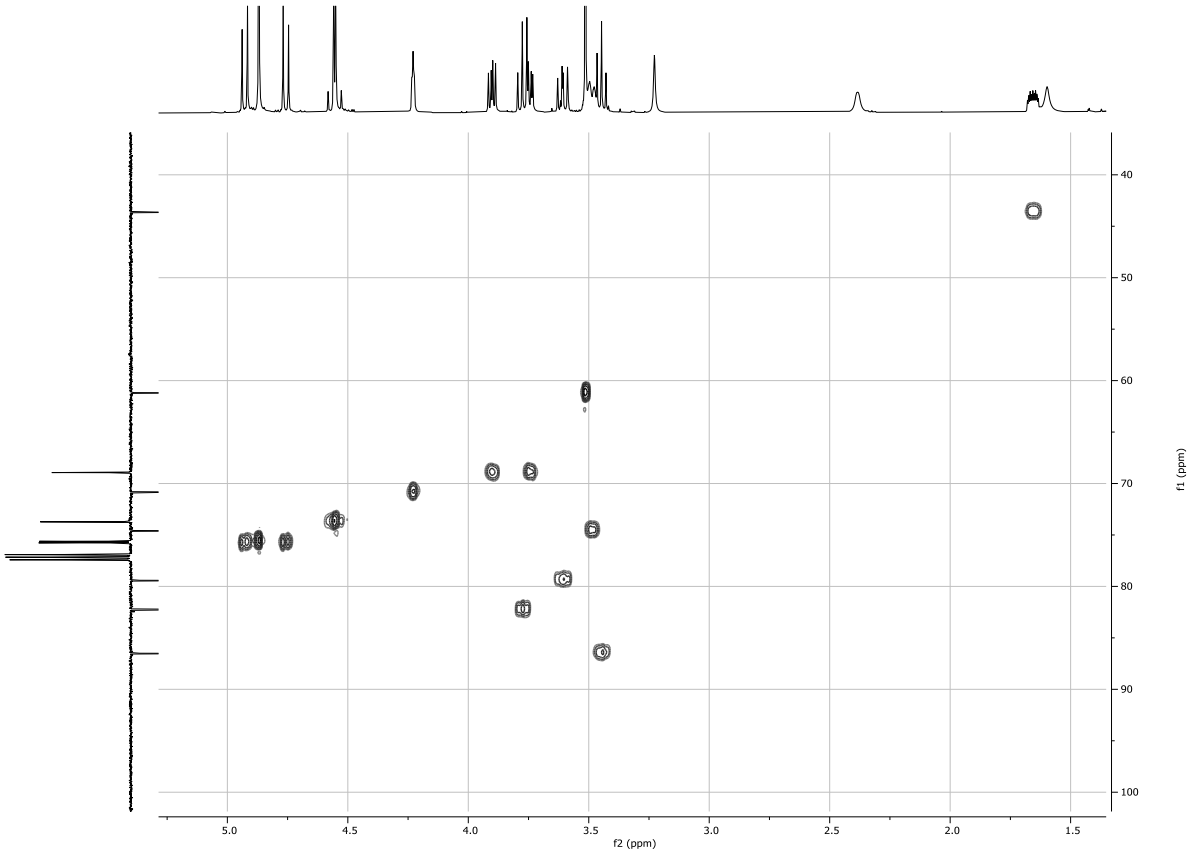

$^{1}$H NMR, 400MHz, $CDCl_3$ of **55**

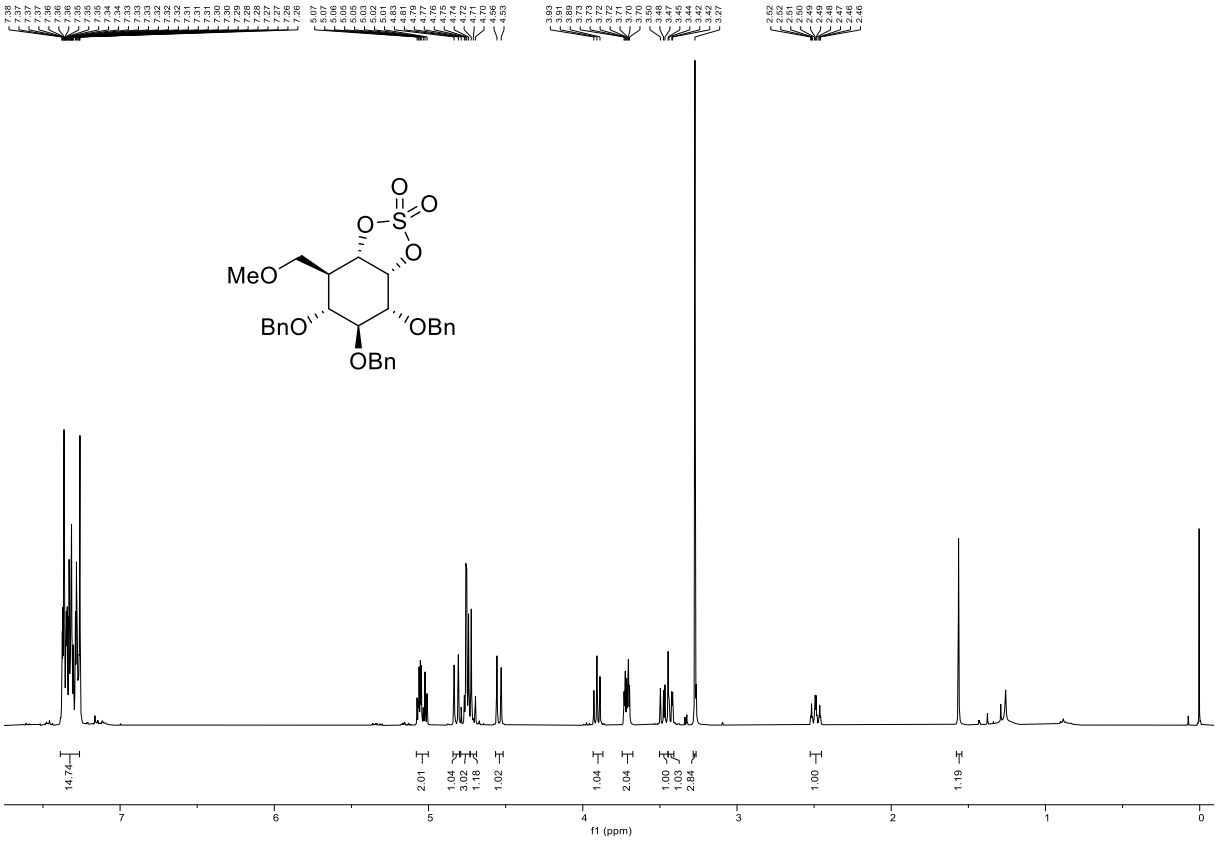


$^{13}$C NMR, 101MHz, $CDCl_3$ of **55**

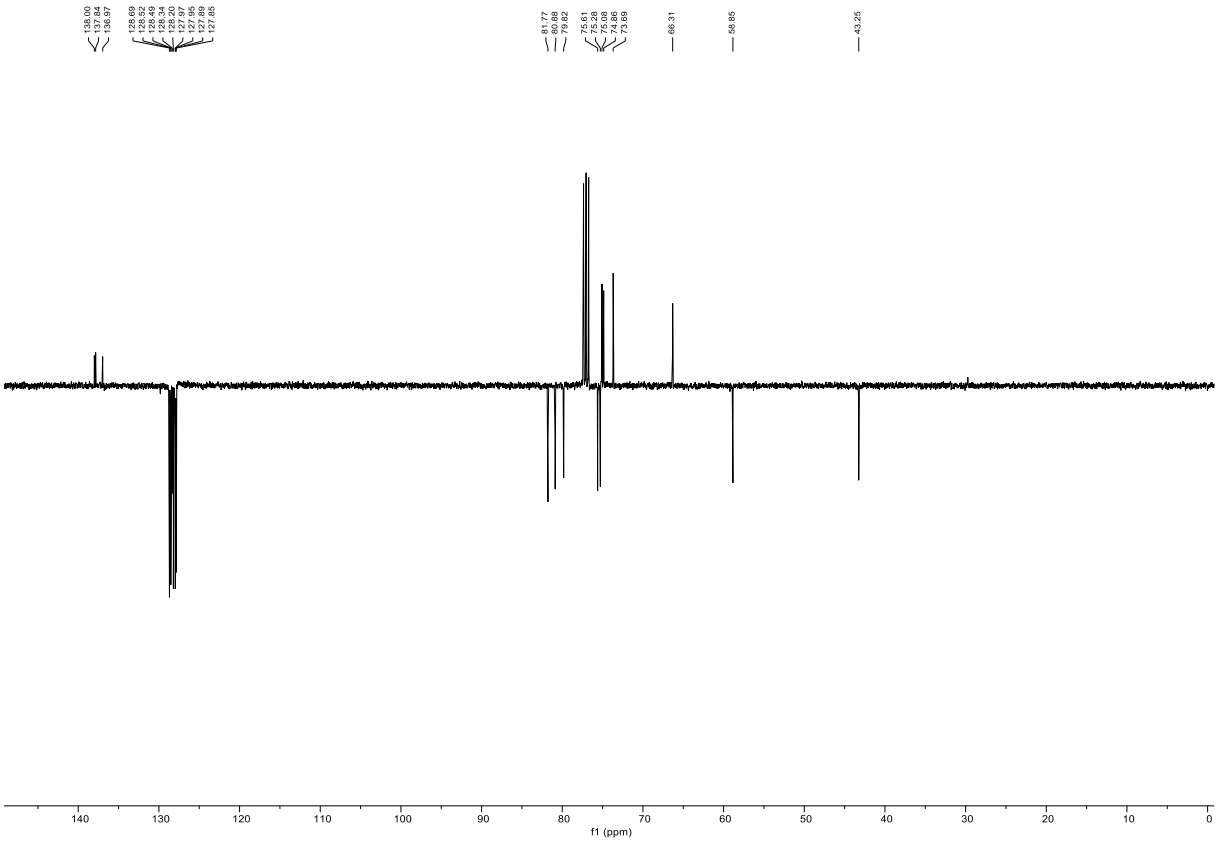

HH-COSY NMR, $CDCl_3$ of **55**

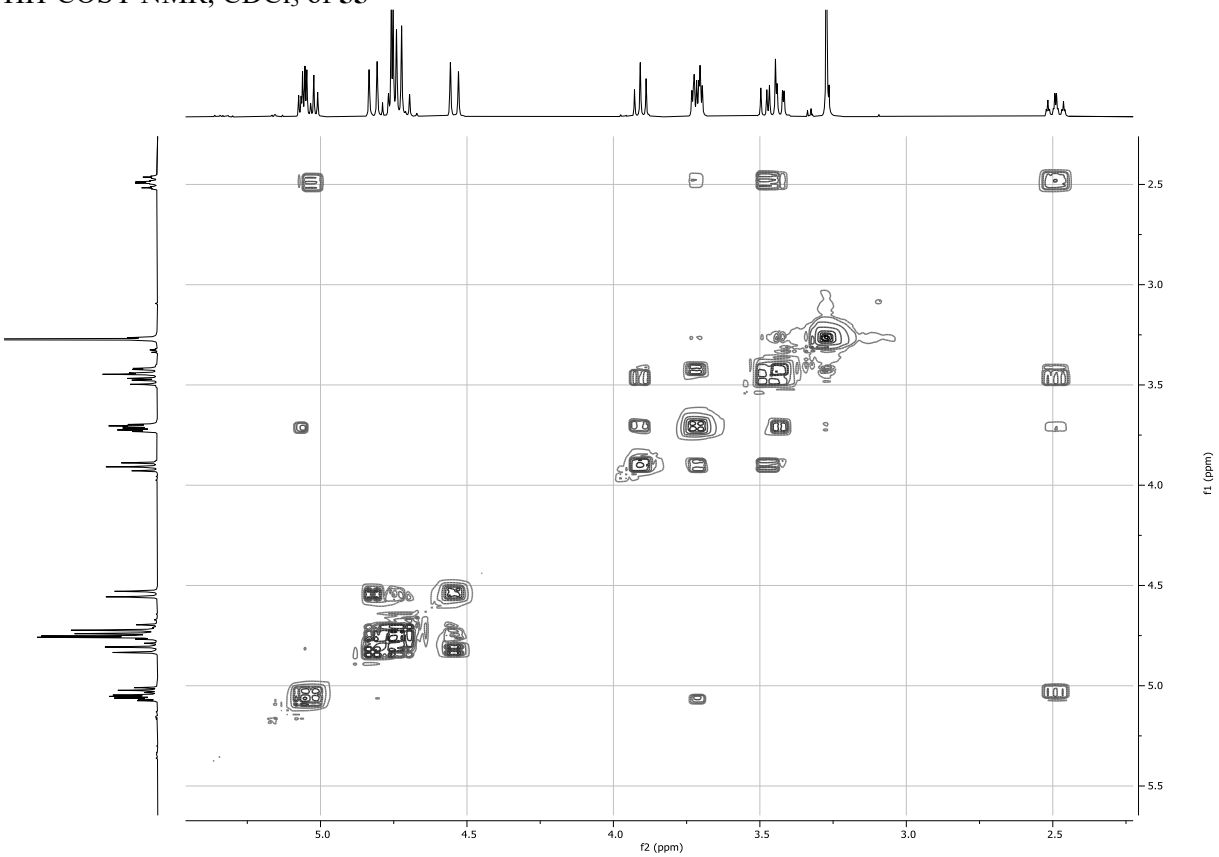


HSQC NMR, $CDCl_3$ of **55**

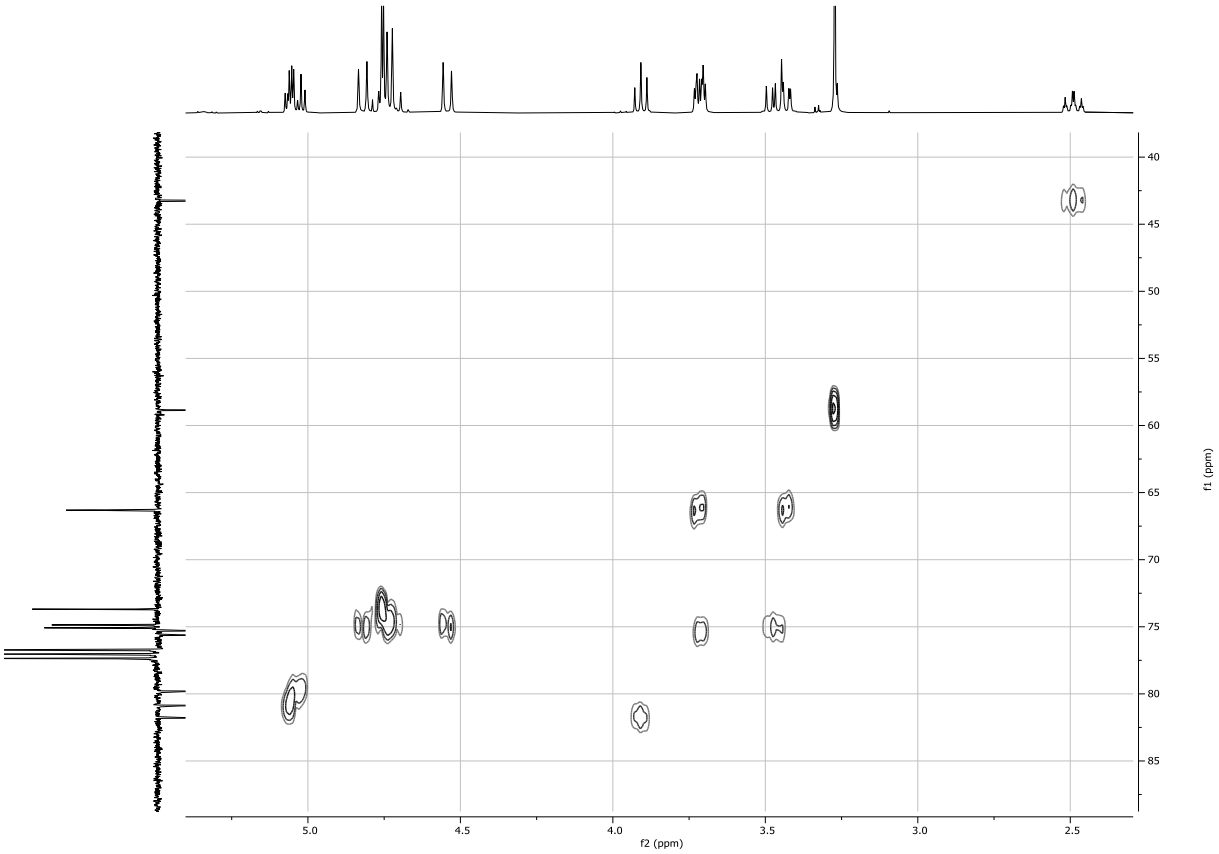

$^{1}$H NMR, 500MHz, MeOD of **8**

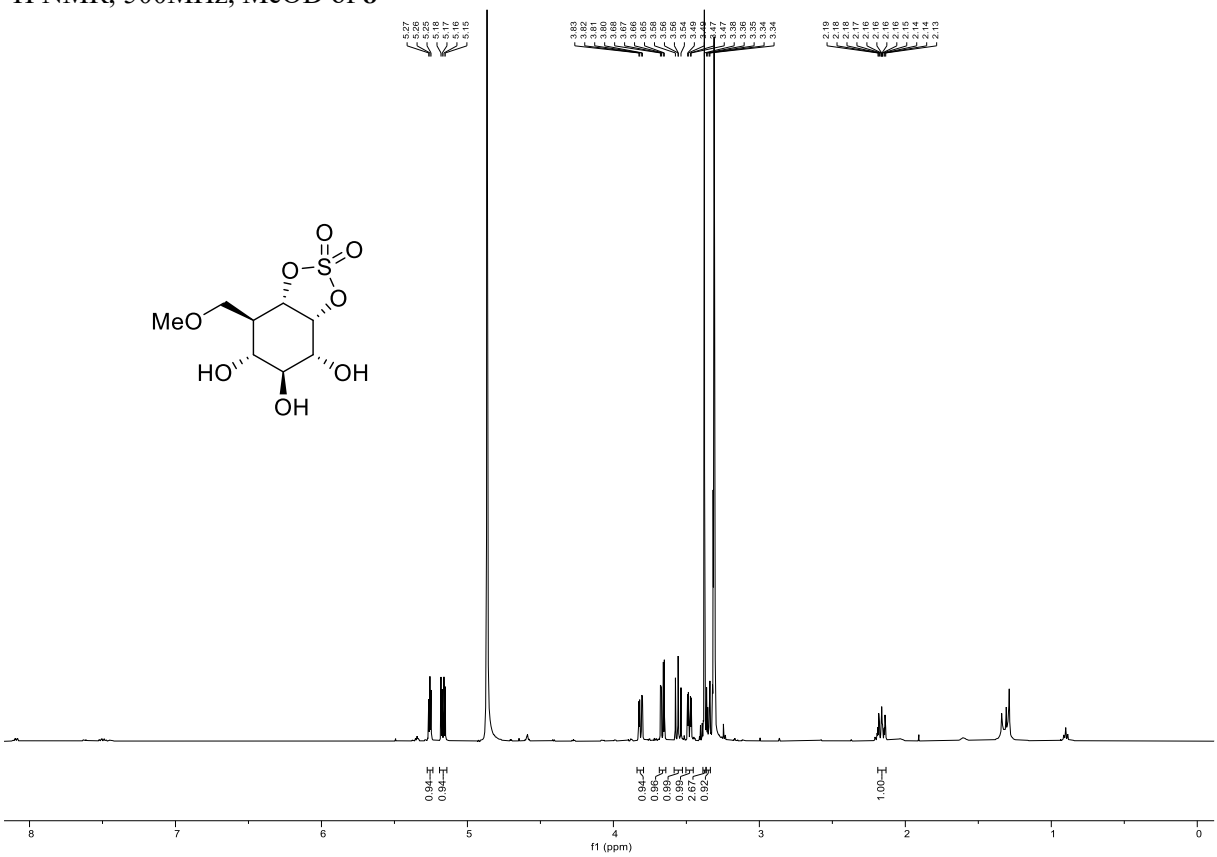


$^{13}$C NMR, 126MHz, MeOD of **8**

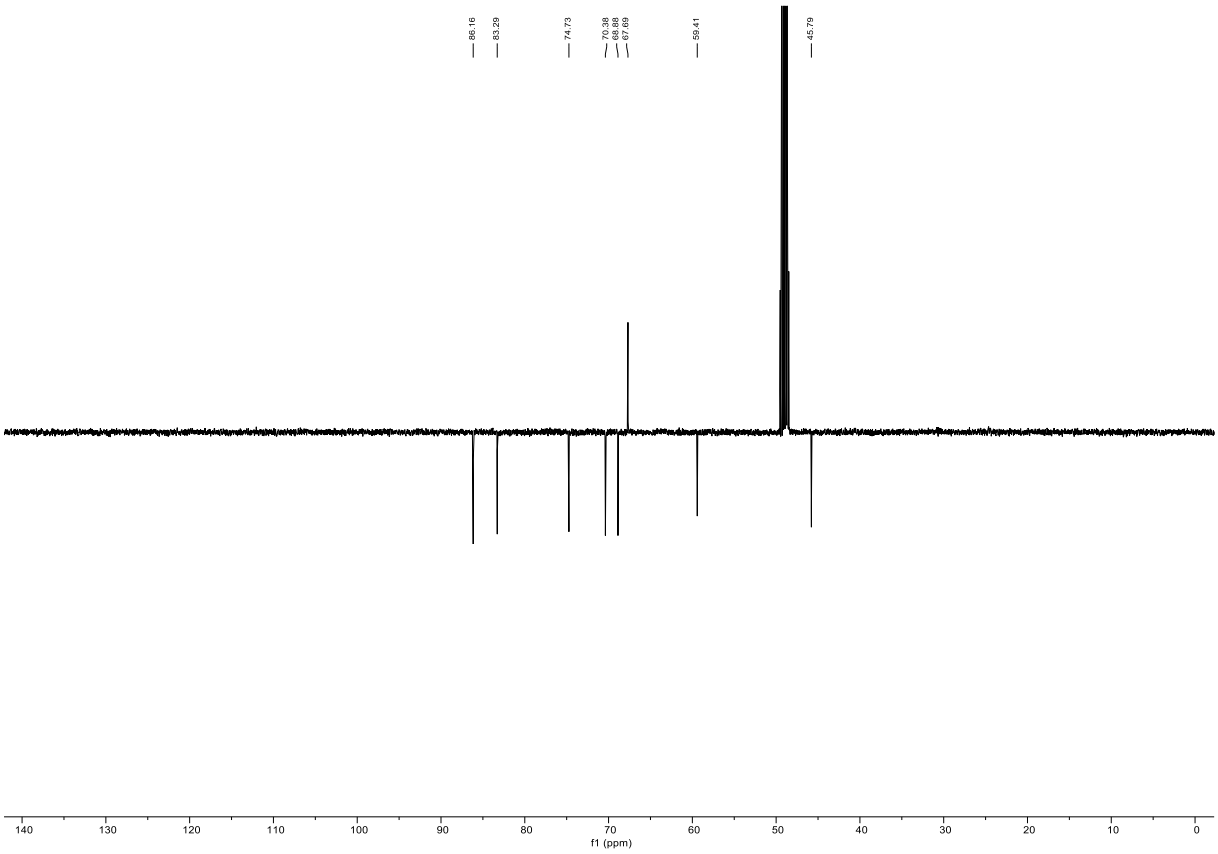

HH-COSY NMR, MeOD of **8**

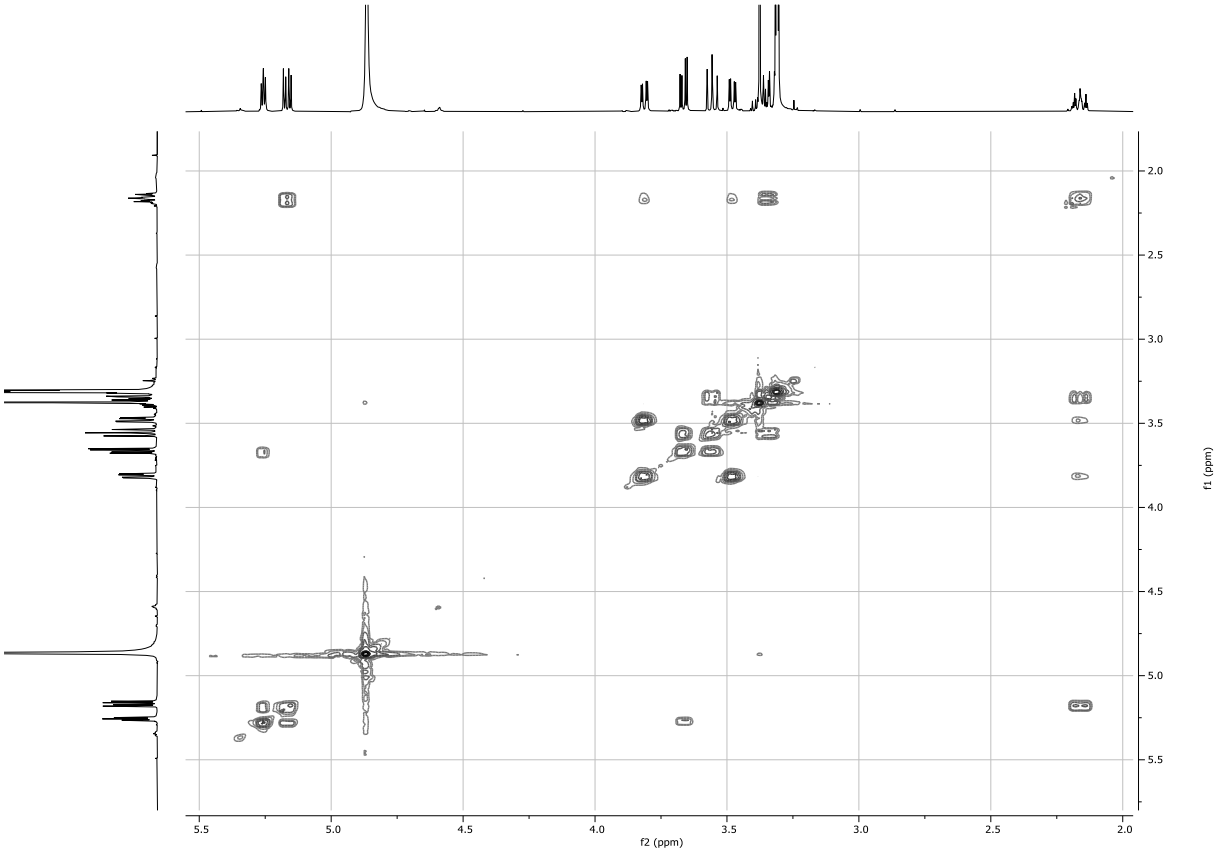


HSQC NMR, MeOD of **8**

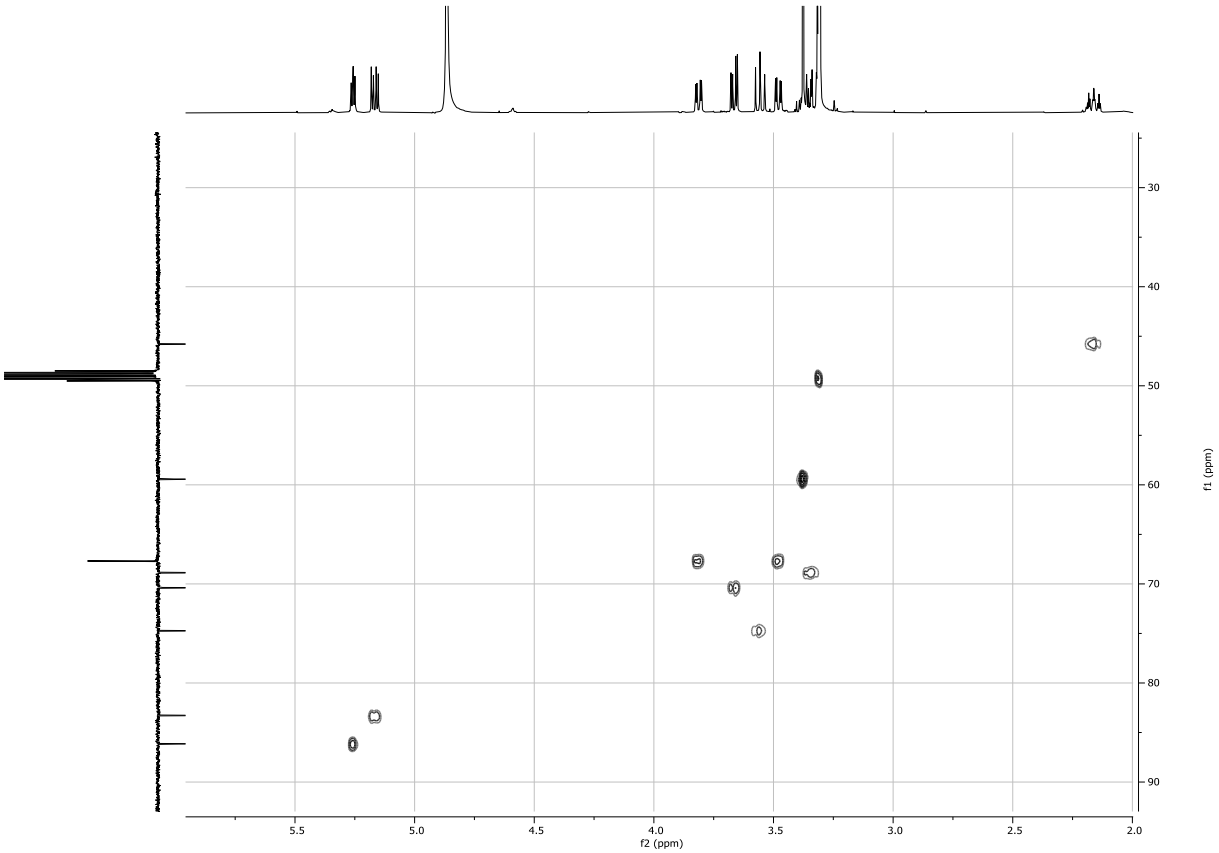

$^{1}$H NMR, 500MHz, MeOD of **13**

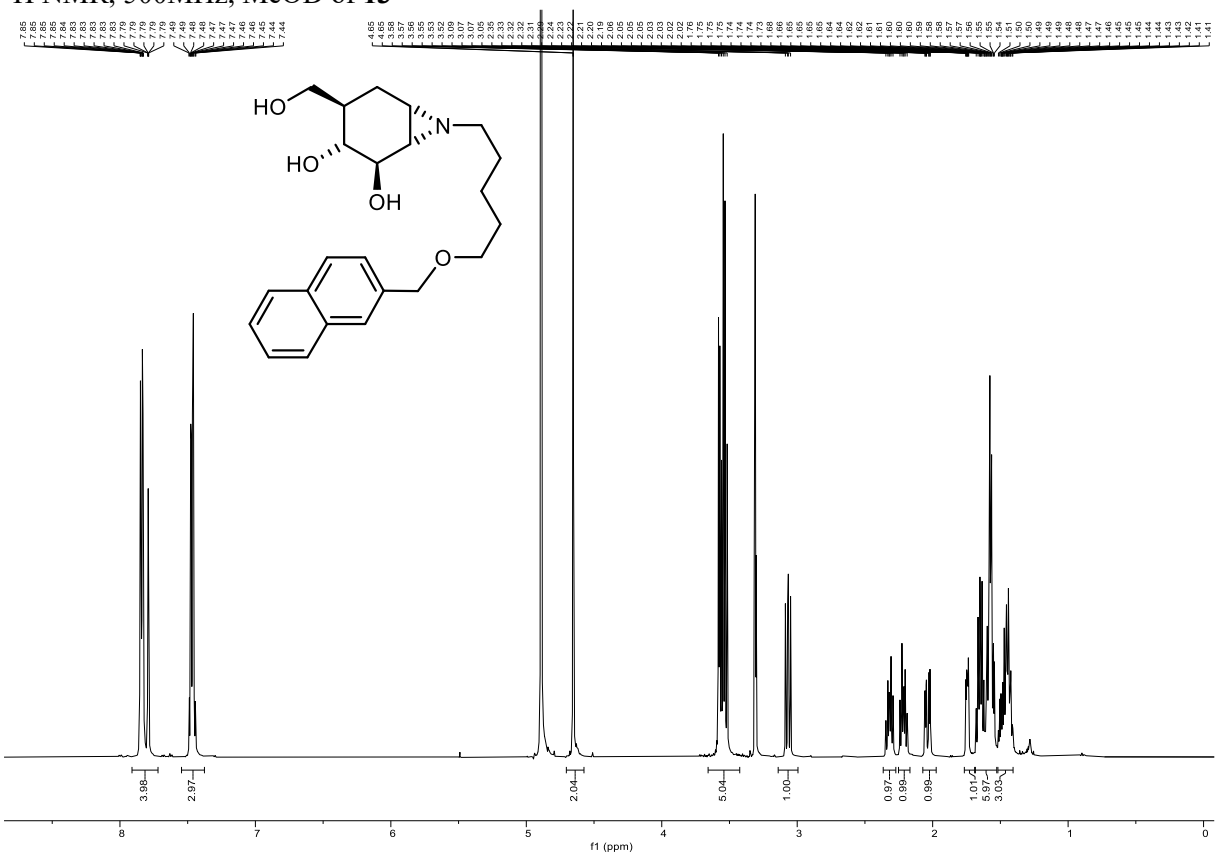


$^{13}$C NMR, 126MHz, MeOD of **13**

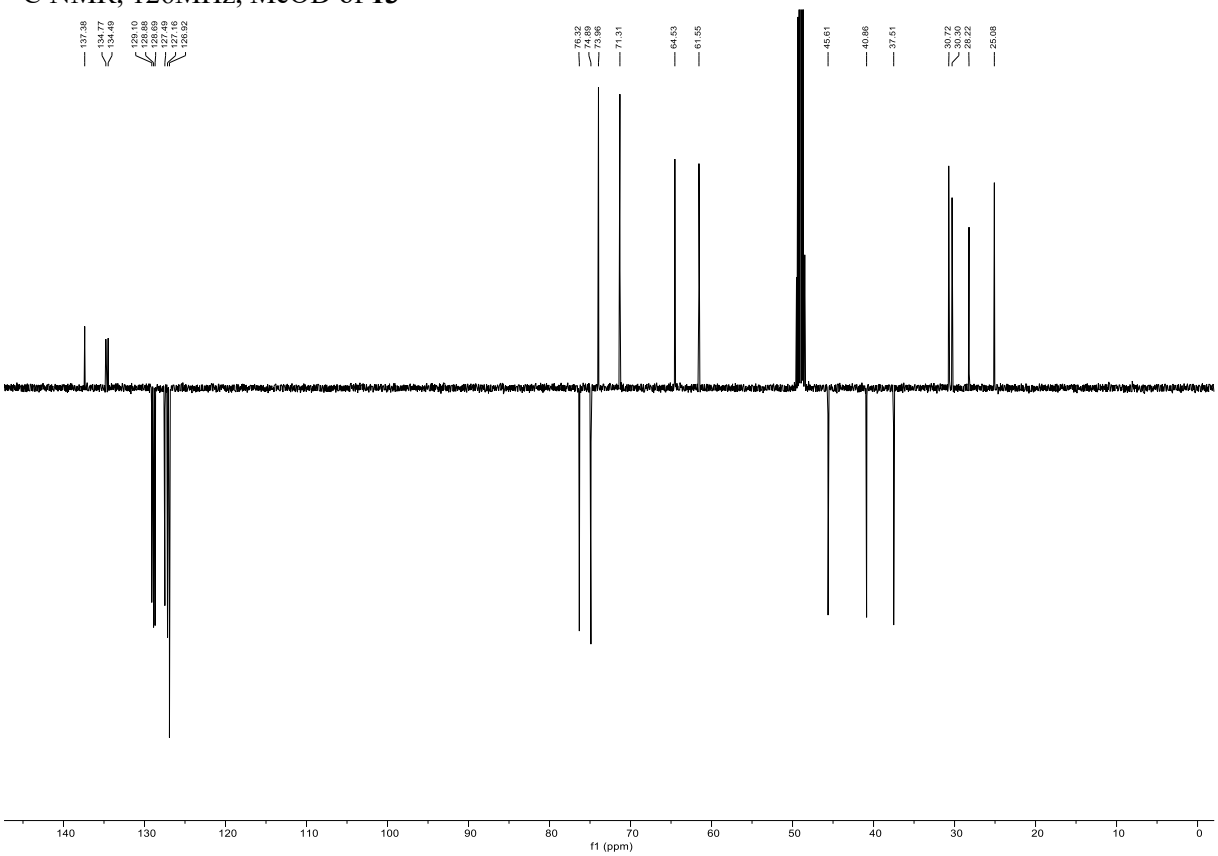

HH-COSY NMR, MeOD of **13**

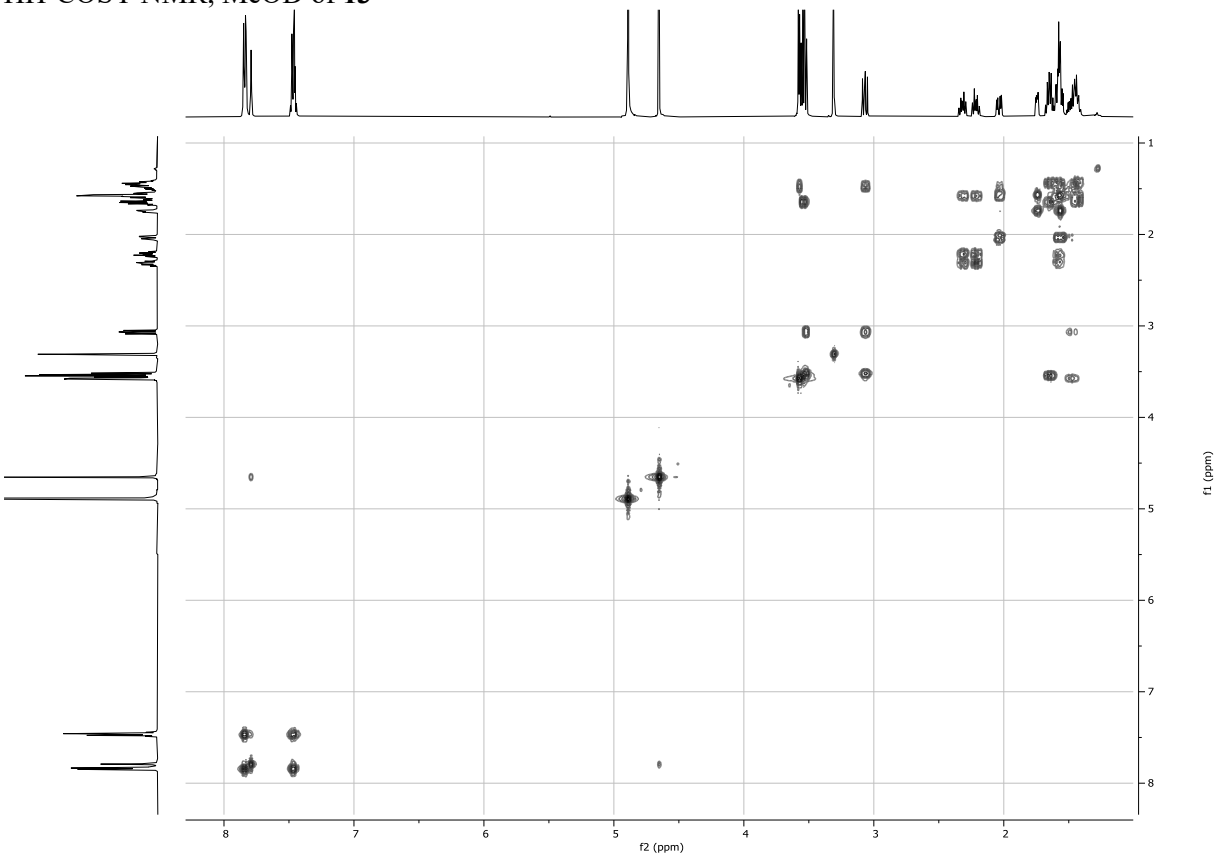


HSQC NMR, MeOD of **13**

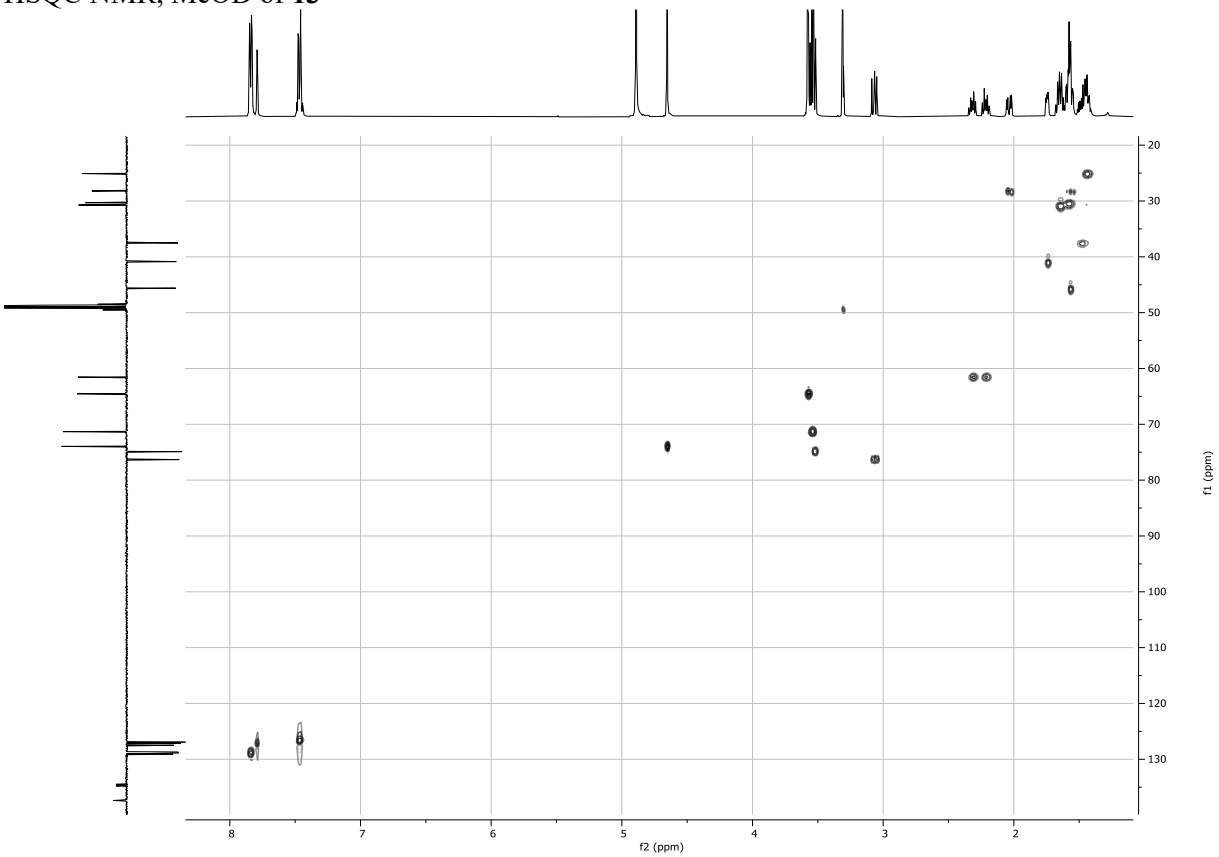

$^{1}$H NMR, 500MHz, MeOD of **14**

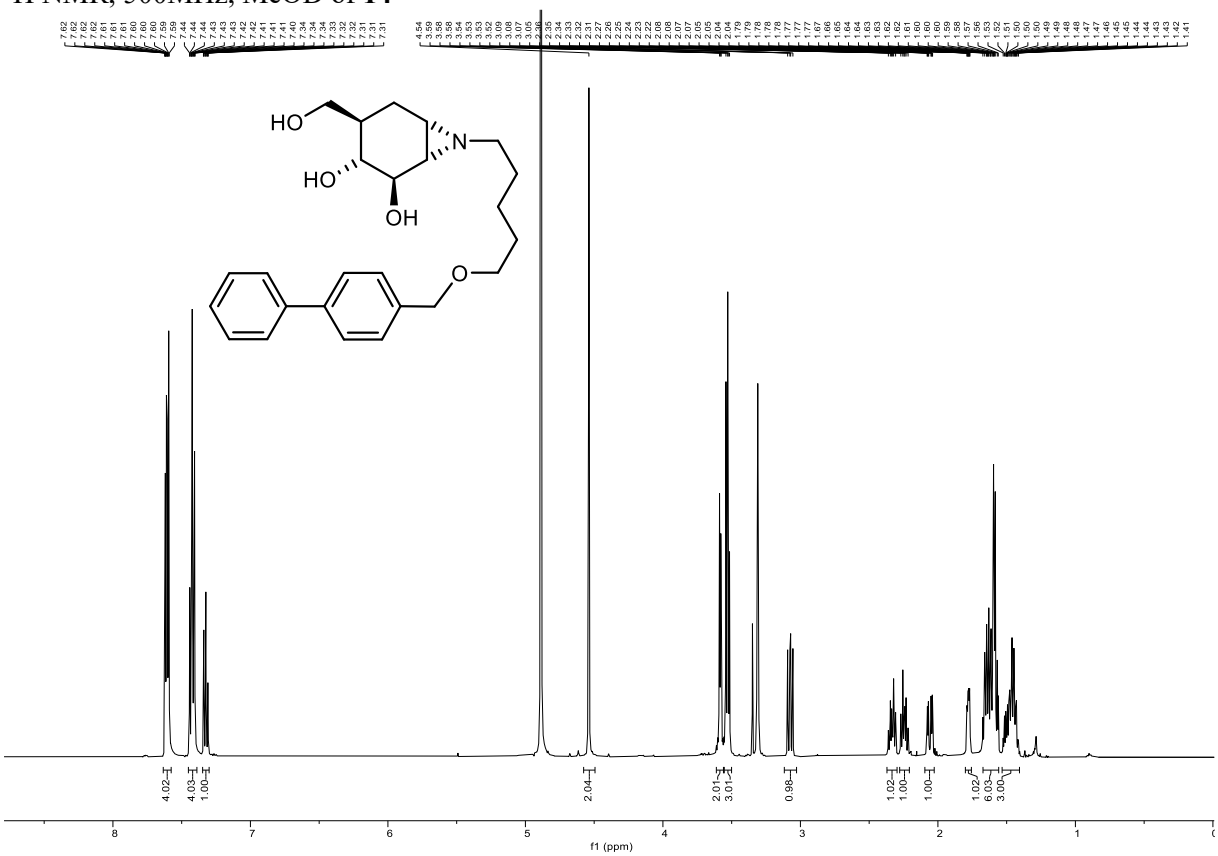


$^{13}$C NMR, 126MHz, MeOD of **14**

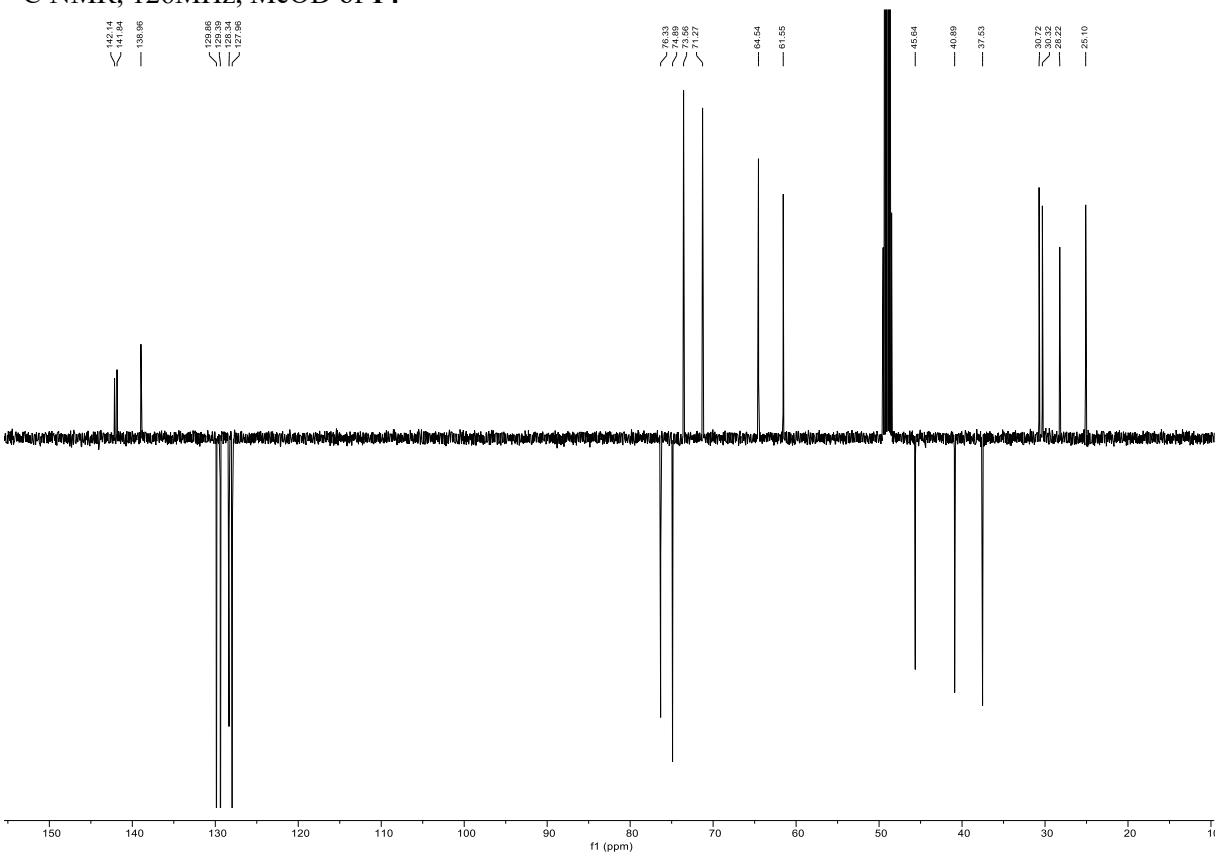

HH-COSY NMR, MeOD of **14**

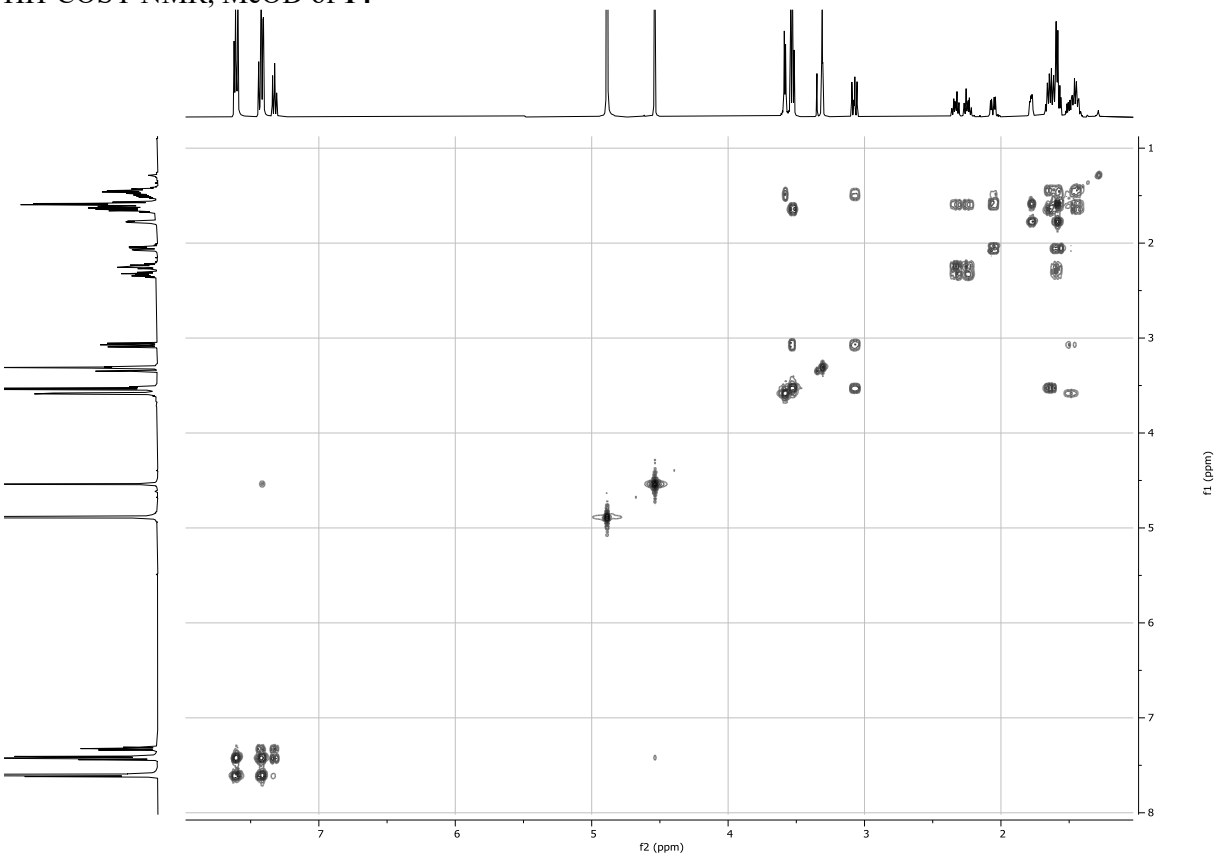


HSQC NMR, MeOD of **14**

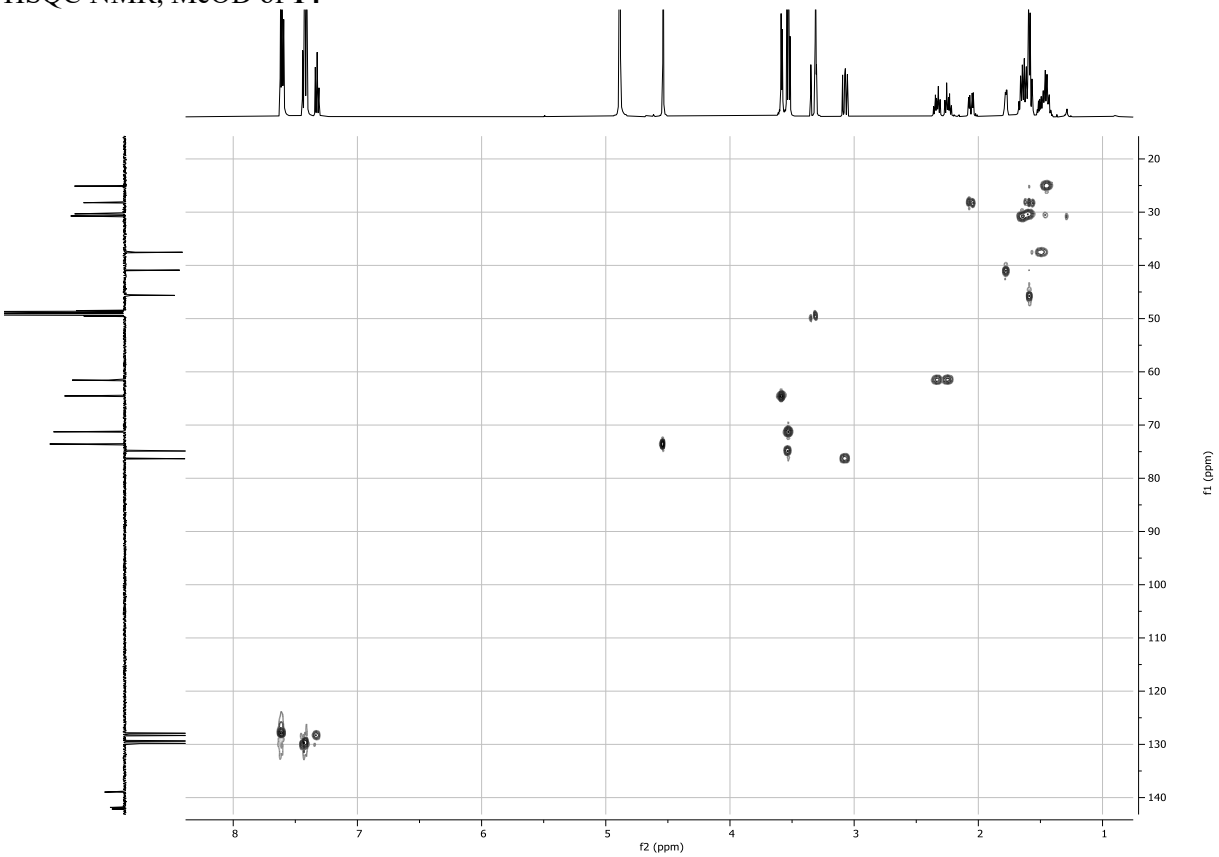

$^{1}$H NMR, 500MHz, MeOD of **17**

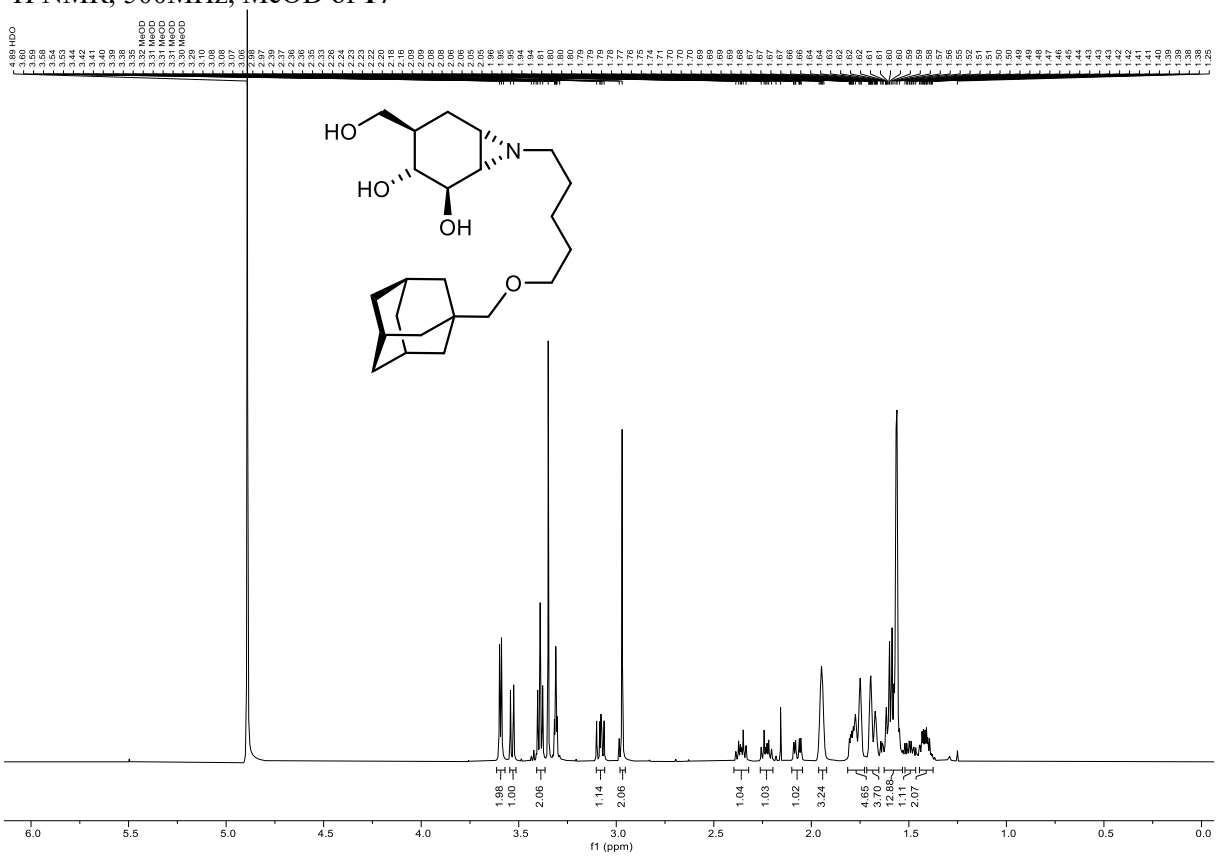


$^{13}$C NMR, 126MHz, MeOD of **17**

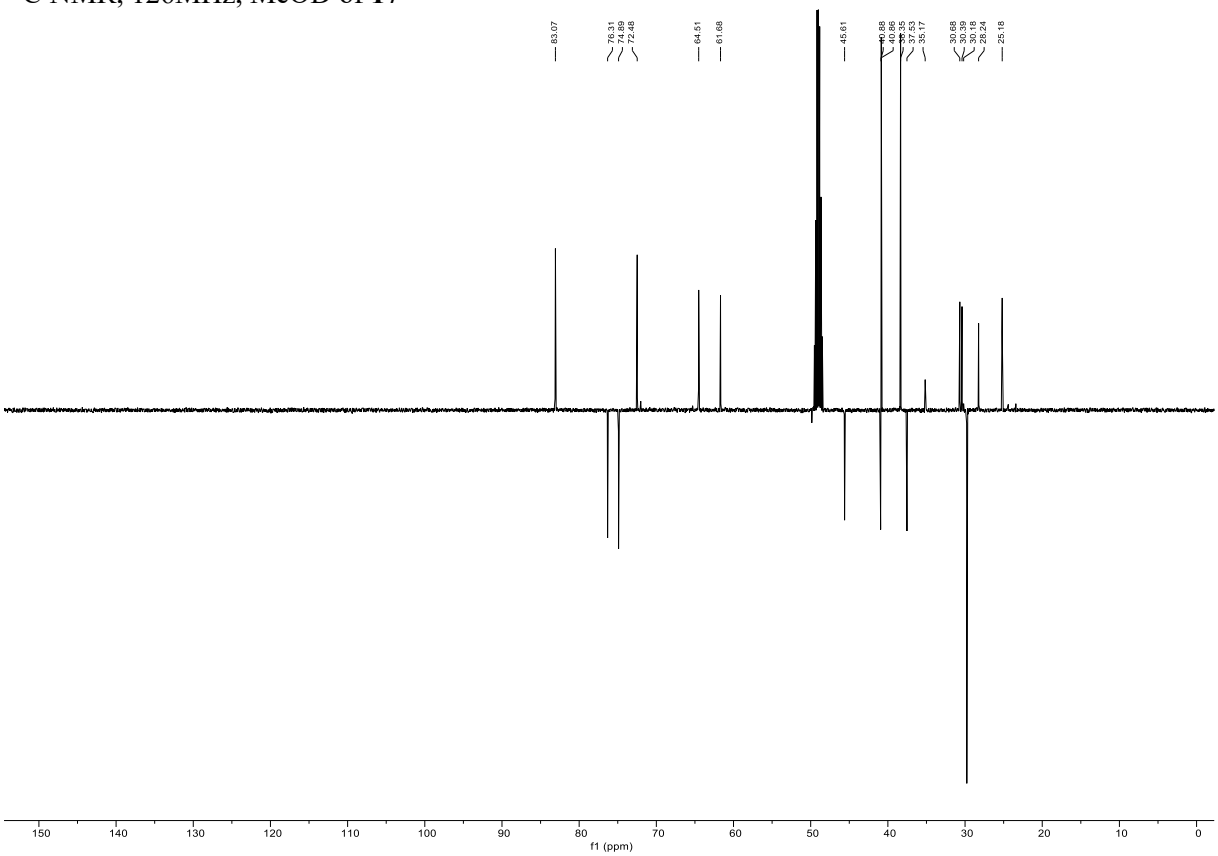

HH-COSY NMR, MeOD of **17**

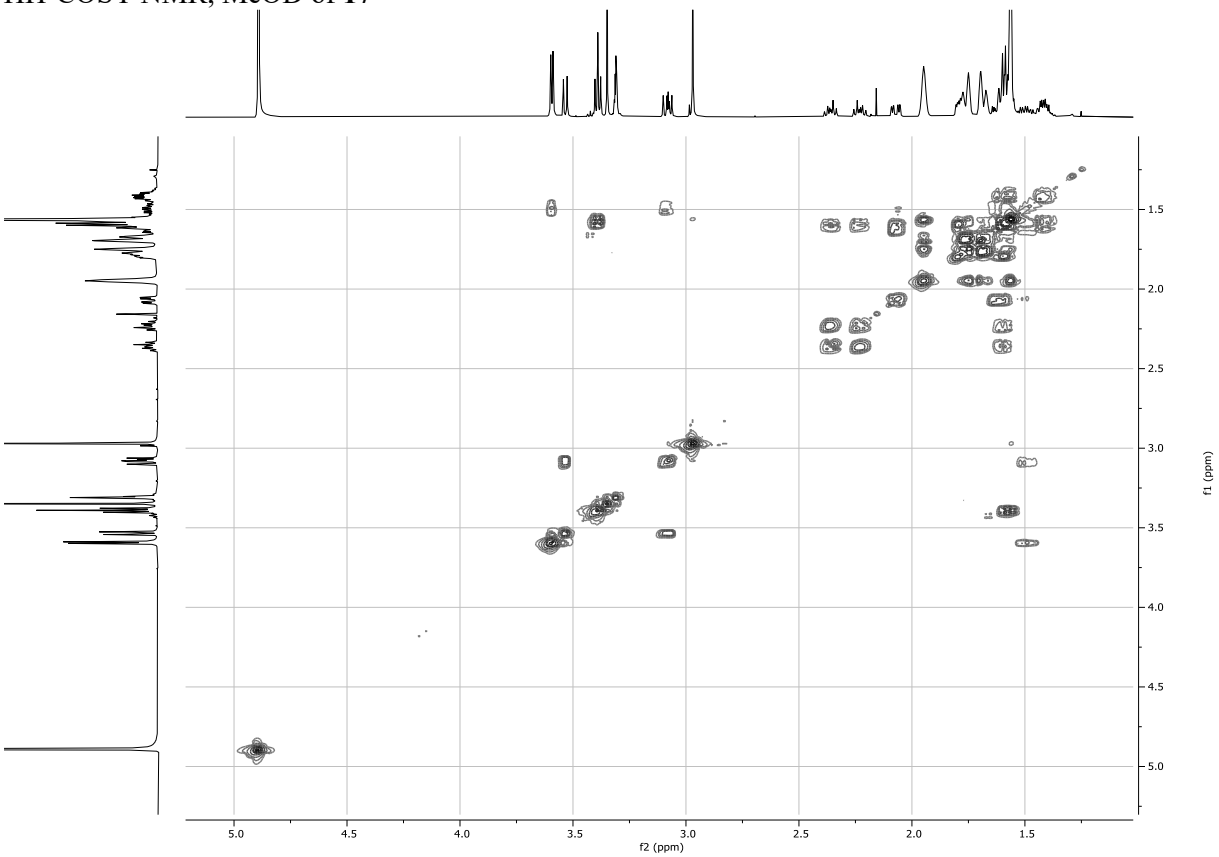


HSQC NMR, MeOD of **17**

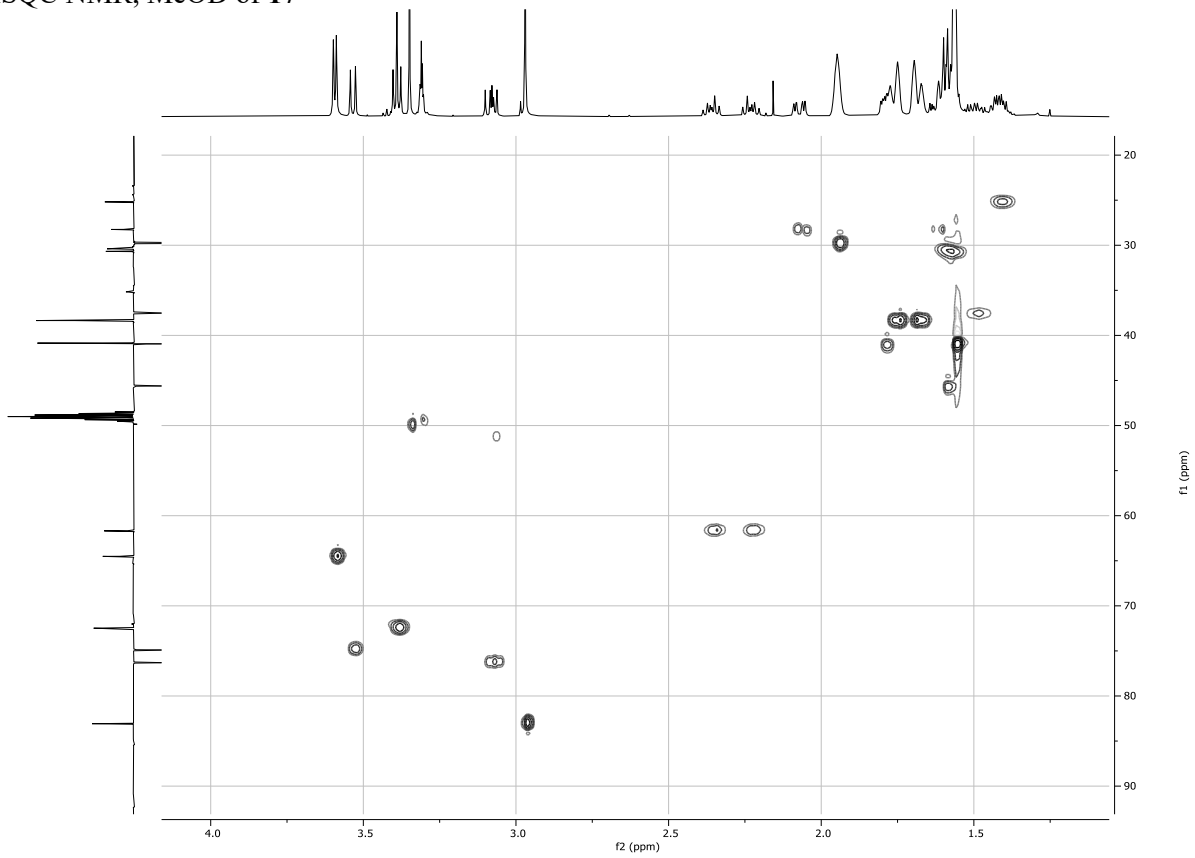

$^{1}$H NMR, 500MHz, MeOD of **18**

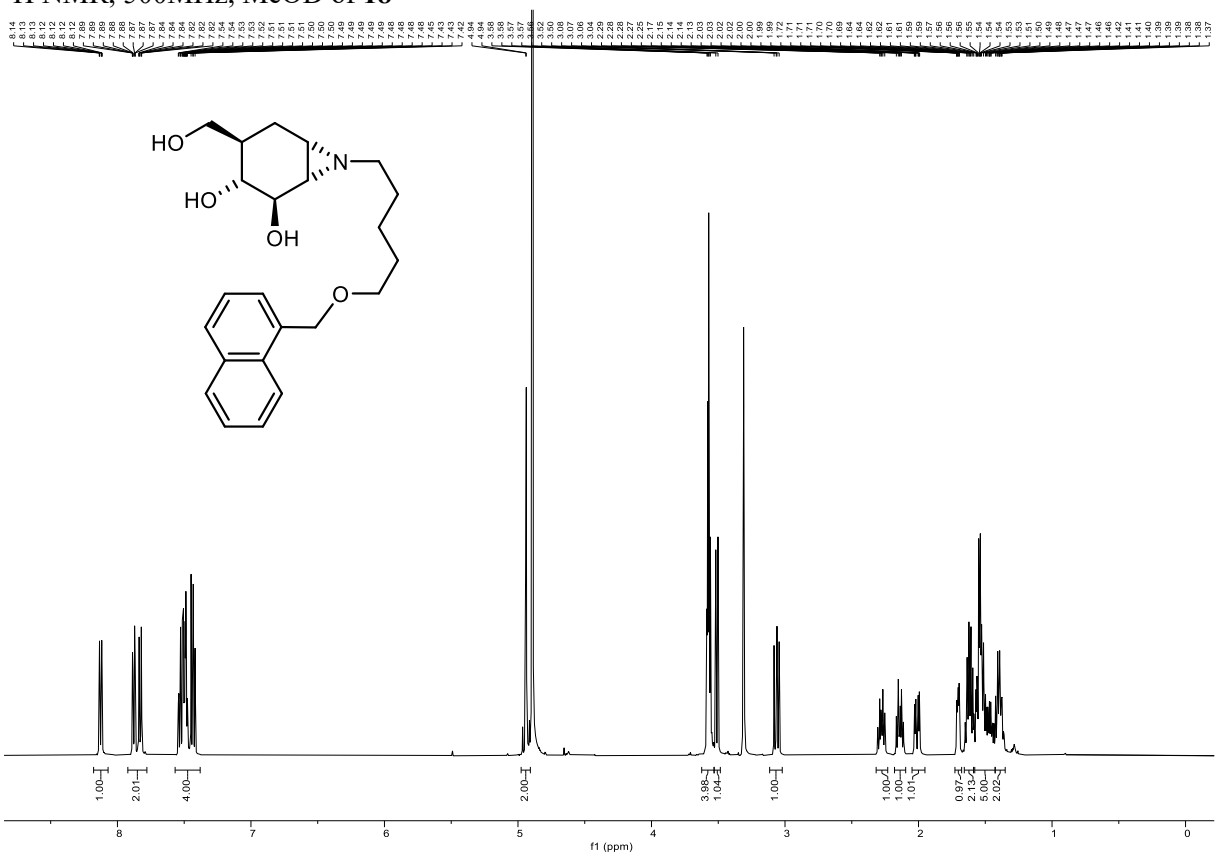


$^{13}$C NMR, 126MHz, MeOD of **18**

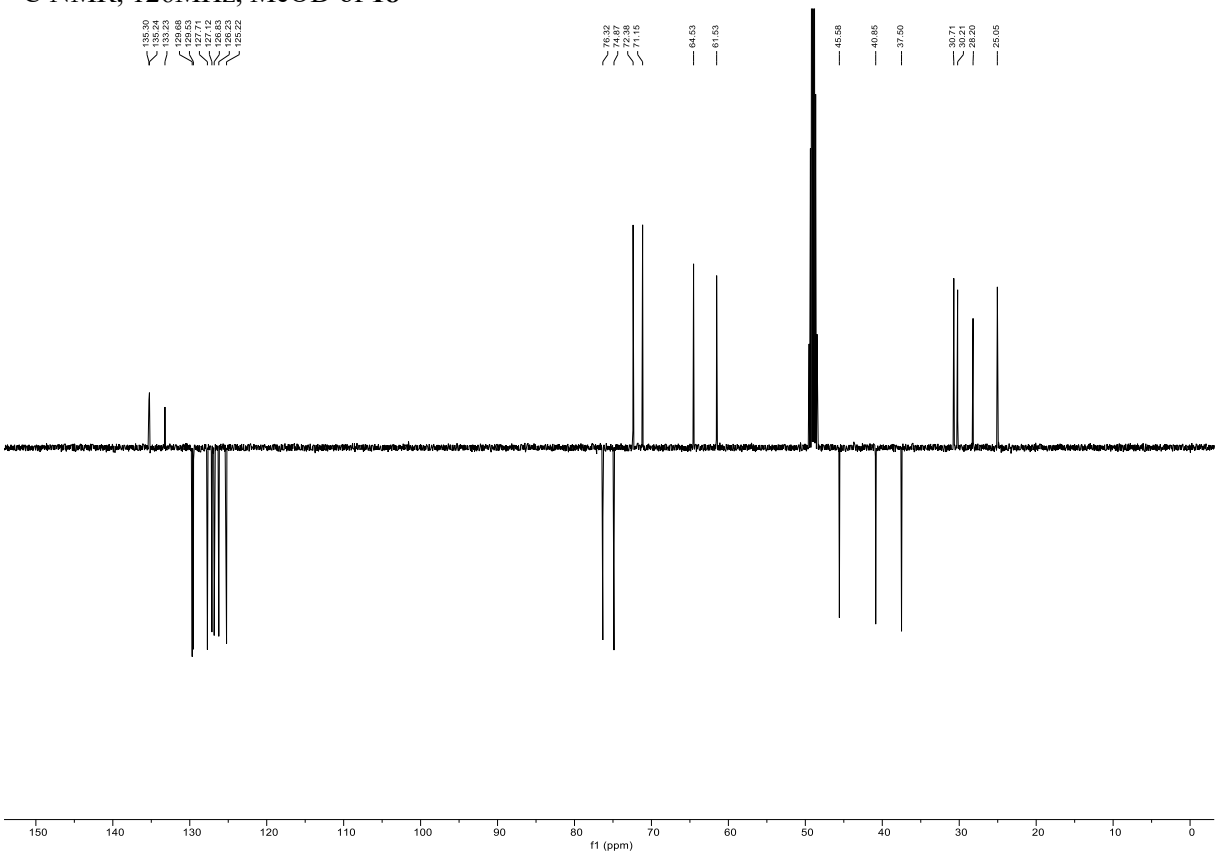

HH-COSY NMR, MeOD of **18**

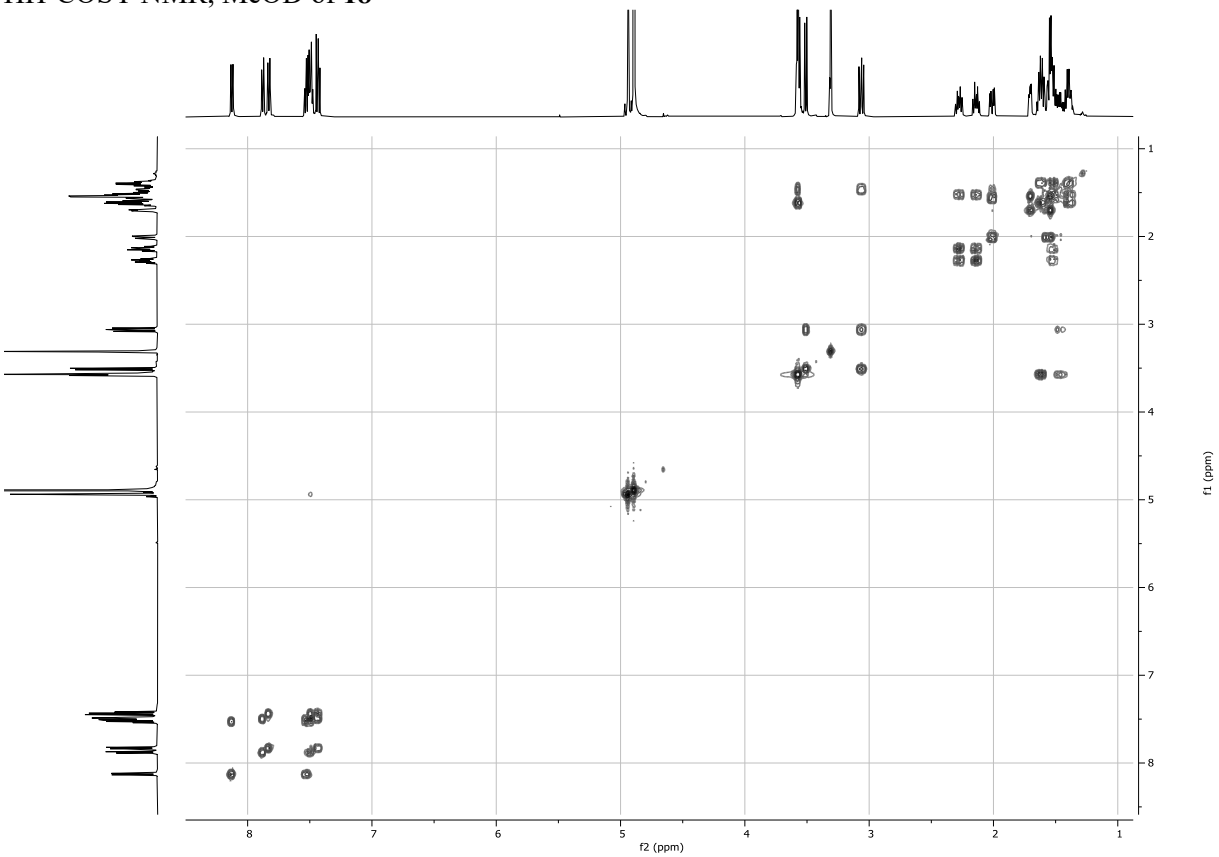


HSQC NMR, MeOD of **18**

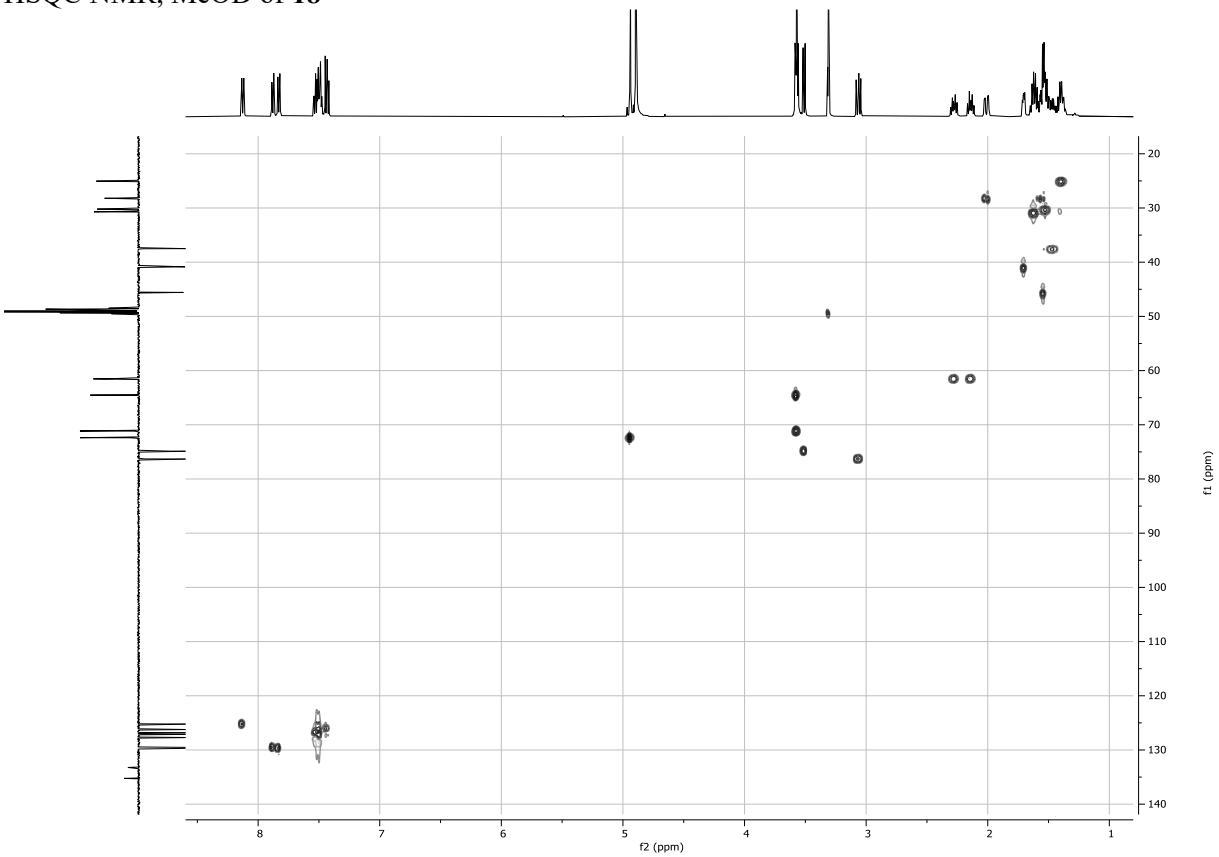

# References


[1] Wennekes, T.; Meijer, A. J.; Groen, A. K.; Boot, R. G.; Groener, J. E.; Van Eijk, M.; Ottenhoff, R.; Bijl, N.; Ghauharali, K.; Song, H.; O'Shea, T. J.; Liu, H.; Yew, N.; Copeland, D.; Van Den Berg, R. J.; Van Der Marel, G. A.; Overkleeft, H. S.; Aerts, J. M. Dual-Action Lipophilic Iminosugar Improves Glycemic Control in Obese Rodents by Reduction of Visceral Glycosphingolipids and Buffering of Carbohydrate Assimilation. J Med Chem 2010, 53, 689–698.

[2] Lahav, D.; Liu, B.; Van Den Berg, R. J. B. H. N.; Van Den Nieuwendijk, A. M. C. H.; Wennekes, T.; Ghisaidoobe, A. T.; Breen, I.; Ferraz, M. J.; Kuo, C. L.; Wu, L.; Geurink, P. P.; Ovaa, H.; Van Der Marel, G. A.; Van Der Stelt, M.; Boot, R. G.; Davies, G. J.; Aerts, J. M. F. G.; Overkleeft, H. S. A Fluorescence Polarization Activity-Based Protein Profiling Assay in the Discovery of Potent, Selective Inhibitors for Human Nonlysosomal Glucosylceramidase. J Am Chem Soc 2017, 139, 14192–14197.

[3] Ghisaidoobe, A. T.; Van Den Berg, R. J. B. H. N.; Butt, S. S.; Strijland, A.; Donker-Koopman, W. E.; Scheij, S.; Van Den Nieuwendijk, A. M. C. H.; Koomen, G. J.; Van Loevezijn, A.; Leemhuis, M.; Wennekes, T.; Van Der Stelt, M.; Van Der Marel, G. A.; Van Boeckel, C. A. A.; Aerts, J. M. F. G.; Overkleeft, H. S. Identification and Development of Biphenyl Substituted Iminosugars as Improved Dual Glucosylceramide Synthase/Neutral Glucosylceramidase Inhibitors. J Med Chem 2014, 57, 9096–9104.

[4] Ghisaidoobe, A.; Bikker, P.; De Bruijn, A. C. J.; Godschalk, F. D.; Rogaar, E.; Guijt, M. C.; Hagens, P.; Halma, J. M.; Van't Hart, S. M.; Luitjens, S. B.; Van Rixel, V. H. S.; Wijzenbroek, M.; Zweegers, T.; Donker-Koopman, W. E.; Strijland, A.; Boot, R.; Van Der Marel, G.; Overkleeft, H. S.; Aerts, J. M. F. G.; Van Den Berg, R. J. B. H. N. Identification of Potent and Selective Glucosylceramide Synthase Inhibitors from a Library of N-Alkylated Iminosugars. ACS Med Chem Lett 2011, 2, 119–123.

[5] https://doi.org/10.1073/pnas.1604463113

[6] Sastry, G. M.; Adzhigirey, M.; Day, T.; Annabhimoju, R.; Sherman, W., "Protein and ligand preparation: Parameters, protocols, and influence on virtual screening enrichments", J. Comput. Aid. Mol. Des., 2013, 27(3), 221-234

[7] Yang, Y; Yao, K; Repasky, M. P.; Leswing, K; Abel, R; Shoichet, B. K.; Jerome, S. V., "Efficient exploration of chemical space with docking and deep learning", J. Chem. Theory Comput. 2021, 17(11), 7106–7119

[8] Friesner, R. A.; Murphy, R. B.; Repasky, M. P.; Frye, L. L.; Greenwood, J. R.; Halgren, T. A.; Sanschagrin, P. C.; Mainz, D. T., "Extra precision Glide: Docking and scoring incorporating a model of hydrophobic enclosure for protein-ligand complexes", J. Med. Chem., 2006, 49, 6177–6196

[9] Halgren, T. A.; Murphy, R. B.; Friesner, R. A.; Beard, H. S.; Frye, L. L.; Pollard, W. T.; Banks, J. L., "Glide: A new approach for rapid, accurate docking and scoring. 2. Enrichment factors in database screening", J. Med. Chem., 2004, 47, 1750–1759

[10] Friesner, R. A.; Banks, J. L.; Murphy, R. B.; Halgren, T. A.; Klicic, J. J.; Mainz, D. T.; Repasky, M. P.; Knoll, E. H.; Shaw, D. E.; Shelley, M.; Perry, J. K.; Francis, P.; Shenkin, P. S., "Glide: A new approach for rapid, accurate docking and scoring. 1. Method and assessment of docking accuracy", J. Med. Chem., 2004, 47, 1739–1749

[11] Lu, C.; Wu, C.; Ghoreishi, D.; Chen, W.; Wang, L.; Damm, W.; Ross, G. A.; Dahlgren, M. K.; Russell, E.; Von Bargen, C. D.; Abel, R.; Friesner, R. A.; Harder, E. D., "OPLS4: Improving force field accuracy on challenging regimes of chemical space", J. Chem. Theory Comput., 2021, 17(7), 4291–4300

[12] Johnston, R. C.; Yao, K.; Kaplan, Z.; Chelliah, M.; Leswing, K.; Seekins, S.; Watts, S.; Calkins, D.; Chief Elk, J.; Jerome, S. V.; Repasky, M. P;. Shelley, J. C., "Epik: pKa and protonation state prediction through machine learning", J. Chem. Theory Comput. 2023, 19, 2380–2388

[13] Zhu, K.; Borrelli, K. W.; Greenwood, J. R.; Day, T.; Abel, R.; Farid, R. S.; Harder, E., "Docking covalent inhibitors: A parameter free approach to pose prediction and scoring", J. Chem. Inf. Model., 2014, 54, 1932−1940

[14] UCSF ChimeraX: Tools for structure building and analysis. Meng EC, Goddard TD, Pettersen EF, Couch GS, Pearson ZJ, Morris JH, Ferrin TE. Protein Sci. 2023 Nov;32(11):e4792.

[15] Salgado-Benvindo C, Leijs AA, Thaler M, Tas A, Arbiser JL, Snijder EJ, van Hemert MJ. 2023. Honokiol Inhibits SARS-CoV-2 Replication in Cell Culture at a Post-Entry Step. Microbiol Spectr 11:e0327322.